

MEDICINAL CHEMISTRY APPROACHES TO ACUTE KIDNEY INJURY

By

Keith Long

B.S. in Pharmaceutical Sciences, University of Pittsburgh, 2015

Doctor of Pharmacy, University of Pittsburgh, 2017

Submitted to the Graduate Faculty of the
School of Pharmacy in partial fulfillment
of the requirements for the degree of
Doctor of Philosophy

University of Pittsburgh

2022

UNIVERSITY OF PITTSBURGH

SCHOOL OF PHARMACY

This thesis was presented

By

Keith Long

It was defended on

November 4, 2022

and approved by

Samuel M. Poloyac, Pharm.D., Ph.D. Dean
The University of Texas at Austin College of Pharmacy

Paul Johnston, Ph.D., Professor
Department of Pharmaceutical Sciences, School of Pharmacy, University of Pittsburgh

Alex Deiters, Ph.D., Professor
Department of Chemistry, University of Pittsburgh

Thesis Advisor/Dissertation Director: **Donna Huryn**, Ph.D.
Department of Pharmaceutical Sciences, School of Pharmacy, University of Pittsburgh

Copyright © by Keith Long

2022

MEDICINAL CHEMISTRY APPROACHES TO ACUTE KIDNEY INJURY

Keith Long PharmD

University of Pittsburgh, 2022

Acute kidney injury (AKI) is a serious condition that negatively contributes to the morbidity and mortality of hospitalized patients. Unfortunately, despite the tremendous need, no specific treatment exists to treat AKI, and there are no clinically validated therapeutic targets. The work described contributes to closing this gap by developing tools to improve interpretation of data in zebrafish assays, to validate a target for AKI using phenotypic screens in zebrafish, to identify drug discovery starting points, and to rationally optimize those starting points. In interpreting results from embryonic zebrafish assays, negative results can be due to no specific biological activity and/or the compound not accessing its target. Using a collection of compounds that are biologically active in zebrafish, a set of predicted chemical property parameters was developed that can improve SAR data interpretation. To validate a therapeutic target for AKI, we evaluated multiple selective inhibitors of HDAC 8 from varied scaffolds in a series of increasingly stringent AKI assays. PCI-34051 was particularly effective in multiple models thus validating HDAC 8 as a target for AKI and providing a starting point for AKI drug discovery. Lead optimization on PCI-34051 focused on the hydroxamic acid zinc binding group (ZBG). Novel analogs to PCI-34051 were designed using known ZBG from the literature, synthesized, and tested. The approaches outlined in this work provide foundational knowledge for the discovery of a small molecule therapy for AKI.

Table of Contents

Title Page.....	i
Committee Page.....	ii
Abstract.....	iv
Table of Contents.....	v
Table of Figures.....	vii
Table of Tables.....	viii
1.0 Introduction.....	1
1.1 Anatomy of the Kidney.....	1
1.2 Acute Kidney Injury and its Consequences.....	1
1.3 Existing Treatments for AKI.....	3
2.0 Development of chemical property descriptors to evaluate small molecule effects in zebrafish.	9
2.1 Introduction.....	9
2.2 Method of Data Acquisition and Hypothesis.....	11
2.3 Cheminformatic Analysis and Results.....	13
2.4 Conclusions.....	18
3.0 Validation of HDAC 8 as a drug target for AKI.	20
3.1 Introduction.....	20
3.2 Experimental Design and zf Results.....	26
3.3 Organoid, Cell, and Mouse Model analysis of Active HDAC 8 Inhibitors.....	32
3.4 Conclusions.....	35
3.5 Future Directions.....	35
4.0 Design of Novel PCI-34051 Analogs.....	37
4.1 Introduction.....	37
4.1.1 PCI-34051.....	37
4.1.2 Hydroxamic Acid Zinc Binding Groups.....	38
4.2 Alternative Zinc Binding Groups.....	39
4.3 Design of PCI-34051 ZBG Isosteres.....	41
4.4 Synthesis of PCI ZBG Analogs.....	42
4.5 <i>In Vitro</i> Analysis of HDAC 8 Activity.....	45
4.6 Analysis of Zinc Chelation Capacity.....	48
4.7 Analysis of Biological activity in AKI Model.....	50
4.8 Future Directions.....	52

4.9 Conclusion.....	54
5.0 Conclusion.....	56
5.1 Summary and Impact	56
Appendix	59
Assay Methods for Chapter 3	59
IC ₅₀ Curves for Chapter 4.....	62
Experimental Data	73
Spectra	111
References	213

Table of Figures

Figure 1 Simple structure of the kidney.....	1
Figure 2 Conundrum presented when interpreting negative assay results.	10
Figure 3 Process for zebrafish permeability data accumulation and curation.	12
Figure 4 The zinc dependent deacetylation of a lysine residue using a nucleophilic water molecule.....	21
Figure 5 Structure of Entinostat.....	25
Figure 6 Structures of selected HDAC 8 inhibitors.....	26
Figure 7 General Synthetic Scheme for synthesis of 2-13	27
Figure 8 Human kidney organoids treated with HDAC 8 inhibitors.....	32
Figure 9 PCI-34051 and Compound 1 reduce expression of inflammatory cytokines in cisplatin-treated human proximal tubule cells.....	33
Figure 10 Effects of PCI-34051 at 10 and 50 mg/kg in DN-IR AKI model.	34
Figure 11 Structure of dansyl amide PCI-34051 analog 14	36
Figure 12 PDB 6HSF PCI-34051 bound to HDAC 8.	37
Figure 13 HDACi "pharmacophore"	37
Figure 14 Constant Linker and Cap Group for PCI-34051 Analogs	41
Figure 15 Synthesis of 15-17, 25, 26, 30, 32, and 33 from Methyl Ester.....	42
Figure 16 Synthesis of 21, 22, and 29 from Weinreb amide.....	43
Figure 17 Synthesis of 18-20 and 31 from amine.	43
Figure 19 Synthesis of 23 and 24 from methyl acetate.	44
Figure 18 Synthesis of 27 and 34-37 from nitrile.....	44
Figure 20 Synthesis of 28 from bromine.....	45
Figure 21 PCI-34051 and selected isosteres tested at various concentrations for fluorescence.....	45
Figure 22 Differences in HDAC 8 affinity assays	46
Figure 23 Structure of Dithizone.....	48
Figure 24 HDAC 8 inhibitors and a representative PCI-34051 analog in a competitive zinc chelation assay against the known zinc chelator EDTA.....	49
Figure 26 Compound 24 at 4uM providing no benefit in the zf AKI assay.	50
Figure 25 Compound 32 dosed at 4uM had a significant improvement of survival in the zf AKI assay.....	50
Figure 27 Attempted Synthesis of Isoxazole Ketone	52
Figure 28 Attempted Synthesis of Methylene Trifluoromethyl Ketone	53
Figure 29 Attempted Synthesis of Hydroxy Pyridone.....	53
Figure 30 Potential Future Analogs of PCI-34051.	54

Table of Tables

Table 1 Potential Drug Targets for AKI.....	4
Table 2 Calculated Properties of Zebrafish Active, Small Molecule Drugs, and Recently Approved Oral Drugs	14
Table 3 Predicted Properties of zf 700 and Small Molecule	17
Table 4 Summary of Effects of pan HDAC inhibition in AKI models.....	22
Table 5 Effects of Selective HDAC inhibition in AKI	24
Table 6 Activity of known HDAC 8 inhibitors in biochemical and zf AKI assays.....	28
Table 7 Activity of Novel THIQs in Biochemical and zf AKI	31
Table 8 PK Parameters for PCI-34051	33
Table 9 Alternative Zinc Binding Groups.....	40
Table 10 Affinity of PCI-34051 Isosteres against HDAC 8 in a Mass Spectrometry Based Assay.	47

1.0 Introduction

1.1 Anatomy of the Kidney

The kidneys, a pair of organs located just below the ribcage, filter the blood of endogenous and exogenous wastes¹. Kidneys are able to filter a cup of blood roughly every two minutes and create urine with excess water². They have additional minor roles in the production of some hormones^{1, 2} as well as in the metabolism of drugs³. The functional unit of the kidney in which the filtration and creation of urine takes place is called the nephron^{1, 2} (Figure 1). The

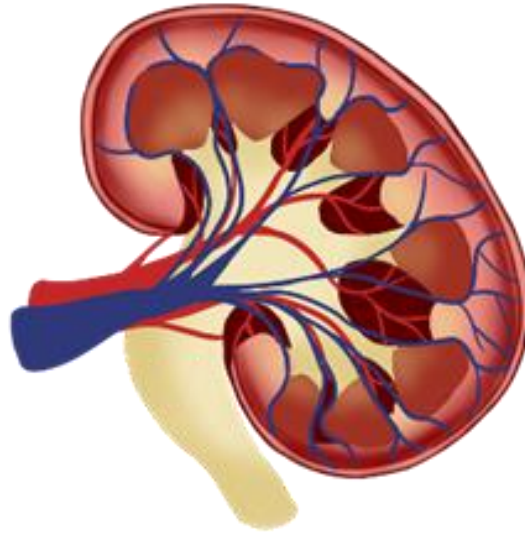


Figure 1 Simple structure of the kidney

filtration of the blood begins in the glomerulus. The filtrate then passes through to the collecting duct where it then travels to the ureter. When the kidneys are damaged, filtration of blood is prevented, and a condition called acute kidney injury (AKI) can result.

1.2 Acute Kidney Injury and its Consequences

AKI can be simply defined as a sudden loss of kidney function, but that simple definition hides the fact that the condition has multiple different etiologies. Furthermore, multiple biological pathways contribute to not only the development, but also the recovery from AKI⁴. To standardize a specific definition of observable AKI, biomarkers like serum creatinine (sCr), glomerular filtration rate (GFR), and urine output (UO) are utilized to reflect injury and its severity⁴. Several groups have defined specific biomarker value cutoffs as a tool for diagnosis⁴, however applying strict definitions may have the consequence of potentially underreporting the true impact of kidney damage⁴.

The causes of kidney damage can be classified into three categories: pre-renal, intra-renal, and post-renal. Pre-renal AKI is characterized by a lack of blood flow to the kidney, which causes hypoxia and ischemia leading to impaired function⁴. Some causes of pre-renal AKI are hypovolemia from traumatic injury, surgery, reduced cardiac output, sepsis, and blood clots⁴. Intra-renal AKI is direct damage to the kidney from an exogenous or endogenous chemicals or through physical trauma⁴. There are multiple classes of drugs that are considered nephrotoxic^{4,5} and can cause intra-renal AKI including: antibiotics, like vancomycin or aminoglycosides; chemotherapy agents, like cisplatin; and contrast dyes utilized in CT scans^{4,5}. Post-renal AKI occurs when a blockage of the ureter, such as kidney stones or swelling of the prostate, prevents the flow of urine, and causes a building up of pressure thus damaging kidney cells⁴. Regardless of the classification or cause of AKI, the consequences are dire.

With impaired kidney function, buildup of both toxins and water in the body occurs. The buildup of water leads to edema which can cause painful swelling in limbs or deadly swelling in the case of pulmonary or cardiac edema. The link between AKI and pulmonary and cardiac edema is reflected in the fact that patients with AKI are twice as likely to require mechanical ventilation than patients without AKI,⁶ and cardiac edema patients with heart failure have a higher chance of mortality with more instances of, and higher severity of, AKI⁷. Without the kidneys' processing of both endogenous and exogenous toxins, organ failure, outside of the kidneys themselves, can occur⁴. Hyperkalemia, which can lead to deadly cardiac arrhythmias, and metabolic acidosis both can occur when the kidneys are unable to excrete potassium and acid metabolites respectively. Damaged kidneys can also affect drug levels, leading to vastly increased drug and metabolite exposures which can increase the likelihood of patients experiencing drug related adverse events.

AKI has a particularly high impact on hospitalized patients. It is estimated that between 5 and 10% of hospitalized patients will experience AKI⁸⁻¹¹, and those patients have a greater likelihood of mortality^{8,9,12}, morbidity⁹, and extended length of stay^{8,10}. In addition to acute effects, a meta-analysis

found that AKI is an independent risk factor for the development of chronic kidney disease (CKD)¹², and the authors suggest that despite functional recovery of the kidney, fibrotic tissue from the acute damage may occur, and over time, that abundance of fibrosis can lead to chronic disease. CKD can then lead to end stage renal disease (ESRD) which requires dialysis and/or transplantation to treat/cure.

The impact of AKI also occurs on the societal level: it is estimated that each case of AKI costs between \$2,000 (for mild cases) and \$33,000 (for severe cases)^{8,10}. One study estimated the total annual cost of AKI in the US to be in the billions of dollars, accounting for roughly 5% of all hospital costs⁸.

1.3 Existing Treatments for AKI

Given the above, there is an urgent need for therapies that could directly treat the underlying cause and/or reverse AKI. An active therapy would result in not only immediate short term benefits (shorter hospital stays and increased survival), but also, given the link between AKI and CKD/ESRD¹², long term impacts on the health of the patient. Unfortunately, there are no specific therapies to treat AKI, and only supportive therapy exists.

Depending on the specific circumstances, AKI treatment can consist of removing nephrotoxic agents, adjusting doses of renally cleared medications, and removing or resolving any obstructions in the ureter or vessels⁹. The removal of nephrotoxic agents is more complicated than just stopping therapy as many of the nephrotoxic agents are lifesaving such as chemotherapy or antibiotics. Fluid replacement is the most effective treatment in pre-renal cases of AKI related to hypovolemia. If none of these are applicable, kidney biomarkers like serum creatinine (sCr) and blood urea nitrogen (BUN) are monitored to see if they recover back to baseline. If the kidneys do not recover on their own, patients may need the drastic intervention of dialysis to remove wastes and toxins.

While there is no approved active therapy to accelerate kidney function recovery after AKI, this is an active area of research. Table 1 lists some recent therapeutic strategies that are directed to specific

biological targets. Rows highlighted in red show targets with clinical trials. Additional rows presented include targets with pre-clinical studies supporting a therapeutic strategy to treat AKI. Additional approaches include administration of general antioxidants as cell damage is associated with oxidative stress. Arguably the most valuable therapy would be one that is effective in all etiologies of AKI through the targeted recovery of kidney cells/nephrons while preventing the development of scar tissue in the kidney.

*Table 1 Potential Drug Targets for AKI. Red indicates targets with associated clinical trials (compound investigated). **Bold and underlined** indicates a negative impact on AKI.*

Drug Target	Results	Reference
ATR-2 Agonist (angiotensin II)	Augmented renal inflammation and apoptosis.	Sharma et al. ¹³
HIF PHD Inhibition (roxadustat)	Improved BUN and sCr. Attenuated renal apoptosis and inflammation.	Yang et al. ¹⁴
MAPK Inhibition	Reduced renal fibrosis and apoptosis. Reduced reactive oxygen species. Suppressed inflammatory response and inhibited apoptosis. Reduced renal fibrosis and inflammation.	Chen et al. ¹⁵ Jiang et al. ¹⁶ Tang et al. ¹⁷
ASK 1 Inhibition	Reduced levels of renal function impairment. Reduced tubular apoptosis. Reduced progressive inflammation and fibrosis and halted GFR decline. Reduced renal apoptosis.	Liles et al. ¹⁸ El Eter ¹⁹
p38 MAPK inhibition	Attenuated elevations of sCr and BUN.	Gong et al. ²⁰
JNK Inhibition	Suppressed renal inflammation, tubular apoptosis, and interstitial fibrosis. Protected against oxidative cytotoxicity in renal cells.	Wang et al. ²¹ Kim et al. ²²
JNK/P38 activation	Reduced renal inflammation.	He et al. ²³
JAK Inhibition	Improved renal function and reduced renal apoptosis. Reduced renal apoptosis. Reduced sCr. Attenuated nephrotoxicity.	Yang et al. ²⁴ Neria et al. ²⁵ Novogrodsky et al. ^{26, 27}
Src inhibition	Reduced inflammation, oxidative stress and tubulointerstitial injury. Reduced renal apoptosis. Alleviated kidney inflammation and apoptosis. Reduced BUN and sCr. Reduced renal inflammation and apoptosis. <u>Aggravated renal failure after I/R injury</u>	Uddin et al. ²⁸ Xiong et al. ²⁹ Sahu et al. ³⁰ Ren et al. ³¹ Takikita-Suzuki et al. ³²
Rho Inhibition	Antioxidant effect.	Wang et al. ³³

	Inhibited tubular damage, inflammation and fibrogenesis.	Prakash et al. ³⁴
ROCK Inhibition	Reduced inflammatory cell infiltration. Less edema and better perfusion.	Kentrup et al. ³⁵
RIPK1 allosteric inhibition	Ameliorated renal injury and reduced renal inflammation.	Xu et al. ³⁶
RIPK1/RIPK3 inhibition	Reduced renal apoptosis.	Qin et al. ³⁷ / Fauster et al. ³⁸
Notch1 inhibition	Reduced renal apoptosis.	Najjar et al. ³⁹
NRF2 Restoration	Reduced renal fibrosis and inflammation.	Aminzadeh et al. ⁴⁰
CB1 inhibition	Reduced renal fibrosis	Chorvat ⁴¹
	Reduced renal fibrosis. Reduced in macrophage infiltration.	Lecru et al. ⁴²
CB2 agonist	Reduced renal inflammation and oxidative stress.	Pacher et al. ⁴³
	Reduced renal oxidative stress and macrophage infiltration.	Mukhopadhyay et al. (2010) ⁴⁴
	Reduced sCr.	Nettekoven et al. ⁴⁵
	Reduced renal fibrosis.	
	Protected against albuminuria and alleviated renal fibrosis.	Barutta et al. ⁴⁶
	Reduced inflammation and tubular injury and reduced renal fibrosis.	
	Reduced renal inflammation and macrophage infiltration.	Horvath et al. ⁴⁷
CB2 inverse agonist	Ameliorated kidney injury, inflammation, and fibrosis.	Zhou et al. ⁴⁸
CB2 partial agonist	Attenuated oxidative stress and inflammation in kidney.	Mukhopadhyay et al. (2016) ⁴⁹
Calpain Inhibition	Reduced apoptosis.	Gutierrez et al. ⁵⁰
S1P1 agonist	Significantly prevented graft rejections in renal transplant patients	Tedesco-Silva et al. ⁵¹
	Reduced infiltrating lymphocytes.	Suleiman et al. ⁵²
	Reduced inflammatory cell recruitment. Reduced renal fibrosis.	Tian et al. ⁵³
	Reduced sCr and infiltrating inflammatory cells.	Lien et al. ⁵⁴
TLR inhibition	Reduced renal inflammation and reduced BUN and sCr.	Peng et al. ⁵⁵
CXCR4 antagonist	Reduced BUN and sCr.	Wu et al. ⁵⁶
CXCR2 inhibition	Reduced inflammatory cell infiltration.	Cugini et al. ⁵⁷
CXCL1/CXCR2 inhibition	Reduced renal inflammation.	Liu et al. ⁵⁸

Current clinical trials for AKI include a study on administering angiotensin II (the endogenous ligand for ATR-2) and a study on administering roxadustat (HIF PHD inhibitor) in the context of coronary artery bypass surgery. Angiotensin II can be administered as a vasoconstrictor⁵⁹. If administered perioperatively, angiotensin II may provide a benefit by improving blood flow to the kidney preventing/treating pre-renal AKI due to hemodynamic instability. This strategy may help with one etiology of AKI, but still damages kidney cells⁶⁰ as a side effect, so its applicability may be limited. As of now, this clinical trial is still ongoing. Roxadustat, while it may provide a great benefit in the context of

blood loss post-surgery, might not provide the same benefit in all etiologies of AKI. Yang et al.¹⁴ found that roxadustat provided benefit from cisplatin induced kidney cell damage. Cisplatin therapy induces hypoxia in kidney cells and Roxadustat prevents the degradation of hypoxia inducible factor (HIF) which stimulates the production of red blood cells in response to hypoxia. Roxadustat is a potential therapy for certain contexts of AKI, but it could also find additional benefit in CKD as those patients are more likely to develop anemia⁶¹. This clinical trial is also ongoing.

Table 1 also contains multiple additional targets that show promising *in vitro* and/or *in vivo* efficacy. What this list highlights is that there are a plethora of biological pathways involved in the development of or the recovery from AKI. Renal apoptosis contributes to the development of acute and chronic kidney injury⁶², so targeting pathways involved in apoptosis is a promising strategy for ameliorating that injury. Kidney cell stress, whether it is due to low blood supply, direct nephrotoxic cell damage, or from increased physical pressure from ureter blockage, leads to mitochondrial injury which starts the apoptotic processes⁶². Targeting pathways involved in apoptosis could prevent further injury and speed up the recovery process. Mitogen-activated protein kinase (MAPK)⁶³, c-Jun N-terminal kinase (JNK)⁶³, janus kinase (JAK)⁶³, apoptosis signal-regulating kinase 1 (ASK 1)⁶⁴, and src family kinase (Src)⁶⁵ are kinases involved in activating the apoptosis pathway. Additionally, Notch1⁶⁶, calpain⁶⁷, and even bile acids⁶⁸ are non-kinase targets that are also involved in promoting apoptosis signaling. In fact, inhibiting MAPK^{15, 16}, ASK 1¹⁹, JNK²¹, JAK^{24, 25}, Src²⁹, Notch1³⁹, and calpain⁵⁰ can each reduce markers of renal apoptosis in models of AKI.

Pathways involved in inflammation are also promising targets for the prevention of or the recovery from AKI⁶⁹. Sphingosine-1-phosphate receptor 1 (S1P1)⁷⁰, toll-like receptor (TLR)⁶⁹, C-X-C motif chemokine receptor family (CXCR)⁶⁹, NF-E2 p45-related factor 2 (NRF2)⁷¹, and cannabinoid receptor type 1 and 2 (CB1 and CB2)⁷² are involved in the activation of inflammatory immune cells. Kinases like rho kinase⁷³ or receptor-interacting protein kinase 1 (RIPK1)⁷⁴ are involved in the proliferation of

inflammatory interleukins. Altering the activity of these targets may interfere with the inflammatory process which could protect kidney cells during injury⁶⁹. *In vivo* studies show that administering an agonist of S1P1^{53, 54} or CB2^{43, 44, 46, 47, 49} or an inhibitor of rho kinases^{34, 35}, RIPK1³⁶, NRF2⁴⁰, CB1⁴², TLR⁵⁵, and CXCR^{57, 58} can reduce inflammation or reduce activity of inflammatory cells in models of AKI. Inflammation is an important component of AKI as it initiates and or extends the injury⁷⁵. Traditional anti-inflammatory medications may not be appropriate as NSAIDs are known to damage kidneys⁷⁶. With that, an agent that can alter the expression of inflammatory cytokines and the activity of inflammatory immune cells in the kidney would be important in the pursuit of a therapeutic for AKI.

There is an ongoing study with an expected completion date of June 15, 2025 looking into fingolimod, an agonist of S1P1, for reduction of renal fibrosis post renal transplant however the generalization to outside of transplant patients may be lacking. BCT197 is an inhibitor of MAPK that was in a clinical trial in 2018 investigating the prevention of AKI post cardiac surgery as well. This trial was terminated early due to lack of effect. There is a completed clinical trial on the efficacy of atorvastatin in preventing AKI post cardiac surgery⁷⁷. Atorvastatin did not reduce the risk of AKI in this patient population. This finding is important as He et al.²³ found that atorvastatin attenuates contrast-induced nephropathy through the regulation of JNK. There are several potential explanations for why atorvastatin was unsuccessful in clinical trials: JNK may not be the best drug target for acute kidney injury, atorvastatin is beneficial in intrarenal causes of AKI but not prerenal, atorvastatin is beneficial in attenuation of injury but not in prevention of injury, atorvastatin is not a specific inhibitor of JNK so off target consequences could have prevented benefit in humans. Selective inhibitors of JNK are in development, but the primary disease state of focus is oncology⁷⁸. Targeting a single kinase in clinical trials has not yet replicated the benefit found in *in vivo* studies. There are dozens of FDA approved kinase inhibitors⁷⁹ for the kinases in Table 1, however none of those inhibitors have appeared in clinical trials for acute kidney injury. This represents a potential avenue, albeit a less promising one after the

failure of clinical trials, for a therapeutic for AKI. While some potential specific biological targets have been considered and investigated, the involvement of multiple biological pathways in this disease state have led others to focus on developing inhibitors to epigenetic targets.

In altering the activity of an epigenetic enzyme, multiple biological pathways can be affected⁸⁰ meaning that a singular therapy has the possibility to impact the activity of many of the targets in Table 1 through induction or repression of their expression. [Chapter 3](#) will investigate one such epigenetic target: the histone deacetylase family. Additionally, the involvement of multiple biological pathways has led to the use of whole organism phenotypic assays to identify potential therapeutics for AKI⁸¹. These assays can provide insight into the interactions of compounds, pathways, cells, and organs which cannot be captured by an *in vitro* target based model of AKI⁸¹.

This thesis will investigate three aspects of an effort to develop a novel therapeutic for AKI. Chapter 2 will discuss phenotypic screening in zebrafish and its application to AKI, and a cheminformatic analysis that allows more accurate interpretation of structure-activity relationship (SAR) data in zebrafish. Chapter 3 will describe the validation of one isoform of the histone deacetylase (HDAC) family, histone deacetylase 8 (HDAC 8), as a target for AKI. Chapter 4 takes advantage of our findings that selective inhibition of HDAC 8 can provide a therapeutic benefit in AKI and focuses on the expansion of the lead PCI-34051. Together, these chapters will contribute to the development of a novel small molecule therapeutics for AKI.

2.0 Development of chemical property descriptors to evaluate small molecule effects in zebrafish.

2.1 Introduction

A compelling strategy for the development of a small molecule therapeutic for multi-factorial diseases or conditions is the use of phenotypic screens as these allow for the testing of compounds against an observable phenotype like survival, disease progression/resolution, or changes in biomarkers⁸². While there is cell-based phenotypic screening, whole organism phenotypic screens can help researchers reach conclusions on a compound's liabilities along with conclusions about activity in a disease model^{82, 83}. Specifically, data from whole organisms can reflect a compound's pharmacokinetic properties and toxicity⁸³⁻⁸⁶.

Zebrafish (*Danio rerio*) are one of the species commonly utilized for whole organism phenotypic screens. They have a rapid reproduction that produces multiple offspring which provides multiple individual whole organisms for a screen^{87, 88}. Zebrafish (zf) embryos and larvae are transparent which allows for direct observation of a phenotype or the observation of changes in anatomy related to a phenotype⁸⁹. Zf embryos do not need to be fed as the yolk sac provides sustenance throughout the assay⁸⁹. The fish can be isolated into individual wells allowing for space efficient, independent analysis between organisms. The genome of zebrafish has been completely sequenced⁸⁷ which gives researchers insight on homology of potential human drug targets. Zebrafish based assays have been included in the development of compounds that are currently in clinical trials⁹⁰. Importantly, zf have provided insights on kidney regeneration^{81, 89}. The process in which kidneys regenerate is conserved across zebrafish, mice, and humans⁸¹ which allows for a translative pipeline of screening compounds, through validation, and then to the clinic. Specifically for this research, a phenotypic model of acute kidney injury in zf was utilized⁹¹.

This zf AKI model induces kidney injury through the administration of a nephrotoxic agent, gentamycin. It is administered, at a nephrotoxic, lethal dose, to zf embryos through microinjection at 2

days post fertilization (dpf) and survival is monitored⁹¹. After gentamycin administration, zf are monitored for the presence of edema, which mimics AKI, and only zf with visible edema are selected in this study to ensure that mortality is linked to the development of severe AKI. With no intervention, ~60-80% of the embryos die within 7 days. Compounds are dissolved in the aqueous solution at 2 days post injury that the fish are kept in which allows for continuous exposure of the test compound. In this model, efficacious compounds result in survival at 7 days post injury of a significantly larger number of embryos as determined by Kaplan-Meier analysis⁹² than vehicle control.

Interpreting data in zf assays comes with some caveats. When the effect is positive, it is assumed that the administered compound reached the site of action to produce the desired effect. If there are no effects after compound treatment, two scenarios are possible (Figure 2).

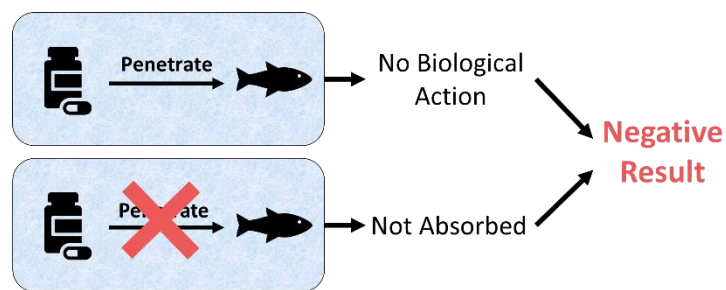


Figure 2 Conundrum presented when interpreting negative assay results.

If the compound was absorbed and reached its site of action, then the conclusion could be that the compound had no biologic activity at that concentration. However, if the compound did not reach its site of action (either because of poor permeability, metabolism, or sequestration), then no conclusions on the biological activity at the target can be made. The implication of not differentiating these two scenarios is particularly important in measuring toxicities, for example, as a false negative due to lack of access may allow a toxic compound to continue along the drug discovery and development process.

There is an abundance of literature on which physical properties of small molecules predict human oral bioavailability. Lipinski and co-workers correlated preferred values for molecular weight ($MW \leq 500$), lipophilicity as measured by octanol–water partition coefficients ($\log P \leq 5$), and the

numbers of hydrogen bond donors (HBD ≤ 5) and acceptors (HBA ≤ 10) to oral bioavailability (Lipinski Rules, Rule of Five⁹³). Veber et al. suggested that total polar surface area (tPSA ≤ 140 Å) of the molecule and the number of rotatable bonds (≤ 10) could predict oral bioavailability.⁹⁴ Others have described characteristics of molecules that are important for cell permeability⁹⁵ and even bacterial permeability.⁹⁶ However, it is not known if these same parameters apply to zf absorption or what similar parameters predict zf absorption. In this absence, the assumption is usually made that the properties that are predictive of human/mammalian absorption will translate to fish; moreover, since the ultimate goal is to treat mammals, not fish, designing for human oral bioavailability is appropriate. However, significant physiological differences between fish and mammals raise questions about the validity of this assumption, and the absence of data may lead to incorrect conclusions about whether a compound is truly biologically inert or did not permeate the fish or reach the target due to other barriers, thereby complicating any structure–activity relationship (SAR) analysis or potentially leading to false conclusions about the toxicity of small molecules.

2.2 Method of Data Acquisition and Hypothesis

To address this knowledge gap, we assembled structures of compounds reported in the literature to exhibit biological activity in zebrafish assays and made the assumption that biological activity necessitated permeability/absorption/access into this model organism (whether it be passive or active). We then calculated and predicted a series of properties and property descriptors and asked (1) what is the range of drug-like properties [e.g., molecular weight (MW), logP, polar surface area (PSA), number of rotatable bonds, H-bond donors (HBD), H-bond acceptors (HBA), solubility, and permeability] exhibited by compounds that are active in zebrafish?; (2) do the general characteristics of zebrafish-active compounds differ from the standard physicochemical property guidelines for oral bioavailability

Reprinted with permission from Long, K.; Kostman, S. J.; Fernandez, C.; Burnett, J. C.; Huryn, D. M., Do Zebrafish Obey Lipinski Rules? *ACS Med Chem Lett*. Copyright 2019 American Chemical Society

used by medicinal chemists or from those of known drugs?; and (3) can we develop a set of guidelines that can be used to interpret zebrafish assay data?

To compile a set of zebrafish-active compounds, we used keywords such as “zebrafish assay” and “zebrafish screen” to search the Scifinder and Pubmed databases for publications reporting data on small molecules’ activity in zebrafish assays. We also directly searched medicinal chemistry and chemical biology journals such as ACS

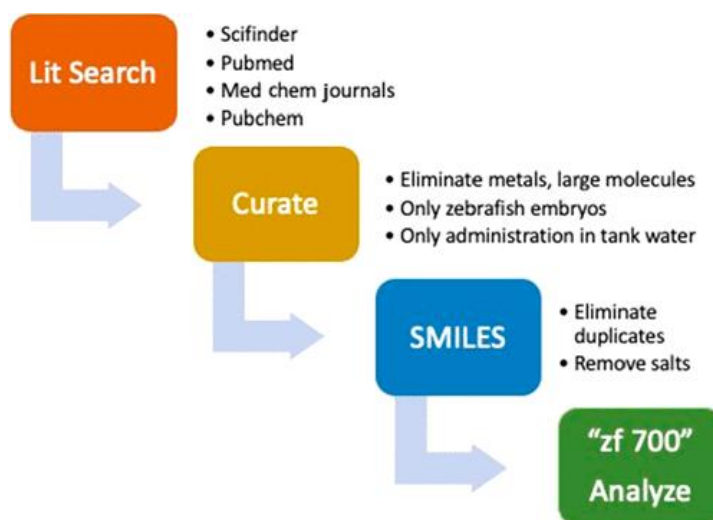


Figure 3 Process for zebrafish permeability data accumulation and curation.

Chemical Biology, ACS Medicinal Chemistry Letters, Bioorganic & Medicinal Chemistry, Bioorganic & Medicinal Chemistry Letters, European Journal of Medicinal Chemistry, Journal of Medicinal Chemistry, and MedChemComm. In total, 158 unique publications were identified, and the structures of active compounds were extracted from them. To supplement the literature data set, we reviewed Pubchem for data reported in zebrafish assays. For this set, we eliminated assays designated as “screening” as they typically report high false positive rates. Thirty-one compounds labeled as “active” in four different confirmatory or secondary assays (AIDs 691, 1137, 504373, 652284) were added to the data set. While it is likely that some publications were not captured, we believe the number and diversity of compounds identified (vide infra) provide a representative data set. Figure 3 outlines the data compilation and curation process.

Reprinted with permission from Long, K.; Kostman, S. J.; Fernandez, C.; Burnett, J. C.; Huryn, D. M., Do Zebrafish Obey Lipinski Rules? *ACS Med Chem Lett*. Copyright 2019 American Chemical Society

Structures of compounds, administered in tank water, that were reported to be active in a zebrafish embryo assay, regardless of potency, degree of efficacy, or time of exposure were collected. We eliminated structures that contained metals or were large peptides or proteins, and those that bypassed the absorption process by administration via injection or other direct method. Structures were prepared as SMILES strings (simplified molecular-input line-entry system); salt counterions and any duplicates were removed. Applying these criteria, 700 unique small molecules (“zf 700”) were identified ([10.1021/acsmmedchemlett.9b00063](https://doi.org/10.1021/acsmmedchemlett.9b00063)).

2.3 Cheminformatic Analysis and Results

We calculated MW, logP (as AlogP), HBD, HBA, number of rotatable bonds, and molecular PSA.⁹⁷

Table 2 shows the range and averages for these properties for the zf 700. Not unexpectedly, the averages all fall within the typical Lipinski/Veber guidelines: MW = 351; AlogP = 3.2; HBD = 1.4; HBA = 4.1; rotatable bonds = 4.4; and tPSA = 72.8 Å. Notable, however, is the wide range of values that appear to be compatible with zebrafish absorption, particularly molecular weight (110 to 1291 Da), AlogP (-14.0 to +7.9), and tPSA (0 to 551 Å). Other properties evaluated, including HBD, HBA, and rotatable bonds, also reveal a very wide range associated with zebrafish active compounds. While some of the extreme values are represented only sparsely, this data suggests that compounds with properties far outside what is typically considered drug-like can, in some cases, be permeable to zebrafish.

To ensure that disproportionate representation of multiple close structural analogs in the zf 700 set were not skewing the averages, we used a computational algorithm (“Affinity Propagation Clustering”⁹⁸) that clustered the 700 based on structural similarity. This algorithm identified 87 exemplars ([10.1021/acsmmedchemlett.9b00063](https://doi.org/10.1021/acsmmedchemlett.9b00063)), representative of the structural diversity of the entire set, for which we calculated the same values for comparison with the full zf 700 set. An independent

evaluation confirmed the diversity of this Exemplar 87 set ([10.1021/acsmmedchemlett.9b00063](https://doi.org/10.1021/acsmmedchemlett.9b00063)). As seen in Table 2, even though the ranges are narrower, the averages calculated for the 87 exemplars is, in most cases, very similar to those generated from the full set of 700. This analysis provides evidence that the presence of large numbers of closely related compounds in the zf 700 set did not bias the calculated averages.

Table 2 Calculated Properties of Zebrafish Active, Small Molecule Drugs, and Recently Approved Oral Drugs

	zf 700 Average	zf 700 Range	Exemplar Average Range (n=87)	zf 700 10 th percentile	zf 700 90 th percentile	Small Molecule Drugs ⁹⁹ Average 10 th – 90 th percentiles (n=1395)	FDA Approved Oral NCEs 1998-2017 ¹⁰⁰ Average 10 th -90 th percentiles (n=409)
MW	351	110 – 1291	365 129 – 958	206	489	386* 182* – 599*	400* 213 – 571*
AlogP	3.2	-14.0 – +7.9	3.3 -2.2 – +7.8	1.3	5.3	1.5* -2.3* – +4.9	2.7* -0.1* – +4.9*#
HBD	1.4	0 – 13	1.5 0 – 8	0	3	2.2* 0 – 4*	2.0* 0 – 4*
HBA	4.1	0 – 23	4.5 0 – 14	1	7	5.1* 1 – 10*	6.4* 2 – 10.2*
Rotatable bonds #	4.4	0 – 35	5.0 0 – 23	0	9	6.1* 1* – 12*	6.5* 2* – 11*
Molecular PSA (Å)	72.8	0 – 551	74.8 0 – 208	20.2	123.5	100.6* 32.0* – 186.3*	88.1* 33.9* – 144.1*

We calculated the 10th and 90th percentiles of the values in Table 2 for the zf 700 set to interrogate the boundaries that can be applied to predict zebrafish absorption. For comparison, we also completed a similar analysis of a set of historical small molecule drugs (approved and experimental, regardless of route of administration) derived from DrugBank (n = 1395)⁹⁹ and a set of >400 oral drugs approved by the FDA in a recent 20-year (1998–2017) span.¹⁰⁰ This data set (Table 2) highlights the differences between the characteristics of the majority of zebrafish-active compounds and

characteristics of approved drugs, and by extension the properties medicinal chemists typically strive for when developing drug-like and/or orally available molecules. Inclusion of the 1998–2017 set allows for specific comparison with orally administered drugs, and also takes into account some of the considerable debate in the literature on which properties reflect “drug-likeness.”¹⁰⁰

The majority of zebrafish-permeable compounds fall within the molecular weight range of 200–500 Da, with an average MW of 351. These numbers are shifted to lower values compared to both drug groups, and by ~50 Da compared to the recent oral drug set. This shift is most apparent at the higher end of the molecular weight range with the 90th percentile of the zf 700 set (489 Da) being ~100 Da lower than the two drug sets (599 and 571 Da), but the 10th percentiles being very close. The molecular weight differences reached statistical significance for all values.

Also divergent are the AlogP values. The zf 700 average (3.2) is significantly higher than the two drug groups (1.5 and 2.7 for the small molecule and recent oral drug sets, respectively), tending toward greater lipophilicity. The 90th percentile for the zf 700 is also greater than the same values for the historical and recent oral drugs (5.3 vs 4.9 for both drug sets); however, for the 90th percentiles, only the difference between the zebrafish and recent oral drug set was significant. This preference for higher lipophilicity could be attributed to zebrafish-active molecules being predominantly absorbed through the yolk sac, which contains high concentrations of lipids.

In accordance with the higher values for AlogP, the HBD and HBA counts for the zf 700 are also shifted toward more lipophilic properties. The 90th percentiles for HBD and HBA are 3 and 7, respectively, with averages of 1.4 (HBD) and 4.1 (HBA) vs the more typical limits (90th percentile) for HBD of 4 and HBA of 10 for both the small molecule and recent oral drugs. The averages for the two drug sets (HBD, 2 for both; HBA, 5.1 and 6.4 for DrugBank and recent oral drugs, respectively) were

Reprinted with permission from Long, K.; Kostman, S. J.; Fernandez, C.; Burnett, J. C.; Huryn, D. M., Do Zebrafish Obey Lipinski Rules? *ACS Med Chem Lett*. Copyright 2019 American Chemical Society

significantly higher than the zf 700 averages. Consistent with the trend toward more lipophilic characteristics, the average PSA of the zebrafish active set was 72.8 Å, and its 90th percentile equaled 123 Å; both significantly lower than the two drug categories. The rotatable bond count average (4.4) is also lower in the zf 700 set compared to the drug sets (6.1 and 6.5), as are the 10th and 90th percentile values.

Overall, zebrafish-absorbed molecules tend to be more lipophilic than known drugs, and in a most cases, their physicochemical properties fall within a narrower range of values. Based on this analysis, in particular the 90th percentiles (which were loosely applied to derive the Lipinski rules), we suggest that compounds most likely to be absorbed by zebrafish will have the following characteristics:

- MW ≤ 500
- clogP ≤ 5.3
- HBD ≤ 3
- HBA ≤ 7
- tPSA ≤ 124 Å
- rotatable bonds ≤ 9

To develop a further understanding of the characteristics of zebrafish-permeable compounds, we predicted¹⁰¹ additional properties such as solubility, various cellular permeability rates, and number of predicted metabolites. Table 3 shows those results and a comparison to the DrugBank drug set.⁹⁹ Of note, the same analysis with the exemplar set was, again, consistent with the full set of 700 compounds. Solubility trended toward lower values (log S average = -4.6 M) compared to typical goals of log S > -4.2 M₂₀ and the drug set (log S = -3.7 M), perhaps confirming the shift toward greater lipophilicity. This result was somewhat unexpected given that the zebrafish actives were administered in tank water,

Reprinted with permission from Long, K.; Kostman, S. J.; Fernandez, C.; Burnett, J. C.; Huryn, D. M., Do Zebrafish Obey Lipinski Rules? *ACS Med Chem Lett*. Copyright 2019 American Chemical Society

Table 3 Predicted Properties of zf 700 and Small Molecule

Property	zf 700 Average (10 th – 90 th Percentile)	Small Molecule Drugs ⁹⁹ Average (10 th – 90 th Percentile)
Recommended Value		
Solubility (QPlogS [#] , M) -6.5 – +0.5	-4.6 (-7.1 – -2.3)	-3.7 (-6.6 – -0.6)
Caco-2 Permeability (QPPCaco [#] , nm/sec) <25=poor; >500=high	1885 (98 – 4903)	772 (3 – 2168)
MDCK Permeability (QPPMDCK [#] , nm/sec) <25=poor; >500=high	1485 (55 – 5304)	819 (2 – 1993)
Number Metabolites [#] [1-8]	3.4 (1 – 7)	4.2 (1 – 8)
MetStabOn ^{102*}	Low: 0 Medium: 691 High: 9	

which requires aqueous solubility at relatively high concentrations (typically $\geq 10 \mu\text{M}$) with low concentrations (typically <0.5% or less) of cosolvents (e.g., DMSO, EtOH, MeOH) present.¹⁰³

Averages for cellular permeability predictions (Caco-2 and MDCK cell lines) were far above the >500 nm/s value that is generally characterized as “excellent”, as were the averages calculated for the small molecule drug set. Of interest, however, the 10th percentiles for both cell lines for the zf 700 set were also

well above the “poor” boundary of <25 nm/s, with values equal to 99 and 56 nm/s, respectively. This metric is at variance from the historic drug set, where the 10th percentiles for both Caco-2 (3 nm/sec) and MDCK (2 nm/sec) permeability fell into the “poor” descriptor. This suggestion that adequate compound permeability is more important for fish embryo absorption than mammalian cell absorption is not unexpected and could be due to a number of factors including differences between mammalian and fish membrane composition or in the activity of ABC efflux transporters.¹⁰⁴ However, this analysis suggests that predicted permeability in either Caco-2 or MDCK cell lines may be useful in evaluating the potential of compounds to be absorbed into zebrafish, and that activity is unlikely to be observed with compounds predicted to be poorly permeable (i.e., <25 nm/s).

Reprinted with permission from Long, K.; Kostman, S. J.; Fernandez, C.; Burnett, J. C.; Huryn, D. M., Do Zebrafish Obey Lipinski Rules? *ACS Med Chem Lett*. Copyright 2019 American Chemical Society

Finally, we considered whether zebrafish-actives would be distinguished from other sets by differences in predicted metabolism. Since the zebrafish yolk is highly metabolically active¹⁰⁵ and assays are often run over the course of days, one could hypothesize that activity in zebrafish assays requires metabolic stability. The prediction of numbers of metabolites indicated that the zf 700 set (average = 3.4; 10th percentile = 1; 90th percentile = 7) fell within the recommended value of 1–8 and was only marginally different from values calculated for small molecule drugs (Table 3).

To evaluate this hypothesis further, we used the open source program MetStabOn¹⁰² to predict human metabolic stability. Of the 700 zebrafish-active compounds, 0 were predicted to exhibit high metabolic stability, and 691 were predicted to have medium metabolic stability; low metabolic stability was predicted for only nine compounds. Based on this analysis, one can conclude that zf-active compounds, as a whole, are not exceptionally stable compared to typical drugs.

2.4 Conclusions

We believe this analysis should be useful when interpreting data from small molecule testing in zebrafish assays; however, there are some limitations to the data set. First, practical limitations in zebrafish testing/assay capacity and/or incorporation of zebrafish assays late in the drug discovery process may have resulted in compounds in the zf 700 data set being prechosen for good/excellent drug-like properties, rather than for a more diverse sampling. For example, when used for screening, libraries that very often contain known drugs¹⁰³ or molecules that are more drug-like than lead-like are frequently used. In other instances, our literature search identified advanced compounds, already optimized for good drug-like properties, that were evaluated in zebrafish assays for specific effects, such as toxicity. In this way, compounds in the zf 700 data set may not represent the broadly diverse scaffolds that are common in more traditional HTS libraries. However, if a preselection of compounds had

Reprinted with permission from Long, K.; Kostman, S. J.; Fernandez, C.; Burnett, J. C.; Huryn, D. M., Do Zebrafish Obey Lipinski Rules? *ACS Med Chem Lett*. Copyright 2019 American Chemical Society

influenced the data, we would have expected no or minimal difference between the zf 700 set and the known drug sets, rather than the significant differences observed.

Second, our criteria for inclusion was binary (active/inactive) and considered neither potency nor degree of efficacy. While most compounds in the zf 700 set exhibited activity at concentrations of 10–20 μM , some were active at concentrations as high as 100 μM . Therefore, future studies should focus on how potencies correlate with properties. Third, due to a lack of data, we do not understand what precludes absorption into zebrafish and can only infer the properties that zebrafish active molecules possess.

Despite these caveats, the reported analyses should be of value to medicinal chemists who rely on SAR data from zebrafish assays to guide drug discovery efforts and translation into mammals. Importantly, our results provide guidelines to aid in determining which compounds are likely to be absorbed by zebrafish and, as a result, can subsequently be used to rationalize when an “inactive” report in a zebrafish assay should be attributed to a lack of biological activity versus a lack of permeability/access. The observation that zebrafish-actives display a different range of the properties typically considered drug-like should help focus medicinal chemistry design that relies on zebrafish assay data and also ensure that optimization of activity in fish can be translated to humans.

3.0 Validation of HDAC 8 as a drug target for AKI.

3.1 Introduction

There are multiple compelling drug targets (Table 1) for developing a small molecule therapy for AKI. Based on previous work showing histone deacetylase (HDAC) involvement in the regeneration of the early kidney in zebrafish¹⁰⁶⁻¹⁰⁸, that drug target emerged as a promising pathway.

HDACs are enzymes that are members of large protein complexes¹⁰⁹ that remove acetyl groups from the ϵ -amino on lysines on proteins, most notably histones¹¹⁰⁻¹¹⁵. This family of enzymes are considered translation repressors as their catalytic activity reveals a positive charge on the histone which condenses the protein preventing transcription and translation of genes^{110-112, 114, 115}. As mentioned previously, HDACs are epigenetic targets which is important in that many of the targets identified in Table 1 can be modulated by HDAC activity. Inhibiting HDACs with trichostatin A (TSA) increases the expression of NRF2¹¹⁶ which attenuates oxidative stress in kidney disease⁴⁰. HDAC inhibition suppresses the Notch pathway^{111, 117} which is associated with protection against renal apoptosis³⁹. Suppression of the JNK pathway was connected to HDAC inhibition^{111, 117} which lead to reductions in renal inflammation and fibrosis post kidney injury²¹. In addition, HDAC inhibitors can inhibit the HIF pathway¹¹⁸ and the MAPK pathway¹¹⁹ which were included in Table 1. HDACs are also considered post-translational modifiers as they can remove the acetyl group from lysines on non-histone proteins as well^{110-115, 120}. α -tubulin is a non-histone substrate of HDACs. Removal of an acetyl group from Lys40 on α -tubulin alters organization of the cytoskeleton indicating that HDACs are involved in this process¹²¹. Additionally deacetylation of unc-51-like kinase 1 (ULK1) deactivates the kinase which is required for autophagy¹²¹. Inhibition of HDACs can alter the activity of multiple biological pathways through the prevention of translation or through the modification of proteins associated with expression or activity of said pathways.

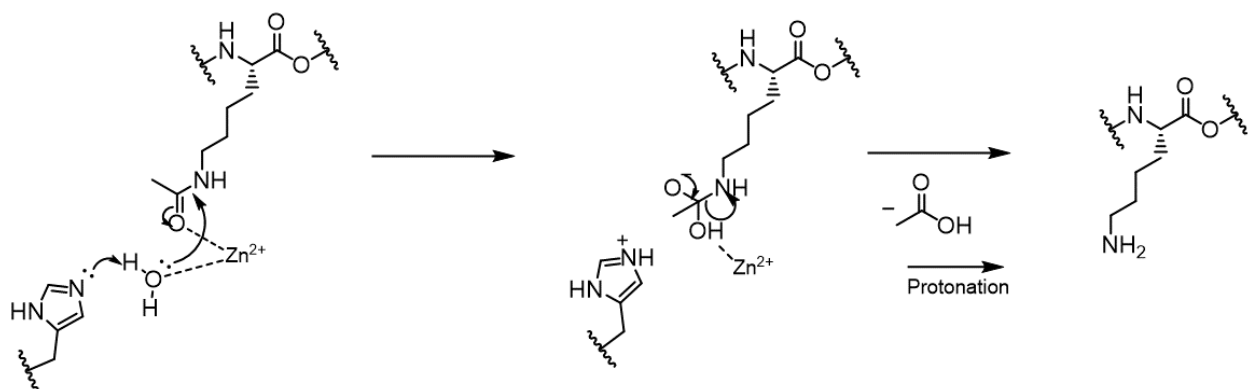


Figure 4 The zinc dependent deacetylation of a lysine residue using a nucleophilic water molecule.

HDACs can be separated into 4 classes dependent on their homology to the yeast orthologs^{110-112, 114}. Class I HDACs include the isoforms HDAC 1, HDAC 2, HDAC 3, and HDAC 8. Class II HDACs are 4, 5, 6, 7, 9, and 10. Class IV consists of one isoform of HDAC 11. These three classes make up the zinc dependent HDACs as they rely on a zinc cation in their active site to activate a water molecule which then acts as a nucleophile to remove an activated (by the same zinc cation) acetyl group from a modified lysine¹¹³ (Figure 4). The class III HDACs are referred to as the sirtuins (SIRTs). Unlike the other classes, sirtuins rely on a NAD⁺ cofactor for their catalytic activity which transfers the acetyl group to a ribose sugar¹¹³. The SIRTs will not be the focus of this document, so the term HDAC from this point forward will refer to the zinc dependent enzymes.

The involvement of HDACs in kidney injury is a relatively recent topic with the earliest relationship documented in 2003. That study found that pan inhibition of HDACs, when used as a potential treatment for lupus, led to a decrease in protein in the urine in a mouse model of lupus¹²². Since then, there have been multiple reports on HDAC activity/inhibition and AKI and other kidney related disorders (Table 4). Interest in inhibitors of HDACs (HDACi) in AKI was based on the

Table 4 Summary of Effects of pan HDAC inhibition in AKI models.

AKI Model	Results	Reference
Streptozotocin induced diabetes mouse model	Reduced renal fibrosis. Reduced reactive oxygen species.	Advani et al. ¹²³
Gentamycin zebrafish model	Promoted renal epithelium dedifferentiation and proliferation.	Brilli Skvarca et al. ¹⁰⁸
Unilateral ureteral obstruction mouse model	Decreased renal fibrosis, inflammation, and markers of oxidative stress.	Choi H. S. et al. ¹²⁴
TGF- β injured HK2 kidney cells	Decreased renal fibrosis. Increased e-cadherin protein.	Choi S. Y. et al. (2016) ¹²⁵
Streptozotocin induced diabetes rat model	Decreased renal apoptosis and inflammation.	Gilbert et al. ¹²⁶
TGF- β injured NRK-49F kidney cells	Decreased fibrosis.	Kang et al. ¹²⁷
Unilateral ureteral obstruction mouse model	Decreased renal inflammation and fibrosis.	
Unilateral ureteral obstruction rat model	Decreased renal inflammation and fibrosis.	Kinugasa et al. ¹²⁸
Cisplatin injured RPTCs	Increased autophagy. Decreased apoptosis.	Liu J. et al. ¹²⁹
Cisplatin mouse model	Decreased sCr, BUN, tubular injury score, and renal apoptosis.	
Unilateral ureteral obstruction mouse model	Restored BMP-7 expression. Decreased renal fibrosis.	Manson et al. ¹³⁰
Systemic lupus erythematosus mouse model (MRL-lpr mice)	Decreased urinary albumin. Decreases glomerular inflammation on histology	Mishra et al. ¹²²
Streptozotocin induced diabetes rat model	Decreased renal fibrosis.	Noh et al. ¹³¹
TGF- β injured NRK52-E kidney cells	Decreased fibrosis.	
Unilateral ureteral obstruction mouse model	Decreased renal fibrosis and apoptosis.	Pang et al. ¹³²
Cisplatin mouse model	Decreased sCr and tubular injury score, renal inflammation, and apoptosis.	Ranganathan et al. ¹³³
Gentamycin zebrafish model	Increases survival.	Skrypyk et al. ¹⁰⁷
Ischemia reperfusion injury mouse model	Decreased renal fibrosis. Decreased sCr, BUN, and renal fibrosis.	
TGF- β treated rat renal fibroblasts	Decreased renal fibrosis.	Tung et al. ¹¹⁷
Unilateral ureteral obstruction mouse model	Decreased renal fibrosis.	
Doxorubicin mouse model	Decreased proteinuria. Decreased renal fibrosis.	Van Beneden et al. ¹³⁴

understanding that HDACi possess anti-fibrotic and anti-inflammatory effects^{109-111, 113, 114}. Furthermore, expression of HDAC isoforms is known to change significantly post kidney injury¹³⁵⁻¹³⁷. Examples in table 4 show that HDACi can provide anti-fibrotic and anti-inflammatory effects in the kidney injury context.

Multiple studies included in Table 4 find that inhibition of HDACs was able to reduce markers of fibrogenesis like decreased fibronectin and collagen production which are large extracellular matrix proteins that create fibrous tissue post injury. HDACi reduce expression of alpha smooth muscle actin (α SMA) which is a marker of myofibroblast activity¹³⁸. These studies also show HDACi benefit as an anti-inflammatory agent in kidney injury with reduction of expression of interleukin 6, 10, and 12 (IL-6, IL-10, IL-12), tumor necrosis factor alpha and beta (TNF- α and TNF- β), and monocyte chemoattractant protein-1 (MCP-1), a chemokine that regulates macrophage infiltration. HDACi are able to decrease apoptosis which is represented by reduced TUNEL positive staining, reduced expression of cleaved caspase, signal transducer and activator of transcription 3 (STAT3), and mothers against decapentaplegic homolog 2 and 3 (SMAD2 and SMAD3). Inhibition of HDACs was shown to result in positive improvements in kidney related biomarkers such as sCr and BUN as well as improved downstream kidney related outcomes like proteinuria. Importantly, HDAC inhibition was effective across multiple etiologies of AKI including examples of pre-renal, intra-renal, and post-renal insults. These results make HDACs an exciting target for the development of an AKI therapy as it could be effective across all etiologies unlike cessation of nephrotoxic agents or fluid resuscitation which are limited to specific situations.

There are some considerations for targeting HDACs with a systemic therapy. Class I HDACs are expressed ubiquitously and Class II and IV HDACs are expressed in multiple organs¹³⁹. Therefore, utilizing a pan-HDAC inhibitor may come with unintended on-target side effects. Regardless, the *in vivo* activity from Table 4 shows a clear benefit in AKI when targeting HDAC with an inhibitor.

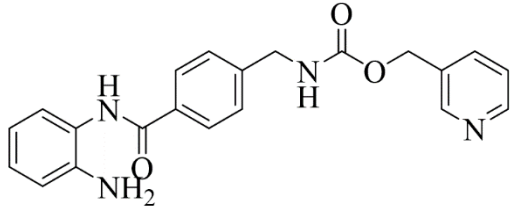
Table 5 Effects of Selective HDAC inhibition in AKI. **Bold and underlined** indicates negative impact on AKI.

Drug Target	AKI Model	Results	Reference
HDAC 1, 2, and 3 inhibition	TGF-B injured HK2 kidney cells	Decreased renal fibrosis. Increased e-cadherin protein.	Choi S. Y. et al. (2016) ¹²⁵
HDAC 8 inhibition	TGF-B injured HK2 kidney cells	Decreased renal fibrosis.	
HDAC 4 and 5 inhibition	TGF-B injured HK2 kidney cells	Decreased renal fibrosis. Increased e-cadherin protein.	
HDAC 6 inhibition	Angiotensin II mouse model	Decreased renal inflammation and fibrosis.	Choi S. Y. et al. (2015) ⁶⁰
HDAC 6 inhibition	Angiotensin II injured HK2 kidney cells	Decreased renal inflammation and fibrosis.	
HDAC 6 inhibition	TGF-B injured HK2 kidney cells	Decreased renal inflammation and fibrosis.	
HDAC 1, 2, and 3 inhibition	Unilateral ureteral obstruction mouse model	Decreased histological fibrous tissue and tubular injury. Decreased renal fibrosis.	Liu N. et al. ¹⁴⁰
HDAC 6 inhibition	Systemic lupus erythematosus mouse model (NZB/W mice)	Decreased proteinuria score. Decreased glomerular inflammation.	Regna et al. ¹⁴¹
HDAC 6 inhibition	Systemic lupus erythematosus mouse model (NZB/W mice)	Decreased proteinuria score.	Ren et al. ¹³⁶
HDAC 6 inhibition	Glycerol mouse model (rhabdomyolysis)	Decreased sCr, BUN, and tubular injury score. Decreased renal inflammation, fibrosis, and apoptosis.	Shi et al. ¹⁴²
HDAC 1, 2, and 3 inhibition	Glycerol mouse model (rhabdomyolysis)	<u>Increased sCr, BUN and tubular injury. Increased renal apoptosis.</u>	Tang et al. ¹⁴³
HDAC 1, 2, and 3 inhibition	Folic acid mouse model	<u>Increased sCr, BUN and tubular injury. Increased renal apoptosis.</u>	
HDAC 8 inhibition	Unilateral ureteral obstruction mouse model	Decreased renal fibrosis and apoptosis. Increases BMP-7 expression.	Zhang et al. ¹³⁷
HDAC 8 inhibition	TGF- β treated renal epithelial cells	Decreased renal fibrosis.	

The benefit of pan inhibition of HDACs in AKI is well documented, but there is also evidence that selective inhibition of individual HDAC isoforms also provides benefit (Table 5). Targeting a specific HDAC isoform may limit the potential side effects from a pan-HDAC inhibitor if inhibiting multiple isoforms in non-kidney cells causes unwanted toxicities. There is compelling data that the class II isoform HDAC 6 is a potential drug target for intra-renal models of AKI^{60, 136, 141, 142, 144}. These studies

show that a selective HDAC 6 inhibitor can provide similar anti-fibrotic, anti-inflammatory, and anti-apoptotic effects as pan inhibitors.

Early work on the benefits of selective class I HDACs in AKI used compound MS-275 (now also known as entinostat, FDA approved as a breakthrough therapy for metastatic or recurrent ER+ breast



cancer (Figure 5)) which is billed as a selective class I HDAC inhibitor. MS-275 has activity at HDAC 1, 2, and 3, (0.18, 1.2, and 2.3 μM), but not against HDAC 8¹⁴⁵⁻¹⁴⁷.

Figure 5 Structure of Entinostat

Using MS-

275, Liu et al.¹⁴⁰ concluded that the compound provided benefit in a unilateral ureteral obstruction (UUO) model of AKI. However, Tang et al.¹⁴³ found that administration of MS-275 potentiated the injury caused in both a folic acid injury model and a

rhabdomyolysis model of AKI. Thus, there are conflicting results in models reflecting two different

etiologies of AKI on the benefits of HDAC 1, 2, and 3 inhibition. The other isoform in class I, HDAC 8, has

fewer studies into its relationship with AKI. Choi et al.¹²⁵ showed the positive impact of specific HDAC 8

inhibition in a kidney cell line injured with TNF- β , but it wasn't until Zhang et al.¹³⁷ that small molecule

inhibition of HDAC 8 would improve outcomes in an unilateral ureteral obstruction (post-renal) mouse

model of AKI. The specific pathways that HDAC 8 inhibition alters are still being elucidated, but one

hypothesis is that the specific HDAC 8 substrate SMC3 plays a critical role. SMC3 is involved in the cell

cycle, and HDAC 8 recycles the protein for further use in mitosis¹⁴⁸. Inhibiting HDAC 8 during kidney

injury may ameliorate the condition by altering differentiation of rapidly proliferating kidney cells.

Support for this therapeutic approach is based on: 1) HDAC 8 is known to be upregulated after ischemia

reperfusion injury (IRI) in the intrarenal vessels¹³⁵ 2) HDAC 8 is known to decrease the expression of

αSMA in myofibroblasts after administration of TGF- β ¹⁴⁹. Based on this premise, this work aims to

further validate and expand HDAC 8 as a viable drug target for multiple etiologies of AKI.

3.2 Experimental Design and Results

To validate HDAC 8 inhibitors as potential starting points for drug discovery, we synthesized and tested a series of known potent, selective HDAC 8 competitive inhibitors with distinct structures. We reasoned that by evaluating inhibitors from multiple scaffolds in increasingly stringent assays, we would reduce the possibility of scaffold-specific effects compromising our conclusions. We also synthesized a small set of novel analogs within one of the series with a goal of identifying HDAC 8 inhibitors that were predicted to have improved properties, particularly solubility. A zebrafish AKI (zfAKI) model was used to prioritize compounds for more extensive evaluation in efficacy studies in human kidney organoid assays and proximal tubule cells. Finally, we report data on the effects of the selective HDAC 8 inhibitor PCI-



Figure 6 Structures of selected HDAC 8 inhibitors.

34051 in a mouse model of AKI.

Together, this work provides further support for HDAC 8

inhibition as a therapeutic target

for AKI and interrogates which HDAC 8 scaffolds may be most promising as starting points for medicinal chemistry optimization. From the potent and selective competitive HDAC 8 inhibitors reported in the literature,^{113, 150} we chose to evaluate the hydroxamic acid-containing PCI-34051¹⁵¹, isoindolyl amide **1**, and a series of tetrahydroisoquinoline (THIQ) hydroxamic acids¹⁵² (**2-13**) that, depending on structure, exhibit a range of HDAC 8 selectivity profiles (Figure 6). This series offered the opportunity to evaluate scaffold-specific effects vs HDAC 8 inhibitory effects. To account for the potential of hydroxamic acids

Reprinted with permission from Long, K.; Vaughn, Z.; McDaniels, M. D.; Joyasawal, S.; Przepiorski, A.; Parasky, E.; Sander, V.; Close, D.; Johnston, P. A.; Davidson, A. J.; de Caestecker, M.; Hukriede, N. A.; Huryn, D. M., Validation of HDAC8 Inhibitors as Drug Discovery Starting Points to Treat Acute Kidney Injury. *ACS Pharmacol Transl Sci*. Copyright 2022 American Chemical Society

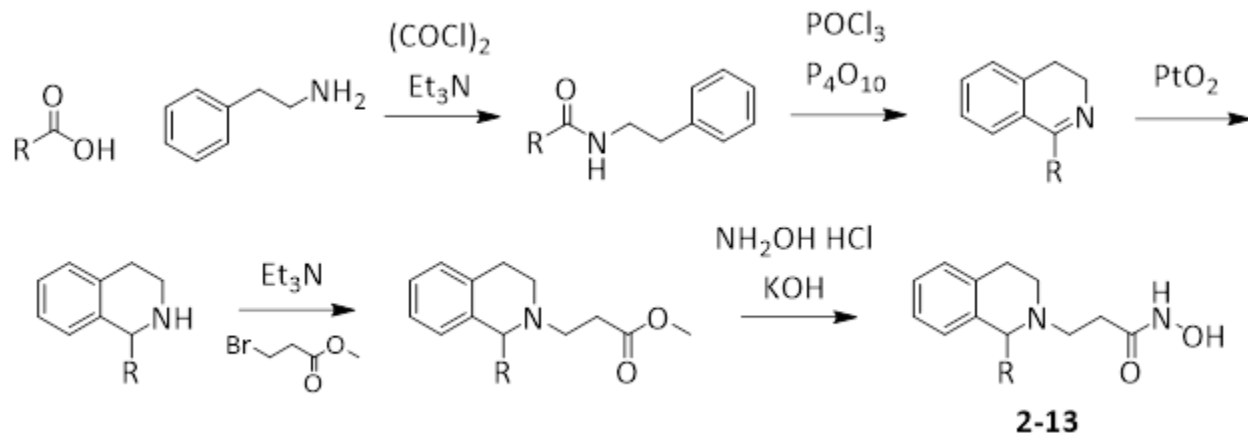


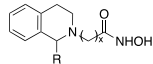
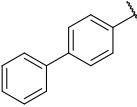
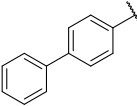
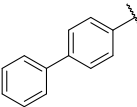
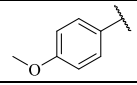
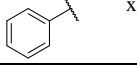
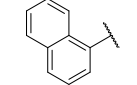
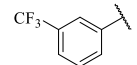
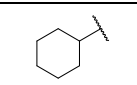
Figure 7 General Synthetic Scheme for synthesis of 2-13.

exerting off-target effects,¹⁵³ as reported for PCI-34051,¹⁵⁴ we evaluated **1** (Figure 6).¹⁵⁵ The pan-HDAC inhibitors SAHA (suberoylanilide hydroxamic acid; Vorinostat) and Belinostat were also evaluated.¹⁴⁷

PCI-34051¹⁵¹ and **1**¹⁵⁵ were synthesized based on previous publications. The synthesis of compounds **2-13** was adapted based on the work of Taha et al.¹⁵² (Figure 7) with exceptions. For **4**, ethyl 2-bromoacetate was used in place of methyl 3-bromopropionate as the alkyl chain connecting the hydroxamic acid to the tetrahydroisoquinoline was shorter. Alkylation with methyl 3-bromopropionate for all other analogs required alterations to conditions to achieve acceptable yields comparable to the original work. Solvent, base, and length of reaction were each investigated. Allowing the reaction to stir for 3 days had the largest positive impact on yield. For the synthesis of **9**, reduction of the dihydroisoquinoline led to dehalogenation of the 4-chlorophenyl ring. Reduction was attempted with sodium borohydride which produced acceptable yields. Full synthetic details are located in the Appendix.

Reprinted with permission from Long, K.; Vaughn, Z.; McDaniels, M. D.; Joyasawal, S.; Przepiorski, A.; Parasky, E.; Sander, V.; Close, D.; Johnston, P. A.; Davidson, A. J.; de Caestecker, M.; Hukriede, N. A.; Huryn, D. M., Validation of HDAC8 Inhibitors as Drug Discovery Starting Points to Treat Acute Kidney Injury. *ACS Pharmacol Transl Sci*. Copyright 2022 American Chemical Society

Table 6 Activity of known HDAC 8 inhibitors in biochemical and zf AKI assays.

Compound	 Tetrahydroisoquinolines 2-13 x=2, except when noted R	HDAC 8 ⁺ IC ₅₀ μM (sd)	Zf AKI [#] Efficacy μM	HDAC Selectivity [†] HDACX/ HDAC 8 vs. HDACs
PCI-34051	-	0.12 (0.05)	4	>200 vs. 1,2,3,6,10 ¹⁵³
1	-	0.15 (0.02)	4	>15 vs. 1,2,6 ¹⁵⁵
[rac]-2		0.42 (0.10)	4	>100 vs. 1,2,3,6 ¹⁵²
(+)-2		0.43 (0.05)	4	>20 vs. 1,2,3,6 [^]
(-)-2		31.2 (NC)	NE	NC
3		2.4 (0.38)	4	>200 vs. 1,2,3,6 ¹⁵²
4	 x=1	>40	NE	=1 vs. 6 ≥5 vs. 1,2,3 ¹⁵²
5		10.8 (3.7)	NE	>6 vs. 1,2,3,6 ¹⁵²
6		9.3 (3.6)	NE	>50 vs. 1,2,3,6 ¹⁵²
7		>40	NE	>4-fold vs. 1,2,3,6 ¹⁵²
SAHA	-	6.1 (0.92)	4	<0.10 vs. 1-4,6,7,9 ^{147,153}
Belinostat	-	1.0 (0.12)	4	<0.6 vs. 1-4,6,7,9 ¹⁴⁷

Our collaborators first confirmed HDAC 8 activity in a commercially available biochemical assay that relied on a fluorescent readout.¹⁵⁶ To prioritize compounds for more extensive (and labor intensive) organoid and *in vivo* studies, we utilized a phenotypic zfAKI assay described in Chapter 2¹⁵⁷¹⁵⁸. In this testing paradigm, when injury is established at 2 dpi, zf larvae are placed in media containing test compound at 4 μM, and survival is assessed on days 3–7

Reprinted with permission from Long, K.; Vaughn, Z.; McDaniels, M. D.; Joyasawal, S.; Przepiorski, A.; Parasky, E.; Sander, V.; Close, D.; Johnston, P. A.; Davidson, A. J.; de Caestecker, M.; Hukriede, N. A.; Huryn, D. M., Validation of HDAC8 Inhibitors as Drug Discovery Starting Points to Treat Acute Kidney Injury. *ACS Pharmacol Transl Sci*. Copyright 2022 American Chemical Society

postinjection. Protective compounds extend survival as measured by the Kaplan–Meier estimator ([10.1021/acsptsci.1c00243](https://doi.org/10.1021/acsptsci.1c00243)).⁹²

Importantly, the properties of all the tested compounds herein fall within the 95th percentile of zf-active small molecules as described in Chapter 2, supporting the probability that there are no obvious barriers to their *in vivo* efficacy in the zfAKI assay ([10.1021/acsptsci.1c00243](https://doi.org/10.1021/acsptsci.1c00243)).

Confirming the literature reports, in our hands, PCI-34051, THIQs **2** (R = biphenyl, x = 2) and **3** (R = p-methoxyphenyl, x = 2), and isoindolyl amide **1** exhibited potent HDAC 8 inhibitory activity (Tables 6 and [10.1021/acsptsci.1c00243](https://doi.org/10.1021/acsptsci.1c00243); reported selectivity vs other HDACs also included). In the zfAKI assay, PCI-34051, compound **1**, and racemic compounds **2** and **3** were efficacious in extending survival when dosed at 4 μ M.

To further explore these findings, we separated the enantiomers of **2**. The (+)-enantiomer was considerably (~100-fold) more potent in the biochemical HDAC 8 assay (IC_{50} = 0.43 μ M) than (–)-**2** (IC_{50} = 31.2 μ M) (Tables 6 and [10.1021/acsptsci.1c00243](https://doi.org/10.1021/acsptsci.1c00243)). Selectivity vs HDACs 1, 2, 3, and 6 was also maintained for (+)-**2**. Consistent with these results, the eutomer was effective in the zfAKI assay at 4 μ M, while the distomer was inactive. These data, in particular the consistent separation of activity between the enantiomers of compound **2**, support our hypothesis that potent HDAC 8 activity can lead to phenotypic zfAKI efficacy and is not scaffold-related.

Within the THIQ series, we evaluated additional analogs chosen for their specific potency and/or selectivity profiles (compounds **4–7**). We reasoned that by testing compounds within the same scaffold with very similar physical properties ([10.1021/acsptsci.1c00243](https://doi.org/10.1021/acsptsci.1c00243)), we would minimize other variables, distinct from biochemical potency, that might contribute to differential effects in the zf phenotypic

Reprinted with permission from Long, K.; Vaughn, Z.; McDaniels, M. D.; Joyasawal, S.; Przepiorski, A.; Parasky, E.; Sander, V.; Close, D.; Johnston, P. A.; Davidson, A. J.; de Caestecker, M.; Hukriede, N. A.; Huryn, D. M., Validation of HDAC8 Inhibitors as Drug Discovery Starting Points to Treat Acute Kidney Injury. *ACS Pharmacol Transl Sci*. Copyright 2022 American Chemical Society

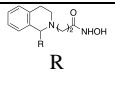
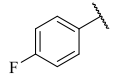
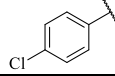
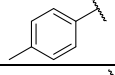
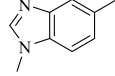
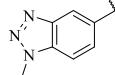
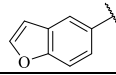
assay. We confirmed HDAC 8 IC₅₀'s internally (Tables 6 and [10.1021/acsptsci.1c00243](https://doi.org/10.1021/acsptsci.1c00243)); in general, the trends for potency were similar to those reported,¹⁵² albeit, under our assay conditions, potencies were lower. None of the compounds showed improvement in survival in the zfAKI assay when tested at 4 μM. The lack of zfAKI activity for analogs **4** and **7** was expected given their lack of HDAC 8 biochemical activity and allows us to conclude that off-target, scaffold-derived effects do not contribute to zf efficacy. However, based on their activity in the biochemical assay, we expected to see some modest effects for compound **5** or **6**. It is possible there is a threshold for potency, and the ~4-fold lower potency of these THIQs was not sufficient for zf efficacy at 4 μM, a concentration selected based on the effects of PCI-34051. The pan-HDAC inhibitors SAHA and Belinostat, with modest HDAC 8 potencies (IC₅₀ = 6 μM and 1.4 μM, respectively) and potent activities at other HDACs, were effective in the zfAKI assay at 4 μM. One hypothesis is that inhibition of other HDACs contributes to the efficacy observed for SAHA and Belinostat, a hypothesis supported by the lack of efficacy of compound **6** with similar potency vs HDAC 8 but no activity at other HDACs.

Some broad conclusions can be drawn from these data. First, highly potent (IC₅₀ < 500 nM) and selective HDAC 8 inhibitors of diverse scaffolds exhibit efficacy in the zfAKI assay, further supporting this therapeutic approach to AKI. Second, the zfAKI assay appears to be valuable for high potency compounds, but for those with modest biochemical potency (e.g., mid-μM), the correlation is less direct. Efficacy or lack of efficacy of compounds such as these may be the result of additional factors (e.g., localization, metabolism, etc.) that can be overcome by more potent analogs. Finally, pan-HDAC inhibition will also result in efficacy in this model, a result consistent with data from studies in proximal tubular cells.¹²⁹

Reprinted with permission from Long, K.; Vaughn, Z.; McDaniels, M. D.; Joyasawal, S.; Przepiorski, A.; Parasky, E.; Sander, V.; Close, D.; Johnston, P. A.; Davidson, A. J.; de Caestecker, M.; Hukriede, N. A.; Huryn, D. M., Validation of HDAC8 Inhibitors as Drug Discovery Starting Points to Treat Acute Kidney Injury. *ACS Pharmacol Transl Sci*. Copyright 2022 American Chemical Society

With the promising data for compounds **(+)-2** and **3** in the zfAKI assay, we prepared a small number of novel analogs that were designed to maintain HDAC 8 potency and selectivity but exhibit improvements in physical and pharmaceutical properties. For example, compound **2** had poor solubility in our hands, requiring a modified formulation in the zfAKI assay. We were also concerned about the potential for metabolic instability due to the presence of the aryl methyl ether in compound **3**. Specific analogs designed to address these issues included the halogenated phenyl analogs **8*** and **9** and tolyl analog **10**. We incorporated heterocycles such as benzimidazole (**11***), benzotriazole (**12***), and benzofuran (**13**) in an effort to improve solubility ([10.1021/acsptsci.1c00243](https://doi.org/10.1021/acsptsci.1c00243)) and mimic the structural features of the biphenyl and para-methoxy phenyl groups found in actives **2** and **3**. Synthesis of these compounds was based on reported methods.¹⁵²

Table 7 Activity of Novel THIQs in Biochemical and zf AKI

Compound		HDAC 8 [†] IC ₅₀ μM (sd)	Zf AKI [#] Efficacy	HDAC Selectivity % inhibition @ 10 μM
8*		8.1 (3.4)	NE	<25% @ HDAC 1,2,3,6
9		3.3 (1.1)	NE	<25% @ HDAC 1,2,3,6
10		4.6 (1.6)	NE	<25% @ HDAC 1,2,3,6
11*		7.5 (3.2)	NE	<25% @ HDAC 1,2,3; ~40% @ HDAC 6
12*		15.4 (7.3)	4	<25% @ HDAC 1,2,3,6
13		4.6 (2.1)	4	<25% @ HDAC 1,2,3,6

Results of biochemical and zfAKI assays for these novel analogs are shown in Tables 7 and [10.1021/acsptsci.1c00243](https://doi.org/10.1021/acsptsci.1c00243). Of the new analogs **8–13**, all exhibited HDAC 8 inhibition in the micromolar range, with analogs **9**, **10**, and **13** being the most potent (IC₅₀ = 3.3, 4.6, and 4.6 μM, respectively) and in the same range as p-methoxy analog **3**. Selectivity was evaluated at 10 μM, and all

* Synthesized by Dr. Sipak Joyasawal

Reprinted with permission from Long, K.; Vaughn, Z.; McDaniels, M. D.; Joyasawal, S.; Przepiorski, A.; Parasky, E.; Sander, V.; Close, D.; Johnston, P. A.; Davidson, A. J.; de Caestecker, M.; Hukriede, N. A.; Huryn, D. M., Validation of HDAC8 Inhibitors as Drug Discovery Starting Points to Treat Acute Kidney Injury. *ACS Pharmacol Transl Sci*. Copyright 2022 American Chemical Society

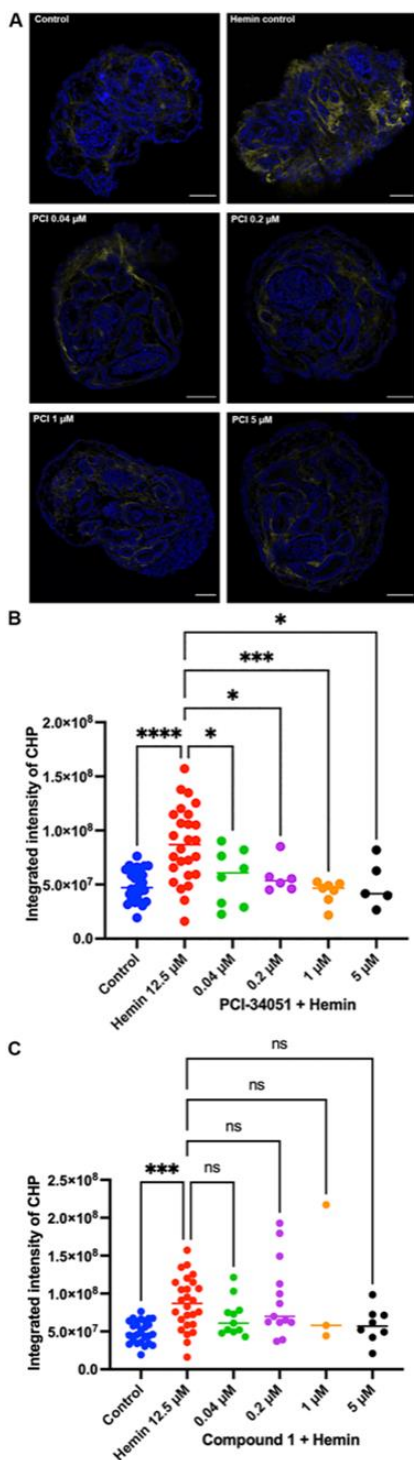


Figure 8 Human kidney organoids treated with HDAC 8 inhibitors.

* Synthesized by Dr. Sipak Joyasawal

Reprinted with permission from Long, K.; Vaughn, Z.; McDaniels, M. D.; Joyasawal, S.; Przepiorski, A.; Parasky, E.; Sander, V.; Close, D.; Johnston, P. A.; Davidson, A. J.; de Caestecker, M.; Hukriede, N. A.; Huryn, D. M., Validation of HDAC8 Inhibitors as Drug Discovery Starting Points to Treat Acute Kidney Injury. *ACS Pharmacol Transl Sci*. Copyright 2022 American Chemical Society

except **11** showed essentially no effects at HDAC 1, 2, 3, or 6. The imidazole **11*** was modestly active at HDAC6, with ~40% inhibition at 10 μ M. All compounds were evaluated in the zFAKI assay, and of these, surprisingly, the most potent compound **9** was inactive, despite potency and physical properties that were very similar to the active compound **3**; also unexpected was the efficacy of the benzotriazole **12***, which exhibits only weak HDAC 8 (IC₅₀ = 15.4 μ M) activity, a similar profile to the zf inactive compound **6** (IC₅₀= 9.3 μ M, >50-fold selective). These data raise the question of whether this THIQ scaffold (vs the PCI-34051 or compound **1** scaffold) is a robust starting point for medicinal chemistry optimization.

3.3 Organoid, Cell, and Mouse Model analysis of Active HDAC 8 Inhibitors

Based on their robust activity in the zFAKI assay and their solubility in our standard assay media (vs compound **2**, which required modification of the assay protocol), our collaborators evaluated PCI-34051, compound **1**, and compound **3** in a human kidney organoid assay to investigate the impact on renal fibrosis. Of the three, PCI-34051 showed significant reduction of collagen deposition at all

concentrations (minimal efficacious dose $\leq 0.04 \mu\text{M}$), but effects were most robust at $1 \mu\text{M}$ (Figure 8A and B). Compound **1** at all doses showed a general trend of decreased CHP staining compared to the hemin-injured control; however, none were statistically significant (Figure 8C). Compound **3** showed no effect at any dose ([10.1021/acsptsci.1c00243](https://doi.org/10.1021/acsptsci.1c00243)).

Our collaborators also tested the effects of PCI-34051 and compound **1** on immortalized human proximal tubule cells (RPTEC/TERT1) injured with the anticancer agent cisplatin, a cause of AKI clinically.¹⁵⁹

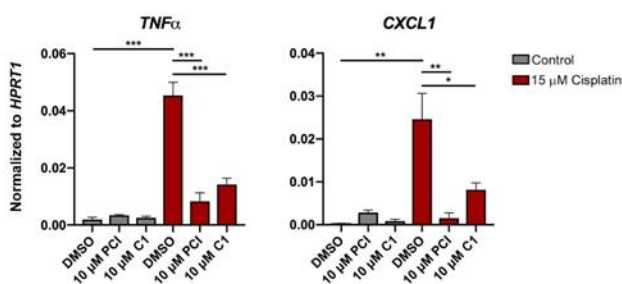


Figure 9 PCI-34051 and Compound **1** reduce expression of inflammatory cytokines in cisplatin-treated human proximal tubule cells.

Treatment with PCI-34051 and compound **1** significantly reduced the upregulation of

these genes (Figure 9). Neither compound had an effect on markers in uninjured cells, except for CCL2, which was induced 4–5-fold. Overall, these results are consistent with HDAC 8 inhibition having an anti-inflammatory effect in the setting of cisplatin-induced injury and support the potential of both scaffolds.

Table 8 PK Parameters for PCI-34051

IP dose (mg/kg)	Tmax (hr)	Cmax (ng/mL)	AUC _{last} (hr*ng/mL)	AUC _{inf} (hr*ng/mL)
10.4	0.25	3808	1851	1954
52	0.08	6157	6680	7636

Given the promising activity of PCI-34051 in both the organoid and proximal tubule cell models, as well as documented selectivity vs HDACs 1–3 and 6 in a cellular environment,^{148, 151}

our collaborators explored its effects in a mouse AKI model that we developed in which an initial AKI event progresses to CKD (unilateral IRI (ischemia reperfusion-induced) followed by delayed contralateral

Reprinted with permission from Long, K.; Vaughn, Z.; McDaniels, M. D.; Joyasawal, S.; Przepiorski, A.; Parasky, E.; Sander, V.; Close, D.; Johnston, P. A.; Davidson, A. J.; de Caestecker, M.; Hukriede, N. A.; Huryn, D. M., Validation of HDAC8 Inhibitors as Drug Discovery Starting Points to Treat Acute Kidney Injury. *ACS Pharmacol Transl Sci*. Copyright 2022 American Chemical Society

nephrectomy; DN-IRI).¹⁶⁰ A pharmacokinetic (PK) study in CD1 mice (Table 8, [10.1021/acsptsci.1c00243](https://doi.org/10.1021/acsptsci.1c00243)) showed measurable levels of the compound up to 24 h after doses of both 10.4 mg/kg and 52 mg/kg ip and, in general, dose-dependent exposure.

Our collaborators dosed mice at 10 and 50 mg/kg ip of PCI-34051 for 7 days after UUO (Figure 10A). Kidney function recovery was monitored through BUN and GFR. Development of fibrosis was monitored through histological staining and Q-RT-PCR of fibrosis markers (collagen 1a1). There was no difference in survival between groups ([10.1021/acsptsci.1c00243](https://doi.org/10.1021/acsptsci.1c00243)). BUN

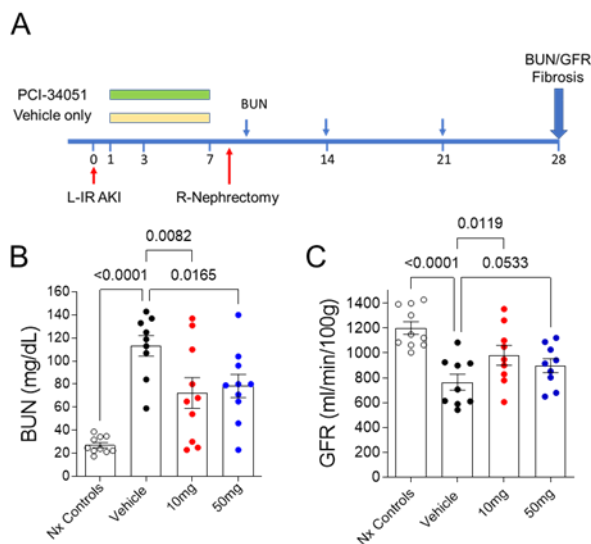


Figure 10 Effects of PCI-34051 at 10 and 50 mg/kg in DN-IR AKI model.

levels were reduced in both treatment groups 9 days after injury (Figure 10B) but equalized between groups over time ([10.1021/acsptsci.1c00243](https://doi.org/10.1021/acsptsci.1c00243)). Transdermal GFR was significantly increased in mice treated with 10 mg/kg PCI-34051 at 28 days; tGFR was also increased in mice treated with 50 mg/kg PCI-34051 27 days after IRI, but these changes failed to reach statistical significance at the accepted $p < 0.05$ level when compared with vehicle control mice ($p = 0.053$), although the effects were trending in the same direction (Figure 10C). There was no significant reduction in renal fibrosis as determined by Sirius red staining, but mRNA markers of renal fibrosis were reduced in mice treated with PCI-34051 ([10.1021/acsptsci.1c00243](https://doi.org/10.1021/acsptsci.1c00243)).

Reprinted with permission from Long, K.; Vaughn, Z.; McDaniels, M. D.; Joyasawal, S.; Przepiorski, A.; Parasky, E.; Sander, V.; Close, D.; Johnston, P. A.; Davidson, A. J.; de Caestecker, M.; Hukriede, N. A.; Huryn, D. M., Validation of HDAC8 Inhibitors as Drug Discovery Starting Points to Treat Acute Kidney Injury. *ACS Pharmacol Transl Sci*. Copyright 2022 American Chemical Society

3.4 Conclusions

In conclusion, we show that selective HDAC 8 inhibitors representing multiple scaffolds (indole hydroxamic acid, THIQ, and indolylamide) can exhibit efficacy in a zf model of AKI, further strengthening and validating this therapeutic approach. Furthermore, applying a stringent compound progression strategy, including biochemical data and zf phenotypic efficacy, we showed that some of these analogs also exhibit efficacy in human kidney organoid models. The most robust effects were observed for PCI-34051, and this translated into efficacy in a rodent model of AKI. Our data supports that selective HDAC 8 inhibitors, and in particular the indole hydroxamic acid scaffold, have the potential to be useful starting points for medicinal chemistry optimization and AKI drug discovery.

3.5 Future Directions

The HDAC 8 validation work showed that administration of an inhibitor of HDAC 8 post injury, no matter the etiology, provided benefit in the model. This study does not show a temporal investigation into potential protective effects of selective HDAC 8 inhibition instead of the recovery effects studied in this chapter. Considering a therapy would be even more useful if it could be administered before an insult to a kidney occurs, such as in the context of surgery or administration of a known nephrotoxin; though there is evidence to point to HDACi being only beneficial post injury^{108, 160}. Additionally, it is known that pan inhibition of HDACs as well as targeting specific HDAC isoforms is effective in AKI models. A future direction would be to investigate the potential synergistic effects of selectively targeting more than one isoform with HDAC 8 utilizing a dual inhibitor or co-treatment of two selective inhibitors. An additional a future direction of this work is further investigation of the relationship between PCI-34051 inhibition of HDAC 8 and the development of or recovery from AKI in zebrafish.

Taking advantage of the fact that zebrafish are translucent while still embryos, studies can be done on

Reprinted with permission from Long, K.; Vaughn, Z.; McDaniels, M. D.; Joyasawal, S.; Przepiorski, A.; Parasky, E.; Sander, V.; Close, D.; Johnston, P. A.; Davidson, A. J.; de Caestecker, M.; Hukriede, N. A.; Huryn, D. M., Validation of HDAC8 Inhibitors as Drug Discovery Starting Points to Treat Acute Kidney Injury. *ACS Pharmacol Transl Sci*. Copyright 2022 American Chemical Society

distribution of a fluorescent analog of PCI-34051 within the zebrafish. This could help establish exposure of the compound to the kidneys and/or predict potential off-target side effects of inhibiting HDAC 8 with PCI-34051 if the compound is sequestered in an organ other than the kidney. A compound synthesized during the research for Chapter 4, the dansyl amide (**14**) (Figure 11), is made from dansyl amine which is a fluorescent dye. The distribution of **14** can be monitored in translucent zf embryos under UV excitation and this could provide insight into the PCI-34051 scaffold in the zf AKI model.

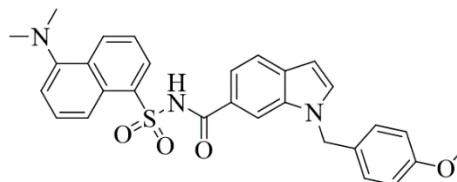


Figure 11 Structure of dansyl amide PCI-34051 analog **14**.

Reprinted with permission from Long, K.; Vaughn, Z.; McDaniels, M. D.; Joyasawal, S.; Przepiorski, A.; Parasky, E.; Sander, V.; Close, D.; Johnston, P. A.; Davidson, A. J.; de Caestecker, M.; Hukriede, N. A.; Huryn, D. M., Validation of HDAC8 Inhibitors as Drug Discovery Starting Points to Treat Acute Kidney Injury. *ACS Pharmacol Transl Sci*. Copyright 2022 American Chemical Society

4.0 Design of Novel PCI-34051 Analogs.

4.1 Introduction

4.1.1 PCI-34051

PCI-34051 is a hydroxamic acid based selective HDAC 8 inhibitor discovered by Balasubramanian et al.^{151, 161, 162}. Its original target patient profile was oncology based on data that it was able to induce apoptosis in a cell model for T-cell lymphomas¹⁵¹. PCI-34051 was also shown to be cytotoxic in a glioblastoma cell line¹⁶³ and could reduce glioma size in mouse models¹⁶⁴ suggesting a utility in non-hematologic cancers.

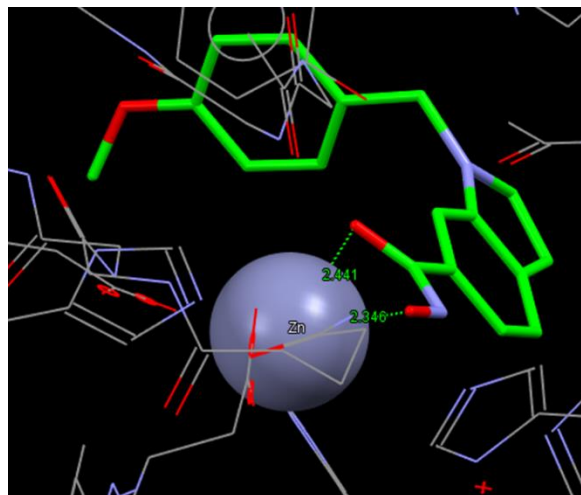


Figure 12 PDB 6HSF PCI-34051 bound to HDAC 8.

A co-crystal structure of PCI-34051 bound to HDAC 8 (Figure 12), illustrates its binding mode. Like the majority of HDAC inhibitors, it conforms to the known **Cap-Linker-ZBG** pharmacophore with the **hydroxamic acid** chelating with the zinc atom

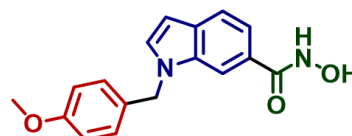
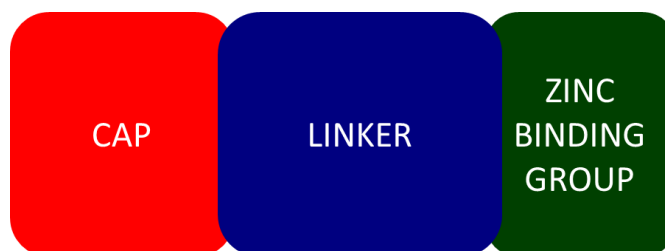


Figure 13 HDACi "pharmacophore". PCI-34051 with regions colored to match with above pharmacophore.

in the active site. Hassan et al.¹⁶⁵ postulates that the **indole group** in PCI-34051 provides the specificity for HDAC 8. Selectivity is believed to be imparted by the "L-shaped" **linker** which forces the **cap** group (Figure 13) into a groove on the surface of specifically HDAC 8. Pan inhibitors, like trichostatin A and vorinostat have a hydrophobic but flexible linker group that allows the zinc binding group to access the active site in multiple isoforms. There have been many studies that prove changes in the cap region¹⁶⁶⁻¹⁸⁰ and in the linker region^{166, 169, 172, 176, 179-183} alters affinity and/or specificity to HDACs.

However, linker alterations might be more challenging for HDAC 8 as they would have to maintain that “L-shape” for selectivity.

4.1.2 Hydroxamic Acid Zinc Binding Groups

The hydroxamic acid is the most commonly used zinc binding group in HDACi¹¹³. In the majority of cases, the carbonyl oxygen and the N-hydroxy oxygen are able form bidentate chelation of the zinc atom in the active site of HDACs¹¹³. While they are present in several approved drugs, hydroxamic acids exhibit some potential liabilities. For example, several are known to be mutagenic¹⁸⁴⁻¹⁸⁶, and the FDA approved hydroxamic acid-containing compounds are positive in the Ames test¹⁸⁴. Skipper et al.¹⁸⁵ showed that a hydroxamic acid derivative would readily form adducts *in vitro* with DNA. This liability would often preclude the compound from being used in humans, but exceptions are made when the indication is for oncology¹⁸⁷. While the target patient population for chemotherapy is older with a shortened life-expectancy, the variety of causes of AKI lead to a much broader patient population where concerns over toxicity and mutagenicity could outweigh the AKI therapeutic benefit. Hydroxamic acids are also sites for glucuronidation¹⁸⁸ and FDA approved hydroxamic acid HDAC inhibitors have short half-lives¹⁸⁹⁻¹⁹³. Together the potential for unacceptable toxicity and poor pharmacokinetics contribute to hydroxamic acid containing compounds, like PCI-34051 being a poor candidate for AKI therapy.

Based on our HDAC 8 validation studies, PCI-34051 became a scaffold of focus due to its robust effects in multiple models of AKI^{137, 194}. Given the liabilities of the hydroxamic acid ZBG, an essential pharmacophoric feature, we focused on replacing this ZBG with alternative moieties.

4.2 Alternative Zinc Binding Groups

Other functional groups have had success as a zinc binding group in replacement of a hydroxamic acid (Table 9). Most notably, is the amino benzamide functional group found in Entinostat, an FDA approved HDACi used for cancer¹⁹⁵. Liu et al¹⁹⁶ investigated 2-substituted benzamides and found that 2-hydroxy benzamide and 2-methylthio benzamide could effectively bind zinc. Liu et al¹⁹⁷ showed an ethyl ketone containing HDACi. A crystal structure illustrates that the ketone readily forms the hydrate in a biological setting which chelates to zinc in a bidentate fashion. The trifluoromethyl ketone is another ketone that has previous success in HDACi research^{198, 199}. He et al.²⁰⁰ found success using ethanolamide and isopropanolamide as ZBGs when developing HDACi. The trifluoromethyl oxazole is billed as a non-chelating ZBG²⁰¹, but crystal structures of the heterocycle in an HDAC active site show that one of the fluorines is 2.7 Å from the zinc atom while the oxygen from the oxazole is at a distance of 3.0 Å showing that, while it may be non-traditional, there is an interaction between electronegative atoms and the zinc cation. The 5-methyl isoxazole ketone and the thiazole ketone are also heterocycle isosteres that have found success as ZBGs in HDACi¹⁹⁷. Roth and Hergenrother²⁰² describe a series of 2-hydroxybenzylidene carbohydrazide analogs for use as zinc chelators, not relating to the HDAC active site, that are functionalized at the 3 and 5 position. Inorganic chemistry research into metal binding ligands²⁰³ was an additional source that produced picolinic acid as an alternative ZBG for replacing a hydroxamic acid. Carboxylic acid containing compounds, like valproic acid, have been successful in inhibiting HDAC function^{134, 204, 205}. There are reviews of alternative zinc binding groups^{168, 205, 206} that report on the varied successes above, but few studies investigate their success on replacing a hydroxamic acid with multiple ZBGs on a single known HDAC inhibitor scaffold. Using these successes as a guide, a library of non-hydroxamate PCI-34051 analogs were proposed (Table 9), synthesized, and tested to see if anything can capture the activity of the parent compound without using the hydroxamic acid functional group.

Table 9 Alternative Zinc Binding Groups

ZBG	Structure	ZBG	Structure
Hydroxamic acid		Isopropanolamide ²⁰⁰ 26	
2-amino benzamide ^{195, 196} 15		Trifluoromethyl oxazole ²⁰¹ 27	
2-hydroxy benzamide ¹⁹⁶ 16		Methylisoxazole ketone ¹⁹⁷ 28	
2-methylthio benzamide ¹⁹⁶ 17		Thiazole ketone ¹⁹⁷ 29	
Flipped 2-amino benzamide 18		2-hydroxybenzylidene carbohydrazide ²⁰² 30	
Flipped 2-hydroxy benzamide 19		Picolinic acid ²⁰³ 31	
Flipped 2-methylthio benzamide 20		Methyl acylsulfonamide ²⁰⁷ 32	
Ethyl ketone ¹⁹⁷ 21		Dimethylamino acylsulfonamide ²⁰⁷ 33	
Trifluoromethyl ketone ^{198, 199} 22		Oxadiazolone ²⁰⁷ 34	
Methylene ethyl ketone 23		Oxadiazole-thione ²⁰⁷ 35	
Methylene hydroxamic acid 24		Tetrazole ²⁰⁷ 36	
Ethanolamide ²⁰⁰ 25		Amidoxime 37	

4.3 Design of PCI-34051 ZBG Isosteres

Based on the literature, we designed analogs that contained a non-hydroxamic acid ZBG on the PCI-34051 scaffold (Figure 14). Additionally, to investigate the importance of the spatial positioning of the heteroatoms in a ZBG, the 2 substituted benzamides (**15-17**) were flipped to provide additional amides (**18-20**). To add to the alkyl ketones (**21,22**) the methylene ethyl ketone (**23**) was synthesized to investigate positioning of the ZBG. The additional methylene before the carbonyl would shift the potential zinc binding group further from the linker changing the geometry of the zinc

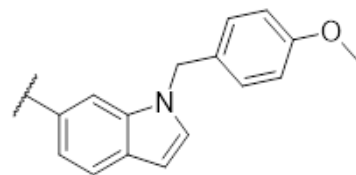


Figure 14 Constant Linker and Cap Group for PCI-34051 Analogs

chelation relative to the rest of the scaffold. The methylene hydroxamic acid (**24**) was synthesized to see the impact of ZBG movement on potency utilizing the established ZBG for the scaffold. Additional ZBGs tested on HDACi scaffolds were investigated as alternatives ZBGs for PCI-34051 (**25-29**) Additional compounds were inspired by the work done by Roth and Hergenrother²⁰² to produce the 2-hydroxybenzylidene carbohydrazide (**30**) and the work done by Dick and Cohen²⁰³ to produce the picolinic acid (**31**).

Carboxylic acids, like valproic acid, are found as a ZBG in some scaffolds. In order to bolster the library and find a potential novel ZBG, a carboxylic acid isostere resource²⁰⁷ was utilized as a source of potential alternatives. Hydroxamic acid is listed as a carboxylic acid isostere, so the rationale was that other carboxylic acid isosteres may act as a hydroxamic acid isostere. From this, the methyl acylsulfonamide (**32**), the dimethylamino acylsulfonamide (**33**), the oxadiazolone (**34**), the oxadiazolethione (**35**), and the tetrazole (**36**) were added to the proposed list of compounds. The amide-oxime (**37**) was similar to the structure of the hydroxamic acid, so it was included as a potential hydroxamic acid isostere (Table 9). In selecting hydroxamic acid replacements, predicted chemical properties, and synthetic feasibility drove the selection process. Specifically, the predicted chemical properties were

tailored to the Zebrafish Rules as the zFAKI assay was utilized as part of the SAR process. These were the compounds proposed and synthesized.

4.4 Synthesis of PCI ZBG Analogs

The synthesis of these compounds is based on the use of advanced intermediates to access multiple analogs. Figure 15 highlights the approach to a series of compounds derived from the methyl ester. The methyl ester intermediate of PCI-34051, was synthesized through benzylation of the 6 substituted indole, and the carboxylic acid was formed from a simple saponification. Amide coupling with EDC or T₃P led to a variety of amide isosteres, **15-17**, **25**, **26**, **32**, and **33**. The acyl hydrazide could be formed directly from the methyl ester with excess hydrazine. The acyl hydrazide was combined with salicylaldehyde to form **30**.

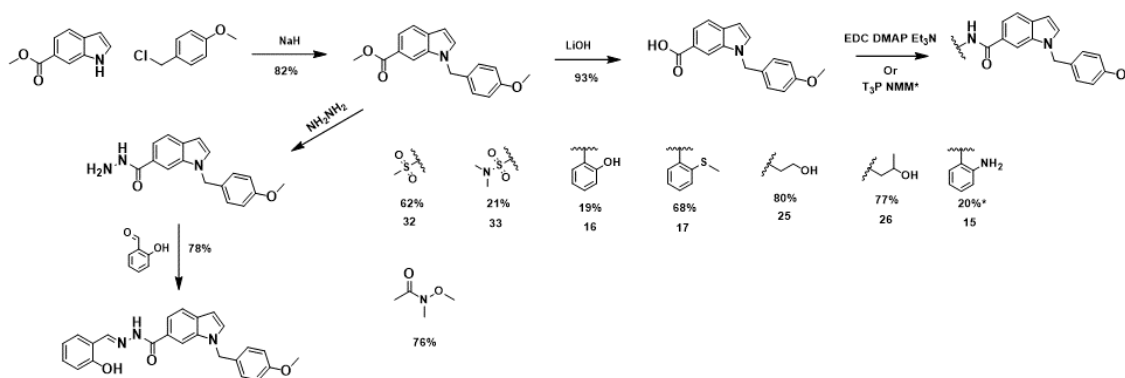


Figure 15 Synthesis of 15-17, 25, 26, 30, 32, and 33 from Methyl Ester.

The Weinreb amide was an additional advanced intermediate that was derived from the methyl ester. From the Weinreb amide, Figure 16 shows the synthesis of **21**, **22**, and **29**. Addition of ethyl Grignard reagent to the Weinreb intermediate formed the ethyl ketone (**21**). In the presence of TMS-CF₃ and catalytic CsF, the conversion to the trifluoromethyl (**22**) was initiated to form an intermediate. The administration of equimolar TBAF converted the intermediate into the final product. To form the

thiazole ketone (**29**), the Weinreb and the halogenated heterocycle were taken into solution before the reaction was initiated by the addition of $i\text{PrMgCl}$.

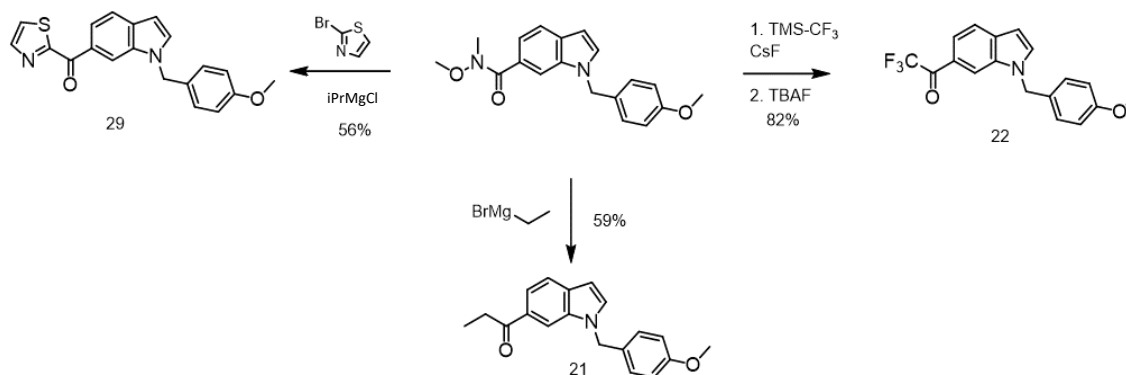


Figure 16 Synthesis of **21**, **22**, and **29** from Weinreb amide.

The benzamides, **15-17** Figure 17 were synthesized by benzylation of 6-nitro indole then reduction to the amine. Amide coupling using EDC and benzoic acid analogs provided **19**, **20**, and **31** in low to moderate yields. To prepare the 2-amino benzamide **18**, the activation of anthranilic acid led to self-coupling, so a synthetic strategy utilizing isatoic anhydride was utilized which provided the desired product.

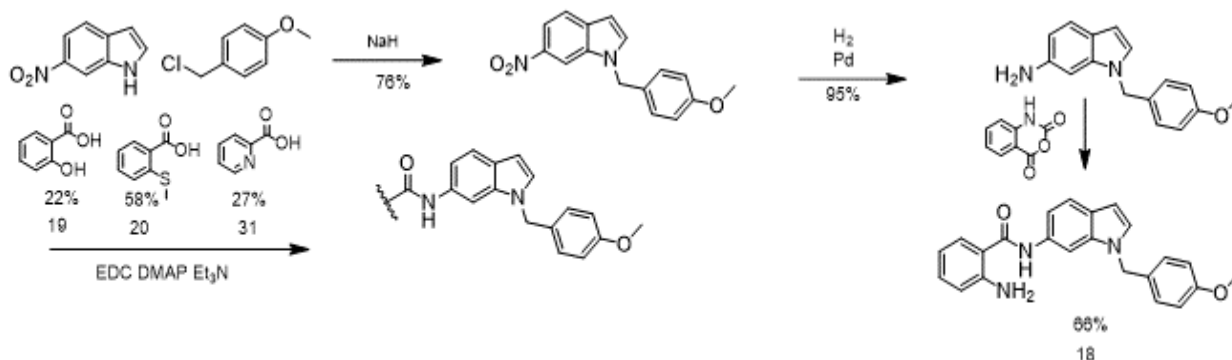


Figure 17 Synthesis of **18-20** and **31** from amine.

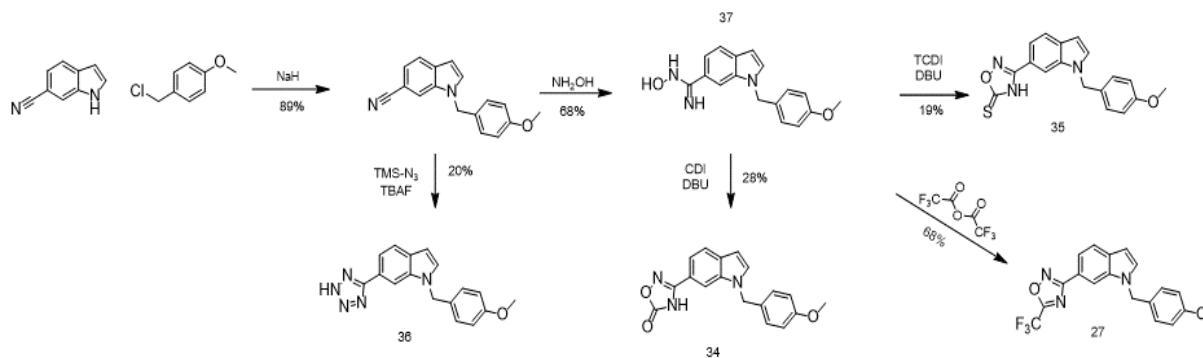


Figure 19 Synthesis of 27 and 34-37 from nitrile.

The nitrile, obtained from the benzylation of 6-cyano indole, was another advanced intermediate that led to multiple final products (Figure 18). The tetrazole (**36**) was formed from reaction with TBAF activated TMS-N₃. After nucleophilic attack of the nitrile with hydroxylamine, the amidoxime (**37**) was synthesized. The trifluoromethyl oxazole (**27**) was formed from the reaction of the amidoxime and trifluoroacetic anhydride. The amidoxime was also reacted with CDI and TCDI in the presence of DBU to form **34** and **35** respectively.

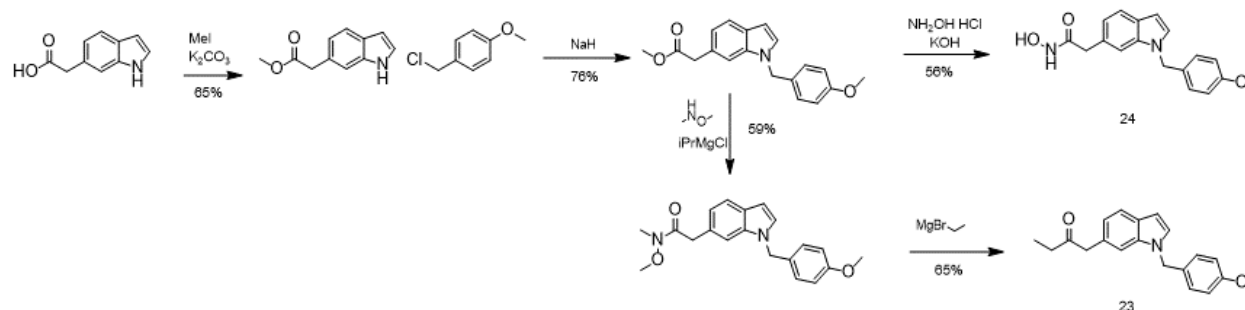


Figure 18 Synthesis of 23 and 24 from methyl acetate.

The synthesis of homologated analogs that moved the ZBG further into the pocket, Figure 19 initiated by thesis synthesis of the methyl ester from indole-6-acetic acid. Benzylation of the indole occurred in the presence of NaH and methoxy benzyl chloride. Conversion of the methyl acetate to the Weinreb amide was attempted over two steps through the carboxylic acid though this led to poor yields. The direct conversion to the Weinreb amide after activation of N,O dimethyl hydroxylamine with iPrMgCl produced acceptable yields. Adding the ethyl Grignard agent to the Weinreb amide formed the

methylene ethyl ketone (**23**). Conversion of the methyl acetate to the methylene hydroxamic acid (**24**) was performed using the previous strategy of activating hydroxylamine with excess KOH.

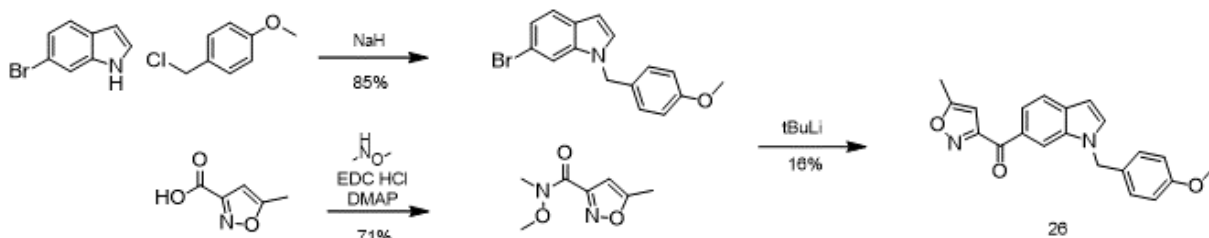


Figure 20 Synthesis of **28** from bromine

The synthesis of the methyl isoxazole ketone (**28**) was attempted through the Weinreb amide similar to the thiazole ketone (**29**) protocol, but no product was formed. An alternative strategy (Figure 20) was to exchange the functional groups by incorporating the Weinreb into the heterocycle and using the brominated indole. This strategy yielded the desired product after lithium-halogen exchange of the bromine indole. Full experimental of each final compound is located in the Appendix.

4.5 *In Vitro* Analysis of HDAC 8 Activity

Our collaborators attempted to assess HDAC 8 activity in a fluorescent readout assay¹⁵⁶. Unfortunately, many of the analogs fluoresced (Figure 21) at the same excitation wavelength used for the HDAC 8 assay, thus rendering conclusions about the activity of the compound inconclusive. In order to assess the HDAC

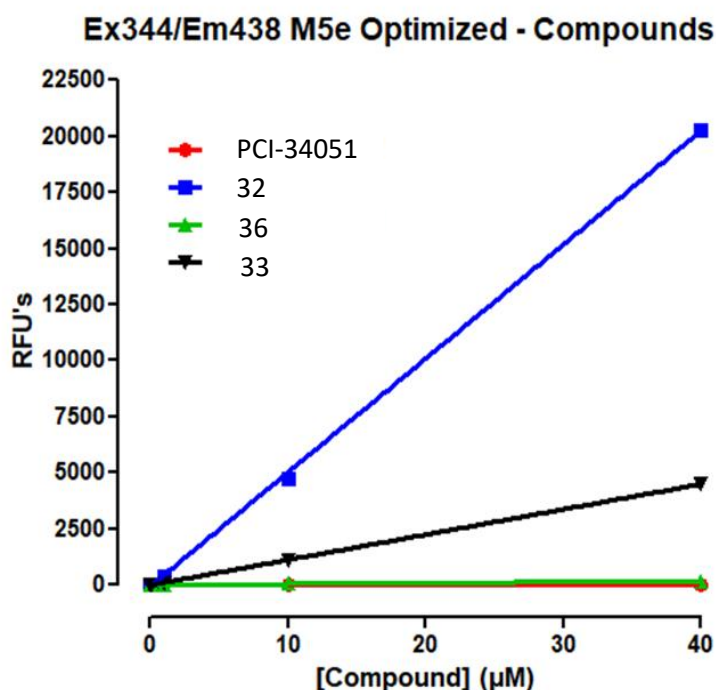
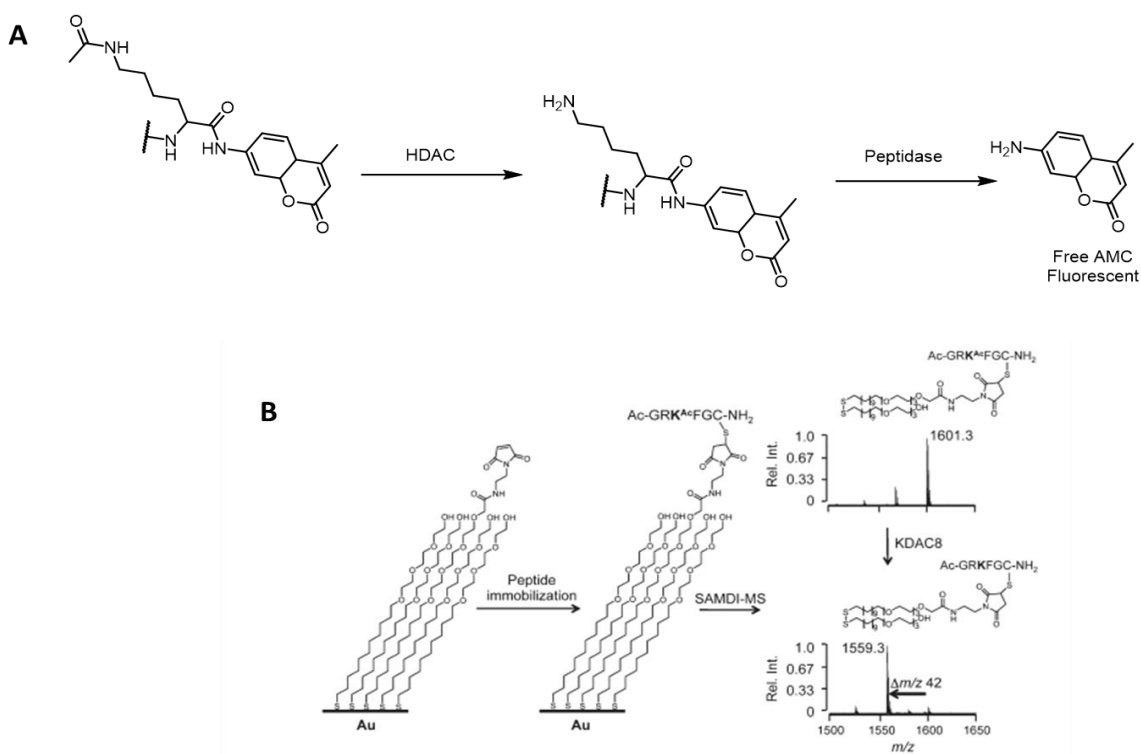


Figure 21 PCI-34051 and selected isosteres tested at various concentrations for fluorescence. Solutions were excited at wavelength 344 and readings were performed at 438 nm.

8 activity of the isosteres, an alternative readout was utilized.

Gurard-Levin et al.²⁰⁸ describes measuring HDAC activity based on mass spectrometry rather than fluorescence (Figure 22A & B). Briefly, test compound and isolated HDAC 8 enzyme are incubated for 15 minutes before a cysteine containing HDAC 8 peptide substrate is added to initiate the reaction. The mixture is transferred to a well plate containing an immobilized monolayer of maleimide containing hydrocarbon chains, which results in a covalent bond between the cysteine in the peptide substrate and the maleimide on the monolayer. After laser removal of the sulfur-gold bond, monolayer-maleimide-peptide conjugate is analyzed on mass spectrometry for the absence/presence of an acetyl group (m/z 1601.3 vs 1559.3) on the peptide substrate. Analyzing the AUC of the two mass peaks gives a



Gurard-Levin et al.

Figure 22 Differences in HDAC 8 affinity assays. A. Fluorescent based readout¹³⁵. B. Mass spectrometry based readout¹⁹³.

measurement of the enzymatic activity of HDAC 8. The results collected by SAMDI Tech Inc. are recorded in Table 10. The highest concentration assessed was 100 μ M. An IC_{50} above 100 μ M is

extrapolated from the data. As can be seen, PCI-34051 exhibits a nanomolar IC₅₀ against HDAC 8. The methylene hydroxamic acid (**24**) is in the low μM range. The ethyl ketone (**21**), 2-amino benzamide and its flipped analog (**15**, **18**), and oxadiazolone (**34**) analogs had an IC₅₀ < 150 μM. The 2-hydroxybenzylidene carbohydrazide (**30**), methyl acylsulfonamide (**32**), tetrazole (**36**), and trifluoromethyl oxazole (**27**) analogs had no detectable IC₅₀ (>1000 μM). Overall, the clear trend is that replacing the hydroxamic acid with any of the selected replacements resulted in a significant loss in activity against HDAC 8. This mirrors what was found when replacing the hydroxamic acid in trichostatin A²⁰⁹, which resulted in a complete loss of potency.

Table 10 Affinity of PCI-34051 Isosteres against HDAC 8 in a Mass Spectrometry Based Assay.

Compound	IC ₅₀ (μM)	Compound	IC ₅₀ (μM)	Compound	IC ₅₀ (μM)
PCI-34051	0.072	Methylisoxazole ketone 28	214.8	2-methylthio benzamide 17	364.9
Methylene hydroxamic acid 24	4.93	2-hydroxy benzamide 16	220.8	Picolinic acid 31	490.1
Ethyl ketone 21	117.8	Methylene ethyl ketone 23	240	Trifluoromethyl ketone 22	571.1
Flipped 2-amino benzamide 18	127.5	Dimethylamino acylsulfonamide 33	316.4	Isopropanolamide 26	891
Oxadiazolone 34	135.1	Oxadiazole-thione 35	327.1	2-hydroxybenzylidene carbohydrazide 30	>1000
2-amino benzamide 15	146.5	Amidoxime 37	341	Methyl acylsulfonamide 32	>1000
Ethanolamide 25	171.6	Flipped 2-methylthio benzamide 20	342	Tetrazole 36	>1000
Thiazole ketone 29	200.4	Flipped 2-hydroxy benzamide 19	360.9	Trifluoromethyl oxazole 27	>1000

While no hydroxamic acid replacement exhibited an IC₅₀ in the nanomolar range, some conclusions that can be drawn from this data. Moving the potential ZBG further into the pocket by

adding a methylene group between the linker and the ZBG had a detrimental effect on the potency; the methylene hydroxamic acid had reduced potency by almost 100-fold compared to PCI-34051, while extending ethyl ketone to the methylene ethyl ketone reduced the potency by about 2-fold compared to the ethyl ketone. Flipping the position of the amide for the benzamide compounds had little to no effect on the potency. Proposed ZBGs from the carboxylic acid isostere work²⁰⁷ did not provide any better or worse inhibition compared to known hydroxamic acid replacements. The overall conclusion is that alternative ZBGs are scaffold specific and cannot be easily swapped out on other scaffolds (such as the indole-methoxybenzyl scaffold of PCI-34051).

4.6 Analysis of Zinc Chelation Capacity

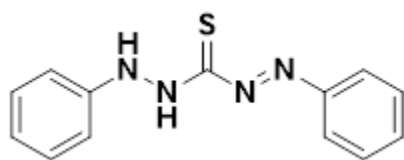


Figure 23 Structure of Dithizone

To investigate why these ZBG replacements did not perform as well as the hydroxamic acid, an *in vitro* zinc chelation assay, as reported by Catapano et al.²¹⁰ was performed on select compounds.

Briefly, the dye dithizone (Figure 23) readily chelates zinc in solution turning the color of the solution from bright orange to bright pink. This also corresponds to a change in the absorbance in the visible light spectra. When a competing zinc chelator is added before dithizone, the color change is prevented. As a standard, compounds' chelation ability was compared to the known metal chelator

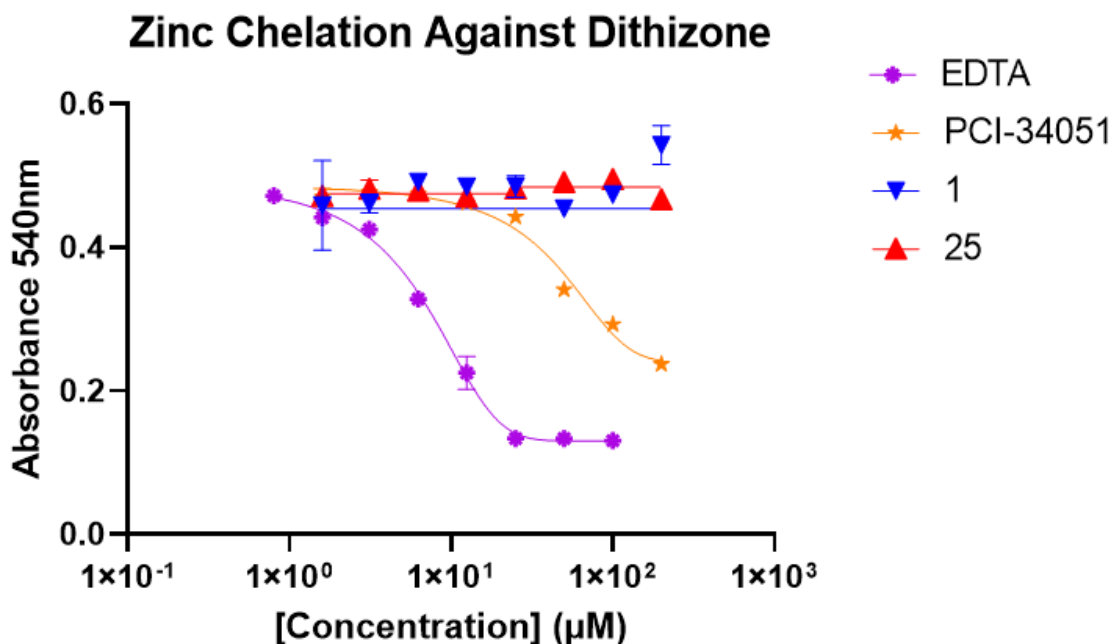


Figure 24 HDAC 8 inhibitors and a representative PCI-34051 analog in a competitive zinc chelation assay against the known zinc chelator EDTA.

Ethylenediaminetetraacetic acid (EDTA). We performed this assay in the presence of dithizone to evaluate the binding affinity to zinc.

The data is shown in Figure 24. Unsurprisingly, the hydroxamic acid, known for its chelation ability²¹¹, was the most effective zinc chelator. However, none of the ZBG analogs showed in the *in vitro* zinc chelation in this assay (Figure 24, contains representative data). The isoindolyl amide **1**, a potent HDAC 8 inhibitor containing a non-hydroxamic acid ZBG, was also tested, and it did not show any ability to compete against dithizone. Despite having a nanomolar HDAC 8 potency, the alpha-amino ketone ZBG had a low capacity for zinc chelation, at least in the context of this assay. From these results, we can propose several conclusions. First, that, at least in these assay conditions, hydroxamic acids are modest zinc chelators; second, this assay is not sensitive enough to detect moderate zinc binding; third, it suggests that zinc chelation ability is not necessarily the primary driving force for high affinity in HDAC 8 inhibitors.

4.7 Analysis of Biological activity in AKI Model

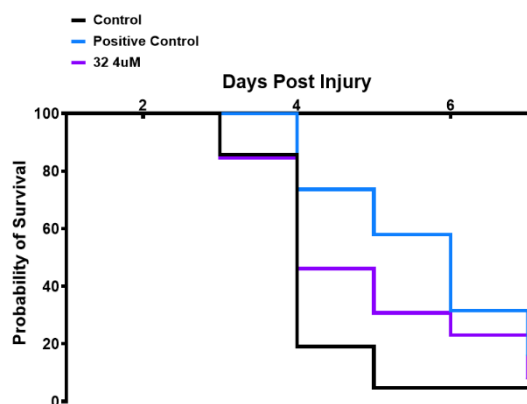


Figure 26 Compound 32 dosed at 4uM had a significant improvement of survival in the zf AKI assay.

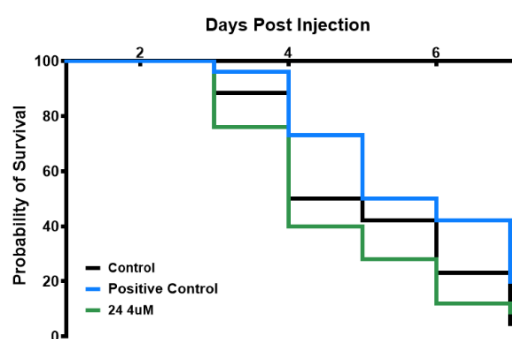


Figure 25 Compound 24 at 4uM providing no benefit in the zf AKI assay.

Despite the lack of HDAC 8 inhibitory activity, select

compounds were tested by our collaborators for activity in the zf AKI assay⁹¹ described in previous chapters. Of those tested the methyl acylsulfonamide (**32**) (Figure 25), the dimethylamino acylsulfonamide (**33**), the tetrazole (**36**), and picolinic acid (**31**) all showed an increase of survival over 5 days in the zf AKI assay. This suggests that the scaffold may exhibit off target effects that also result in efficacy in the zf AKI assay. Additionally, this may suggest that the inhibition of HDAC 8 is not the only determinant in the amelioration of AKI in this model, {though previous data¹³⁷ would refute that claim}. This is an area for future investigation.

The methylene hydroxamic acid (**24**), which had an IC50 of 5 μ M against HDAC 8, provided no benefit in the

assay (Figure 26) where PCI-34051 showed significant benefit. These results highlight the benefit of using a phenotypic screen during drug development. Despite compounds not being active at the desired target, they were still able to improve survival in a model of AKI. This could be a result of untested off-target effects that these compounds provide. Regardless, a small molecule administered in this context was able to exhibit effects in this model.

An alternative explanation for the phenotypic assay results could be that the HDAC 8 assay used does not accurately reflect activity in the biological context. A recent study²¹² evaluated the binding kinetics of hydroxamic acid based HDAC inhibitors and non-hydroxamic acid based inhibitors. They

found that the non-hydroxamic acid inhibitors exhibited slow binding kinetics and that letting the compounds incubate longer with the enzyme led to a lower IC_{50} ²¹², suggesting that a short incubation time for assays (e.g. 15 minutes for the mass spectrometry assay and 30 minutes for the fluorescent assay) may not accurately reflect activity of slow binding inhibitors. It's possible that the non-hydroxamic acid PCI-34051 analogs exhibited similar kinetics and the incubation was too short to capture the true activity of the compound. In future studies, longer incubation times or biophysical (e.g. SPR) studies to determine compound binding to HDAC 8 could potentially elucidate if this relationship occurs. Furthermore, it would be important to investigate other isoforms of HDAC to establish selectivity of these compounds. A potential explanation for some compound's activity is that they do not inhibit HDAC 8 but in fact inhibit HDAC 6 or another HDAC that potentiates AKI (Table 5).

4.8 Future Directions

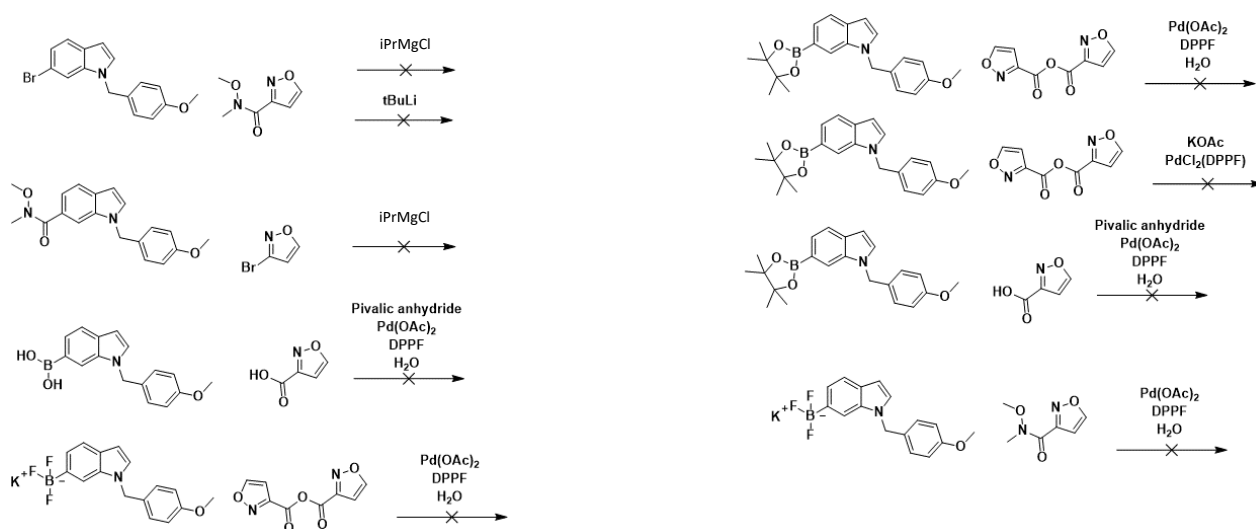


Figure 27 Attempted Synthesis of Isoxazole Ketone

While we prepared 23 PCI-34051 analogs with ZBG replacements, there are additional ZBG analogs that could be synthesized and tested. The isoxazole ketone, an analog of the methylisoxazole ketone (**28**) and the thiazole ketone (**29**) was attempted to be synthesized through multiple reaction strategies (Figure 27). Additional synthetic routes based on palladium coupling²¹³ utilizing the boronic acid, the boronic ester, and the trifluoroborate were attempted as well (Figure 27). Altering the activating anhydride was investigated as well as changing the ligand for the palladium catalyst. Regardless, there are additional opportunities to investigate alternative pathways to the final compound. The isoxazole ketone was the most potent analog from the literature¹⁹⁷ and as such would be an important additional compound for this series.

Additionally, exploration of making the homologated trifluoromethyl ketone was attempted (Figure 28). The methyl ester, the carboxylic acid, and the Weinreb amide were all utilized as potential

advanced intermediates but the reactions were unsuccessful. This would further solidify the benefit or

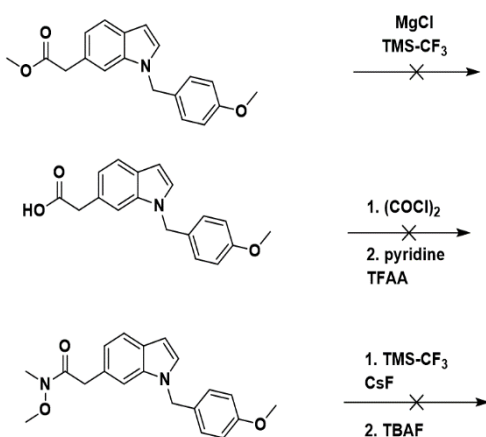


Figure 28 Attempted Synthesis of Methylene Trifluoromethyl Ketone

There are additional assays to be completed to more fully understand PCI ZBG isosteres. While there is convincing evidence that these analogs do not have nearly the same potency against HDAC 8, it would be still

beneficial to investigate if the compounds maintained selectivity over other isoforms. This data would solidify the assertion that Hassan et al.¹⁶⁵ made that the “L shape” provided by the linker region creates the selectivity and not the ZBG. Additionally, further testing of the compounds to see if replacement of the hydroxamic acid impacts pharmacokinetic properties as well as toxicologic outcomes. While this work did not find an alternative, these tests would reemphasize the importance of finding an analog that does recapture activity against HDAC 8 by replacing the hydroxamic acid.

Based on the mass spec HDAC 8 assay data, the extended hydroxamic acid analog exhibited the lowest potency among the analogs. This data highlights that positioning of the ZBG matters, but the hydroxamic acid is still the best ZBG for the PCI scaffold in the context of potency. There is preliminary

lack thereof for the extension of the ZBG further into the pocket.

The hydroxy pyridone and hydroxy pyridin-thione²¹⁴⁻²¹⁶ were also attempted (Figure 29). The synthesis was attempted through Buchwald-Hartwig coupling with the methoxy pyridone as well as synthesis of the heterocycle through the amine utilizing furfural²¹⁷.

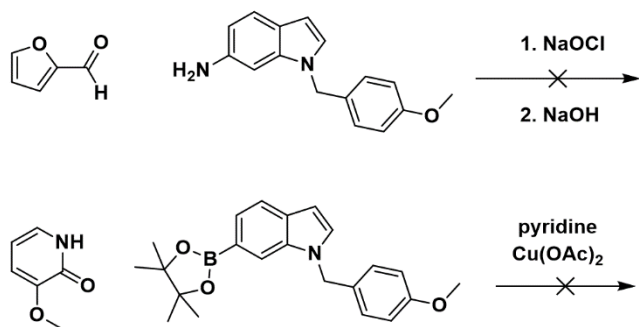


Figure 29 Attempted Synthesis of Hydroxy Pyridone

data (unpublished) that indicates that replacing the hydroxamic acid has a significant impact on extending the half-life of the compound. This would need to be assessed for other ZBG isosteres to investigate the impact of hydroxamic acid replacement.

Future directions for compounds to be synthesized includes the compounds that were attempted in Chapter 4 but were unable to be synthesized. Additionally, there are other known ZBGs in the literature that were not the focus of this work. The oxime²¹⁸, the 1-hydroxy pyridine-2-thiones²¹⁹, glycine and alanine²²⁰ (similar to the α -amino ketone **1**¹⁵⁵), and the α -thio ketone²²¹ were other ZBG alternatives that were not included (Figure 30). There are also computational studies^{199, 222} that have looked into investigating zinc chelating functional groups or the work in the inorganic chemistry literature looking into metal chelation^{203, 216} that could be the basis of additional analogs.

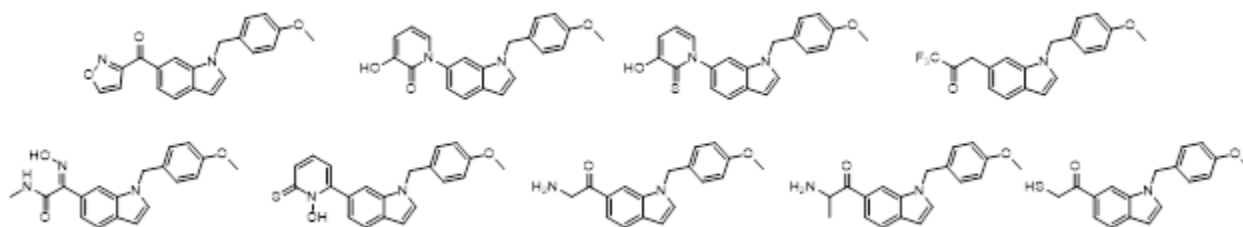


Figure 30 Potential Future Analogs of PCI-34051.

4.9 Conclusion

In conclusion, replacing hydroxamic acids with different zinc binding functional groups while maintaining potency remains a difficult task. This work provides evidence that success on one scaffold does not guarantee success on a scaffold of interest. In fact, for the PCI-34051 scaffold, there seems to be no replacement for the hydroxamic acid when it comes to achieving nanomolar potency against HDAC 8. However, these compounds may still have an advantage as a starting point for future compounds. Hydroxamic acids still remain a toxicity and metabolic liability, so their replacement is still a necessity for use in a kidney disease context.

The unconventional pharmacophore assigned to **1** may lead to a potential pathway for some of the PCI-34051 isosteres presented in this work. **1** extends past the zinc atom in the active site into what is known as the “acetate release channel”¹⁵⁵. That work shows that hydrophobic and aromatic substitutions lead to nanomolar inhibitors utilizing a non-hydroxamic acid zinc binding group. A potential next step for this series would be to build out aromatic functionalization off of the benzamide series or the methyl isoxazole ketone and triazole ketone. While none of the ZBG isosteres were a complete success, there is still an avenue to pursue in replacing the hydroxamic acid on the PCI-34051 scaffold. Once a sub-micromolar compound is synthesized, it would be paramount to assess the pharmacokinetics and mutagenic capabilities of said compound to highlight the significance of the replacement.

5.0 Conclusion

5.1 Summary and Impact

The work detailed in this document outlines a series of steps towards a small molecule therapy for AKI. Phenotypic zebrafish screens are a useful tool in drug development. This work addresses assumptions made in the interpretation of results from zebrafish-based assays. Utilizing zebrafish assays along with organoids and mouse models, our research expanded the validation of HDAC 8 as a drug target for AKI with the use of multiple HDAC 8 inhibitor scaffolds. We were able to investigate the validity of replacement of the hydroxamic acid with various functional groups in order to obtain novel HDAC inhibitors. Cumulatively, this contributed to the medicinal chemistry understanding of a potential drug for AKI.

Chapter 2 introduced the “Zebrafish Rules” ($\text{clogP} \leq 5.3$, $\text{HBD} \leq 3$, $\text{HBA} \leq 7$, $\text{tPSA} \leq 124 \text{ \AA}$, $\text{rotatable bonds} \leq 9$) which allowed us to make more informed statements about the negative results from the gentamycin induced AKI zebrafish assay that was used in the following chapters. The “Zebrafish Rules” have expansive utility outside of the AKI context. Any phenotypic screen using zebrafish for any disease state now can be more confident in the results found from hit screening. The application of “Zebrafish Rules” can also be before the assay selection process if a series of compounds of interest have predicted properties that lie outside of the parameters outlined by the rules. Zebrafish are utilized frequently in toxicologic screens and an application of the “Zebrafish Rules” would remove doubt that compounds may still exhibit toxicity outlined in the assay.

Chapter 3 expanded on the validation of HDAC 8 as a target for AKI. A previous study showed targeting HDAC 8 was able to ameliorate AKI in a post-renal model of AKI¹³⁷. This work established HDAC 8 as a target in multiple contexts with AKI models utilizing pre-renal and intra-renal etiologies of the condition, and highlighted efficacy of multiple scaffolds. This work also established selective inhibitors outside PCI-34051 as effective in some contexts while also concluding that success in one model does not guarantee success in a separate model. Similarly, it would be important to investigate if inhibiting

HDAC 8 in AKI had any correlation to the cancer models that were the original focus of selective HDAC 8 inhibitors. This could reinforce the relationship between HDAC 8 activity and multiple pathologies. Regardless, there is now compelling evidence that HDAC 8 is a valid drug target for AKI and developing a small molecule inhibitor is a sound pathway towards a therapeutic.

This work also highlighted the utilization of phenotypic assays in zf in medicinal chemistry, and specifically for AKI. While zebrafish assays have been used in the development of compounds for oncology and orphan diseases, such as Dravet Syndrome⁹⁰ and models of AKI are known,⁸¹ this establishes that zebrafish AKI assays can be a valuable step in a AKI medicinal chemistry optimization process. In our case, while enzymatic activity was required, the zf assays were used to as a funnel to evaluate the efficacy of compounds in a disease state model. Specifically, the potent HDAC8 inhibitor, PCI-34051 was active in the zebrafish AKI model, and that activity was further corroborated in a mouse AKI model supporting the translatability of the zf AKI model.

In that regard, Chapter 4 looked into the PCI-34051 scaffold and asked if alterations could be made to the hydroxamic acid ZBG. This work highlights the importance of the hydroxamic acid to the PCI-34051 scaffold as no replacement for the zinc binding group produced a compound with a nanomolar potency against HDAC 8. While the alternatives to the hydroxamic acid found success on other scaffolds, on the PCI-34051 scaffold, the ZBG isosteres do not provide significant affinity to make up for the loss of affinity from replacing the hydroxamic acid. If replacing a hydroxamic acid as a ZBG, or as a metal chelator on a different scaffold, is imperative, simply swapping out to another successful ZBG is not a straightforward pathway. This research shows that there are scaffold specific challenges to non-hydroxamic acid inhibitors, and that investigation into linker, cap group, and acetate release channel changes will have to accompany the change to the ZBG.

This chapter also highlighted the value of zebrafish assays and phenotypic screening. Despite the lack of activity at HDAC8, compounds **31**, **32**, **33**, and **36** all showed increased survival in the

zebrafish assay. This result highlights the potential to find active compounds regardless of mechanism using these types of assays, which could lead to novel hypotheses for further research. By utilizing zebrafish assays for this series of compounds, we were able to identify agents that were active in an AKI model due to their measuring biological activity in the context of a whole organism also provides insight on these compounds' ADMET properties at the starting point. This strategy eliminates compounds with poor PK properties or high toxicities from advancing in the pipeline saving time and money. With zebrafish established for AKI drug development, researchers can be more selective and confident with the compounds that they are promoting to mammalian studies.

This work advances the understanding in AKI: specifically in pursuit of a HDAC inhibitor small molecule therapy. This work validates some strategies, such as targeting the HDAC 8 isoform, while it investigates the shortcomings of other strategies, such as hydroxamic acid replacement. This document provides a foundation for the development of a small molecule HDAC inhibitor for use in AKI and raises additional scientific questions for further work.

Appendix

Assay Methods for Chapter 3

Zebrafish Assay – Courtesy of Neil Hukreide Lab, University of Pittsburgh

Studies were approved by the University of Pittsburgh IACUC. Zebrafish were maintained as described,²²³ and embryos from Pitt AB wildtype were used. Zebrafish larvae were injected with a single dose of gentamicin at 3 days post fertilization (dpf) with 7 ng of gentamicin as previously described.¹⁵⁷ Prior to the gentamicin injection, 3 dpf zebrafish larvae were anesthetized in 0.2% tricaine/E3 medium (5 mM NaCl, 0.33 mM CaCl₂, 0.33 mM MgSO₄, and 0.17 mM KCl). Glass capillaries were pulled to produce microneedles and were aspirated with 10 µL of 7 ng/nL gentamicin solution diluted with filtered saline solution (Aspen Veterinary Resources, Cat No. 17861615). The larvae were injected with 1 nL of gentamicin solution, delivered via the common cardinal vein. After injection, larvae were incubated in 50 µg/mL penicillin/streptomycin diluted in E3 medium. Test compounds were diluted in E3 medium containing 0.5% DMSO, except for [rac]-2, (+)-2, and (-)-2, which were diluted in Danieau's solution instead of E3. Larvae were treated with either DMSO, UPHD25, or test compounds (4 µM) from 2 days postinjection. Data were analyzed as compounds that extend survival as measured by the Kaplan–Meier estimator. UPHD25 (HDAC inhibitor previously shown to be protective in kidney injury¹⁰⁷) was used as a positive control and was statistically significant in all survival assays.

Organoid Assay – Courtesy of Neil Hukreide Lab, University of Pittsburgh

All work was carried out with the approval of IRB approval STUDY19020238 and biosafety approval IBC201600244. iPSCs were maintained on 10 cm cell culture dishes coated with Geltrex (Thermo Fisher) and mTeSR1 (Stemcell Technologies) medium. All experiments were performed with the MANZ-2-2 iPSC line, courtesy of the Alan Davidson laboratory.²²⁴ Kidney organoid assays were performed as described previously.^{225, 226} Briefly after Dispase treatment iPSC clusters were suspended in medium composed of TeSR-E5 (Stemcell Technologies), 0.1% ITS-X, 1% CD lipid concentrate (Gibco), 0.25% polyvinyl alcohol, 1% penicillin/streptomycin (Gibco), and 2.5 µg/mL Plasmocin. On day 3 of the assay, embryoid bodies were transferred to the Stage II medium consisting of DMEM-low glucose, 10% KOSR (Thermo Fisher), 1% nonessential amino acids, 1% penicillin/streptomycin, 1% HEPES, 1% GlutaMAX, 0.25% polyvinyl alcohol, and 2.5 mg/mL Plasmocin. Hemin was made up in 0.1 M NaOH. Day 14 organoids were washed thrice with DMEM-low glucose before being placed into protein-free medium (1:1 ratio of DMEM-low glucose and Hams F-12 nutrient mixture), 1% HEPES, 1% penicillin/streptomycin (Gibco), and 2.5 µg/mL Plasmocin containing Hemin in a 6-well ultralow attachment plate. The hemin concentration was at 12.5 µM. The control well contained an equivalent volume of 0.1 M NaOH as a vehicle control. All treatments were maintained for 48 h. Kidney organoids at day 16 post hemin treatment were washed 3× with Stage II medium. For compound treatment Stage II medium was supplemented with 0.3% DMSO. A 2× solution of compound was prepared in Stage II-DMSO, and a calculated amount was added to each well to make up 1× stock in a 3 mL volume, per well of a 6-well ULA plate. The plates were maintained on the magnetic stirrer at 25% power and 120 revolutions until day 23. Deparaffinized sections of kidney organoids were washed with DPBS. A working solution of CHP was first heated for 5 min at 80 °C, cooled on ice immediately, and distributed onto each section. Sections were stained overnight at 4 °C in a

Reprinted with permission from Long, K.; Vaughn, Z.; McDaniels, M. D.; Joyasawal, S.; Przepiorski, A.; Parasky, E.; Sander, V.; Close, D.; Johnston, P. A.; Davidson, A. J.; de Caestecker, M.; Hukriede, N. A.; Huryn, D. M., Validation of HDAC8 Inhibitors as Drug Discovery Starting Points to Treat Acute Kidney Injury. *ACS Pharmacol Transl Sci*. Copyright 2022 American Chemical Society

humidified chamber. The next day, sections were washed twice, and nuclei were stained with DAPI and mounted before imaging on a Zeiss LSM700 instrument. All images were taken with the same settings and analyzed using Fiji software. Statistical significance was tested with one-way ANOVA with Dunnett's multiple comparisons test in GraphPad Prism 9 software. PK Studies. PK studies on PCI-34051 were performed at SAI Life Sciences Ltd., Pune, India, using male BALB/c mice following a single intraperitoneal dose of PCI-34051 in 5% NMP, 5% Solutol HS, 30% PEG-400, and 60% normal saline at 10.4 and 52 mg/kg. Blood samples (approximately 120 μ L) were collected from retro-orbital plexus of three mice predose and at 0.08, 0.25, 0.5, 1, 2, 4, 8, and 24 h. Samples were collected into labeled microtubes, containing 20% K2EDTA as anticoagulant. Immediately, aliquots (50 μ L) of blood were hemolyzed with an equal volume of water (50 μ L) and quenched with three volumes (150 μ L) of acetonitrile (IS containing acetonitrile) and samples were stored below -70°C until bioanalysis. This study was performed with approval of Institutional Animal Ethics Committee (IAEC) in accordance with requirements of the Committee for the Purpose of Control and Supervision of Experiments on Animals, India. All samples were processed for analysis by protein precipitation using acetonitrile and analyzed with the fit for purpose LC/MS/MS method. PK parameters were calculated using the noncompartmental analysis tool of Phoenix WinNonlin (Version 7.0). Maximum concentration (C_{max}) and time to reach maximum concentration (T_{max}) were taken from the observed values. The areas under the concentration time curve (AUC_{last} and AUC_{inf}) and elimination half-life were calculated by the linear trapezoidal rule.

Proximal Tubule Cell Assay – Courtesy of Alan Davidson Lab, University of Auckland

Human immortalized renal proximal tubule epithelial cells (RPTEC/TERT1; ATCC CRL-4031) were maintained in renal epithelial cell growth medium (REGM; Lonza Bioscience). Cells were synchronized by double thymidine block and then treated with 15 μM cisplatin (Sigma) for 48 h, followed by 10 μM PCI-34051 or compound 1 in fresh REGM for an additional 48 h. RNA isolation (GENEZol TriRNA Pure Kit) and cDNA synthesis (SuperScript IV VILO Master Mix; Invitrogen) were carried out, and expression levels were measured on a QuantStudio 6 Flex Real-Time PCR system, using the following primers: CCL2 fwd, CAGCCAGATGCAATCAATGCC; rev, TGGAATCCTGAACCCACTTCT; CXCL1 fwd, GCGCCCAAACCGAAGTCATA; rev, ATGGGGGATGCAGGATTGAG; CXCL5 fwd, CAGACCACGCAAGGAGTTCATC; rev, TTCCTTCCCGTTCTTCAGGGAG; HPRT1 fwd, CATTATGCTGAGGATTTGAAAGG; rev, CTTGAGCACACAGAGGGCTACA; IL6 fwd, AGACAGCCACTCACCTCTTCAG; rev, TTCTGCCAGTGCCTCTTTGCTG; IL8 (CXCL8) fwd, GAGAGTGATTGAGAGTGGACCAC; rev, CACAACCCTCTGCACCCAGTTT; SERPINE1 fwd, CTCATCAGCCACTGGAAAGGCA; rev, GACTCGTGAAGTCAGCCTGAAAC; TNFa fwd, CTCTTCTGCCTGCTGCACTTTG; rev, ATGGGCTACAGGCTTGCTCACTC. Measurements were performed in triplicate. Statistical analysis was performed using one-way ANOVA in Prism.

Ischemia Reperfusion-Induced Acute Kidney Injury Assay – Courtesy of Mark DeCaestecker Lab, Vanderbilt University

Surgeries were performed on a water bath-heated platform at 38°C on 10- to 12-week-old male BALB/c mice purchased from Charles River Laboratories. To induce IRIAKI, mice underwent left renal pedicle clamping for 30–31 min, and delayed contralateral nephrectomy was performed after 8 days, as

Reprinted with permission from Long, K.; Vaughn, Z.; McDaniels, M. D.; Joyasawal, S.; Przepiorski, A.; Parasky, E.; Sander, V.; Close, D.; Johnston, P. A.; Davidson, A. J.; de Caestecker, M.; Hukriede, N. A.; Huryn, D. M., Validation of HDAC8 Inhibitors as Drug Discovery Starting Points to Treat Acute Kidney Injury. *ACS Pharmacol Transl Sci*. Copyright 2022 American Chemical Society

described^{226, 227}. Separate cohorts of mice underwent contralateral nephrectomy alone for comparison. Mouse numbers and survival after the surgeries are documented over time in [10.1021/acsptsci.1c00243](https://doi.org/10.1021/acsptsci.1c00243), and mice were euthanized for tissue harvesting and terminal blood draw 28 days after the initiating injury. Blood urea nitrogen (BUN) was determined in duplicate samples using a colorimetric assay kit (Infinity Urea, Thermo Scientific) at days 9, 14, 21, and 28 after IRI. Transdermal FITC-sinistrin clearance was performed to measure glomerular filtration rate (GFR) in conscious mice 28 days after the initiation injury, as described²²⁶. FITCsinistrin half-life was calculated using a 3-compartment model with linear fit using MPD Studio software (MediBeacon, Germany). All compound treatments were initiated 24 h after the initiating injury once a day for 7 days, and the investigator handling the mice and performing the assays (including histology) was blinded to treatment groups until all studies for that experiment were completed. PCI-34051 was solubilized in 10% Solutol HS, 20% PEG-400, and 70% water at pH 4.3, sonicated for 2 h at 60 °C, and administered by IP injection at 10 mg/kg and 50 mg/kg/day. All experimental protocols were approved by the Vanderbilt Institutional Animal Care and Use Committee. To assess fibrosis, kidneys were harvested, fixed, and mounted in paraffin, and Sirius red staining and quantification were performed to evaluate renal fibrosis/collagen accumulation in the outer stripe of the outer medulla, as described²²⁶. Image capture and semiquantitative evaluation were performed by an observer blinded to treatment using ImageJ software. RNA isolation and quantitative RT-PCR were performed to evaluate expression of renal fibrosis markers in snap frozen kidneys using primer sequences and RNA extraction, as previously described²²⁷. Statistical analyses were performed using GraphPad Prism V9 (San Diego, CA), using Student's one-way ANOVA for multiple between-group comparisons. The minimal level of significance is indicated from pairwise comparisons and was set at $p \leq 0.05$ for ANOVA studies. The p values shown were adjusted for multiple between group comparisons with false discovery rates of $p < 0.05$ using the two-stage step up method of Benjamini, Krieger, and Yekutieli. Two-way ANOVA used to compare changes over time for BUN time course studies.

Zinc Chelating Assay – Performed in collaboration with Paul Johnston Lab, University of Pittsburgh

To 20 μM Zn Cl_2 was added either test compounds in 6% DMSO, positive control EDTA, or null 6% DMSO. The assays were run at an 8 point 2-fold serial dilution concentrations starting at 200 μM (except EDTA curve started at 100 μM). 50 μM dithizone in 0.5% DMSO was added to initiate the reaction. Absorbance at 540 nm was recorded. Absorbance at 540 nm was compared to maximum absorbance of no test compound added and minimum absorbance of no zinc added. Assays were run in triplicate.

Mass Spectrometry HDAC 8 Inhibition Assay – Courtesy of SAMDI Tech Inc.

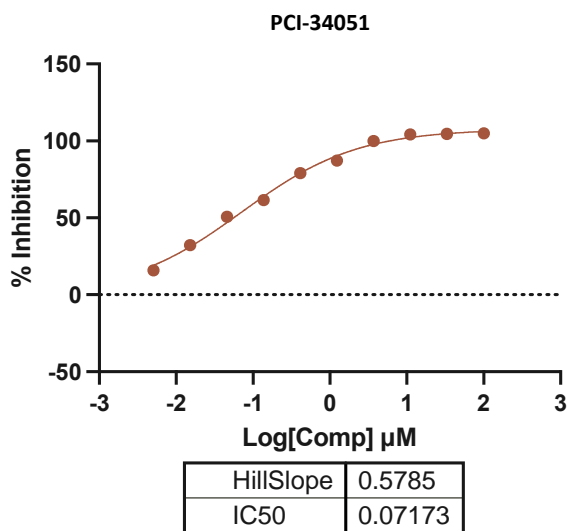
Assay performed by SAMDI Tech incorporated Chicago, Illinois. Briefly, 10 nM isolated HDAC 8 enzyme is incubated with buffer (50 mM Hepes pH 8, 137 mM NaCl, 2.7 mM KCl, 0.005% BSG, 0.002% Tween, 1 mM MgCl_2 , 1 mM DTT) and test compound, standard control (trichostatin A), or without compound for 15 minutes with a 10 point 3-fold serial dilution. 10 μM HDAC 8 substrate (Biotin-RHKK(TFA)) was added to initiate the reaction which took place over 60 minutes at room temperature. Reactions were concluded with the addition of 0.5% formic acid. "The array plates were then rinsed with deionized ultrafiltered water, ethanol, dried with nitrogen, and treated with matrix (trihydroxyacetophenone, 50 mg mL in acetone). Each plate was analyzed with an Applied Biosystems 4800 MALDI TOF/TOF

Reprinted with permission from Long, K.; Vaughn, Z.; McDaniels, M. D.; Joyasawal, S.; Przepiorski, A.; Parasky, E.; Sander, V.; Close, D.; Johnston, P. A.; Davidson, A. J.; de Caestecker, M.; Hukriede, N. A.; Huryn, D. M., Validation of HDAC8 Inhibitors as Drug Discovery Starting Points to Treat Acute Kidney Injury. *ACS Pharmacol Transl Sci*. Copyright 2022 American Chemical Society

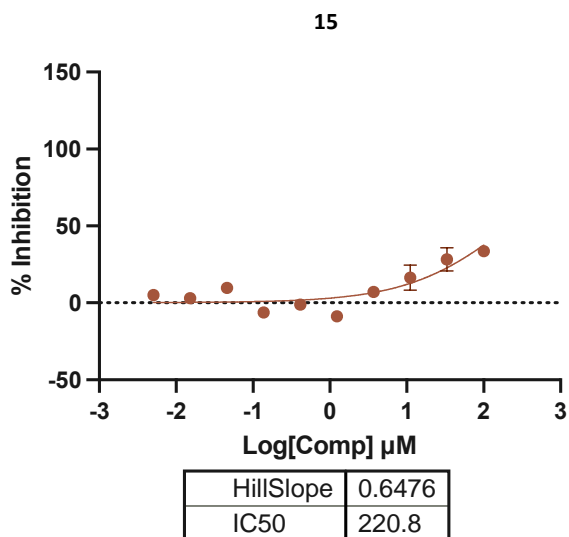
spectrometer using an automated protocol (20 kV accelerating voltage, positive reflector mode, 200 laser shots per spot)²⁰⁸. AUCs of the corresponding peaks at 1601.3 and 1559.3 were analyzed by Applied Biosystems Data Explorer Software and the difference between the AUCs were used to calculate percent inhibition and create IC₅₀ curves. Assays were performed in duplicate.

IC₅₀ Curves for Chapter 4

PCI-34051

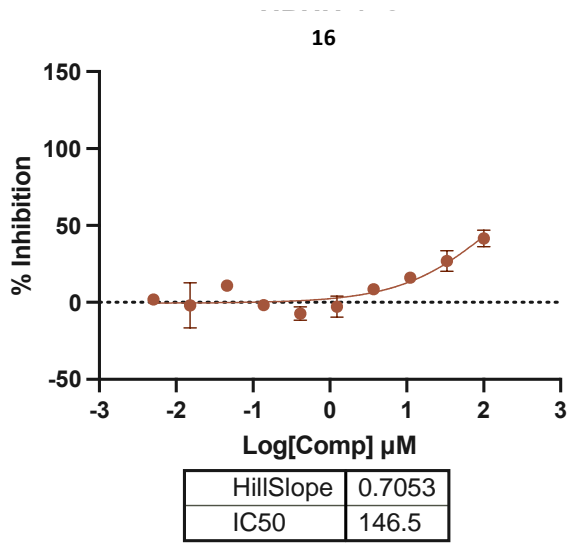


15



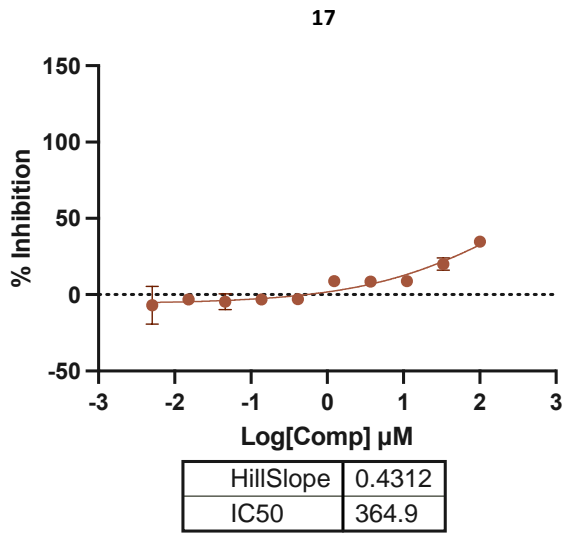
IC₅₀ extrapolated.

16



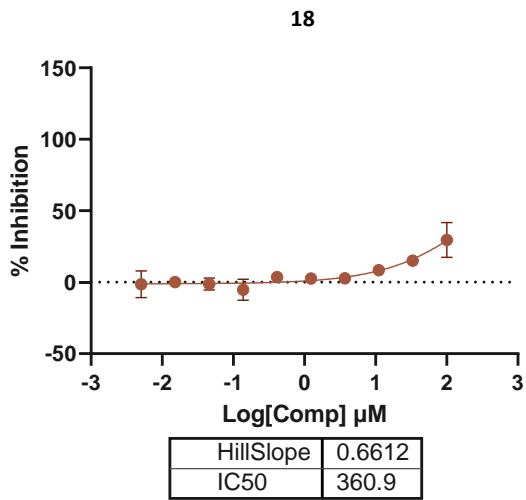
IC₅₀ extrapolated.

17



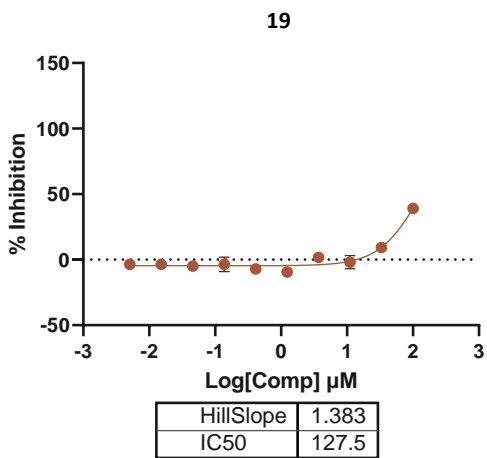
IC₅₀ extrapolated.

18



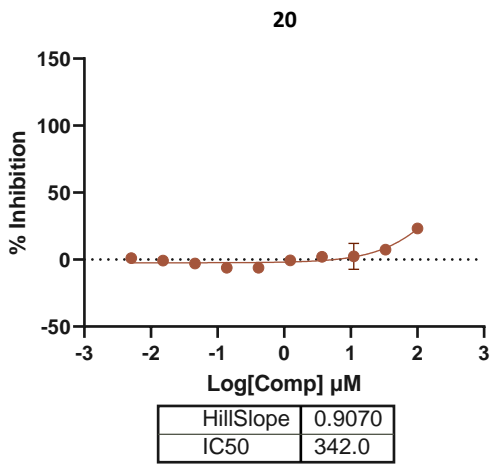
IC₅₀ extrapolated.

19



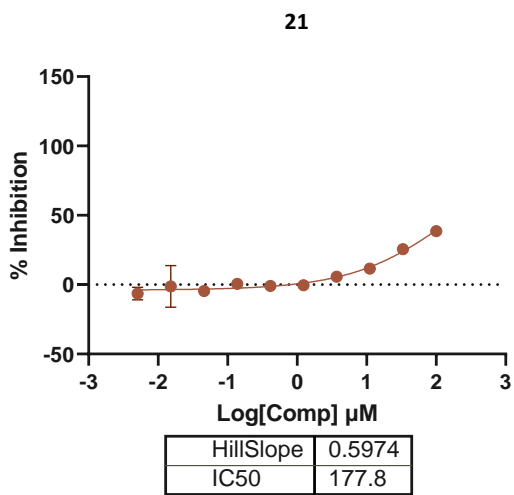
IC₅₀ extrapolated.

20



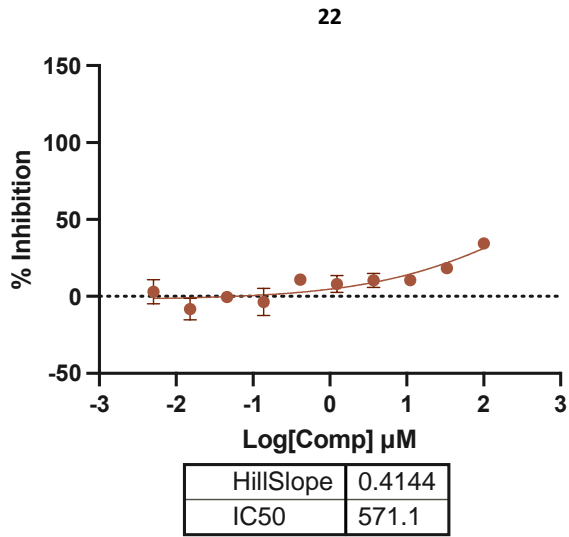
IC₅₀ extrapolated.

21



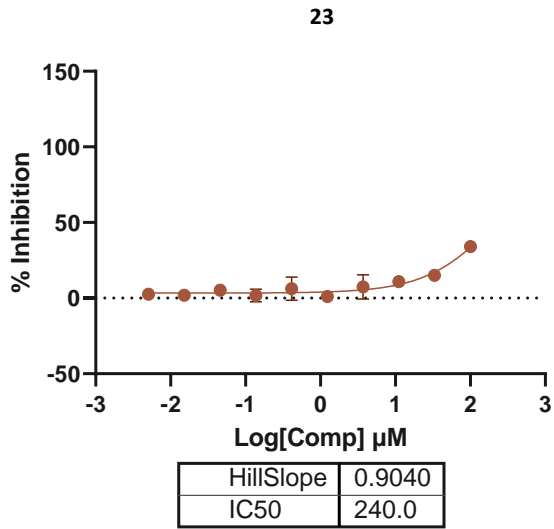
IC₅₀ extrapolated.

22



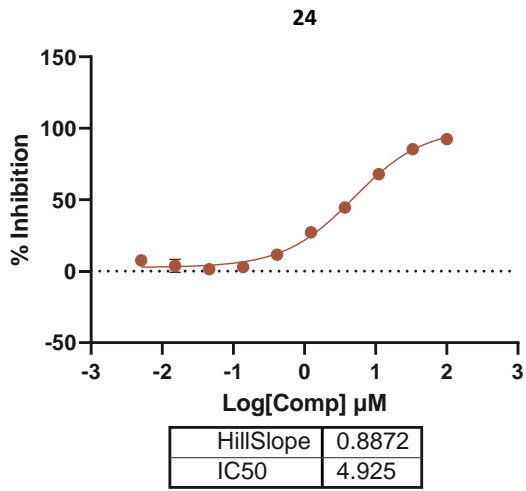
IC₅₀ extrapolated.

23

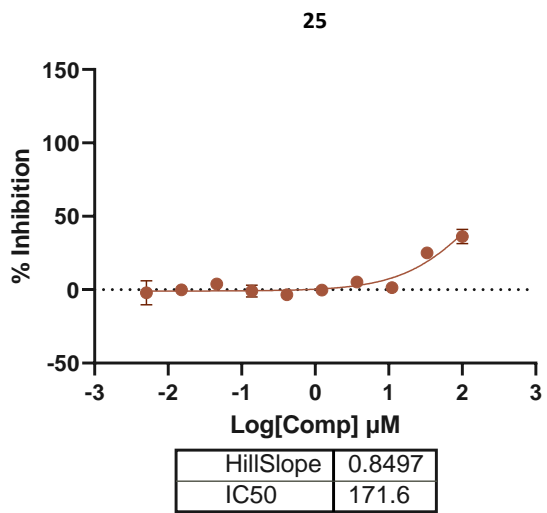


IC₅₀ extrapolated.

24

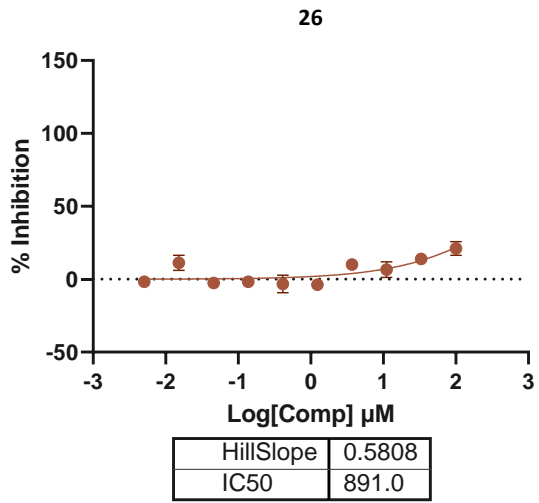


25



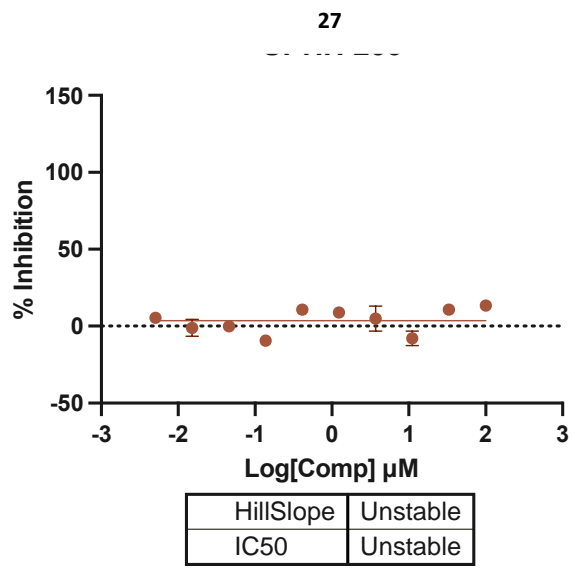
IC₅₀ extrapolated.

26

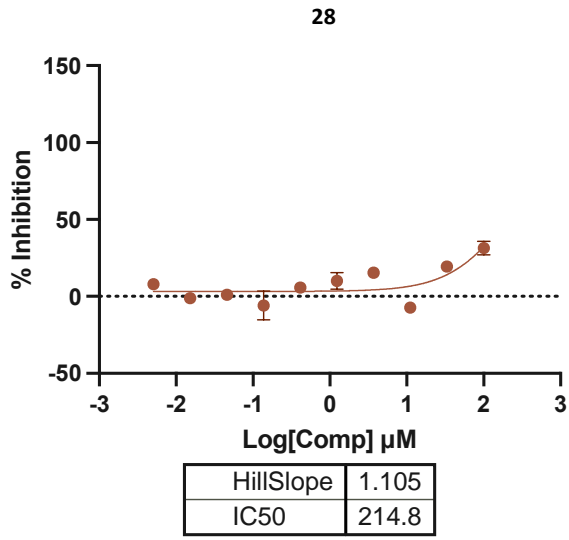


IC₅₀ extrapolated.

27

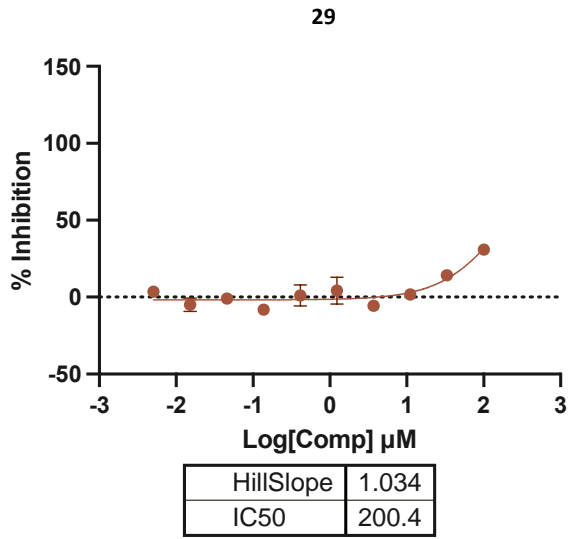


28



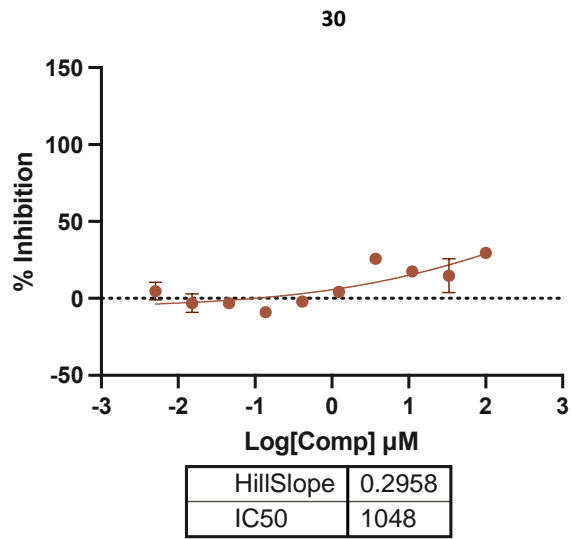
IC₅₀ extrapolated.

29



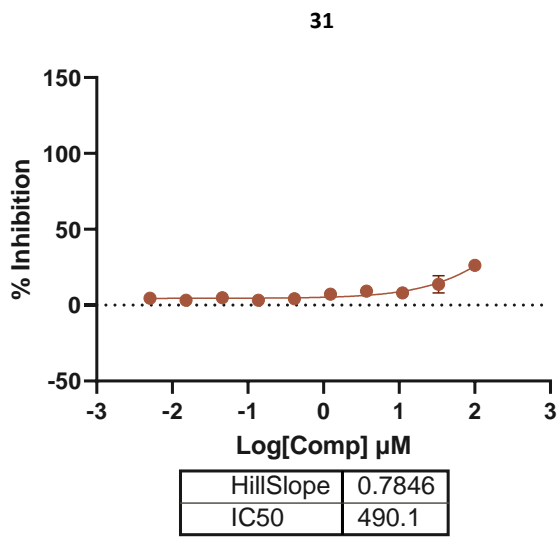
IC₅₀ extrapolated.

30



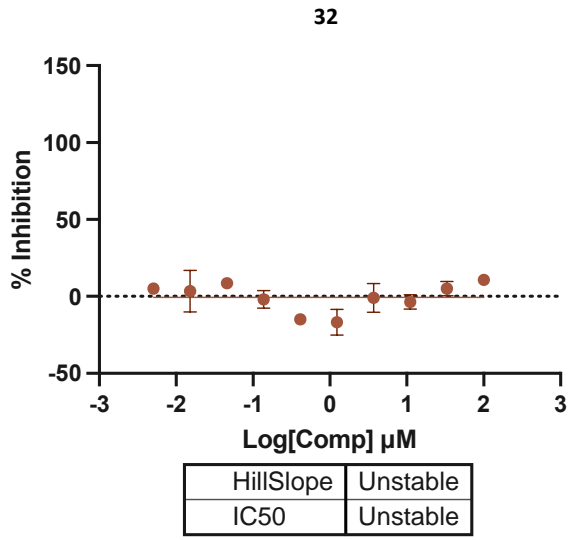
IC₅₀ extrapolated.

31

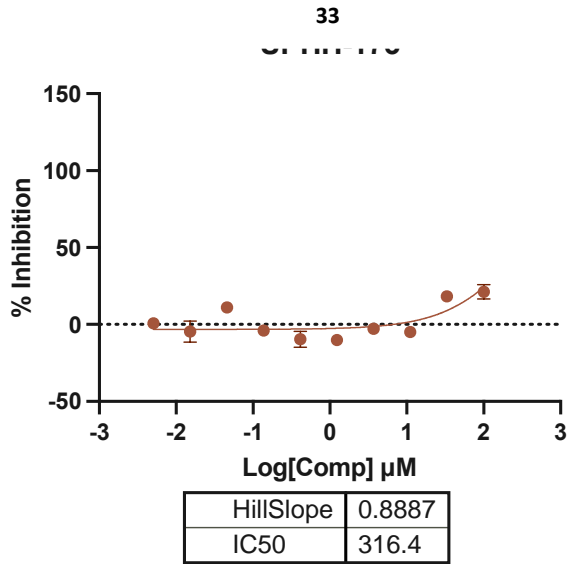


IC₅₀ extrapolated.

32

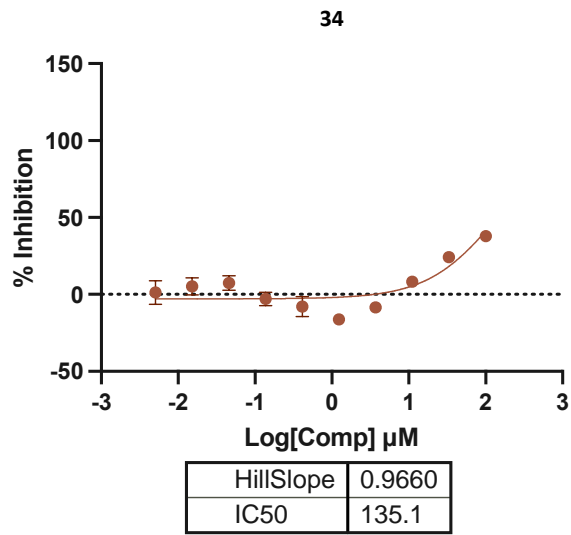


33



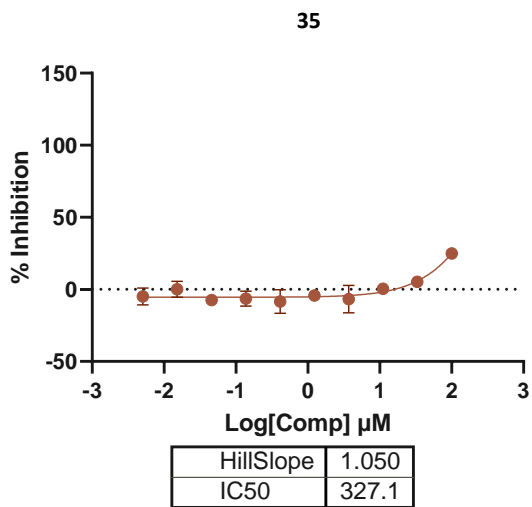
IC₅₀ extrapolated.

34



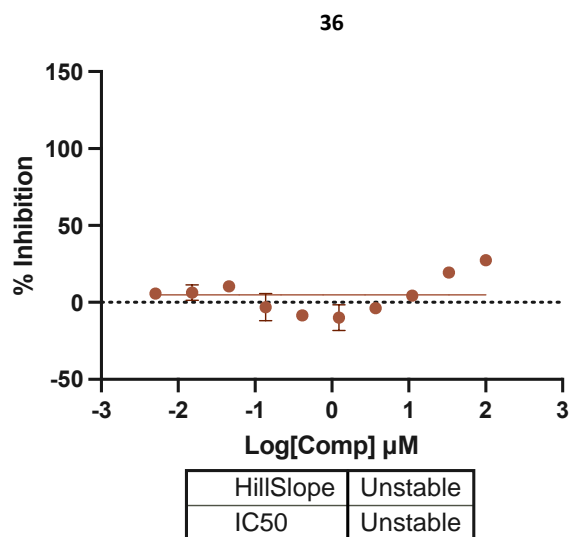
IC₅₀ extrapolated.

35

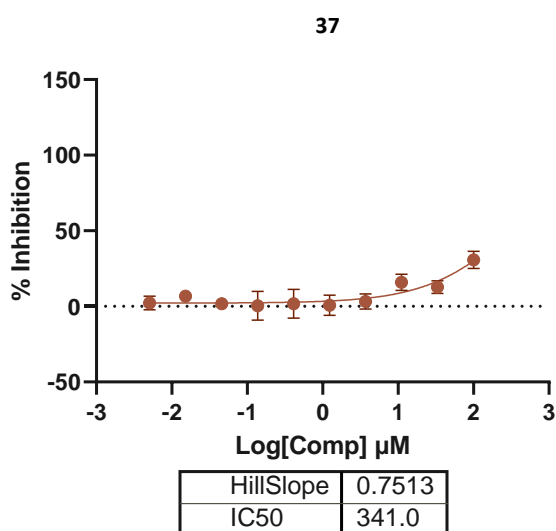


IC₅₀ extrapolated.

36



37



IC₅₀ extrapolated.

Experimental Data

General Chemistry Protocols

All air and moisture sensitive reactions were performed under a dry N₂ or Ar atmosphere. Chemicals and reagents were obtained from commercial sources and used as received. All solvents were reagent grade or HPLC grade. Reactions were monitored by thin layer chromatography using silica gel 60 F₂₅₄ plates and visualized with 254 nm UV light or iodine staining. Column chromatography was performed using the CombiFlash RF + ISCO system. ¹H and ¹³C NMR spectra of final products were recorded on a Bruker 600/150 MHz instrument using deuterated solvents. Intermediate products' NMRs were recorded on a Bruker 600/150, 400/100, or 300/75 system using deuterated solvents. ¹⁹F NMR spectra were recorded

on a Bruker 500 MHz instrument at 470 MHz. The following abbreviations designate multiplicities: s=singlet, d=doublet, t=triplet, q=quartet, m=multiplet, and br=broad. Chemical shifts (δ) are reported in ppm relative to tetramethylsilane (TMS) as the internal standard or to solvent residual peak (7.26/77.16 (CDCl₃), 2.50/39.52 (DMSO-d₆)). All assayed final compounds were >95% pure as determined by LC/MS using a Thermo Scientific Ultimate 3000 LC and TSQ Quantum Ultra MS LCMS system (Thermo Scientific Hypersil GOLD column) with UV detection using MeOH/H₂O. HPLC was conducted using a Dionex Ultimate 3000 HPLC system with UV detection using isopropanol. HRMS was conducted using Waters SYNAPT G2S HDMS Q-TOF Mass Spectrometer. Melting points were determined using a Mel-Temp instrument. SAHA, Belinostat and Panobinostat was purchased from Ambeed, and confirmed to be >95% pure based on LC-MS. Optical rotations were measured on a Jasco P-2000 Polarimeter.

PCI-34051

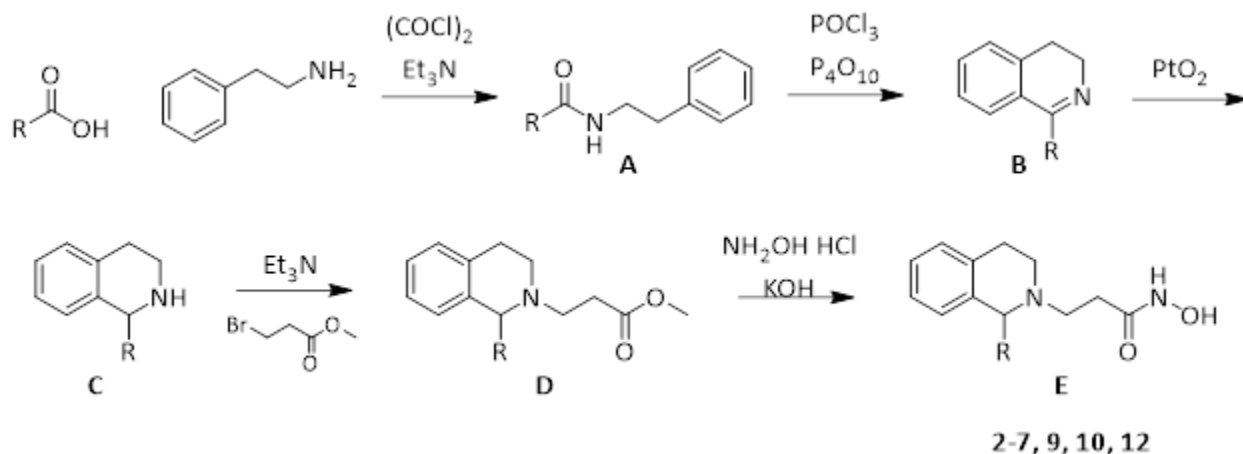
PCI-34051 was synthesized according to methods reported in patents.^{161, 162} ¹H NMR was consistent with published data. IR cm⁻¹: 627, 727, 756, 791, 815, 869, 944, 1030, 1084, 1135, 1176, 1241, 1305, 1315, 1357, 1438, 1466, 1511, 1558, 1605, 2833, 2902, 3102, 3216.

1

Compound **1** was synthesized according to methods in Whitehead et al.¹⁵⁵ ¹H NMR was consistent with published data. IR cm⁻¹: 750, 794, 811, 854, 1048, 1091, 1180, 1261, 1280, 1359, 1425, 1471, 1584, 1638, 2864, 2923.

Compounds **2-7** were resynthesized based on an adaptation of reported methods¹⁵². Spectra characterization was consistent with those reported in the literature. Novel compounds **9, 10**, and **13** were prepared using the adapted protocol.

Appendix Scheme 1 General Synthesis for THIQ analogs. Some exceptions apply and are noted in the experimental.



General Procedure A, adapted.¹⁵²

To a solution of carboxylic acid (1.0 eq.) in DCM (0.3 M with respect to carboxylic acid) in an ice bath was added DMF (0.04 eq.) and oxalyl chloride (1.5 eq.), and the mixture was stirred for 3 hours. The reaction mixture was concentrated under reduced pressure and used without further purification. The crude acyl chloride in DCM (0.3 M with respect to acyl chloride) in an ice bath was treated with phenylethylamine

(1.0 eq.) and triethylamine (1.5 eq.). The reaction was warmed up to room temperature and stirred overnight. Upon disappearance of starting material based on TLC, the reaction was diluted with DCM and the organic layer was washed with 1N aqueous HCl (5.0 mL), saturated NaHCO₃ solution (10 mL), and brine (10 mL). The organic phase was dried over Na₂SO₄, filtered, and concentrated under reduced pressure to provide amide A.

General Procedure B, adapted.¹⁵²

To a solution of A (1.0 eq.) in xylenes (0.1 M with respect to amide) was added phosphorus oxychloride (5.0 eq.) and phosphorus pentoxide (4.0 eq.). The mixture was refluxed at 160 °C for 6 hours, at which time TLC indicated consumption of starting material. The liquid was separated, and the remaining solids were basified to pH of ~12 with 20% aqueous KOH, then combined with the liquid. The aqueous phase was extracted with ethyl acetate (2 x 100 mL) and the organic phase was dried over Na₂SO₄ and filtered. The crude product was purified using silica column chromatography (0-30% ethyl acetate in hexanes) to give dihydroisoquinoline B.

General Procedure C, adapted.¹⁵²

A solution of dihydroisoquinoline B (1.0 eq.) in ethanol (0.1 M with respect to dihydroisoquinoline) was degassed with argon. Platinum(IV) oxide (0.05 eq.) was added to the solution. The reaction was stirred overnight under H₂ atmosphere (balloon), at which time TLC showed the disappearance of starting material. The solution was filtered through Celite and concentrated under reduced pressure to give tetrahydroisoquinoline C.

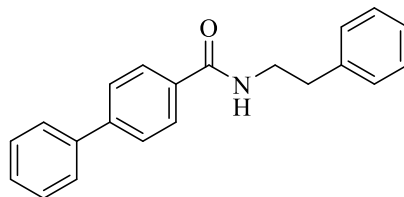
General Procedure D, adapted.¹⁵²

To a solution of tetrahydroisoquinoline C (1.0 eq.) in acetonitrile (0.1 M with respect to tetrahydroisoquinoline) under a N₂ atmosphere was added methyl 3-bromopropionate (4.0 eq.) dropwise. Triethylamine (4.0 eq.) was added dropwise to the solution and the reaction stirred at room temperature for 3 days, while monitoring by TLC. The reaction was diluted with water, and the aqueous phase was extracted with ethyl acetate (2 x 25 mL). The organic phase was dried over Na₂SO₄, filtered, and concentrated under reduced pressure. The crude product was purified using silica gel column chromatography (0-30% ethyl acetate in hexanes) to give tetrahydroisoquinoline methyl ester D.

General Procedure E, adapted.¹⁵²

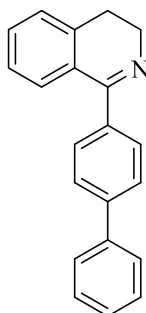
To a solution of hydroxylamine hydrochloride in methanol (0.6 M with respect to hydroxylamine) in an ice bath was added KOH (25 eq.). The mixture was stirred in an ice bath for 1 hour. The hydroxylamine solution was filtered and added to a solution of tetrahydroisoquinoline methyl ester (1.0 eq.) in methanol (0.06 M with respect to ester) in an ice bath under nitrogen. KOH (10 eq.) was added to the

mixture and the reaction was removed from the ice bath and stirred overnight at room temperature. The reaction mixture was neutralized to pH 7 with 1 N HCl. The mixture was diluted with water, and the aqueous phase was extracted with ethyl acetate (2 x 25 mL). The organic phase was dried over Na₂SO₄, filtered, and concentrated under reduced pressure. The crude product was purified with silica column chromatography (0-10% methanol in DCM) to give tetrahydroisoquinoline hydroxamic acid.



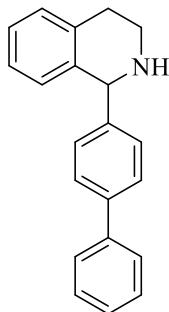
Preparation of *N*-phenethyl-[1,1'-biphenyl]-4-carboxamide (2A):

Prepared according to General Procedure A using [1,1'-biphenyl]-4-carboxylic acid (2.0 g, 10.09 mmol) to afford 3.0 g of *N*-phenethyl-[1,1'-biphenyl]-4-carboxamide (98%) as an off-white solid. ¹H NMR (600 MHz, CDCl₃) δ 7.76 (d, *J* = 8.4 Hz, 2H), 7.63 (d, *J* = 8.4 Hz, 2H), 7.61-7.59 (m, 2H), 7.46 (t, *J* = 7.6, 2H), 7.40-7.37 (m, 2H), 7.35 (t, *J* = 7.5 Hz, 2H), 7.27 (s, 2H), 6.15 (bs, 1H), 3.75 (q, *J* = 6.6 Hz, 2H), 2.96 (t, *J* = 6.9 Hz, 2H) ppm.



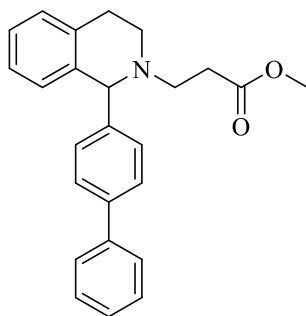
Preparation of 1-([1,1'-biphenyl]-4-yl)-3,4-dihydroisoquinoline (2B):

Prepared according to General Procedure B using *N*-phenethyl-[1,1'-biphenyl]-4-carboxamide (3.0 g, 9.96 mmol) to afford 2.06 g of 1-([1,1'-biphenyl]-4-yl)-3,4-dihydroisoquinoline (73%) as a brown solid. ¹H NMR (600 MHz, CDCl₃) δ 7.69 (d, *J* = 6.4 Hz, 2H), 7.65 (t, *J* = 6.5 Hz, 4H), 7.46 (t, *J* = 6.7 Hz, 2H), 7.41-7.35 (m, 3H), 7.28 (bs, 2H), 3.87 (t, *J* = 6.2 Hz, 2H), 2.82 (t, *J* = 6.5 Hz, 2H) ppm.



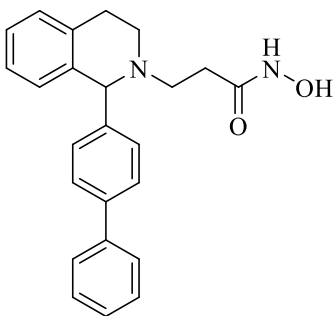
Preparation of 1-([1,1'-biphenyl]-4-yl)-1,2,3,4-tetrahydroisoquinoline (2C):

Prepared according to General Procedure C using 1-([1,1'-biphenyl]-4-yl)-3,4-dihydroisoquinoline (2.0 g, 7.06 mmol) to afford 1.98 g of 1-([1,1'-biphenyl]-4-yl)-1,2,3,4-tetrahydroisoquinoline (98%) as an off-white solid. $^1\text{H NMR}$ (400 MHz, CDCl_3) δ 7.60-7.54 (m, 4H), 7.43 (t, $J = 7.3$, 2H), 7.34 (d, $J = 8.1$ Hz, 3H), 7.16 (d, $J = 3.8$, 2H), 7.08-7.04 (m, 1H), 6.82 (d, $J = 8.0$ Hz, 1H), 5.16 (s, 1H), 3.32-3.28 (m, 1H), 3.16-3.03 (m, 2H), 2.88-2.82 (m, 1H) ppm.



Preparation of Methyl 3-(1-([1,1'-biphenyl]-4-yl)-3,4-dihydroisoquinolin-2(1H)-yl)propanoate (2D):

Prepared according to General Procedure D using 1-([1,1'-biphenyl]-4-yl)-1,2,3,4-tetrahydroisoquinoline (1.15 g, 4.03 mmol) to afford 240 mg of methyl 3-(1-([1,1'-biphenyl]-4-yl)-3,4-dihydroisoquinolin-2(1H)-yl)propanoate (16%) after 24 hours as a white solid. $^1\text{H NMR}$ (CDCl_3 , 600 MHz) δ 7.59 (d, $J = 7.8$ Hz, 2H), 7.52 (d, $J = 6.0$ Hz, 2H), 7.43 (t, $J = 7.92$ Hz, 2H), 7.33-7.30 (m, 3H), 7.13-7.08 (m, 2H), 7.02 (t, $J = 7.3$ Hz, 1H), 6.76 (d, $J = 7.8$ Hz, 1H), 4.65 (s, 1H), 3.61 (s, 3H), 3.22-3.18 (m, 1H), 3.13-3.08 (m, 1H), 2.97-2.93 (m, 1H), 2.89-2.84 (m, 1H), 2.73-2.65 (m, 2H), 2.51 (t, $J = 6.0$ Hz, 2H) ppm.

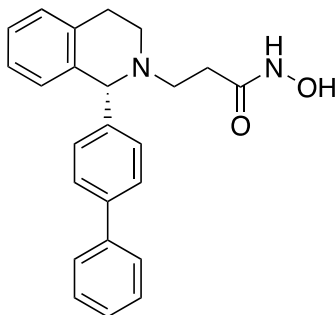


Preparation of 3-(1-([1,1'-biphenyl]-4-yl)-3,4-dihydroisoquinolin-2(1H)-yl)-N-hydroxypropanamide ([rac]-2):

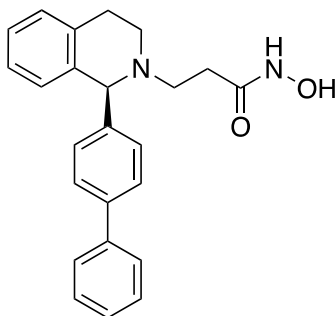
Prepared according to General Procedure E using Methyl 3-(1-([1,1'-biphenyl]-4-yl)-3,4-dihydroisoquinolin-2(1H)-yl)propanoate (40.0 mg, 0.108 mmol) to afford 25.0 mg of 3-(1-([1,1'-biphenyl]-4-yl)-3,4-dihydroisoquinolin-2(1H)-yl)-*N*-hydroxypropanamide (62%) as a white solid. Melting Point 78 – 90°C. ¹H NMR (600 MHz, CDCl₃) δ 10.93 (bs, 1H), 7.57 (appt, *J* = 8.9 Hz, 5H), 7.43 (t, *J* = 7.5 Hz, 2H + CHCl₃), 7.34 (t, *J* = 7.3 Hz, 1H), 7.24 (s, 1H + CHCl₃), 7.18 (bs, 2H + CHCl₃), 7.07 (d, *J* = 7.6 Hz, 1H + CHCl₃), 6.75 (d, *J* = 7.8 Hz, 1H), 4.65 (s, 1H), 3.28-3.32 (m, 1H), 3.12-3.17 (m, 1H), 2.95-2.98 (m, 1H), 2.88-2.93 (m, 1H), 2.61-2.68 (m, 2H), 2.55-2.58 (m, 1H), 2.36-2.39 (m, 1H); ¹³C NMR (150 MHz, DMSO-*d*₆) δ 168.0, 143.1, 139.9, 138.8, 138.0, 134.4, 129.8, 128.9, 128.4, 128.4, 127.3, 126.6, 126.4, 125.8, 125.5, 66.1, 50.1, 46.1, 29.9, 28.4 ppm. *m/z* calculated for C₂₄H₂₄N₂O₂ [M+H]⁺ 373.19, found 373.20. IR cm⁻¹: 695, 737, 760, 829, 1007, 1074, 1123, 1295, 1339, 1354, 1369, 1405, 1427, 1450, 1485, 1515, 1645, 2834, 2901, 3024, 3059, 3185.

Preparation of *R* and *S*-3-(1-([1,1'-biphenyl]-4-yl)-3,4-dihydroisoquinolin-2(1H)-yl)-*N*-hydroxypropanamide (+) – 2 and (-) – 2:

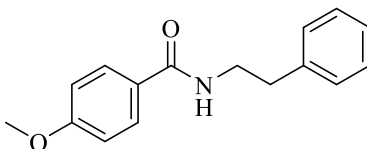
[rac] – 2 was separated on a Phenomenex Lux 5 μm Amylose-1 (250 x 10 mm) column using isocratic *i*-PrOH as eluant. The first eluting peak (RT= 6.5 min) corresponded to the (-) enantiomer. The second eluting peak (RT = 8.0 min) corresponded to the (+) – enantiomer. **Stereochemistry drawn is arbitrarily assigned.**



(-)-3-(1-([1,1'-biphenyl]-4-yl)-3,4-dihydroisoquinolin-2(1H)-yl)-*N*-hydroxypropanamide (-) – 2: ¹H NMR (600 MHz, CDCl₃) δ 10.91 (bs, 1H), 7.57 (appdd, *J* = 8.0 Hz, 1.6 Hz, 5H), 7.43 (t, *J* = 7.5 Hz, 2H + CHCl₃), 7.34 (t, *J* = 7.3 Hz, 1H), 7.24 (d, *J* = 7.9 Hz, 1H + CHCl₃), 7.18 (d, *J* = 5.5 Hz, 2H), 7.07 (appdd, *J* = 8.3 Hz, 5.6 Hz, 1H), 6.75 (d, *J* = 7.8 Hz, 1H), 4.65 (s, 1H), 3.27-3.30 (m, 1H), 3.21-3.18 (m, 1H), 2.95-2.98 (m, 1H), 2.88-2.91 (m, 1H), 2.61-2.66 (m, 2H), 2.55-2.58 (m, 1H), 2.34-2.37 (m, 1H). RT= 6.5 min (Phenomenex Lux 5 μm Amylose-1; *i*-PrOH). [α]_D = -64.7 (c = 0.50, MeOH).

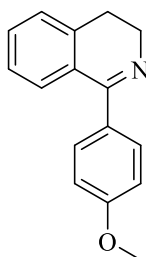


(+)-3-(1-([1,1'-biphenyl]-4-yl)-3,4-dihydroisoquinolin-2(1H)-yl)-*N*-hydroxypropanamide (+) – 2: ¹H NMR (600 MHz, CDCl₃) δ 7.57 (q, *J* = 6.1 Hz, 5H), 7.43 (t, *J* = 7.5 Hz, 2H + CHCl₃), 7.34 (t, *J* = 7.3 Hz, 1H), 7.24 (d, *J* = 7.9 Hz, 1H + CHCl₃), 7.18 (appdd, *J* = 8.3 Hz, 1.3 Hz, 2H), 7.07 (appdd, *J* = 2.5 Hz, 5.6 Hz, 1H), 6.75 (d, *J* = 7.8 Hz, 1H), 4.65 (s, 1H), 3.27-3.31 (m, 1H), 3.11-3.16 (m, 1H), 2.94-2.98 (m, 1H), 2.87-2.92 (m, 1H), 2.61-2.66 (m, 2H), 2.54-2.58 (m, 1H), 2.33-2.38 (m, 1H). RT= 8.0 min (Phenomenex Lux 5 μm Amylose-1; *i*-PrOH). [α]_D = +62.2 (c = 0.48, MeOH).



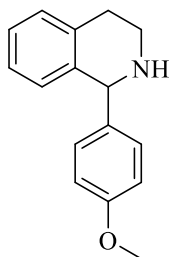
Preparation of 4-methoxy-*N*-phenethylbenzamide (3A):

Prepared according to General Procedure A using 4-methoxybenzoic acid (2.0 g, 13.14 mmol) to afford 3.3 g of 4-methoxy-*N*-phenethylbenzamide (98%) as a white solid. ¹H NMR (600 MHz, CDCl₃) δ 7.65 (d, *J* = 8.8 Hz, 2H), 7.33 (t, *J* = 7.5 Hz, 2H), 2.74 (d, *J* = 7.0 Hz, 3H) 6.90 (d, *J* = 8.8 Hz, 2H), 6.02 (bs, 1H), 3.84 (s, 3H), 3.71 (q, *J* = 6.6 Hz, 2H), 2.93 (t, *J* = 6.9 Hz, 2H) ppm.



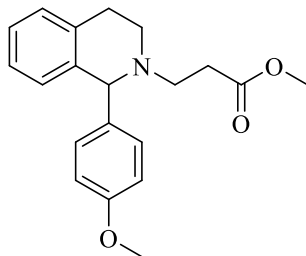
Preparation of 1-(4-methoxyphenyl)-3,4-dihydroisoquinoline (3B):

Prepared according to General Procedure B using 4-methoxy-*N*-phenethylbenzamide (3.3 g, 12.93 mmol) to afford 2.3 g of 1-(4-methoxyphenyl)-3,4-dihydroisoquinoline (75%) as an orange oil. ¹H NMR (600 MHz, CDCl₃) δ 7.57 (d, *J* = 8.7 Hz, 2H), 7.40-7.37 (m, 1H), 7.32-7.30 (m, 3H), 6.95 (d, *J* = 8.8 Hz, 2H), 3.86 (s, 3H), 3.82-3.80 (m, 2H), 2.79 (t, *J* = 7.3 Hz, 2H) ppm.



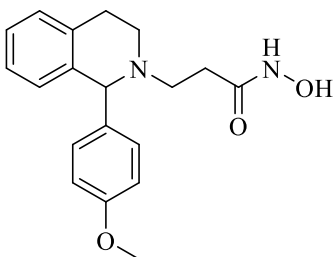
Preparation of 1-(4-methoxyphenyl)-1,2,3,4-tetrahydroisoquinoline (3C):

Prepared according to General Procedure C using 1-(4-methoxyphenyl)-3,4-dihydroisoquinoline (2.0 g, 8.43 mmol) to afford 2.0 g of 1-(4-methoxyphenyl)-1,2,3,4-tetrahydroisoquinoline (99%) as an off-white solid. ¹H NMR (600 MHz, CDCl₃) δ 7.18 (d, *J* = 8.6 Hz, 2H), 7.14 (d, *J* = 3.8 Hz, 2H), 7.05-7.02 (m, 1H), 6.85 (d, *J* = 8.7 Hz, 2H), 6.76 (d, *J* = 7.6 Hz, 1H), 5.06 (s, 1H), 3.80 (s, 3H), 3.29-3.25 (m, 1H), 3.11-3.07 (m, 1H), 3.06-3.01 (m, 1H), 2.84-2.80 (m, 1H) ppm.



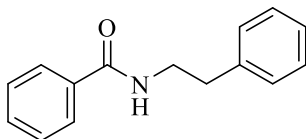
Preparation of Methyl 3-(1-(4-methoxyphenyl)-3,4-dihydroisoquinolin-2(1H)-yl)propanoate (3D):

Prepared according to General Procedure D using 1-(4-methoxyphenyl)-1,2,3,4-tetrahydroisoquinoline (325 mg, 1.36 mmol) to afford 310 mg of methyl 3-(1-(4-methoxyphenyl)-3,4-dihydroisoquinolin-2(1H)-yl)propanoate (70%) as an amber solid. ^1H NMR (600 MHz, CDCl_3) δ 7.15 (d, $J = 8.7$ Hz, 2H), 7.11-7.07 (m, 2H), 7.00-6.98 (m, 1H), 6.83 (d, $J = 8.7$ Hz, 2H), 6.70 (d, $J = 7.8$ Hz, 1H), 4.54 (s, 1H), 3.80 (s, 3H), 3.61 (s, 3H), 3.18-3.14 (m, 1H), 3.10-3.05 (m, 1H), 2.93-2.88 (m, 1H), 2.85-2.81 (m, 1H), 2.67-2.62 (m, 2H), 2.49-2.46 (m, 2H) ppm.



Preparation of N-hydroxy-3-(1-(4-methoxyphenyl)-3,4-dihydroisoquinolin-2(1H)-yl)propanamide (3):

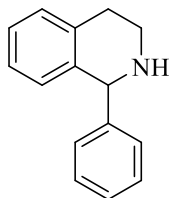
Prepared according to General Procedure E using methyl 3-(1-(4-methoxyphenyl)-3,4-dihydroisoquinolin-2(1H)-yl)propanoate (40 mg, 0.123 mmol) to afford 27.0 mg of N-hydroxy-3-(1-(4-methoxyphenyl)-3,4-dihydroisoquinolin-2(1H)-yl)propanamide (67%) as a white solid. Melting Point: 58 – 68 °C. ^1H NMR (600 MHz, DMSO-d_6) δ 10.36 (bs, 1H), 8.67 (bs, 1H), 7.12 (t, $J = 8.2$ Hz 3H), 7.07 (t, $J = 7.4$ Hz, 1H) 6.98 (t, $J = 7.3$ Hz 1H), 6.86 (d, $J = 8.5$ Hz, 2H), 6.61 (d, $J = 7.7$ Hz, 1H), 4.57 (s, 1H), 3.73 (s, 3H), 3.06-3.03 (m, 1H), 2.98-2.93 (m, 1H), 2.81-2.78 (m, 1H), 2.66-2.62 (m, 1H), 2.58-2.56 (m, 1H), 2.22-2.18 (m, 1H), 2.09-2.04 (m, 1H). ^{13}C NMR (150 MHz, CDCl_3) δ 169.1, 159.2, 137.4, 134.2, 133.9, 130.8, 129.0, 128.4, 126.5, 126.1, 114.0, 68.5, 55.3, 48.8, 45.7, 30.0, 28.3 ppm. m/z calculated for $\text{C}_{19}\text{H}_{22}\text{N}_2\text{O}_3$ $[\text{M}+\text{H}]^+$ 327.17, found 327.19. IR cm^{-1} : 741, 787, 825, 940, 1031, 1074, 1172, 1246, 1302, 1371, 1452, 1508, 1608, 1643, 2834, 2918, 3171.



Preparation of N-phenethylbenzamide (4A):

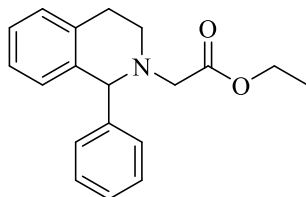
Prepared according to General Procedure A using benzoic acid (500 mg, 4.10 mmol) to afford 610 mg of N-phenethylbenzamide (66%) as an off-white solid. ^1H NMR (400 MHz, CDCl_3) δ 7.70-7.67 (m, 2H), 7.50-

7.46 (m, 1H), 7.43-7.39 (m, 2H), 7.34 (t, $J = 7.3$ Hz, 2H), 7.25 (t, $J = 6.1$ Hz, 3H), 6.09 (bs, 1H), 3.73 (q, $J = 6.6$ Hz, 2H), 2.95 (t, $J = 6.8$ Hz, 2H) ppm.



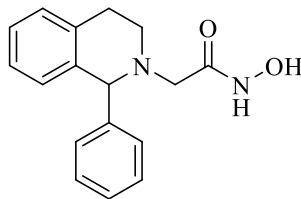
Preparation of 1-phenyl-1,2,3,4-tetrahydroisoquinoline (4C):

To a solution of *N*-phenethylbenzamide (500 mg, 2.22 mmol) in xylenes (25 mL) was added phosphorus oxychloride (1.0 mL, 11.1 mmol) and phosphorus pentoxide (2.52 g, 8.88 mmol). The mixture was refluxed at 160 °C for 6 hours. The liquid mixture was transferred to a large collecting flask, and the left-over solid material was basified with 20% aqueous KOH solution and added to the liquid mixture. The aqueous phase was extracted twice with ethyl acetate (100 mL) and the organic phase was dried over Na₂SO₄, filtered, and concentrated under reduced pressure. The crude mixture was taken into ethanol (35 mL) and degassed under nitrogen. Platinum(IV) oxide (42 mg, 0.19 mmol) was added to the solution. The reaction was stirred overnight under hydrogen atmosphere. The solution was filtered through Celite and concentrated under reduced pressure, and the crude product was purified with silica column chromatography (0-100% ethyl acetate in hexanes) to give 257 mg of 1-phenyl-1,2,3,4-tetrahydroisoquinoline (55%) as a white solid. ¹H NMR (400 MHz, CDCl₃) δ 7.33-7.27 (m, 5H), 7.14 (d, $J = 3.8$ Hz, 2H), 7.06-7.01 (m, 1H), 6.75 (d, $J = 7.9$ Hz, 1H), 5.11 (s, 1H), 3.31-3.26 (m, 1H), 3.13-3.03 (m, 2H), 2.85-2.80 (m, 1H) ppm.



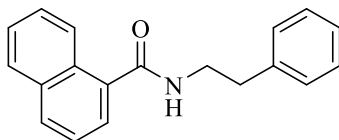
Preparation of Ethyl 2-(1-phenyl-3,4-dihydroisoquinolin-2(1H)-yl)acetate (4D):

To a solution of 1-phenyl-1,2,3,4-tetrahydroisoquinoline (200 mg, 0.97 mmol) in acetonitrile (10 mL) under nitrogen gas was added ethyl bromoacetate (420 μL, 3.80 mmol) dropwise. Triethylamine (530 μL, 3.82 mmol) was added dropwise to the solution and the reaction stirred at room temperature overnight. The reaction was diluted with water (20 mL), and the aqueous phase was extracted twice with ethyl acetate (25 mL). The organic phase was dried over Na₂SO₄, filtered, and concentrated under reduced pressure. The crude product was purified with silica column chromatography (0-30% ethyl acetate in hexanes) to give 250 mg of ethyl 2-(1-phenyl-3,4-dihydroisoquinolin-2(1H)-yl)acetate (87%) as a viscous yellow oil. ¹H NMR (600 MHz, CDCl₃) δ 7.30-7.27 (m, 5H), 7.13-7.08 (m, 2H), 6.99 (t, $J = 7.3$ Hz, 1H), 6.68 (d, $J = 7.8$ Hz, 1H), 4.96 (s, 1H), 4.17-4.10 (m, 2H), 3.33 (d, $J = 16.9$ Hz, 1H), 3.23 (d, $J = 16.9$ Hz, 1H), 3.20-3.17 (m, 2H), 3.07-3.03 (m, 1H), 2.86-2.83 (m, 1H), 1.26-1.24 (t, $J = 7.1$ Hz, 3H) ppm.



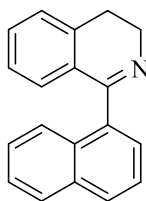
Preparation of *N*-hydroxy-2-(1-phenyl-3,4-dihydroisoquinolin-2(1H)-yl)acetamide (4):

Prepared according to General Procedure E using ethyl 2-(1-phenyl-3,4-dihydroisoquinolin-2(1H)-yl)acetate (100 mg, 0.338 mmol) to afford 70 mg of *N*-hydroxy-2-(1-phenyl-3,4-dihydroisoquinolin-2(1H)-yl)acetamide (70%) as a white solid. Melting Point: 136 – 138 °C. ¹H NMR (600 MHz, DMSO-_{d6}) δ 10.34 (bs, 1H), 8.75 (bs, 1H), 7.35-7.30 (m, 4H), 7.26 (t, *J* = 6.9 Hz, 1H), 7.13 (d, *J* = 7.5 Hz, 1H), 7.08 (t, *J* = 7.4 Hz, 1H), 6.99 (t, *J* = 7.3 Hz, 1H), 6.60 (d, *J* = 7.7 Hz, 1H), 4.75 (s, 1H), 3.19-3.14 (m, 1H), 3.05-3.02 (m, 1H), 2.95 (d, *J* = 15.3 Hz, 1H), 2.86 (d, *J* = 15.3 Hz, 1H), 2.79-2.70 (m, 2H). ¹³C NMR (150 MHz, DMSO-_{d6}) δ 166.3, 143.5, 137.9, 134.2, 129.4, 128.3, 128.3, 128.1, 127.2, 125.7, 125.5, 66.7, 55.5, 48.1, 28.6 ppm. *m/z* calculated for C₁₇H₁₈N₂O₂ [M+H]⁺ 283.14, found 283.14. IR cm⁻¹: 635, 701, 742, 991, 1017, 1093, 1143, 1283, 1303, 1456, 1487, 1523, 1629, 2842, 2917, 3147, 3304, 3334.



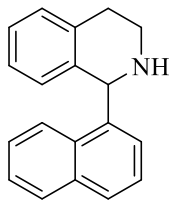
Preparation of *N*-phenethyl-1-naphthamide (5A):

Prepared according to General Procedure A using 1-naphthoic acid (500 mg, 2.90 mmol) to afford 702 mg of *N*-phenethyl-1-naphthamide (88%) as a pale-yellow solid. ¹H NMR (600 MHz, CDCl₃) δ 8.20-8.19 (m, 1H), 7.89 (d, *J* = 8.2 Hz, 1H), 7.85-7.84 (m, 1H), 7.52-7.49 (m, 3H), 7.42 (t, *J* = 7.6 Hz, 1H), 7.33 (t, *J* = 7.5 Hz, 2H), 7.28 (d, *J* = 7.1 Hz, 3H), 5.96 (bs, 1H), 3.84 (q, *J* = 6.5 Hz, 2H), 3.01 (t, *J* = 6.8 Hz, 2H) ppm.



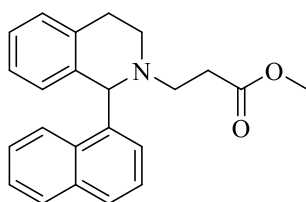
Preparation of 1-(naphthalen-1-yl)-3,4-dihydroisoquinoline (5B):

Prepared according to General Procedure B using *N*-phenethyl-1-naphthamide (600 mg, 2.18 mmol) to afford 430 mg of 1-(naphthalen-1-yl)-3,4-dihydroisoquinoline (77%) as an amber solid. ¹H NMR (600 MHz, CDCl₃) δ 7.92-7.91 (m, 1H), 7.89 (d, *J* = 3.1 Hz, 1H), 7.71 (d, *J* = 8.5 Hz, 1H), 7.54-7.52 (m, 2H), 7.46 (t, *J* = 7.2 Hz, 1H), 7.36 (q, *J* = 5.3 Hz, 2H), 7.30 (d, *J* = 7.7 Hz, 1H), 7.08 (t, *J* = 7.4 Hz, 1H), 6.85 (d, *J* = 7.7 Hz, 1H), 4.03 (bs, 2H), 2.97 (t, *J* = 7.3 Hz, 2H) ppm.



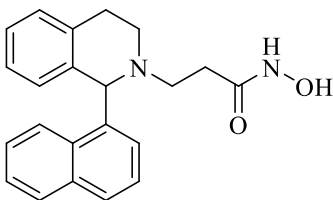
Preparation of 1-(naphthalen-1-yl)-1,2,3,4-tetrahydroisoquinoline (5C):

Prepared according to General Procedure C using 1-(naphthalen-1-yl)-3,4-dihydroisoquinoline (430 mg, 1.67 mmol) to afford 428 mg of 1-(naphthalen-1-yl)-1,2,3,4-tetrahydroisoquinoline (99%) as a viscous amber oil. ^1H NMR (600 MHz, CDCl_3) δ 8.24-8.23 (m, 1H), 7.89-7.87 (m, 1H), 7.79 (d, $J = 8.2$ Hz, 1H), 7.48-7.47 (m, 2H), 7.38 (t, $J = 7.7$ Hz, 1H), 7.21 (t, $J = 6.3$ Hz, 2H), 7.17 (t, $J = 7.4$ Hz, 1H), 7.01 (t, $J = 7.3$ Hz, 1H), 6.77 (d, $J = 7.7$ Hz, 1H), 5.87 (s, 1H), 3.29-3.26 (m, 1H), 3.17-3.08 (m, 2H), 2.96-2.91 (m, 1H) ppm.



Preparation of Methyl 3-(1-(naphthalen-1-yl)-3,4-dihydroisoquinolin-2(1H)-yl)propanoate (5D):

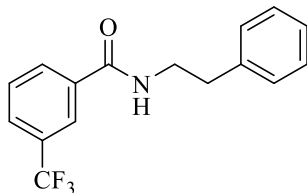
Prepared according to General Procedure D using 1-(naphthalen-1-yl)-1,2,3,4-tetrahydroisoquinoline (425 mg, 1.64 mmol) to afford 112 mg of methyl 3-(1-(naphthalen-1-yl)-3,4-dihydroisoquinolin-2(1H)-yl)propanoate (20%) after 1 day as a dark brown viscous oil. ^1H NMR (600 MHz, CDCl_3) δ 8.26 (d, $J = 8.6$ Hz, 1H) 7.82-7.79 (m, 2H), 7.43-7.39 (m, 3H) 7.32 (s, 1H), 7.15 (d, $J = 7.6$ Hz, 1H), 7.07 (t, $J = 7.5$ Hz, 1H), 6.87 (t, $J = 7.5$ Hz, 1H), 6.59 (d, $J = 7.8$ Hz, 1H), 5.10 (s, 1H), 3.34 (s, 3H), 3.33-3.27 (m, 2H), 3.00-2.91 (m, 2H), 2.71-2.68 (m, 1H), 2.60-2.55 (m, 1H), 2.45-2.36 (m, 2H) ppm.



Preparation of *N*-hydroxy-3-(1-(naphthalen-1-yl)-3,4-dihydroisoquinolin-2(1H)-yl)propenamide (5):

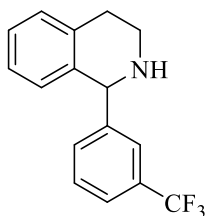
Prepared according to General Procedure E using methyl 3-(1-(naphthalen-1-yl)-3,4-dihydroisoquinolin-2(1H)-yl)propanoate (50 mg, 0.145 mmol) to afford 15.0 mg of *N*-hydroxy-3-(1-(naphthalen-1-yl)-3,4-dihydroisoquinolin-2(1H)-yl)propenamide (30%) as a yellow-solid. Melting Point: 87 – 110 °C. ^1H NMR (600 MHz, $\text{DMSO-}d_6$) δ 10.30 (bs, 1H), 8.60 (bs, 1H), 8.32 (d, $J = 8.5$ Hz, 1H), 7.90-7.86 (m, 2H), 7.48 (appd, $J = 5.3$ Hz, 2H), 7.43 (t, $J = 7.5$ Hz, 1H), 7.34 (bs, 1H), 7.18 (d, $J = 7.6$ Hz, 1H), 7.06 (t, $J = 7.3$ Hz, 1H), 6.87 (t, $J = 7.4$ Hz, 1H), 6.46 (d, $J = 7.7$ Hz, 1H), 5.16 (bs, 1H), 3.26-3.16 (bm, 2H), 2.91 (d, $J = 16.3$ Hz, 1H), 2.76-2.71 (m, 2H), 2.68-2.63 (m, 1H), 2.24-2.19 (m, 1H), 2.02-1.98 (m, 1H); ^{13}C NMR (150 MHz, $\text{DMSO-}d_6$) δ 167.9, 138.8, 138.4, 134.1, 134.0, 131.1, 128.9, 128.4, 128.3, 128.1, 127.1, 125.8, 125.6, 125.4, 125.3, 125.1, 50.3, 47.5, 29.3, 28.4 ppm. m/z calculated for $\text{C}_{22}\text{H}_{22}\text{N}_2\text{O}_2$ $[\text{M}+\text{H}]^+$ 347.17, found 347.18. IR cm^{-1} :

733, 785, 939, 1014, 1077, 1100, 1123, 1292, 1355, 1392, 1428, 1451, 1491, 1508, 1648, 2834, 2912, 3054, 3177.



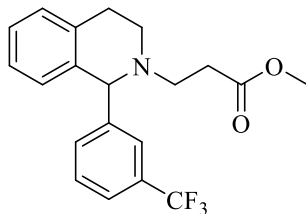
Preparation of *N*-phenethyl-3-(trifluoromethyl)benzamide (6A):

Prepared according to General Procedure A using 3-(trifluoromethyl)benzoic acid (500 mg, 2.63 mmol) to afford 730 mg of *N*-phenethyl-3-(trifluoromethyl)benzamide (95%) as an off-white solid. ¹H NMR (400 MHz, CDCl₃) δ 7.95 (s, 1H), 7.86 (d, *J* = 7.7 Hz, 1H), 7.74 (d, *J* = 7.8 Hz, 1H), 7.55 (t, *J* = 7.8 Hz, 1H), 7.34 (t, *J* = 7.2 Hz, 2H), 7.26 (m, 3H), 6.11 (bs, 1H), 3.75 (q, *J* = 6.6 Hz, 2H), 2.96 (t, *J* = 6.9 Hz, 2H) ppm.



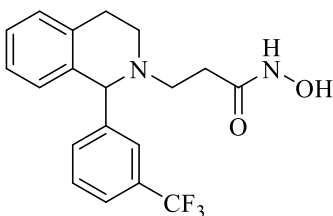
Preparation of 1-(3-(trifluoromethyl)phenyl)-1,2,3,4-tetrahydroisoquinoline (6C):

To a solution of *N*-phenethyl-3-(trifluoromethyl)benzamide (500 mg, 1.79 mmol) in xylenes (25 mL) was added phosphorus oxychloride (830 μL, 8.88 mmol) and phosphorus pentoxide (2.05 g, 7.23 mmol). The mixture was refluxed at 160 °C for 6 hours. The liquid mixture was transferred to a large collecting flask, and the left-over solid material was basified with 20% KOH solution and added to the liquid mixture. The aqueous phase was extracted twice with ethyl acetate (100 mL) and the organic phase was dried over Na₂SO₄, filtered, and concentrated under reduced pressure. The crude mixture was taken into ethanol (35 mL) and was degassed under nitrogen. Platinum(IV) oxide (39 mg, 0.17 mmol) was added to the solution. The reaction was stirred overnight under hydrogen atmosphere. The solution was filtered through Celite and concentrated under reduced pressure, and the crude product was purified with silica column chromatography (0-100% ethyl acetate in hexanes) to give 290 mg of 1-(3-(trifluoromethyl)phenyl)-1,2,3,4-tetrahydroisoquinoline (58%) as an off-white solid. ¹H NMR (400 MHz, CDCl₃) δ 7.57-7.54 (m, 2H), 7.45-7.43 (m, 2H), 7.17 (d, *J* = 3.8 Hz, 2H), 7.08-7.04 (m, 1H), 6.70 (d, *J* = 7.6 Hz, 1H), 5.19 (s, 1H), 3.30-3.25 (m, 1H), 3.16-3.03 (m, 2H), 2.87-2.82 (m, 1H) ppm.



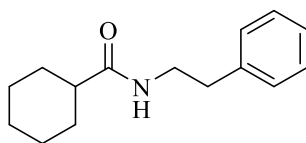
Preparation of Methyl 3-(1-(3-(trifluoromethyl)phenyl)-3,4-dihydroisoquinolin-2(1H)-yl)propanoate (6D):

Prepared according to General Procedure D using 1-(3-(trifluoromethyl)phenyl)-1,2,3,4-tetrahydroisoquinoline (250 mg, 0.901 mmol) to afford 210 mg of methyl 3-(1-(3-(trifluoromethyl)phenyl)-3,4-dihydroisoquinolin-2(1H)-yl)propanoate (64%) as a yellow oil. ¹H NMR (600 MHz, CDCl₃) δ 7.54 (s, 1H), 7.51 (d, *J* = 7.0 Hz, 1H), 7.41 (q, *J* = 8.1 Hz, 2H), 7.12 (q, *J* = 7.5 Hz, 2H), 7.01 (t, *J* = 7.2 Hz, 1H), 6.65 (d, *J* = 7.8 Hz, 1H), 4.65 (s, 1H), 3.60 (s, 3H), 3.19-3.16 (m, 1H), 3.09-3.05 (m, 1H), 2.91-2.83 (m, 2H), 2.67-2.62 (m, 2H), 2.47 (t, *J* = 7.1 Hz, 2H) ppm.



Preparation of *N*-hydroxy-3-(1-(3-(trifluoromethyl)phenyl)-3,4-dihydroisoquinolin-2(1H)-yl)propanamide (6):

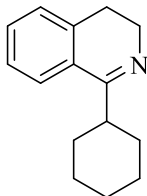
Prepared according to General Procedure E using methyl 3-(1-(3-(trifluoromethyl)phenyl)-3,4-dihydroisoquinolin-2(1H)-yl)propanoate (100 mg, 0.275 mmol) to afford 75 mg of *N*-hydroxy-3-(1-(3-(trifluoromethyl)phenyl)-3,4-dihydroisoquinolin-2(1H)-yl)propanamide (75%) as a white solid. Melting Point: 55 – 72 °C. ¹H NMR (600 MHz, DMSO-*d*₆) δ 10.37 (bs, 1H), 8.68 (bs, 1H), 7.63-7.61 (m, 1H), 7.59 (s, 1H), 7.56 (appd, *J* = 5.8, 2H), 7.16 (d, *J* = 7.4 Hz, 1H), 7.11 (t, *J* = 7.4 Hz, 1H), 7.02 (t, *J* = 7.3 Hz, 1H), 6.63 (d, *J* = 7.7 Hz, 1H), 4.81 (s, 1H), 3.07-3.03 (m, 1H), 3.01-2.96 (m, 1H), 2.84-2.81 (m, 1H), 2.64-2.61 (m, 2H), 2.56-2.53 (m, 1H), 2.23-2.21 (m, 1H), 2.11-2.07 (m, 1H). ¹³C NMR (150 MHz, DMSO-*d*₆) δ 167.9, 145.5, 137.1, 134.5, 133.3, 129.2, 128.8 (q, *J*_{C-CF₃} = 31.4 Hz), 128.6, 128.4, 126.1, 125.7, 125.3 (d, *J*_{αC} = 3.4 Hz), 124.2 (q, *J*_{CF₃} = 272.3 Hz), 123.9 (d, *J*_{αC} = 3.7 Hz), 65.7, 49.9, 46.1, 29.8, 28.2; ¹⁹F NMR (376 MHz, DMSO-*d*₆) δ -60.8 (s) ppm. *m/z* calculated for C₁₉H₁₉F₃N₂O₂ [M+H]⁺ 365.14, found 365.14. IR cm⁻¹: 660, 690, 741, 806, 1013, 1069, 1117, 1160, 1264, 1323, 1447, 1492, 1630, 1655, 2825, 2918, 3198.



Preparation of *N*-phenethylcyclohexanecarboxamide (7A):

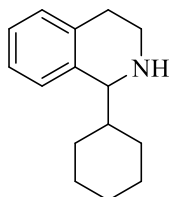
Prepared according to General Procedure A using cyclohexanecarboxylic acid (750 mg, 5.85 mmol) to afford 1.3 g of *N*-phenethylcyclohexanecarboxamide (96%) as an off-white solid. ¹H NMR (600 MHz, CDCl₃) δ 7.32 (t, *J* = 7.5 Hz, 2H), 7.24 (d, *J* = 7.7 Hz, 1H), 7.19 (d, *J* = 7.4 Hz, 2H), 5.40 (bs, 1H), 3.51 (q, *J* =

6.5 Hz, 2H), 2.81 (t, $J = 6.8$ Hz, 2H), 2.02-1.98 (m, 1H), 1.81-1.75 (m, 4H), 1.65 (bs, 1H), 1.38 (q, $J = 11.3$ Hz, 2H), 1.26-1.18 (m, 3H) ppm.



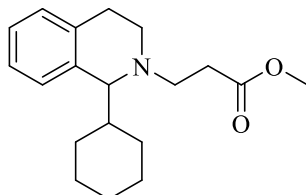
Preparation of 1-cyclohexyl-3,4-dihydroisoquinoline (7B):

Prepared according to General Procedure B using *N*-phenethylcyclohexanecarboxamide (1.0 g, 4.32 mmol) to afford 740 mg of 1-cyclohexyl-3,4-dihydroisoquinoline (80%) as a yellow oil. ^1H NMR (600 MHz, CDCl_3) δ 7.52 (d, $J = 7.4$ Hz, 1H), 7.34-7.26 (m, 2H), 7.19 (d, $J = 7.1$ Hz, 1H), 3.66 (t, $J = 7.3$ Hz, 2H), 2.90 (t, $J = 11.0$ Hz, 1H), 2.65 (t, $J = 7.3$ Hz, 2H), 1.87 (q, $J = 13.7$ Hz, 4H), 1.74 (d, $J = 13.0$ Hz, 1H), 1.42 (m, 4H), 1.28 (m, 1H) ppm.



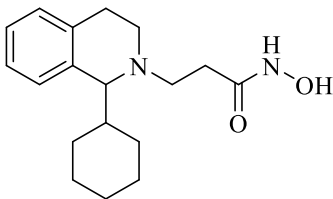
Preparation of 1-cyclohexyl-1,2,3,4-tetrahydroisoquinoline (7C):

Prepared according to General Procedure C using 1-cyclohexyl-3,4-dihydroisoquinoline (740 mg, 3.47 mmol) to afford 745 mg of 1-cyclohexyl-1,2,3,4-tetrahydroisoquinoline (99%) as a yellow oil. ^1H NMR (600 MHz, CDCl_3) δ 7.15 (d, $J = 3.1$ Hz, 2H), 7.12-7.10 (m, 1H), 7.07 (d, $J = 7.3$ Hz, 1H), 3.90 (bs, 1H), 3.29-3.26 (m, 1H), 2.95-2.91 (m, 1H), 2.86-2.80 (m, 1H), 2.69-2.65 (m, 1H), 1.94-1.90 (m, 1H), 1.84-1.81 (m, 1H), 1.70 (q, $J = 12.7$, 3H), 1.59 (s, 1H), 1.41-1.30 (m, 3H), 1.18-1.07 (m, 3H) ppm.



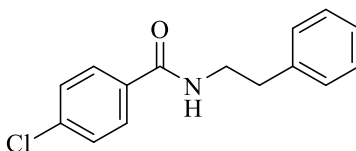
Preparation of Methyl 3-(1-cyclohexyl-3,4-dihydroisoquinolin-2(1H)-yl)propanoate (7D):

Prepared according to General Procedure D using 1-cyclohexyl-1,2,3,4-tetrahydroisoquinoline (700 mg, 3.26 mmol) to afford 800 mg of Methyl 3-(1-cyclohexyl-3,4-dihydroisoquinolin-2(1H)-yl)propanoate (81%) as a yellow oil. ^1H NMR (600 MHz, CDCl_3) δ 7.13-7.06 (m, 3H), 6.99 (d, $J = 7.2$ Hz, 1H), 3.67 (s, 3H), 3.29-3.24 (m, 1H), 3.19 (d, $J = 7.7$ Hz, 1H), 2.87-2.75 (m, 4H), 2.60-2.56 (m, 1H), 2.48 (t, $J = 7.0$ Hz, 2H), 1.98 (d, $J = 13.1$ Hz, 1H), 1.74-1.67 (m, 2H), 1.60 (d, $J = 12.1$ Hz, 2H), 1.50-1.45 (m, 1H), 1.17-1.09 (m, 3H), 1.00-0.94 (m, 2H) ppm.



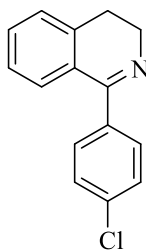
Preparation of 3-(1-cyclohexyl-3,4-dihydroisoquinolin-2(1H)-yl)-N-hydroxypropanamide (7):

Prepared according to General Procedure E using methyl 3-(1-cyclohexyl-3,4-dihydroisoquinolin-2(1H)-yl)propanoate (100 mg, 0.332 mmol) to afford 59 mg of 3-(1-cyclohexyl-3,4-dihydroisoquinolin-2(1H)-yl)-N-hydroxypropanamide (59%) as a pale-yellow solid. Melting Point: 44 – 57 °C. ¹H NMR (600 MHz, DMSO-*d*₆) δ 10.35 (bs, 1H), 8.67 (bs, 1H), 7.11-7.06 (m, 3H), 7.00 (d, *J* = 7.0 Hz, 1H), 3.20 (d, *J* = 7.6 Hz, 1H), 3.16-3.14 (m, 1H), 2.79-2.76 (m, 1H), 2.70-2.68 (m, 2H), 2.59-2.57 (m, 1H), 2.53 (bs, 1H), 2.12 (t, *J* = 7.2 Hz, 2H), 1.93 (bd, *J* = 12.7 Hz, 1H), 1.69-1.64 (m, 2H), 1.57 (bs, 1H), 1.51 (bd, *J* = 12.2 Hz, 1H), 1.44-1.41 (m, 1H), 1.09-1.07 (m, 3H), 1.00-0.96 (m, 2H); ¹³C NMR (150 MHz, DMSO-*d*₆) δ 168.0, 136.5, 134.9, 129.2, 128.5, 125.8, 124.6, 65.7, 50.4, 43.7, 42.8, 31.7, 30.3, 30.1, 26.2, 26.1, 26.0, 23.9 ppm. *m/z* calculated for C₁₈H₂₆N₂O₂ [M+H]⁺ 303.20, found 303.19. IR cm⁻¹: 649, 744, 892, 964, 1009, 1072, 1103, 1263, 1360, 1448, 1488, 1634, 1645, 2847, 2918, 3019, 3160.



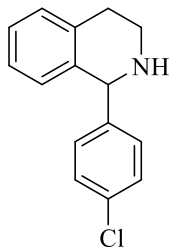
Preparation of 4-chloro-N-phenethylbenzamide (9A):

Prepared according to General Procedure A using 4-chlorobenzoic acid (750 mg, 4.79 mmol) to afford 1.2 g of 4-chloro-N-phenethylbenzamide (96%) as an off-white solid. ¹H NMR (600 MHz, CDCl₃) δ 7.62 (d, *J* = 8.5 Hz, 2H), 7.38 (d, *J* = 8.5 Hz, 2H), 7.34 (t, *J* = 7.5 Hz, 2H), 7.23 (t, *J* = 7.5 Hz, 3H), 6.04 (bs, 1H), 3.72 (q, *J* = 6.5 Hz, 2H), 2.94 (t, *J* = 6.9 Hz, 2H) ppm.



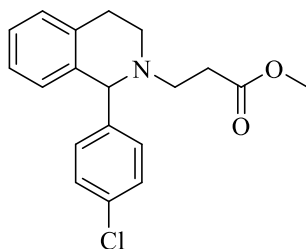
Preparation of 1-(4-chlorophenyl)-3,4-dihydroisoquinoline (9B):

Prepared according to General Procedure B using 4-chloro-N-phenethylbenzamide (1.0 g, 3.85 mmol) to afford 760 mg of 1-(4-chlorophenyl)-3,4-dihydroisoquinoline (92%) as an off-white solid. ¹H NMR (600 MHz, CDCl₃) δ 7.55 (d, *J* = 8.4 Hz, 2H) 7.41-7.39 (m, 3H), 7.28 (d, *J* = 7.9 Hz, 2H), 7.23 (t, *J* = 8.1 Hz, 1H), 3.84 (t, *J* = 7.3 Hz, 2H), 2.80 (t, *J* = 7.3 Hz, 2H) ppm.



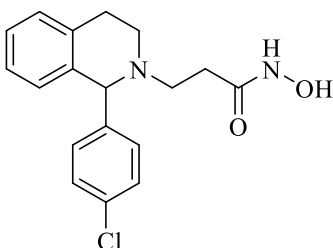
Preparation of 1-(4-chlorophenyl)-1,2,3,4-tetrahydroisoquinoline (9C):

To a solution of 1-(4-chlorophenyl)-3,4-dihydroisoquinoline (700 mg, 2.90 mmol) in methanol (30 mL) in an ice bath under argon was added sodium borohydride (164 mg, 4.34 mmol). The reaction was raised from the ice bath and stirred for two hours at room temperature. The reaction was quenched with water (10 mL), and the aqueous phase was extracted with DCM (50 mL). The organic phase was dried over Na_2SO_4 , filtered, and concentrated under reduced pressure to give 670 mg of 1-(4-chlorophenyl)-1,2,3,4-tetrahydroisoquinoline (95%) as an off-white solid. ^1H NMR (600 MHz, CDCl_3) δ 7.29 (d, $J = 8.4$ Hz, 2H), 7.21 (d, $J = 8.4$ Hz, 2H), 7.15 (d, $J = 4.0$ Hz, 2H), 7.06-7.04 (m, 1H), 6.71 (d, $J = 7.7$ Hz, 1H), 5.08 (s, 1H), 3.27-3.24 (m, 1H) 3.12-3.01 (m, 2H), 2.84-2.80 (m, 1H) ppm.



Preparation of Methyl 3-(1-(4-chlorophenyl)-3,4-dihydroisoquinolin-2(1H)-yl)propanoate (9D):

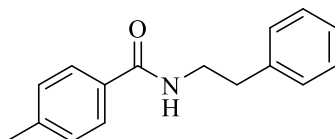
Prepared according to General Procedure D using 1-(4-chlorophenyl)-1,2,3,4-tetrahydroisoquinoline (600 mg, 2.46 mmol) to afford 540 mg of methyl 3-(1-(4-chlorophenyl)-3,4-dihydroisoquinolin-2(1H)-yl)propanoate (67%) as a white solid. ^1H NMR (600 MHz, CDCl_3) δ 7.26 (d, $J = 7.6$ Hz, 2H), 7.19 (d, $J = 8.3$ Hz, 2H), 7.12-7.08 (m, 2H), 7.00 (t, $J = 8.0$ Hz, 1H), 6.66 (d, $J = 7.8$ Hz, 1H), 4.56 (s, 1H), 3.61 (s, 3H), 3.18-3.14 (m, 1H), 3.09-3.04 (m, 1H), 2.91-2.86 (m, 1H), 2.85-2.81 (m, 1H) 2.66-2.61 (m, 2H), 2.47 (t, $J = 7.2$ Hz, 2H) ppm.



3-(1-(4-chlorophenyl)-3,4-dihydroisoquinolin-2(1H)-yl)-N-hydroxypropanamide (9)

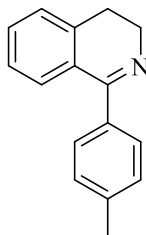
Prepared according to General Procedure E using methyl 3-(1-(4-chlorophenyl)-3,4-dihydroisoquinolin-2(1H)-yl)propanoate (100 mg, 0.303 mmol) to afford 61 mg of 3-(1-(4-chlorophenyl)-3,4-

dihydroisoquinolin-2(1H)-yl)-*N*-hydroxypropanamide (61%) as a white solid. Melting Point: 61 – 75°C. ¹H NMR (600 MHz, DMSO-*d*₆) δ 10.36 (bs, 1H), 8.68 (bs, 1H), 7.36 (d, *J* = 8.3 Hz, 2H), 7.26 (d, *J* = 8.3 Hz, 2H), 7.14 (d, *J* = 7.4 Hz, 1H), 7.09 (t, *J* = 7.4 Hz, 1H), 7.01 (t, *J* = 7.3 Hz, 1H), 6.63 (d, *J* = 7.7 Hz, 1H), 4.66 (s, 1H), 3.07-3.03 (m, 1H), 2.99-2.94 (m, 1H), 2.82-2.79 (m, 1H), 2.65-2.60 (m, 1H), 2.59-2.55 (m, 1H), 2.22-2.18 (m, 1H), 2.10-2.05 (m, 1H); ¹³C NMR (150 MHz, DMSO-*d*₆) δ 167.9, 143.0, 137.6, 134.4, 131.5, 131.0, 128.4, 128.3, 128.1, 125.9, 125.6, 65.7, 50.0, 46.2, 29.9, 28.4 ppm. *m/z* calculated for C₁₈H₁₉ClN₂O₂ [M+H]⁺ 331.1213, found 331.1219. IR cm⁻¹: 741, 816, 939, 1013, 1086, 1125, 1373, 1427, 1450, 1489, 1648, 2829, 2919, 3019, 3179.



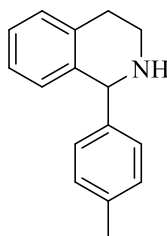
Preparation of 4-methyl-*N*-phenethylbenzamide (10A):

Prepared according to General Procedure A using p-toluic acid (750 mg, 5.51 mmol) to afford 1.2 g of 4-methyl-*N*-phenethylbenzamide (91%) as an off-white solid. ¹H NMR (600 MHz, CDCl₃) δ 7.58 (d, *J* = 8.1 Hz, 2H), 7.33 (t, *J* = 7.5 Hz, 2H), 7.24 (d, *J* = 7.8 Hz, 3H), 7.21 (d, *J* = 7.9 Hz, 2H), 6.07 (bs, 1H), 3.72 (q, *J* = 6.6 Hz, 2H), 2.93 (t, *J* = 6.9 Hz, 2H), 2.38 (s, 3H) ppm.



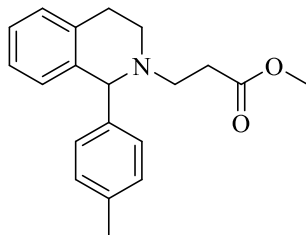
Preparation of 1-(p-tolyl)-3,4-dihydroisoquinoline (10B):

Prepared according to General Procedure B using 4-methyl-*N*-phenethylbenzamide (1.0 g, 4.18 mmol) to afford 420 mg of 1-(p-tolyl)-3,4-dihydroisoquinoline (45%) as an off-white solid. ¹H NMR (600 MHz, CDCl₃) δ 7.50 (d, *J* = 8.0 Hz, 2H), 7.38 (t, *J* = 6.9 Hz, 1H), 7.28 (t, *J* = 6.4 Hz, 2H), 7.23 (d, *J* = 7.8 Hz, 3H), 3.83 (t, *J* = 7.3 Hz, 2H), 2.80 (t, *J* = 7.2 Hz, 2H), 2.41 (s, 3H) ppm.



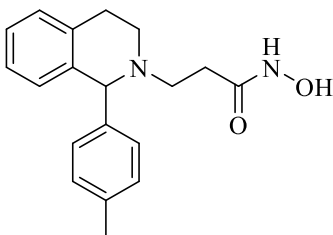
Preparation of 1-(p-tolyl)-1,2,3,4-tetrahydroisoquinoline (10C):

Prepared according to General Procedure C using 1-(p-tolyl)-3,4-dihydroisoquinoline (420 mg, 1.9 mmol) to afford 413 mg of 1-(p-tolyl)-1,2,3,4-tetrahydroisoquinoline (97%) as an amber solid. ¹H NMR (600 MHz, CDCl₃) δ 7.16-7.11 (m, 6H), 7.04-7.01 (m, 1H), 6.76 (d, *J* = 7.7 Hz, 1H), 5.07 (s, 1H), , 3.29-3.25 (m, 1H), 3.11-3.01 (m, 2H), 2.85-2.81 (m, 1H), 2.34 (s, 3H), 1.79 (bs, 1H).



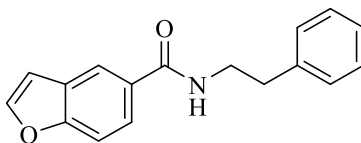
Preparation of Methyl 3-(1-(p-tolyl)-3,4-dihydroisoquinolin-2(1H)-yl)propanoate (10D):

Prepared according to General Procedure D using 1-(p-tolyl)-1,2,3,4-tetrahydroisoquinoline (300 mg, 1.34 mmol) to afford 275 mg of methyl 3-(1-(p-tolyl)-3,4-dihydroisoquinolin-2(1H)-yl)propanoate (66%) as an off-white solid. ^1H NMR (600 MHz, CDCl_3) δ 7.13-7.07 (m, 6H), 6.98 (t, $J = 7.1$ Hz, 1H), 6.70 (d, $J = 7.8$ Hz, 1H), 4.56 (s, 1H), 3.60 (s, 3H), 3.17-3.15 (m, 1H), 3.11-3.06 (m, 1H), 2.91-2.88 (m, 1H), 2.86-2.82 (m, 1H), 2.67-2.62 (m, 2H), 2.47 (t, $J = 6.2$ Hz, 2H), 2.33 (s, 3H) ppm.



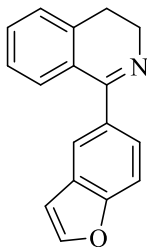
Preparation of N-hydroxy-3-(1-(p-tolyl)-3,4-dihydroisoquinolin-2(1H)-yl)propanamide (10):

Prepared according to General Procedure E using ethyl 3-(1-(p-tolyl)-3,4-dihydroisoquinolin-2(1H)-yl)propanoate (100 mg, 0.323 mmol) to afford 63 mg of N-hydroxy-3-(1-(p-tolyl)-3,4-dihydroisoquinolin-2(1H)-yl)propanamide (63%) as a white solid. Melting Point: 60 – 69 °C. ^1H NMR (600 MHz, $\text{DMSO-}d_6$) δ 10.36 (bs, 1H), 8.67 (bs, 1H), 7.11 (apps, 5H), 7.07 (t, $J = 7.3$ Hz, 1H), 6.98 (t, $J = 7.3$ Hz, 1H), 6.61 (d, $J = 7.7$ Hz, 1H), 4.58 (s, 1H), 3.07-3.04 (m, 1H), 2.99-2.94 (m, 1H), 2.81-2.78 (m, 1H), 2.66-2.61 (m, 1H), 2.58-2.56 (m, 2H + DMSO), 2.28 (s, 3H), 2.23-2.18 (m, 1H), 2.09-2.04 (m, 1H); ^{13}C NMR (150 MHz, $\text{DMSO-}d_6$) δ 168.0, 140.7, 138.3, 136.0, 134.3, 129.1, 128.7, 128.4, 128.3, 125.7, 125.4, 66.4, 50.0, 46.3, 29.8, 28.5, 20.7 ppm. m/z calculated for $\text{C}_{19}\text{H}_{22}\text{N}_2\text{O}_2$ $[\text{M}+\text{H}]^+$ 311.1760, found 311.1766. IR cm^{-1} : 739, 813, 938, 1013, 1073, 1297, 1374, 1425, 1450, 1491, 1509, 1630, 1638, 2821, 2892, 3018, 3166.



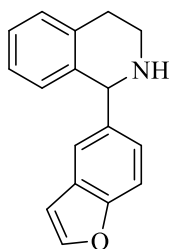
Preparation of N-phenethylbenzofuran-5-carboxamide (13A):

Prepared according to General Procedure A using benzofuran-5-carboxylic acid (500 mg, 3.09 mmol) to afford 675 mg of N-phenethylbenzofuran-5-carboxamide (82%) as an off-white solid. ^1H NMR (300 MHz, CDCl_3) δ 7.98 (d, $J = 1.7$ Hz, 1H), 7.68-7.62 (m, 2H), 7.51 (d, $J = 8.6$ Hz, 1H), 7.37-7.32 (m, 2H), 7.27 (s, 3H), 6.81 (d, $J = 1.4$ Hz, 1H), 6.12 (bs, 1H), 3.76 (q, $J = 6.5$ Hz, 2H), 2.96 (t, $J = 6.9$ Hz, 2H) ppm.



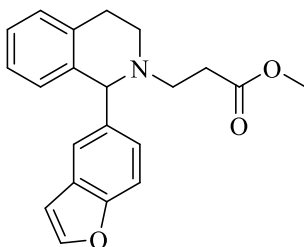
Preparation of 1-(benzofuran-5-yl)-3,4-dihydroisoquinoline (13B):

Prepared according to General Procedure B using *N*-phenethylbenzofuran-5-carboxamide (600 mg, 2.26 mmol) to afford 245 mg of 1-(benzofuran-5-yl)-3,4-dihydroisoquinoline (44%) as a yellow oil. ¹H NMR (600 MHz, CDCl₃) δ 7.86 (s, 1H), 7.67 (d, *J* = 2.0 Hz, 1H), 7.58-7.53 (m, 2H), 7.40 (t, *J* = 6.6 Hz, 1H), 7.30 (t, *J* = 7.8 Hz, 2H), 6.80 (d, *J* = 1.6 Hz, 1H), 3.86 (t, *J* = 7.3 Hz, 2H), 2.83 (t, *J* = 7.2 Hz, 2H) ppm.



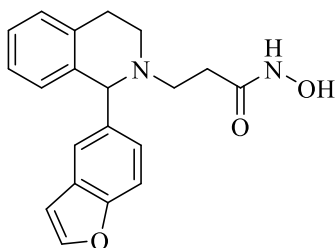
Preparation of 1-(benzofuran-5-yl)-1,2,3,4-tetrahydroisoquinoline (13C):

Prepared according to General Procedure C using 1-(benzofuran-5-yl)-3,4-dihydroisoquinoline (245 mg, 0.99 mmol) to afford 230 mg of 1-(benzofuran-5-yl)-1,2,3,4-tetrahydroisoquinoline (93%) as an off-white solid. ¹H NMR (600 MHz, CDCl₃) δ 7.61 (d, *J* = 2.0 Hz, 1H), 7.48 (d, *J* = 1.1 Hz, 1H), 7.45 (d, *J* = 8.5 Hz, 1H), 7.26-7.22 (m, 1H), 7.17-7.13 (m, 2H), 7.04-7.01 (m, 1H), 6.76 (d, *J* = 7.7 Hz, 1H), 6.71 (d, *J* = 1.3 Hz, 1H), 5.21 (s, 1H), 3.32-3.29 (m, 1H), 3.15-3.06 (m, 2H), 2.86-2.83 (m, 1H) ppm.



Preparation of Methyl 3-(1-(benzofuran-5-yl)-3,4-dihydroisoquinolin-2(1H)-yl)propanoate (13D):

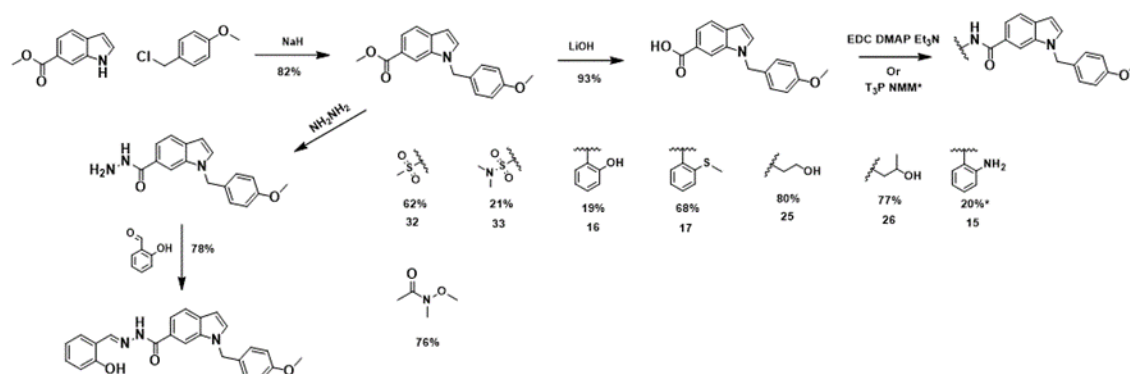
Prepared according to General Procedure D using 1-(benzofuran-5-yl)-1,2,3,4-tetrahydroisoquinoline (200 mg, 0.8 mmol) to afford 200 mg of Methyl 3-(1-(benzofuran-5-yl)-3,4-dihydroisoquinolin-2(1H)-yl)propanoate (75%) as an off-white solid. ¹H NMR (600 MHz, CDCl₃) δ 7.60 (s, 1H), 7.48 (s, 1H), 7.42 (d, *J* = 8.4 Hz, 1H), 7.20 (d, *J* = 8.4 Hz, 1H), 7.12 (d, *J* = 7.4 Hz, 1H), 7.09 (t, *J* = 7.2 Hz, 1H), 6.97 (t, *J* = 7.3 Hz, 1H), 6.71 (s, 1H), 6.69 (d, *J* = 7.7 Hz, 1H), 4.67 (s, 1H), 3.57 (s, 3H), 3.23-3.19 (m, 1H), 3.16-3.11 (m, 1H), 2.96-2.91 (m, 1H), 2.87-2.84 (m, 1H), 2.69-2.63 (m, 2H), 2.47 (t, *J* = 7.2 Hz, 2H) ppm.



Preparation of 3-(1-(benzofuran-5-yl)-3,4-dihydroisoquinolin-2(1H)-yl)-N-hydroxypropanamide (13):

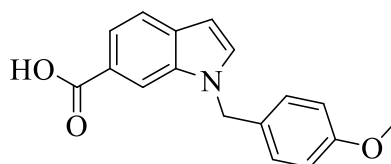
Prepared according to General Procedure E using methyl 3-(1-(benzofuran-5-yl)-3,4-dihydroisoquinolin-2(1H)-yl)propanoate (100 mg, 0.297 mmol) to afford 64 mg of 3-(1-(benzofuran-5-yl)-3,4-dihydroisoquinolin-2(1H)-yl)-N-hydroxypropanamide (64%) as a white solid. Melting Point: 72-87°C. ¹H NMR (600 MHz, DMSO-*d*₆) δ 10.35 (bs, 1H), 8.66 (bs, 1H), 7.97 (d, *J* = 2.1 Hz, 1H), 7.52 (s, 1H), 7.50 (d, *J* = 8.5 Hz, 1H), 7.18 (appdd, *J* = 1.2 Hz, 7.3 Hz, 1H), 7.14 (d, *J* = 7.6 Hz, 1H), 7.07 (t, *J* = 7.4 Hz, 1H), 6.97 (t, *J* = 7.3 Hz, 1H), 6.92 (appd, *J* = 1.3 Hz, 1H), 6.62 (d, *J* = 7.8 Hz, 1H), 4.72 (s, 1H), 3.12-3.08 (m, 1H), 3.04-2.99 (m, 1H), 2.84-2.81 (m, 1H), 2.69-2.65 (m, 1H), 2.62-2.57 (m, 2H), 2.24-2.19 (m, 1H), 2.10-2.05 (m, 1H); ¹³C NMR (150 MHz, DMSO-*d*₆) δ 168.0, 153.5, 146.1, 138.6, 134.3, 128.5, 128.3, 126.9, 125.7, 125.6, 125.4, 121.8, 110.9, 106.8, 106.7, 66.6, 50.0, 46.4, 29.8, 28.6 ppm. *m/z* calculated for C₂₀H₂₀N₂O₃ [M+H]⁺ 337.1552, found 337.1554. IR cm⁻¹: 657, 738, 765, 814, 883, 1014, 1027, 1107, 1190, 1260, 1450, 1463, 1490, 1535, 1639, 2828, 2902, 3016, 3155.

Appendix Scheme 2 General Synthesis for methyl ester analogs.



Preparation of Methyl 1-(4-methoxybenzyl)-1H-indole-6-carboxylate:

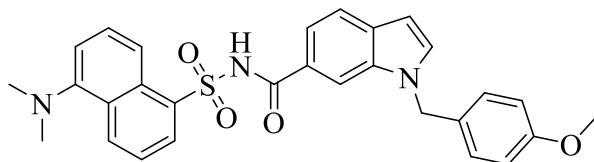
To a solution of methyl 1H-indole-6-carboxylate (1 g, 5.71 mmol) in acetonitrile (30 mL) stirred in an ice bath was added washed NaH (221 mg) as a slurry in acetonitrile (10 mL). The reaction mixture was aged in an ice bath for 30 minutes. 1-(chloromethyl)-4-methoxybenzene (1.2 mL) was added dropwise to the mixture and the reaction was raised from the ice bath and stirred at room temperature overnight. The reaction mixture was stirred in an ice bath and quenched with saturated NH_4Cl solution (15 mL). The mixture was diluted with EtOAc (150 mL) and washed with brine (15 mL). The organic phase was dried over Na_2SO_4 , filtered, and concentrated under reduced pressure to provide crude product. The product was purified on a silica gel column (0-20% EtOAc in hexanes) to give 900 mg of methyl 1-(4-methoxybenzyl)-1H-indole-6-carboxylate (53%) as a pale-yellow solid. ^1H NMR (400 MHz, CDCl_3) δ 8.11 (s, 1H), 7.80 (q, $J = 3.3$ Hz, 1H), 7.65 (d, $J = 8.4$, 1H), 7.25 (d, $J = 3.1$ Hz, 1H + CDCl_3), 7.08 (d, $J = 8.7$ Hz, 2H), 6.84 (d, $J = 8.7$ Hz, 2H), 6.57 (d, $J = 1.3$ Hz, 1H), 5.32 (s, 2H), 3.92 (s, 3H), 3.78 (s, 3H) ppm.



Preparation of 1-(4-methoxybenzyl)-1H-indole-6-carboxylic acid:

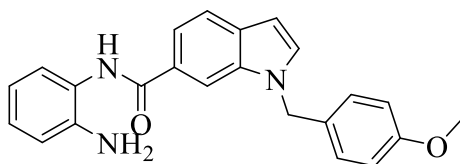
To a solution of methyl 1-(4-methoxybenzyl)-1H-indole-6-carboxylate (845 mg, 2.86 mmol) in methanol (4 mL) was added THF (4 mL) and H_2O (3 mL). LiOH (277 mg, 11.5 mmol) was added, and the reaction stirred at room temperature overnight. The reaction was quenched with 1 M HCl (10 mL), and the aqueous phase was extracted twice with EtOAc (30 mL). The organic phase was dried over Na_2SO_4 , filtered, and concentrated under reduced pressure to provide 750 mg of 1-(4-methoxybenzyl)-1H-indole-6-carboxylic acid (93%) as a yellow solid. ^1H NMR (400 MHz, CDCl_3) δ 8.17 (s, 1H), 7.85 (q, $J = 3.2$

Hz, 1H), 7.68 (d, $J = 8.3$ Hz, 1H), 7.28 (d, $J = 3.1$ Hz, 1H), 7.10 (d, $J = 8.7$ Hz, 2H), 6.85 (d, $J = 8.7$ Hz, 2H), 6.59 (d, $J = 2.5$ Hz, 1H), 5.33 (s, 2H), 3.78 (s, 3H) ppm.



Preparation of N-((5-(dimethylamino)naphthalen-1-yl)sulfonyl)-1-(4-methoxybenzyl)-1H-indole-6-carboxamide (14):

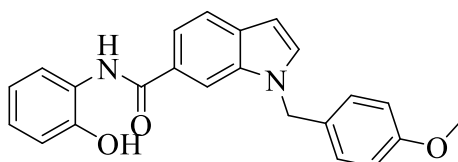
To a solution of EDC HCl (35.3 mg, 0.185 mmol) in DCM (1 mL) was added DMAP (41.6 mg, 0.341 mmol). The mixture was stirred at room temperature for 5 minutes. The mixture was stirred in an ice bath, and 1-(4-methoxybenzyl)-1H-indole-6-carboxylic acid (40 mg, 0.142 mmol) was added. The reaction was stirred for 15 minutes in an ice bath. Dansyl amide (35.5 mg, 0.142 mmol) was added, and the reaction was stirred at room temperature overnight. The reaction was quenched with 1 M HCl until the pH was roughly 7, and the mixture was diluted with DCM (10 mL). The organic phase was washed with saturated NH_4Cl solution (10 mL). The organic phase was dried over Na_2SO_4 , filtered, and concentrated under reduced pressure to provide crude product. The crude product was purified on a silica gel column (0-20% EtOAc in hexanes) to give 65 mg of N-((5-(dimethylamino)naphthalen-1-yl)sulfonyl)-1-(4-methoxybenzyl)-1H-indole-6-carboxamide (89%) as a bright yellow solid. ^1H NMR (500 MHz, CDCl_3) δ 8.94 (bs, 1H), 8.61 (appt, $J = 8.5$ Hz, 2H), 8.33 (d, $J = 8.7$ Hz, 1H), 7.83 (s, 1H), 7.62 (appt, $J = 7.82$, 2H), 7.54 (t, $J = 8.1$ Hz, 1H), 7.38 (d, $J = 8.4$ Hz, 1H), 7.24 (d, $J = 3.1$ Hz, 1H), 7.14 (d, $J = 7.6$ Hz, 1H), 6.99 (d, $J = 8.6$ Hz, 2H), 6.79 (d, $J = 8.7$ Hz, 2H), 6.53 (d, $J = 2.7$ Hz, 1H), 5.22 (s, 2H), 3.76 (s, 3H), 2.86 (s, 6H) ppm. ^{13}C NMR (126 MHz, CDCl_3) δ 165.06, 159.27, 135.62, 133.47, 132.67, 131.87, 131.75, 129.76, 129.68, 129.39, 128.78, 128.52, 128.31, 128.21, 124.06, 123.39, 121.06, 118.33, 118.22, 115.19, 114.24, 110.80, 102.13, 55.24, 49.57, 45.41 ppm. m/z calculated for $\text{C}_{29}\text{H}_{27}\text{N}_3\text{O}_4\text{S}$ $[\text{M}+\text{H}]^+$ 514.17, found 514.1. IR cm^{-1} : 622, 726, 758, 787, 819, 872, 944, 1030, 1054, 1090, 1142, 1200, 1243, 1317, 1337, 1397, 1413, 1512, 1572, 1586, 1610, 1674, 2786, 2833, 2867, 2928, 3279.



Preparation of N-(2-aminophenyl)-1-(4-methoxybenzyl)-1H-indole-6-carboxamide (15):

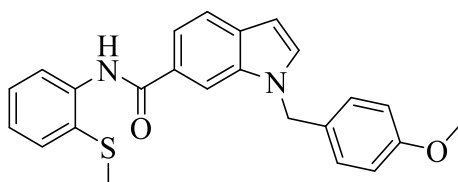
To a solution of 1-(4-methoxybenzyl)-1H-indole-6-carboxylic acid (100 mg, 0.355 mmol) in acetonitrile (8 mL) was added propanephosphonic acid anhydride (0.41 mL, 50% solution). N-methylmorpholine (0.19 mL, 207 mg, 2.03 mmol) was added to the solution, and the mixture was stirred at room temperature for 10 minutes. Benzene-1,2-diamine (40 mg, 3.73 mmol) was added, and the reaction was stirred at room temperature overnight. Reaction was diluted with DCM (10 mL) and washed with saturated NH_4Cl solution (2 mL) and water (2 mL). The organic phase was dried over Na_2SO_4 , filtered, and concentrated under reduced pressure to provide crude product. The crude product was purified on a silica gel column (0-20% EtOAc in DCM) to give 27 mg of N-(2-aminophenyl)-1-(4-methoxybenzyl)-1H-indole-6-carboxamide (20%) as an off-white solid. ^1H NMR (600 MHz, CDCl_3) δ 8.04 (s, 1H), 7.85 (bs, 1H), 7.71 (d, J

= 8.2 Hz, 1H), 7.57 (d, $J = 8.3$ Hz, 1H), 7.33 (d, $J = 6.8$ Hz, 1H), 7.08-7.10 (m, 3H), 6.85 (dd, $J = 7.8, 12.0$ Hz, 4H), 6.59 (d, $J = 2.9$ Hz, 2H), 5.33 (s, 2H), 3.93 (bs, 1H), 3.78 (s, 3H) ppm. ^{13}C NMR (151 MHz, CDCl_3) δ 159.26, 140.74, 135.98, 131.62, 131.06, 128.89, 128.36, 127.38, 127.01, 125.15, 124.96, 120.96, 119.74, 118.34, 117.66, 114.27, 110.36, 101.96, 55.29, 49.75 ppm. m/z calculated for $\text{C}_{23}\text{H}_{21}\text{N}_3\text{O}_2$ $[\text{M}+\text{H}]^+$ 372.16, found 372.3. IR cm^{-1} : 649, 721, 755, 820, 1028, 1176, 1246, 1294, 1315, 1352, 1450, 1511, 1610, 2836, 2927, 3216.



Preparation of N-(2-hydroxyphenyl)-1-(4-methoxybenzyl)-1H-indole-6-carboxamide (16):

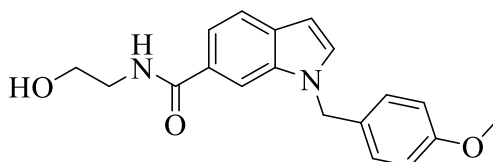
To a solution of 1-(4-methoxybenzyl)-1H-indole-6-carboxylic acid (60 mg, 0.213 mmol) in DCM (3 mL) in an ice bath was added 2-aminophenol (30.1 mg, 0.276 mmol), triethylamine (0.075 mL, 0.534 mmol), and DMAP (2.5 mg, 0.021 mmol). EDC HCl (36 mg, 0.234 mmol) was added to the solution and the reaction was stirred on ice for 1 hour. The reaction was raised from the ice bath and stirred at room temperature overnight. The reaction was diluted with EtOAc (20 mL) and washed with 1 M HCl (3 mL), saturated NaHCO_3 solution (3 mL), and brine (3 mL). The organic phase was dried over Na_2SO_4 , filtered, and concentrated under reduced pressure to provide crude product. The crude product was purified on a silica gel column (0-25% EtOAc in hexanes) to give 15 mg of N-(2-hydroxyphenyl)-1-(4-methoxybenzyl)-1H-indole-6-carboxamide (19%) as a pale amber solid. ^1H NMR (600 MHz, CDCl_3) δ 9.13 (s, 1H), 8.12 (s, 1H), 8.07 (s, 1H), 7.75 (d, $J = 8.3$ Hz, 1H), 7.56 (q, $J = 3.1$ Hz, 1H), 7.19 (appt, $J = 7.1$ Hz, 1H), 7.10-7.12 (m, 4H), 6.94 (appt, $J = 7.1$ Hz, 1H), 6.87 (d, $J = 8.6$ Hz, 2H), 6.63 (d, $J = 2.9$ Hz, 1H), 5.37 (s, 2H), 3.80 (s, 3H) ppm. ^{13}C NMR (151 MHz, CDCl_3) δ 169.20, 159.38, 149.22, 135.97, 132.10, 131.58, 128.67, 128.38, 127.28, 127.28, 125.92, 122.39, 121.17, 120.46, 120.26, 117.42, 114.33, 110.76, 102.13, 55.31, 49.82 ppm. m/z calculated for $\text{C}_{23}\text{H}_{20}\text{N}_2\text{O}_3$ $[\text{M}+\text{H}]^+$ 373.15, found 373.1. IR cm^{-1} : 698, 734, 748, 771, 796, 883, 962, 1030, 1151, 1175, 1238, 1289, 1315, 1335, 1432, 1491, 1509, 1588, 1612, 1685, 2836, 2925, 3020, 3091, 3276.



Preparation of 1-(4-methoxybenzyl)-N-(2-(methylthio)phenyl)-1H-indole-6-carboxamide (17):

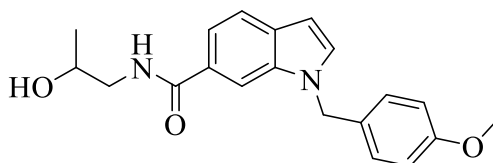
To a solution of EDC HCl (35.3 mg, 0.185 mmol) in DCM (1 mL) was added DMAP (41.6 mg, 0.341 mmol). The mixture was stirred at room temperature for 5 minutes. The mixture was stirred in an ice bath, and 1-(4-methoxybenzyl)-1H-indole-6-carboxylic acid (40 mg, 0.142 mmol) was added. The reaction was stirred for 15 minutes in an ice bath. 2-(methylthio)aniline (0.017 mL, 0.142 mmol) was added, and the reaction was stirred at room temperature overnight. The reaction was quenched with 1 M HCl until the pH was roughly 1, and the mixture was diluted with DCM (10 mL). The organic phase was washed with brine (5 mL). The organic phase was dried over Na_2SO_4 , filtered, and concentrated under reduced pressure to provide crude product. The crude product was purified on a silica gel column (0-20% EtOAc

in hexanes) to give 47 mg of 1-(4-methoxybenzyl)-N-(2-(methylthio)phenyl)-1H-indole-6-carboxamide (82%) as an orange solid. ^1H NMR (600 MHz, CDCl_3) δ 9.33 (s, 1H), 8.58 (d, $J = 8.0$ Hz, 1H), 8.07 (s, 1H), 7.73 (d, $J = 8.2$ Hz, 1H), 7.64 (d, $J = 8.0$ Hz, 1H), 7.55 (d, $J = 7.3$ Hz, 1H), 7.36 (d, $J = 7.3$ Hz, 1H), 7.29 (d, $J = 2.8$ Hz, 1H), 7.07-7.13 (m, 3H), 6.84 (d, $J = 8.5$ Hz, 2H), 6.60 (d, $J = 2.3$ Hz, 1H), 5.35 (s, 2H), 3.77 (s, 3H), 2.38 (s, 3H) ppm. ^{13}C NMR (126 MHz, CDCl_3) δ 166.11, 159.32, 139.24, 136.01, 133.56, 131.71, 131.12, 129.33, 128.86, 128.39, 128.16, 125.15, 124.02, 121.05, 120.28, 117.57, 114.33, 110.24, 101.93, 55.28, 49.91, 19.27 ppm. m/z calculated for $\text{C}_{24}\text{H}_{22}\text{N}_2\text{O}_2\text{S}$ $[\text{M}+\text{H}]^+$ 403.14, found 403.0. IR cm^{-1} : 632, 731, 747, 772, 814, 879, 1030, 1177, 1236, 1306, 1352, 1435, 1464, 1511, 1574, 1610, 1647, 2925, 2971, 3324.



Preparation of N-(2-hydroxyethyl)-1-(4-methoxybenzyl)-1H-indole-6-carboxamide (25):

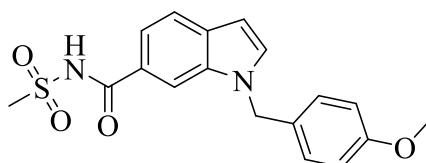
To a solution of EDC HCl (35.3 mg, 0.185 mmol) in DCM (1 mL) was added DMAP (41.6 mg, 0.341 mmol). The mixture was stirred at room temperature for 5 minutes. The mixture was stirred in an ice bath, and 1-(4-methoxybenzyl)-1H-indole-6-carboxylic acid (40 mg, 0.142 mmol) was added. The reaction was stirred for 15 minutes in an ice bath. 2-aminoethan-1-ol (0.009 mL, 0.142 mmol) was added, and the reaction was stirred at room temperature overnight. The reaction was quenched with 1 M HCl until the pH was roughly 2, and the mixture was diluted with DCM (10 mL). The organic phase was washed with water (5 mL). The organic phase was dried over Na_2SO_4 , filtered, and concentrated under reduced pressure to provide crude product. The crude product was purified on a silica gel column (0-60% EtOAc in hexanes) to give 37 mg of N-(2-hydroxyethyl)-1-(4-methoxybenzyl)-1H-indole-6-carboxamide (80%) as an orange solid. ^1H NMR (500 MHz, CDCl_3) δ 7.96 (s, 1H), 7.64 (d, $J = 8.3$ Hz, 1H), 7.42 (dd, $J = 1.5, 8.3$ Hz, 1H), 7.22 (d, $J = 3.1$ Hz, 1H), 7.07 (d, $J = 8.7$ Hz, 2H), 6.83 (d, $J = 8.7$ Hz, 2H), 6.64 (bs, 1H), 6.56 (d, $J = 2.6$ Hz, 1H), 5.31 (s, 2H), 3.85 (t, $J = 4.9$ Hz, 2H), 3.77 (s, 3H), 3.65 (q, $J = 5.2$ Hz, 2H) ppm. ^{13}C NMR (126 MHz, CDCl_3) δ 169.66, 159.29, 135.99, 131.37, 130.76, 128.95, 128.33, 127.29, 120.75, 117.40, 114.29, 110.02, 101.89, 62.88, 55.29, 49.62, 43.17 ppm. m/z calculated for $\text{C}_{19}\text{H}_{20}\text{N}_2\text{O}_3$ $[\text{M}+\text{H}]^+$ 325.15, found 325.1. IR cm^{-1} : 655, 696, 725, 754, 771, 810, 1028, 1058, 1107, 1172, 1241, 1290, 1349, 1437, 1460, 1509, 1534, 1606, 1627, 2929, 3305.



Preparation of N-(2-hydroxypropyl)-1-(4-methoxybenzyl)-1H-indole-6-carboxamide (26):

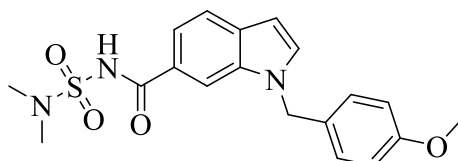
To a solution of EDC HCl (35.3 mg, 0.185 mmol) in DCM (1 mL) was added DMAP (41.6 mg, 0.341 mmol). The mixture was stirred at room temperature for 5 minutes. The mixture was stirred in an ice bath, and 1-(4-methoxybenzyl)-1H-indole-6-carboxylic acid (40 mg, 0.142 mmol) was added. The reaction was stirred for 15 minutes in an ice bath. 1-aminopropan-2-ol (0.011 mL, 0.142 mmol) was added, and the reaction was stirred at room temperature overnight. The reaction was quenched with 1 M HCl until the pH was roughly 1, and the mixture was diluted with DCM (10 mL). The organic phase was washed with

brine (10 mL). The organic phase was dried over Na₂SO₄, filtered, and concentrated under reduced pressure to provide crude product. The crude product was purified on a silica gel column (0-60% EtOAc in hexanes) to give 37 mg of N-(2-hydroxypropyl)-1-(4-methoxybenzyl)-1H-indole-6-carboxamide (78%) as a yellow oil. ¹H NMR (500 MHz, CDCl₃) δ 7.96 (s, 1H), 7.64 (d, *J* = 8.3 Hz, 1H), 7.42 (dd, *J* = 1.4, 8.3 Hz, 1H), 7.22 (d, *J* = 3.1 Hz, 1H), 7.08 (d, *J* = 8.6 Hz, 2H), 6.83 (d, *J* = 8.7 Hz, 2H), 6.60 (bs, 1H), 6.56 (d, *J* = 3.1 Hz, 1H), 5.31 (s, 2H), 4.06 (bs, 1H), 3.77 (s, 3H), 3.64-3.69 (m, 1H), 3.33-3.38 (m, 1H), 2.72 (d, *J* = 3.7 Hz, 1H), 1.26 (d, *J* = 6.3 Hz, 3H + grease) ppm. ¹³C NMR (126 MHz, CDCl₃) δ 169.51, 159.27, 135.98, 131.34, 130.74, 128.95, 128.36, 127.35, 120.74, 117.39, 114.28, 110.06, 101.88, 67.89, 55.29, 49.63, 47.76, 21.09 ppm. *m/z* calculated for C₂₀H₂₂N₂O₃ [M+H]⁺ 339.16, found 339.1. IR cm⁻¹: 650, 678, 728, 759, 820, 873, 1023, 1080, 1111, 1136, 1176, 1245, 1305, 1319, 1354, 1438, 1462, 1510, 1534, 1608, 2925, 2959, 3093, 3323.



Preparation of 1-(4-methoxybenzyl)-N-(methylsulfonyl)-1H-indole-6-carboxamide (32):

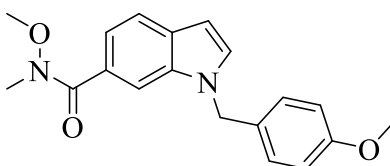
To a solution of EDC HCl (664 mg, 3.47 mmol) in DCM (15 mL) was added DMAP (782 mg, 6.40 mmol). The mixture was stirred at room temperature for 5 minutes. The mixture was stirred in an ice bath, and 1-(4-methoxybenzyl)-1H-indole-6-carboxylic acid (750 mg, 2.67 mmol) was added. The reaction was stirred for 15 minutes in an ice bath. Methanesulfonamide (254 mg, 2.67 mmol) was added, and the reaction was stirred at room temperature overnight. The reaction was quenched with 1 M HCl until the pH was roughly 1, and the mixture was diluted with DCM (10 mL). The organic phase was washed with saturated NH₄Cl solution (10 mL). The organic phase was dried over Na₂SO₄, filtered, and concentrated under reduced pressure to provide crude product. The crude product was purified on a silica gel column (0-20% EtOAc in hexanes) to give 600 mg of 1-(4-methoxybenzyl)-N-(methylsulfonyl)-1H-indole-6-carboxamide (63%) as an off-white solid. ¹H NMR (600 MHz, CDCl₃) δ 8.40 (s, 1H), 7.96 (s, 1H), 7.72 (d, *J* = 8.3 Hz, 2H), 7.47-7.45 (m, 2H), 7.34 (d, *J* = 3.1 Hz, 2H), 7.08 (d, *J* = 8.6 Hz, 2H), 6.87 (d, *J* = 8.6 Hz, 2H), 6.63 (d, *J* = 2.9 Hz, 2H), 5.35 (s, 2H), 3.80 (s, 3H), 3.46 (s, 3H) ppm. ¹³C NMR (151 MHz, CDCl₃) δ 165.98, 159.39, 135.72, 133.05, 132.39, 128.43, 128.24, 123.77, 121.35, 117.95, 114.37, 110.93, 102.31, 55.31, 49.86, 41.85 ppm. *m/z* calculated for C₁₈H₁₈N₂O₄S [M+H]⁺ 359.10, found 359.14. IR cm⁻¹: 733, 771, 808, 835, 866, 962, 1025, 1093, 1151, 1177, 1237, 1318, 1335, 1392, 1427, 1491, 1612, 1685, 2833, 2937, 3020, 3271.



Preparation of N-(N,N-dimethylsulfonyl)-1-(4-methoxybenzyl)-1H-indole-6-carboxamide (33):

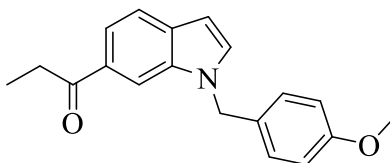
To a solution of 1-(4-methoxybenzyl)-1H-indole-6-carboxylic acid (60 mg, 0.213 mmol) in DCM (3 mL) in an ice bath was added methanesulfonamide (35 mg, 0.276 mmol), triethylamine (0.075 mL, 0.534 mmol), and DMAP (2.5 mg, 0.021 mmol). EDC HCl (36 mg, 0.234 mmol) was added to the solution and

the reaction was stirred on ice for 1 hour. The reaction was raised from the ice bath and stirred at room temperature overnight. The reaction was diluted with EtOAc (20 mL) and washed with 1 M HCl (2 mL), saturated NaHCO₃ solution (2 mL), and brine (2 mL). The organic phase was dried over Na₂SO₄, filtered, and concentrated under reduced pressure to provide crude product. The crude product was purified on a silica gel column (0-25% EtOAc in hexanes) to give 17 mg of N-(N,N-dimethylsulfamoyl)-1-(4-methoxybenzyl)-1H-indole-6-carboxamide (21%) as a pale amber solid. ¹H NMR (500 MHz, CDCl₃) δ 8.38 (s, 1H), 7.94 (s, 1H), 7.69 (d, *J* = 8.4 Hz, 1H), 7.43 (q, *J* = 3.3 Hz, 1H), 7.30 (d, *J* = 3.2 Hz, 1H), 7.06 (d, *J* = 8.7 Hz, 2H), 6.85 (d, *J* = 8.7 Hz, 2H), 6.60 (d, *J* = 2.7 Hz, 1H), 5.32 (s, 2H), 3.78 (s, 3H), 3.05 (s, 6H) ppm. ¹³C NMR (126 MHz, CDCl₃) δ 165.72, 159.39, 135.82, 132.70, 132.03, 128.54, 128.28, 124.22, 121.23, 117.86, 114.37, 110.71, 102.25, 55.31, 49.75, 38.42 ppm. *m/z* calculated for C₁₉H₂₁N₃O₄S [M]⁻ 386.13, found 386.1. IR cm⁻¹: 651, 708, 727, 767, 820, 872, 981, 1032, 1065, 1094, 1128, 1154, 1177, 1246, 1351, 1406, 1430, 1486, 1512, 1561, 1612, 1644, 2849, 2917, 3169.



Preparation of N-methoxy-1-(4-methoxybenzyl)-N-methyl-1H-indole-6-carboxamide:

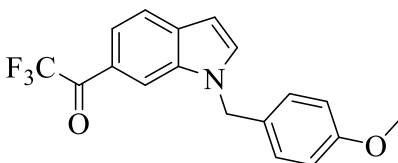
To a solution of methyl 1-(4-methoxybenzyl)-1H-indole-6-carboxylate (200 mg, 0.677 mmol) in THF (2 mL) in a -20°C bath was added N,O-dimethylhydroxylamine hydrochloride (102.4 mg, 1.05 mmol). 1 M iPrMgCl in MeTHF (2 mL) was added dropwise over 10 minutes. The reaction was allowed to warm to room temperature and stir for 30 minutes. The mixture was quenched with saturated NH₄Cl solution (2 mL) and diluted with EtOAc (10 mL). The organic phase was dried over Na₂SO₄, filtered, and concentrated under reduced pressure to provide crude product. The crude product was purified on a silica gel column (0-30% EtOAc in hexanes) to give 165 mg of N-methoxy-1-(4-methoxybenzyl)-N-methyl-1H-indole-6-carboxamide (75%) as a yellow oil. ¹H NMR (600 MHz, CDCl₃) δ 7.77 (s, 1H), 7.62 (d, *J* = 8.2 Hz, 1H), 7.47 (d, *J* = 8.2 Hz, 1H), 7.21 (d, *J* = 2.8 Hz, 1H), 7.08 (d, *J* = 8.4 Hz, 2H), 6.83 (d, *J* = 8.4 Hz, 2H), 6.55 (d, *J* = 2.5 Hz, 1H), 5.29 (s, 2H), 3.77 (s, 3H), 3.51 (s, 3H), 3.35 (s, 3H) ppm.



Preparation of 1-(1-(4-methoxybenzyl)-1H-indol-6-yl)propan-1-one (21):

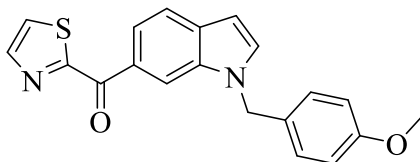
To a solution of N-methoxy-1-(4-methoxybenzyl)-N-methyl-1H-indole-6-carboxamide (30 mg, 0.092 mmol) in THF (1 mL) in an ice bath was added ethyl magnesium bromide (0.08 mL, 0.222 mmol). The reaction was raised to room temperature and stirred for 1 hour. The reaction was quenched with saturated NH₄Cl solution (1 mL) and diluted with EtOAc (10 mL). The organic phase was dried over Na₂SO₄, filtered, and concentrated under reduced pressure to provide crude product. The crude product was purified on a silica gel column (0-20% EtOAc in hexanes) to give 16 mg of 1-(1-(4-methoxybenzyl)-1H-indol-6-yl)propan-1-one (59%) as a pale-yellow oil. ¹H NMR (600 MHz, CDCl₃) δ 8.05 (s, 1H), 7.74 (d, *J* = 8.2 Hz, 1H), 7.65 (d, *J* = 8.3 Hz, 1H), 7.09 (d, *J* = 8.4 Hz, 2H), 6.84 (d, *J* = 8.4 Hz, 2H), 6.56 (d, *J* = 2.4 Hz,

1H), 5.32 (s, 2H), 3.78 (s, 3H), 3.05 (q, $J = 7.2$ Hz, 2H), 1.24 (t, $J = 7.3$ Hz, 3H + grease) ppm. ^{13}C NMR (126 MHz, CDCl_3) δ 201.00, 159.32, 135.91, 132.41, 131.59, 130.89, 128.91, 128.38, 120.54, 119.61, 114.30, 110.29, 101.94, 55.29, 49.72, 31.86, 8.68 ppm. m/z calculated for $\text{C}_{19}\text{H}_{19}\text{NO}_2$ $[\text{M}+\text{H}]^+$ 294.14, found 294.2. IR cm^{-1} : 640, 724, 754, 791, 821, 894, 915, 1029, 1171, 1234, 1302, 1316, 1350, 1454, 1512, 1605, 1673, 2905, 2933.



Preparation of 2,2,2-trifluoro-1-(1-(4-methoxybenzyl)-1H-indol-6-yl)ethan-1-one (22):

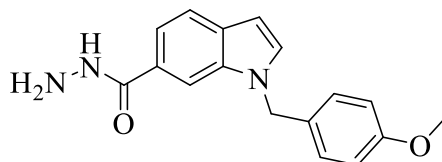
To a solution of N-methoxy-1-(4-methoxybenzyl)-N-methyl-1H-indole-6-carboxamide (30 mg, 0.092 mmol) in toluene (1 mL) stirred on ice was added CsF (6 mg, 0.036 mmol). The reaction was vented and TMS-CF_3 (27 μL , 0.185) was added. The reaction was stirred in an ice bath for 10 minutes. The solvent was removed under reduced pressure and the mixture was taken back up into THF (0.5 mL). 1 drop of water (20 μL) and 1M TBAF in THF (0.1 mL) was added and the reaction was refluxed for 2 hours. The solvent was removed under reduced pressure, diluted with EtOAc (20 mL) and washed with water (5 mL) and brine (5 mL). The organic phase was dried over Na_2SO_4 , filtered, and concentrated under reduced pressure to provide crude product. The crude product was purified on a silica gel column (0-20% EtOAc in hexanes) to give 25 mg of 2,2,2-trifluoro-1-(1-(4-methoxybenzyl)-1H-indol-6-yl)ethan-1-one (82%) as a yellow oil. ^1H NMR (600 MHz, CDCl_3) δ 8.13 (s, 1H), 7.81 (d, $J = 8.3$ Hz, 1H), 7.71 (d, $J = 8.4$ Hz, 1H), 7.38 (d, $J = 2.5$ Hz, 1H), 7.12 (d, $J = 8.3$ Hz, 2H), 6.86 (d, $J = 8.4$ Hz, 2H), 6.61 (d, $J = 2.0$ Hz, 1H), 5.33 (s, 2H), 3.78 (s, 3H) ppm. ^{13}C NMR (126 MHz, CDCl_3) δ 179.41 (q, $J = 33.7$ Hz, 1C), 158.47, 134.50, 133.43, 132.61, 127.54, 127.19, 122.26, 120.22, 119.85, 116.17 (q, $J = 291.6$ Hz, 1C), 113.37, 112.30, 101.52, 54.29, 49.02 ppm. ^{19}F (471 MHz, CDCl_3) δ -70.07 ppm. m/z calculated for $\text{C}_{18}\text{H}_{14}\text{F}_3\text{NO}_2$ $[\text{M}+\text{H}]^+$ 334.10, found 334.0. IR cm^{-1} : 733, 798, 884, 1020, 1086, 1136, 1259, 1466, 1513, 1609, 1698, 2853, 2924, 2962.



Preparation of 1-(1-(4-methoxybenzyl)-1H-indol-6-yl)(thiazol-2-yl)methanone (29):

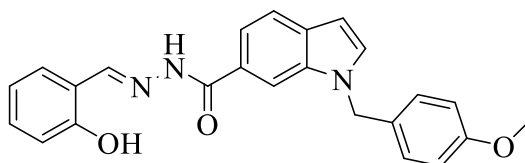
To a solution of N-methoxy-1-(4-methoxybenzyl)-N-methyl-1H-indole-6-carboxamide (30 mg, 0.092 mmol) in THF (1 mL) stirring in a -15°C bath was added 2-bromothiazole (0.01 mL, 0.115 mmol). Isopropyl magnesium chloride (0.36 mL, 0.115 mmol) was added dropwise to the solution. The reaction was aged in a -15°C bath for 30 minutes. The mixture was raised from the bath and stirred at room temperature overnight. The crude mixture was purified on a silica gel column (0-15% EtOAc in hexanes) to give 18 mg of 1-(1-(4-methoxybenzyl)-1H-indol-6-yl)(thiazol-2-yl)methanone (56%) as a bright orange solid. ^1H NMR (500 MHz, CDCl_3) δ 8.79 (s, 1H), 8.26 (dd, $J = 8.4, 1.4$ Hz, 1H), 8.08 (d, $J = 3.1$ Hz, 1H), 7.71 (d, $J = 8.5$ Hz, 1H), 7.68 (d, $J = 3.1$ Hz, 1H), 7.31 (d, $J = 3.1$ Hz, 1H), 7.15 (d, $J = 8.7$ Hz, 2H), 6.85 (d, $J = 8.7$ Hz, 2H), 6.58 (d, $J = 2.6$ Hz, 1H), 5.36 (s, 2H), 3.77 (s, 3H) ppm. ^{13}C NMR (126 MHz, CDCl_3) δ 183.75, 169.22, 159.32, 144.50, 135.72, 133.15, 132.20, 128.86, 128.65, 128.56, 125.48, 122.15, 120.64, 114.58,

114.27, 102.20, 55.29, 49.88 ppm. m/z calculated for $C_{20}H_{16}N_2O_2S$ $[M+H]^+$ 349.09, found 349.1. IR cm^{-1} : 612, 650, 682, 723, 759, 798, 819, 843, 878, 943, 1031, 1072, 1106, 1157, 1172, 1244, 1280, 1303, 1356, 1390, 1490, 1512, 1556, 1604, 1629, 2838, 2926, 2959, 3079, 3114.



Preparation of 1-(4-methoxybenzyl)-1H-indole-6-carbohydrazide:

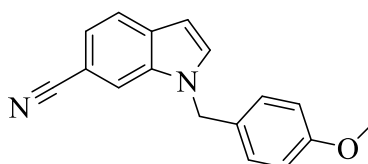
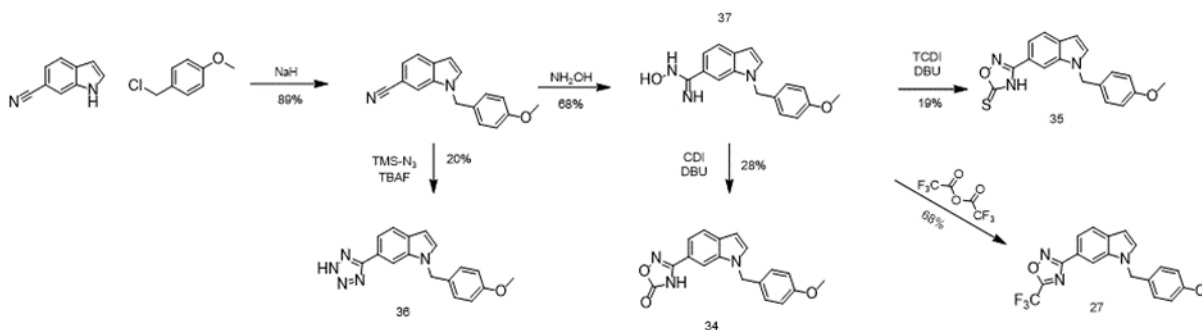
To a solution of methyl 1-(4-methoxybenzyl)-1H-indole-6-carboxylate (98.7 mg, .334 mmol) in EtOH (3 mL) was added hydrazine monohydrate (0.5 mL, 10.14 mmol). The reaction was heated to reflux, and the reaction stirred overnight. The mixture was filtered to give 61 mg of 1-(4-methoxybenzyl)-1H-indole-6-carbohydrazide (62%) and a pale-yellow solid that was used in the next step without further purification. 1H NMR (500 MHz, $CDCl_3$) δ 9.63 (bs, 1H), 8.04 (s, 1H), 7.63 (d, J = 3.1 Hz, 1H), 7.57 (d, J = 8.2 Hz, 1H), 7.53 (dd, J = 8.3, 1.4 Hz, 1H), 7.20 (d, J = 8.7 Hz, 2H), 6.88 (d, J = 8.8 Hz, 2H), 6.51 (d, J = 3.0 Hz, 1H), 5.36 (s, 2H), 4.44 (bs, 2H), 3.70 (s, 3H) ppm.



Preparation of N'-(2-hydroxybenzylidene)-1-(4-methoxybenzyl)-1H-indole-6-carbohydrazide (30):

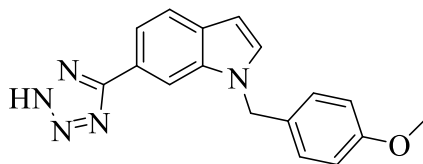
To a solution of salicylaldehyde (20.6 mg, .169 mmol) in ether (0.8 mL) was added 1-(4-methoxybenzyl)-1H-indole-6-carbohydrazide (40.6 mg, .137 mmol). MeOH and THF (0.8 mL and 0.4 mL respectively) were added to the mixture. The reaction was stirred at room temperature overnight. The crude mixture was purified with no further work-up on a silica gel column (0-40% EtOAc in hexanes) to give 42 mg of N'-(2-hydroxybenzylidene)-1-(4-methoxybenzyl)-1H-indole-6-carbohydrazide (78%) as an amber solid. 1H NMR (500 MHz, $CDCl_3$) δ 12.01 (s, 1H), 11.44 (s, 1H), 8.66 (s, 1H), 8.16 (s, 1H), 7.64-7.69 (m, 3H), 7.53 (d, J = 7.2 Hz, 1H), 7.31 (appt, J = 7.1 Hz, 1H), 7.20 (d, J = 8.6 Hz, 2H), 6.94 (appt, J = 8.8 Hz, 2H), 6.89 (d, J = 8.7 Hz, 2H), 6.58 (d, J = 2.6 Hz, 1H), 5.45 (s, 2H), 3.71 (s, 3H) ppm. ^{13}C NMR (126 MHz, $CDCl_3$) δ 159.31, 135.90, 131.93, 131.80, 131.31, 130.84, 128.73, 128.40, 125.44, 121.04, 119.33, 117.51, 117.25, 114.30, 110.70, 102.60, 55.29, 49.78 ppm. m/z calculated for $C_{24}H_{21}N_3O_3$ $[M+H]^+$ 400.16, found 400.2. IR cm^{-1} : 640, 662, 718, 754, 795, 828, 855, 923, 950, 1028, 1073, 1125, 1151, 1172, 1246, 1266, 1284, 1318, 1356, 1435, 1463, 1485, 1510, 1526, 1572, 1610, 1631, 2858, 2915, 2961, 3034, 3097, 3220.

Appendix Scheme 3 General scheme for nitrile analogs.



Preparation of 1-(4-methoxybenzyl)-1H-indole-6-carbonitrile:

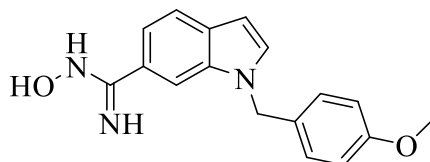
To a solution of 1H-indole-6-carbonitrile (1 g, 7.03 mmol) in acetonitrile (10 mL) stirred in an ice bath was added washed NaH (253 mg) as a slurry in acetonitrile (20 mL). The reaction mixture was aged in an ice bath for 30 minutes. 1-(chloromethyl)-4-methoxybenzene (1.4 mL) was added dropwise to the mixture and the reaction was raised from the ice bath and stirred at room temperature overnight. The reaction mixture was stirred in an ice bath and quenched with saturated NH_4Cl solution (10 mL). The mixture was diluted with EtOAc (50 mL). The organic phase was dried over Na_2SO_4 , filtered, and concentrated under reduced pressure to provide crude product. Product was purified on a silica gel column (0-20% EtOAc in hexanes) to give 1.75 g of 1-(4-methoxybenzyl)-1H-indole-6-carbonitrile (95%) as a pale orange solid. ^1H NMR (400 MHz, CDCl_3) δ 7.68 (d, J = 8.3 Hz, 1H), 7.62 (s, 1H), 7.31-7.33 (m, 2H), 7.06 (d, J = 8.7 Hz, 2H), 6.86 (d, J = 8.6 Hz, 2H), 6.59 (d, J = 3.0 Hz, 1H), 5.28 (s, 2H), 3.79 (s, 3H) ppm.



Preparation of 1-(4-methoxybenzyl)-6-(2H-tetrazol-5-yl)-1H-indole (36):

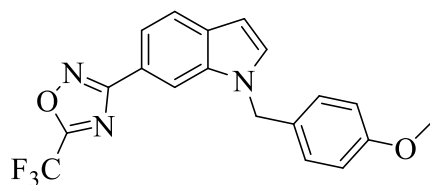
To a flask containing 1-(4-methoxybenzyl)-1H-indole-6-carbonitrile (65 mg, 0.248 mmol) was added TMS-N_3 (0.127 mL, 0.957 mmol) and 1M TBAF in THF (0.12 mL). The reaction was refluxed at 85°C for 4 hours. The mixture was diluted with EtOAc (20 mL) and was washed with 1M HCl solution (4 mL) and brine (4 mL). The organic phase was dried over Na_2SO_4 , filtered, and concentrated under reduced pressure to provide crude product. Product was purified on a silica gel column (0-70% EtOAc in hexanes) to give 15 mg of 1-(4-methoxybenzyl)-6-(2H-tetrazol-5-yl)-1H-indole (20%) as an off-white solid. ^1H NMR (600 MHz, DMSO) δ 8.20 (s, 1H), 7.75 (d, J = 8.2 Hz, 1H), 7.68-7.70 (m, 2H), 7.22 (d, J = 8.6 Hz, 2H), 6.88 (d, J = 8.6 Hz, 2H), 6.59 (d, J = 2.9 Hz, 1H), 5.44 (s, 2H), 3.69 (s, 3H) ppm. ^{13}C NMR (151 MHz, DMSO) δ

158.60, 135.35, 131.82, 130.40, 129.73, 128.40, 121.36, 117.78, 113.98, 109.15, 101.45, 55.01, 48.69 ppm. m/z calculated for $C_{17}H_{15}N_5O$ $[M+H]^+$ 306.13, found 306.2. IR cm^{-1} : 722, 740, 756, 813, 881, 1029, 1055, 1151, 1175, 1244, 1320, 1443, 1467, 1513, 1560, 1612, 2714, 2916, 3060.



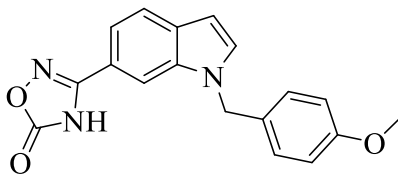
Preparation of N-hydroxy-1-(4-methoxybenzyl)-1H-indole-6-carboximidamide (37):

To a solution of 1-(4-methoxybenzyl)-1H-indole-6-carbonitrile (1 g, 3.81 mmol) in EtOH (4 mL) was added hydroxylamine 50% in water (0.5 mL) in a sealed tube. The reaction was stirred at 75°C overnight. The solvent was removed under reduced pressure to give crude product. The product was purified on a silica gel column (0-50% EtOAc in hexanes) to give 766 mg of N-hydroxy-1-(4-methoxybenzyl)-1H-indole-6-carboximidamide (68%) as a pale-yellow solid. 1H NMR (500 MHz, $CDCl_3$) δ 7.62-7.65 (m, 2H), 7.36 (q, J = 3.2 Hz, 1H), 7.16 (d, 3.1 Hz, 1H), 7.06 (d, J = 8.7 Hz, 2H), 6.83 (d, J = 8.7 Hz, 2H), 6.54 (q, J = 1.2 Hz, 1H), 5.27 (s, 2H), 4.87 (bs, 2H), 3.77 (s, 3H) ppm. ^{13}C NMR (126 MHz, $CDCl_3$) δ 159.22, 154.20, 136.04, 130.23, 129.72, 129.12, 128.31, 125.82, 121.09, 117.36, 114.26, 107.69, 101.75, 55.28, 49.59 ppm. m/z calculated for $C_{17}H_{17}N_3O_2$ $[M+H]^+$ 296.13, found 296.14. IR cm^{-1} : 646, 695, 725, 760, 814, 917, 940, 1026, 1175, 1242, 1304, 1315, 1356, 1371, 1439, 1462, 1510, 1583, 1610, 1633, 2835, 2931, 2964, 3096, 3361, 3484.



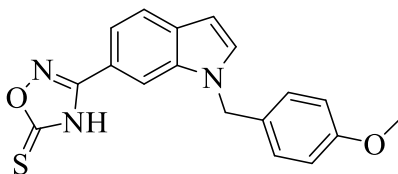
Preparation of 3-(1-(4-methoxybenzyl)-1H-indol-6-yl)-5-(trifluoromethyl)-1,2,4-oxadiazole (27):

To a solution of N-hydroxy-1-(4-methoxybenzyl)-1H-indole-6-carboximidamide (25 mg, 0.085 mmol) in THF (0.5 mL) stirring in an ice bath was added trifluoroacetic anhydride (24 μ L, 0.17 mmol). The reaction was raised from the bath and stirred at room temperature overnight. The mixture was diluted with EtOAc (10 mL) and washed with saturated $NaHCO_3$ solution (2 mL). The organic phase was dried over Na_2SO_4 , filtered, and concentrated under reduced pressure to provide crude product. Product was purified on a silica gel column (0-20% EtOAc in hexanes) to give 22 mg of 3-(1-(4-methoxybenzyl)-1H-indol-6-yl)-5-(trifluoromethyl)-1,2,4-oxadiazole (69%) as a yellow oil. 1H NMR (600 MHz, $CDCl_3$) δ 8.13 (s, 1H), 7.86 (d, J = 8.3 Hz, 1H), 7.74 (d, J = 8.3 Hz, 1H), 7.24 (d, J = 3.1 Hz, 1H), 7.10 (d, J = 8.5 Hz, 2H), 6.85 (d, J = 8.6 Hz, 2H), 6.60 (d, J = 2.9 Hz, 1H), 5.34 (s, 2H), 3.78 (s, 3H). ^{13}C NMR (151 MHz, $CDCl_3$) δ 170.21, 159.30, 136.00, 131.75, 130.93, 128.78, 128.34, 121.69, 118.68, 117.96, 114.28, 109.82, 102.32, 55.29, 49.66 ppm. ^{13}C NMR (126 MHz, $CDCl_3$) δ 170.22, 165.37 (q, J = 44.1 Hz, 1C), 159.33, 136.03, 131.78, 130.92, 128.79, 128.36, 121.69, 118.69, 117.99, 116.12 (q, J = 273.4 Hz, 1C), 114.30, 109.83, 102.33, 55.29, 49.68 ppm. ^{19}F NMR (471 MHz, $CDCl_3$) δ -65.39 ppm. m/z calculated for $C_{19}H_{14}F_3N_3O_2$ $[M+H]^+$ 374.10, found 374.0. IR cm^{-1} : 612, 632, 661, 713, 731, 755, 769, 817, 871, 947, 992, 1032, 1071, 1109, 1156, 1170, 1210, 1246, 1305, 1350, 1401, 1440, 1467, 1510, 1533, 1584, 1613, 1634, 2838, 2932, 2963, 2998, 3372, 3486.



Preparation of 3-(1-(4-methoxybenzyl)-1H-indol-6-yl)-1,2,4-oxadiazol-5(4H)-one (34):

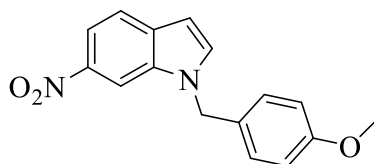
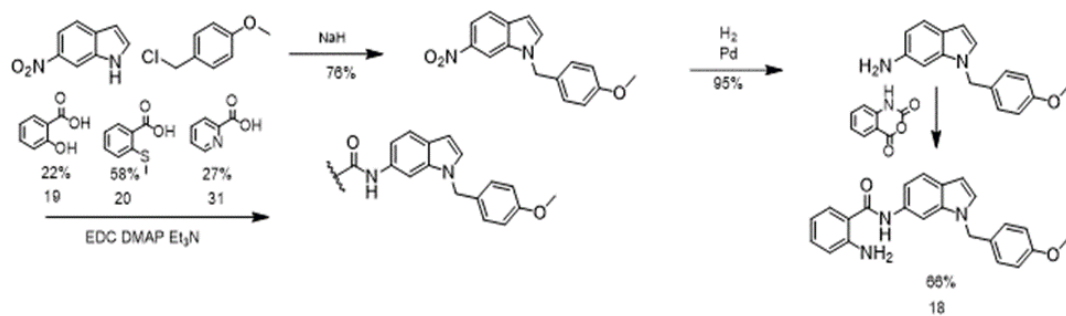
To a solution of N-hydroxy-1-(4-methoxybenzyl)-1H-indole-6-carboximidamide (60 mg, 0.203 mmol) in dioxane (8 mL) was added CDI (50 mg, 0.305 mmol) and DBU (50 μ L, 0.305 mmol). The reaction was heated to 100°C for 1 hour. The solvent was removed under reduced pressure, and the crude mixture was diluted with DCM (10 mL). The mixture was washed with 1M HCl twice (5 mL). The organic phase was dried over Na₂SO₄, filtered, and concentrated under reduced pressure to provide crude product. Product was purified on a silica gel column (0-70% EtOAc in hexanes) to give 18 mg of 3-(1-(4-methoxybenzyl)-1H-indol-6-yl)-1,2,4-oxadiazol-5(4H)-one (28%) as a brown solid. ¹H NMR (600 MHz, DMSO) δ 12.87 (s, 1H), 8.00 (s, 1H), 7.71-7.73 (m, 2H), 7.47 (d, *J* = 8.1 Hz, 1H), 7.23 (d, *J* = 8.4 Hz, 2H), 6.89 (d, *J* = 8.6 Hz, 2H), 6.59 (d, *J* = 2.6 Hz, 1H), 5.39 (s, 2H), 3.71 (s, 3H) ppm. ¹³C NMR (151 MHz, DMSO) δ 160.09, 158.64, 158.28, 134.97, 132.18, 130.95, 129.62, 128.50, 121.28, 116.39, 115.64, 113.97, 108.60, 101.65, 55.02, 48.68 ppm. *m/z* calculated for C₁₈H₁₅N₃O₃ [M]⁺ 320.11, found 320.1. IR cm⁻¹: 653, 686, 721, 758, 815, 877, 968, 1033, 1108, 1173, 1246, 1305, 1353, 1441, 1512, 1551, 1586, 1612, 1749, 1774, 2833, 2822, 3093.



Preparation of 3-(1-(4-methoxybenzyl)-1H-indol-6-yl)-1,2,4-oxadiazole-5(4H)-thione (35)

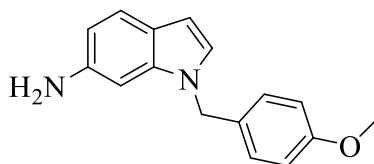
To a solution of N-hydroxy-1-(4-methoxybenzyl)-1H-indole-6-carboximidamide (50 mg, 0.17 mmol) in dioxane (2 mL) was added TCDI (51 mg, 0.255 mmol) and DBU (100 μ L, 0.677 mmol). The reaction was heated to 100°C for 2 hours. The solvent was removed under reduced pressure, and the crude mixture was diluted with DCM (10 mL). The mixture was washed with 1M HCl (5 mL), saturated NH₄Cl solution (5 mL), and brine (5 mL). The organic phase was dried over Na₂SO₄, filtered, and concentrated under reduced pressure to provide crude product. Product was purified on a silica gel column (0-70% EtOAc in hexanes) to give 11 mg of 3-(1-(4-methoxybenzyl)-1H-indol-6-yl)-1,2,4-oxadiazole-5(4H)-thione (19%) as a light brown solid. ¹H NMR (500 MHz, CDCl₃) δ 8.74 (s, 1H), 8.17 (s, 1H), 7.90 (dd, *J* = 8.2, 1.3 Hz, 1H), 7.75 (d, *J* = 8.3 Hz, 1H), 7.24 (d, *J* = 3.1 Hz, 1H), 7.12 (d, *J* = 8.7 Hz, 2H), 6.86 (d, *J* = 8.7 Hz, 2H), 6.61 (d, *J* = 3.1 Hz, 1H), 5.36 (s, 2H), 3.79 (s, 3H) ppm. ¹³C NMR (101 MHz, CDCl₃) δ 168.73, 164.32, 159.26, 136.11, 131.20, 130.40, 128.99, 128.33, 121.48, 119.45, 118.77, 114.27, 109.48, 102.16, 55.29, 49.63 ppm. *m/z* calculated for C₁₈H₁₅N₃O₂S [M]⁺ 336.09, found 336.1. IR cm⁻¹: 605, 665, 738, 758, 819, 871, 971, 1027, 1101, 1173, 1245, 1302, 1321, 1347, 1440, 1510, 1529, 1583, 1611, 1634, 2837, 2926, 2957, 3105, 3138, 3188.

Appendix Scheme 4 General synthesis for amine analogs.



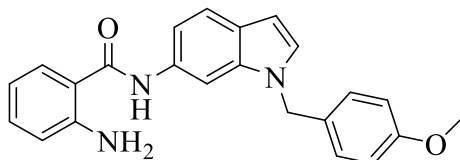
Preparation of 1-(4-methoxybenzyl)-6-nitro-1H-indole:

To a solution of 1H-indole-6-carbonitrile (500 g, 3.08 mmol) in acetonitrile (10 mL) stirred in an ice bath was added washed NaH (111 mg) as a slurry in acetonitrile (5 mL). The reaction mixture was aged in an ice bath for 30 minutes. 1-(chloromethyl)-4-methoxybenzene (0.62 mL) was added dropwise to the mixture and the reaction was raised from the ice bath and stirred at room temperature overnight. The reaction mixture was stirred in an ice bath and quenched with saturated NH_4Cl solution (10 mL). The mixture was diluted with EtOAc (50 mL). The organic phase was dried over Na_2SO_4 , filtered, and concentrated under reduced pressure to provide crude product. The product was purified on a silica gel column (0-20% EtOAc in hexanes) to give 689 g of 1-(4-methoxybenzyl)-6-nitro-1H-indole (80%) as a yellow solid. ^1H NMR (500 MHz, CDCl_3) δ 8.31 (d, J = 1.7 Hz, 1H), 8.01 (q, J = 3.6 Hz, 1H), 7.67 (d, J = 8.8 Hz, 1H), 7.38 (d, J = 3.1 Hz, 1H), 7.10 (d, J = 8.6 Hz, 2H), 6.86 (d, J = 8.7 Hz, 2H), 6.63 (d, J = 2.9 Hz, 1H), 5.33 (s, 2H), 3.79 (s, 3H) ppm.



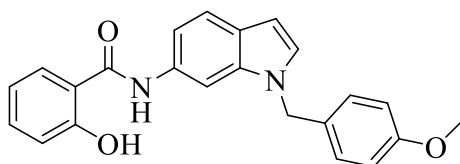
Preparation of 1-(4-methoxybenzyl)-1H-indol-6-amine:

To a solution of 1-(4-methoxybenzyl)-6-nitro-1H-indole (70 mg, 0.248 mmol) in methanol (8 mL) was added 10% Pd on C (27 mg, 0.025 mmol). The reaction was stirred under a hydrogen atmosphere at room temperature overnight. The mixture was filtered through celite and concentrated to give 52 mg of 1-(4-methoxybenzyl)-1H-indol-6-amine (83%) as a brown solid. ^1H NMR (600 MHz, CDCl_3) δ 7.40 (d, J = 7.8 Hz, 1H), 7.05 (d, J = 8.7 Hz, 2H), 6.91 (d, J = 3.2 Hz, 1H), 6.82 (d, J = 8.7 Hz, 2H), 6.56 (m, 2H), 6.40 (d, J = 3.1 Hz, 1H), 5.14 (s, 2H), 3.77 (s, 3H), 3.59 (bs, 2H) ppm.



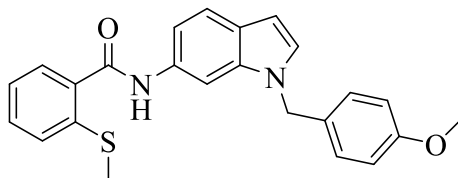
Preparation of 2-amino-N-(1-(4-methoxybenzyl)-1H-indol-6-yl)benzamide (18):

To a solution of 1-(4-methoxybenzyl)-1H-indol-6-amine (30 mg, 0.119 mmol) in toluene (1 mL) was added isatoic anhydride (19.4 mg, 0.119 mmol). DMF (0.1 mL) was added to improve solubility. The mixture was heated to reflux and stirred overnight. The solvent was evaporated under reduced pressure to give crude product. The crude product was purified on a silica gel column (0-25% EtOAc in hexanes) to give 29 mg of 2-amino-N-(1-(4-methoxybenzyl)-1H-indol-6-yl)benzamide (66%) as a pale brown solid. ¹H NMR (500 MHz, CDCl₃) δ 7.92 (bs, 1H), 7.80 (bs, 1H), 7.58 (d, *J* = 8.3 Hz, 1H), 7.48 (dd, *J* = 8.2, 1.3 Hz, 1H), 7.24 (d, *J* = 8.9 Hz, 1H), 7.10 (d, *J* = 8.6 Hz, 2H), 7.08 (d, *J* = 3.2 Hz, 1H), 7.02 (dd, *J* = 8.4, 1.8 Hz, 1H), 6.84 (d, *J* = 8.7 Hz, 2H), 6.720-6.73 (m, 2H), 6.50 (d, *J* = 2.8 Hz, 1H), 5.48 (bs, 2H), 5.26 (s, 2H), 3.77 (s, 3H) ppm. ¹³C NMR (126 MHz, CDCl₃) δ 167.37, 159.13, 136.41, 132.52, 132.37, 130.65, 129.37, 128.39, 127.16, 125.96, 121.13, 117.91, 117.45, 114.19, 113.78, 102.26, 101.61, 55.28, 49.53 ppm. *m/z* calculated for C₂₃H₂₁N₃O₂ [M+H]⁺ 372.16, found 372.3. IR cm⁻¹: 627, 661, 686, 745, 805, 959, 1032, 1109, 1151, 1173, 1240, 1281, 1304, 1392, 1439, 1485, 1509, 1523, 1578, 1617, 1639, 2832, 2921, 3294, 3415.



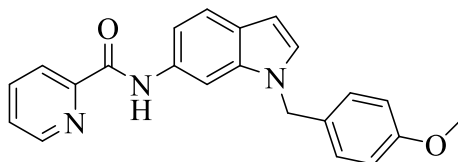
Preparation of 2-hydroxy-N-(1-(4-methoxybenzyl)-1H-indol-6-yl)benzamide (19)

To a solution of EDC HCl (50 mg, 0.258 mmol) in DCM (3 mL) was added DMAP (58.2 mg, 0.476 mmol). The mixture was stirred at room temperature for 5 minutes. The mixture was stirred in an ice bath, and salicylic acid (29.3 mg, 0.212 mmol) was added. The reaction was stirred for 15 minutes in an ice bath. 1-(4-methoxybenzyl)-1H-indol-6-amine (51 mg, 0.202 mmol) was added, and the reaction was stirred at room temperature overnight. The reaction was quenched with 1 M HCl until the pH was roughly 1, and the mixture was diluted with DCM (10 mL). The organic layer was washed with saturated NH₄Cl solution (5 mL), washed with brine (5 mL), collected, dried over Na₂SO₄, filtered, and concentrated to give crude product. The crude product was purified on a silica gel column (0-20% EtOAc in hexanes) to give 37 mg of 2-hydroxy-N-(1-(4-methoxybenzyl)-1H-indol-6-yl)benzamide (50%) as a pale-yellow solid. ¹H NMR (500 MHz, CDCl₃) δ 7.98 (bs, 1H), 7.87 (s, 1H), 7.62 (d, *J* = 8.3 Hz, 1H), 7.52 (d, *J* = 6.7 Hz, 1H), 7.42-7.47 (m, 1H), 7.10-7.13 (m, 3H), 7.05 (appt, *J* = 8.1 Hz, 2H), 6.92 (appt, *J* = 8.1 Hz, 1H), 6.85 (d, *J* = 8.7 Hz, 2H), 6.52 (d, *J* = 3.2 Hz, 1H), 5.27 (s, 2H), 3.78 (s, 3H) ppm. ¹³C NMR (126 MHz, CDCl₃) δ 168.22, 161.87, 159.19, 136.28, 134.43, 131.03, 129.18, 128.86, 128.38, 126.55, 125.24, 121.29, 118.93, 118.85, 114.84, 114.23, 114.10, 103.11, 101.68, 55.28, 49.67 ppm. *m/z* calculated for C₂₃H₂₀N₂O₃ [M+H]⁺ 373.15, found 373.1. IR cm⁻¹: 621, 668, 710, 740, 793, 813, 851, 955, 1034, 1096, 1159, 1174, 1192, 1234, 1303, 1363, 1456, 1511, 1547, 1586, 1609, 2698, 2832, 2905, 2935, 3032, 3317, 3375.



Preparation of N-(1-(4-methoxybenzyl)-1H-indol-6-yl)-2-(methylthio)benzamide (20):

To a solution of EDC HCl (27.6 mg, 0.144 mmol) in DCM (1 mL) was added DMAP (32.5 mg, 0.266 mmol). The mixture was stirred at room temperature for 5 minutes. The mixture was stirred in an ice bath, and 2-(methylthio)benzoic acid (18.5 mg, 0.11 mmol) was added. The reaction was stirred for 15 minutes in an ice bath. 1-(4-methoxybenzyl)-1H-indol-6-amine (28 mg, 0.11 mmol) was added, and the reaction was stirred at room temperature overnight. The reaction was quenched with 1 M HCl until the pH was roughly 1, and the mixture was diluted with DCM (10 mL). The organic layer was washed with brine twice (5 mL), collected, dried over Na₂SO₄, filtered, and concentrated to give crude product. The crude product was purified on a silica gel column (0-30% EtOAc in hexanes) to give 26 mg of N-(1-(4-methoxybenzyl)-1H-indol-6-yl)-2-(methylthio)benzamide (58%) as a white solid. ¹H NMR (500 MHz, CDCl₃) δ 8.37 (bs, 1H), 8.19 (s, 1H), 7.75 (d, *J* = 7.6, 1H), 7.57 (d, *J* = 8.4 Hz, 1H), 7.38-7.43 (m, 2H), 7.29 (d, *J* = 6.7 Hz, 1H), 7.12 (d, *J* = 8.5 Hz, 2H), 7.08 (d, *J* = 3.1 Hz, 1H), 7.00 (d, *J* = 6.8 Hz, 1H), 6.84 (d, *J* = 8.7 Hz, 2H), 6.49 (d, *J* = 2.7 Hz, 1H), 5.27 (s, 2H), 3.77 (s, 3H), 2.49 (s, 3H) ppm. ¹³C NMR (126 MHz, CDCl₃) δ 159.12, 136.52, 136.46, 135.66, 132.63, 130.90, 129.41, 129.18, 128.53, 128.29, 128.21, 125.84, 121.07, 114.18, 112.97, 101.60, 55.28, 49.49, 17.10 ppm. *m/z* calculated for C₂₄H₂₂N₂O₂S [M+H]⁺ 403.14, found 403.0. IR cm⁻¹: 620, 687, 726, 780, 812, 857, 957, 1029, 1057, 1110, 1168, 1248, 1274, 1302, 1408, 1432, 1464, 1488, 1513, 1546, 1588, 1619, 1638, 1651, 2833, 2917, 2959, 2991, 3032, 3076, 3124, 3261.

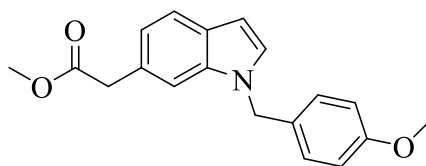
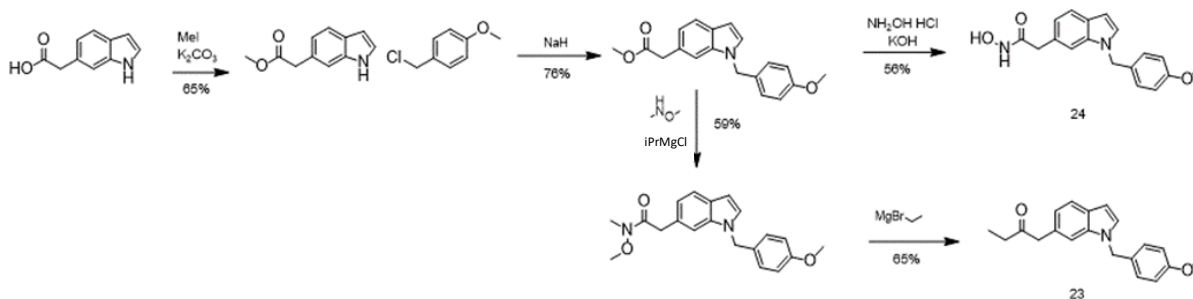


Preparation of N-(1-(4-methoxybenzyl)-1H-indol-6-yl)picolinamide (31):

To a solution of EDC HCl (50 mg, 0.258 mmol) in DCM (3 mL) was added DMAP (58.2 mg, 0.476 mmol). The mixture was stirred at room temperature for 5 minutes. The mixture was stirred in an ice bath, and picolinic acid (25.2 mg, 0.204 mmol) was added. The reaction was stirred for 15 minutes in an ice bath. 1-(4-methoxybenzyl)-1H-indol-6-amine (50 mg, 0.198 mmol) was added, and the reaction was stirred at room temperature overnight. The reaction was quenched with saturated NH₄Cl solution (2 mL), and the mixture was diluted with DCM (10 mL). The organic layer was washed with brine (5 mL), collected, dried over Na₂SO₄, filtered, and concentrated to give crude product. The crude product was purified on a silica gel column (0-20% EtOAc in hexanes) to give 19 mg of N-(1-(4-methoxybenzyl)-1H-indol-6-yl)picolinamide (27%) as a pale brown solid. ¹H NMR (400 MHz, CDCl₃) δ 10.10 (bs, 1H), 8.62 (d, *J* = 5.6 Hz, 1H), 8.28-8.32 (m, 2H), 7.91 (appt, *J* = 7.0 Hz, 1H), 7.60 (d, *J* = 8.1 Hz, 1H), 7.47-7.52 (m, 1H), 7.20 (d, *J* = 1.6 Hz, 1H plus CHCl₃), 7.12 (d, *J* = 8.5 Hz, 2H), 7.08 (d, *J* = 3.0 Hz, 1H), 6.84 (d, *J* = 8.7 Hz, 2H), 6.50 (d, *J* = 3.0 Hz, 1H), 5.28 (s, 2H), 3.77 (s, 3H) ppm. ¹³C NMR (126 MHz, CDCl₃) δ 161.69, 159.11, 150.14, 147.88, 137.72, 136.50, 132.56, 129.46, 128.43, 128.23, 126.23, 125.67, 122.27, 121.11, 114.19, 113.02, 101.65, 101.08, 55.27, 49.46 ppm. *m/z* calculated for C₂₂H₁₉N₃O₂ [M+H]⁺ 358.15, found 358.2. IR cm⁻¹: 620, 671,

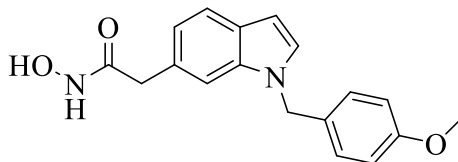
724, 747, 805, 853, 925, 953, 994, 1027, 1107, 1173, 1245, 1290, 1323, 1351, 1431, 1458, 1494, 1511, 1527, 1576, 1612, 1669, 2844, 2923, 2965, 3061, 3338.

Appendix Scheme 5 General synthesis for methyl acetate analogs.



Preparation of methyl 2-(1-(4-methoxybenzyl)-1H-indol-6-yl)acetate:

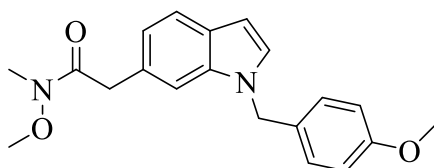
To a solution of methyl 2-(1H-indol-6-yl)acetate (800 mg, 4.23 mmol) in DMF (12 mL) was added 1-(chloromethyl)-4-methoxybenzene (0.57 mL, 4.23 mmol) dropwise. K_2CO_3 (1.17 g, 8.46 mmol) was added, and the reaction was stirred in an 80°C bath overnight. The reaction was quenched with 4 N HCl until pH \sim 7. The aqueous layer was extracted with DCM twice (30 mL). The organic layers were collected, dried over Na_2SO_4 , filtered, and concentrated to give crude product. The crude product was purified on a silica gel column (0-20% EtOAc in hexanes) to give 580 mg of methyl 2-(1-(4-methoxybenzyl)-1H-indol-6-yl)acetate (44%) as an orange oil. 1H NMR (500 MHz, $CDCl_3$) δ 7.57 (d, J = 8.1 Hz, 1H), 7.22 (s, 1H), 7.06-7.08 (m, 3H), 7.02 (dd, J = 8.1, 1.4 Hz, 1H), 6.83 (d, J = 8.7 Hz, 2H), 6.49 (d, J = 2.6 Hz, 1H), 5.24 (s, 2H), 3.77 (s, 3H), 3.70 (s, 2H), 3.66 (s, 3H) ppm.



Preparation of N-hydroxy-2-(1-(4-methoxybenzyl)-1H-indol-6-yl)acetamide (24):

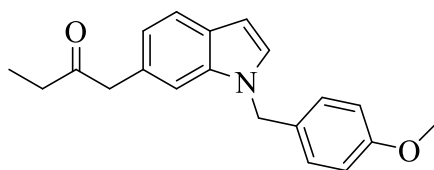
To a solution of NH_2OH HCl (449 mg, 6.46 mmol) in MeOH (3 mL) stirred in an ice bath was added KOH (453 mg, 8.08 mmol). The mixture was stirred in an ice bath for 1 hour. The mixture was filtered and added to a solution methyl 2-(1-(4-methoxybenzyl)-1H-indol-6-yl)acetate (95.6 mg, .309 mmol) in MeOH (2 mL). The reaction was stirred at room temperature for 2 hours. The reaction was quenched with 4N HCl until pH \sim 7. The cloudy solution was extracted with EtOAc twice (30 mL). The organic phase was dried over Na_2SO_4 , filtered, and concentrated under reduced pressure to give 56 mg of N-hydroxy-2-(1-(4-methoxybenzyl)-1H-indol-6-yl)acetamide (56%) as a yellow solid without further purification. 1H NMR (500 MHz, DMSO) δ 10.59 (bs, 1H), 8.75 (bs, 1H), 7.46 (d, J = 8.1 Hz, 1H), 7.40 (d, J = 3.2 Hz, 1H), 7.34 (s,

1H), 7.15 (d, $J = 8.5$ Hz, 2H), 6.93 (d, $J = 8.0$ Hz, 1H), 6.87 (d, $J = 8.6$ Hz, 2H), 6.42 (d, $J = 3.0$ Hz, 1H), 5.30 (s, 2H), 3.71 (s, 3H), 3.33 (s, 2H plus water) ppm. ^{13}C NMR (101 MHz, CDCl_3) δ 159.23, 136.50, 129.03, 128.91, 128.67, 128.35, 128.25, 125.75, 121.76, 120.89, 114.25, 110.66, 101.60, 55.29, 49.64, 40.97 ppm. m/z calculated for $\text{C}_{18}\text{H}_{18}\text{N}_2\text{O}_3$ [M] $^+$ 309.13, found 309.1. IR cm^{-1} : 608, 662, 714, 757, 818, 872, 974, 992, 1033, 1155, 1210, 1246, 1305, 1350, 1402, 1441, 1469, 1510, 1533, 1584, 1613, 1633, 2838, 2904, 2997, 3167.



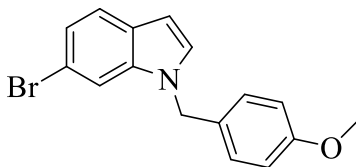
Preparation of N-methoxy-2-(1-(4-methoxybenzyl)-1H-indol-6-yl)-N-methylacetamide:

To a solution of methyl 2-(1-(4-methoxybenzyl)-1H-indol-6-yl)acetate (101.2 mg, 0.327 mmol) in THF (2 mL) was added N,O-Dimethylhydroxylamine hydrochloride (50.4 mg, 0.517 mmol). The mixture was stirred in a -30°C bath. Isopropyl magnesium chloride (0.5 mL, 1.0 mmol) was added dropwise to the solution and the mixture was raised from the bath to stir at room temperature for 30 minutes. The mixture was quenched with saturated NH_4Cl solution (5 mL), and the aqueous layer was extracted twice with EtOAc (20 mL). The organic layers were collected, dried over Na_2SO_4 , filtered, and concentrated to give crude product. The crude product was purified on a silica gel column (0-35% EtOAc in hexanes) to give 64 mg of N-methoxy-2-(1-(4-methoxybenzyl)-1H-indol-6-yl)-N-methylacetamide (59%) as a brown oil. ^1H NMR (500 MHz, CDCl_3) δ 7.49 (d, $J = 8.1$ Hz, 1H), 7.18 (s, 1H), 6.96-7.00 (m, 4H), 6.75 (d, $J = 8.7$ Hz, 2H), 6.41 (d, $J = 2.8$ Hz, 1H), 5.17 (s, 2H), 3.78 (bs, 2H), 3.70 (s, 3H), 3.41 (bs, 3H), 3.09 (s, 3H) ppm.



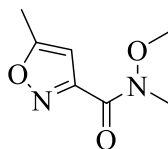
Preparation of 1-(1-(4-methoxybenzyl)-1H-indol-6-yl)butan-2-one (23):

To a solution of N-methoxy-2-(1-(4-methoxybenzyl)-1H-indol-6-yl)-N-methylacetamide (30 mg, 0.089 mmol) in THF (1 mL) stirred in a -20°C bath was added ethyl magnesium bromide (0.1 mL, 0.3 mmol) dropwise. The reaction was aged in an -20°C bath for 30 minutes. The reaction was quenched with saturated NH_4Cl solution (2 mL), and the aqueous layer was extracted with EtOAc twice (20 mL). The organic layers were collected, dried over Na_2SO_4 , filtered, and concentrated to give crude product. The crude product was purified on a silica gel column (0-20% EtOAc) to give 17 mg of 1-(1-(4-methoxybenzyl)-1H-indol-6-yl)butan-2-one (65%) as a clear oil. ^1H NMR (500 MHz, CDCl_3) δ 7.58 (d, $J = 8.1$ Hz, 1H), 7.13 (s, 1H), 7.05-7.08 (m, 3H), 6.95 (dd, $J = 8.1, 1.2$ Hz, 1H), 6.83 (d, $J = 8.7$ Hz, 2H), 6.50 (d, $J = 3.1$ Hz, 1H), 5.23 (s, 2H), 3.77 (s, 3H), 3.74 (s, 2H), 2.43 (q, $J = 7.3$ Hz, 2H), 0.97 (t, $J = 7.3$ Hz, 3H) ppm. ^{13}C NMR (126 MHz, CDCl_3) δ 159.17, 136.63, 129.34, 128.29, 128.25, 128.00, 127.76, 121.20, 121.16, 114.18, 110.28, 101.48, 55.28, 50.50, 49.54, 34.76, 7.81 ppm. m/z calculated for $\text{C}_{20}\text{H}_{21}\text{NO}_2$ [M+H] $^+$ 308.16, found 308.2. IR cm^{-1} : 614, 659, 718, 761, 799, 813, 943, 1030, 1107, 1175, 1244, 1304, 1318, 1346, 1462, 1511, 1585, 1612, 1706, 2835, 2934, 2971.



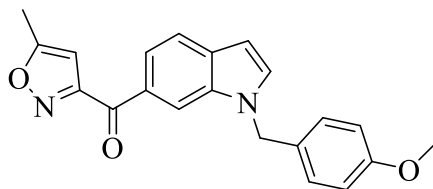
Preparation of 6-bromo-1-(4-methoxybenzyl)-1H-indole:

To a solution of 6-bromo-1H-indole (2.0 g, 10.2 mmol) in DMF (20 mL) stirred in an ice bath was added 60% NaH in mineral oil (800 mg, 20.4 mmol). The mixture was stirred in an ice bath for 30 minutes. 1-(chloromethyl)-4-methoxybenzene (1.5 mL, 15.3 mmol) was added dropwise and the reaction was stirred at room temperature overnight. The reaction was quenched with saturated NH₄Cl solution (10 mL), and the aqueous layer was extracted with EtOAc twice (30 mL). The organic layers were collected, dried over Na₂SO₄, filtered, and concentrated to give crude product. The crude product was purified on a silica gel column (0-5% EtOAc in hexanes) to give 2.75 g of 6-bromo-1-(4-methoxybenzyl)-1H-indole (85%) as a dark amber oil. ¹H NMR (500 MHz, CDCl₃) δ 7.49 (d, *J* = 8.4 Hz, 1H), 7.45 (s, 1H), 7.19 (dd, *J* = 8.4, 1.5 Hz, 1H), 7.07 (d, *J* = 3.2 Hz, 1H), 7.05 (d, *J* = 8.6 Hz, 2H), 6.84 (d, *J* = 8.6 Hz, 2H), 6.50 (d, *J* = 3.0 Hz, 1H), 5.21 (s, 2H), 3.78 (s, 3H) ppm.



Preparation of N-methoxy-N,5-dimethylisoxazole-3-carboxamide:

To a solution of EDC HCl (393 mg, 2.05 mmol) in DCM (3 mL) was added DMAP (654 mg, 5.35 mmol). The mixture was stirred at room temperature for 5 minutes. The mixture was stirred in an ice bath, and 5-methylisoxazole-3-carboxylic acid (200 mg, 1.57 mmol) was added. The reaction was stirred for 15 minutes in an ice bath. N,O-Dimethylhydroxylamine hydrochloride (153 mg, 1.57 mmol) was added, and the reaction was stirred at room temperature overnight. The reaction was quenched with saturated NH₄Cl solution (2 mL), and the mixture was diluted with DCM (10 mL). The aqueous layer was further extracted with DCM (10 mL). The organic layers were collected, dried over Na₂SO₄, filtered, and concentrated to give crude product. The crude product was purified on a silica gel column (0-30% EtOAc in hexanes) to give 191 mg of N-methoxy-N,5-dimethylisoxazole-3-carboxamide (71%) as a clear oil. ¹H NMR (500 MHz, CDCl₃) δ 6.32 (s, 1H), 3.79 (s, 3H), 3.39 (bs, 3H), 2.48 (s, 3H) ppm.



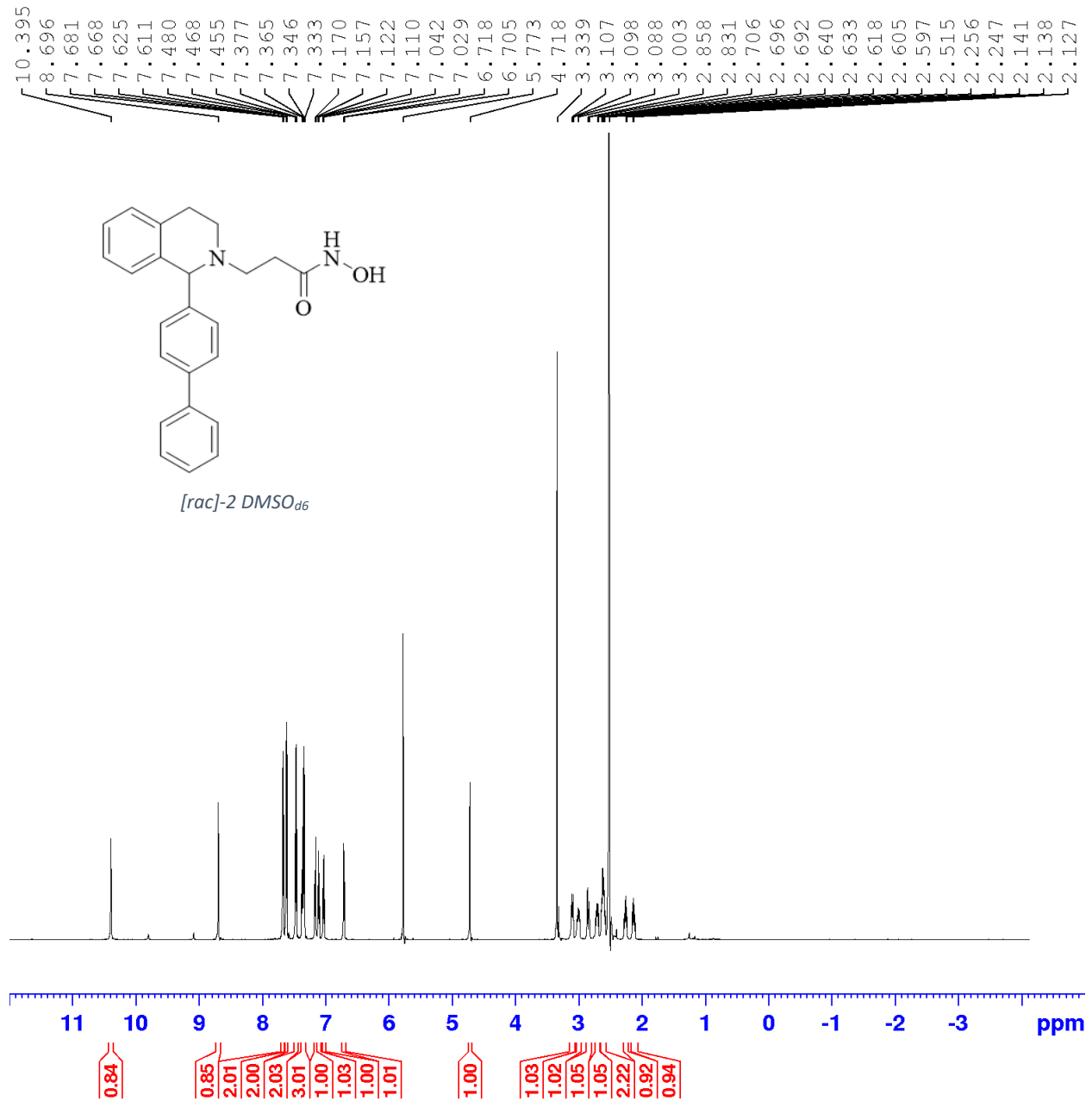
Preparation of (1-(4-methoxybenzyl)-1H-indol-6-yl)(5-methylisoxazol-3-yl)methanone (28):

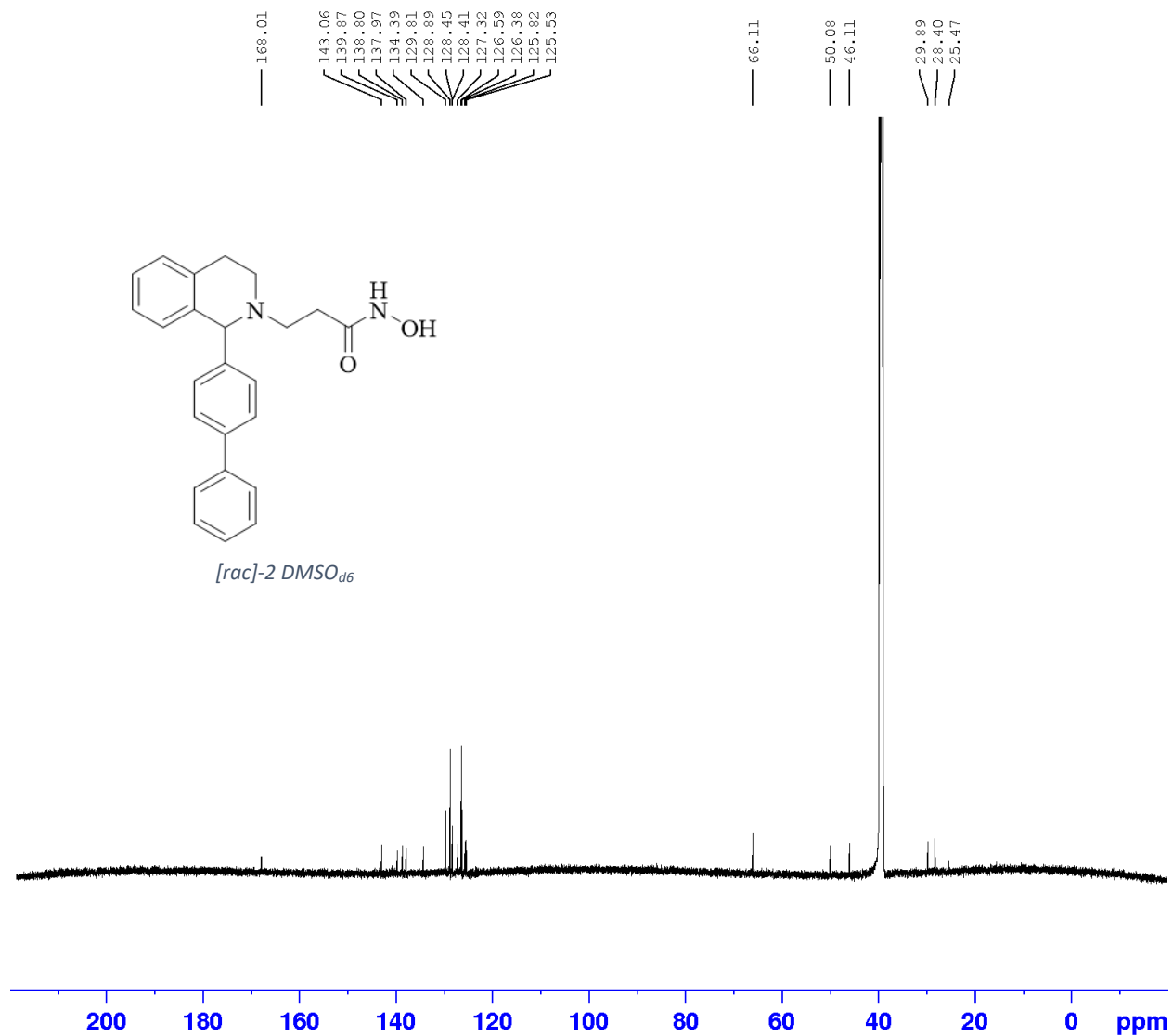
To a solution of 6-bromo-1-(4-methoxybenzyl)-1H-indole (167 mg, 0.528 mmol) in ether (5 mL) stirred in a -78°C bath was added t-butyl lithium in hexanes (0.66 mL, 1.06 mmol) dropwise. The reaction was stirred in a -78°C bath for 30 minutes. A solution of N-methoxy-N,5-dimethylisoxazole-3-carboxamide

(30 mg, 0.176 mmol) in ether (1 mL) was added drop wise and the reaction stirred in a -78°C bath for 30 minutes. The reaction was quenched with 1 M phosphoric acid (2 mL). The mixture was diluted with EtOAc (20 mL) and washed with saturated NaHCO₃ solution (2 mL). The aqueous layer was further extracted with EtOAc (20 mL). The organic layers were collected, dried over Na₂SO₄, filtered, and concentrated to give crude product. The crude product was purified on a silica gel column (0-15% EtOAc in hexanes) to give 10 mg of (1-(4-methoxybenzyl)-1H-indol-6-yl)(5-methylisoxazol-3-yl)methanone (16%) as a yellow oil. ¹H NMR (500 MHz, CDCl₃) δ 8.48 (s, 1H), 8.04 (dd, *J* = 8.4, 1.4 Hz, 1H), 7.70 (d, *J* = 8.4 Hz, 1H), 7.30 (d, *J* = 3.1 Hz, 1H), 7.12 (d, *J* = 8.7 Hz, 2H), 6.85 (d, *J* = 8.7 Hz, 2H), 6.58 (d, *J* = 3.1 Hz, 1H), 6.49 (s, 1H), 5.33 (s, 2H), 3.77 (s, 3H), 2.53 (s, 3H) ppm. ¹³C NMR (126 MHz, CDCl₃) δ 185.84, 169.84, 162.69, 159.34, 135.70, 133.35, 132.32, 129.48, 128.76, 128.62, 121.65, 120.77, 114.29, 113.95, 102.79, 102.24, 55.29, 49.80, 12.21 ppm. *m/z* calculated for C₂₁H₁₈N₂O₃ [M+H]⁺ 347.13, found 347.2. IR cm⁻¹: 603, 630, 657, 678, 727, 761, 773, 821, 861, 909, 953, 1030, 1080, 1124, 1175, 1191, 1245, 1271, 1318, 1355, 1445, 1496, 1512, 1559, 1602, 1646, 2851, 2922, 2955.

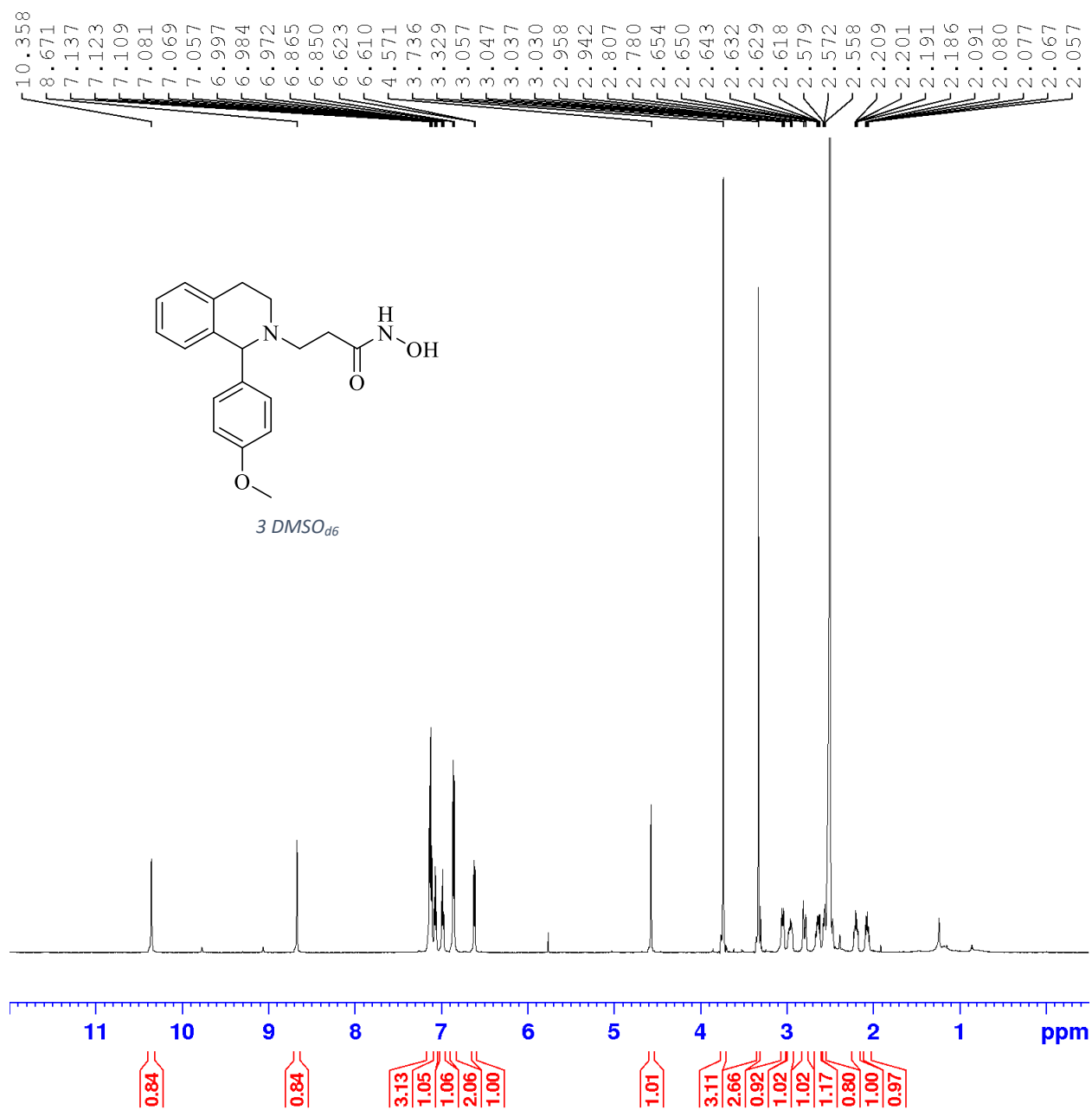
Spectra

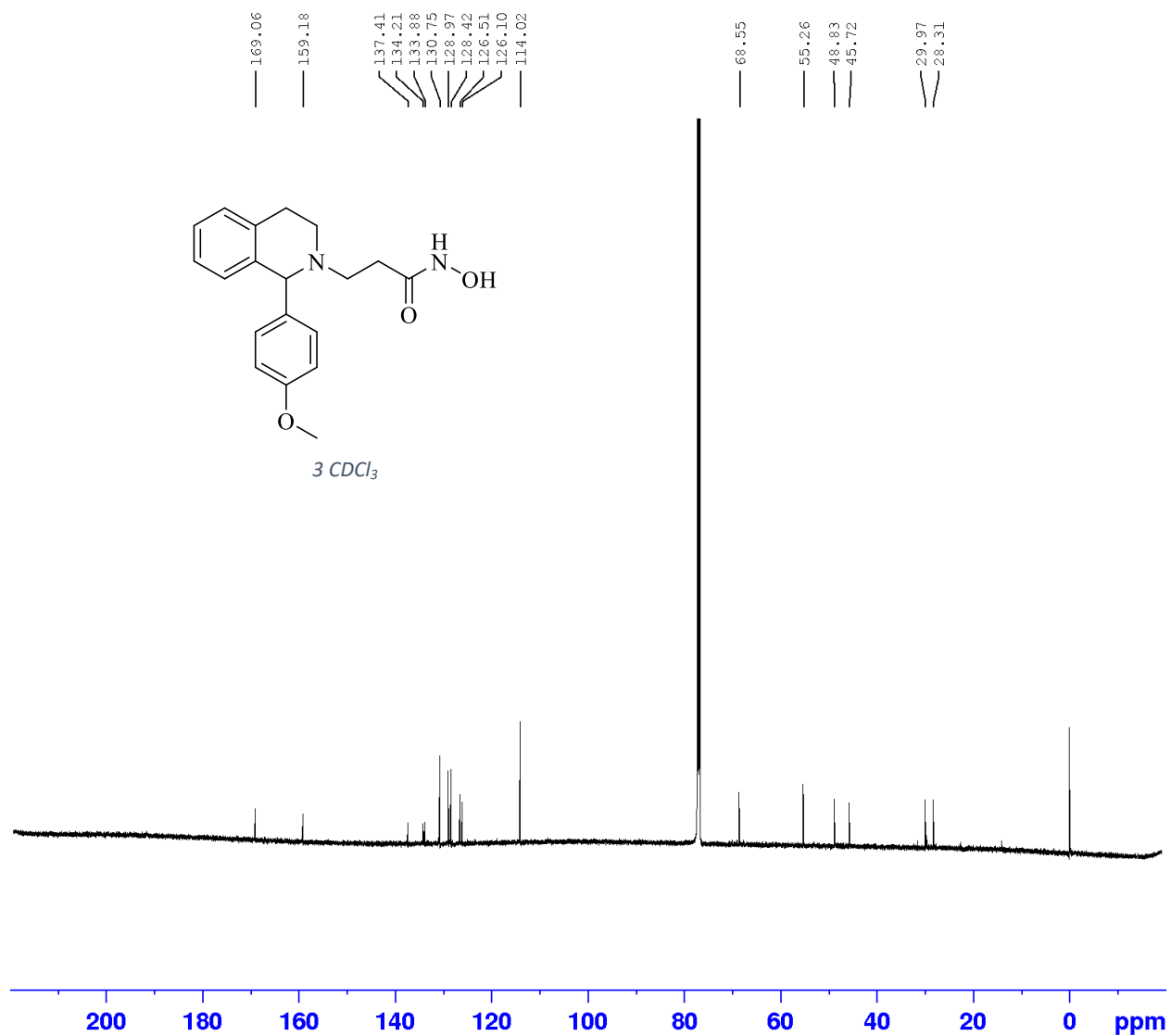
[rac]-2

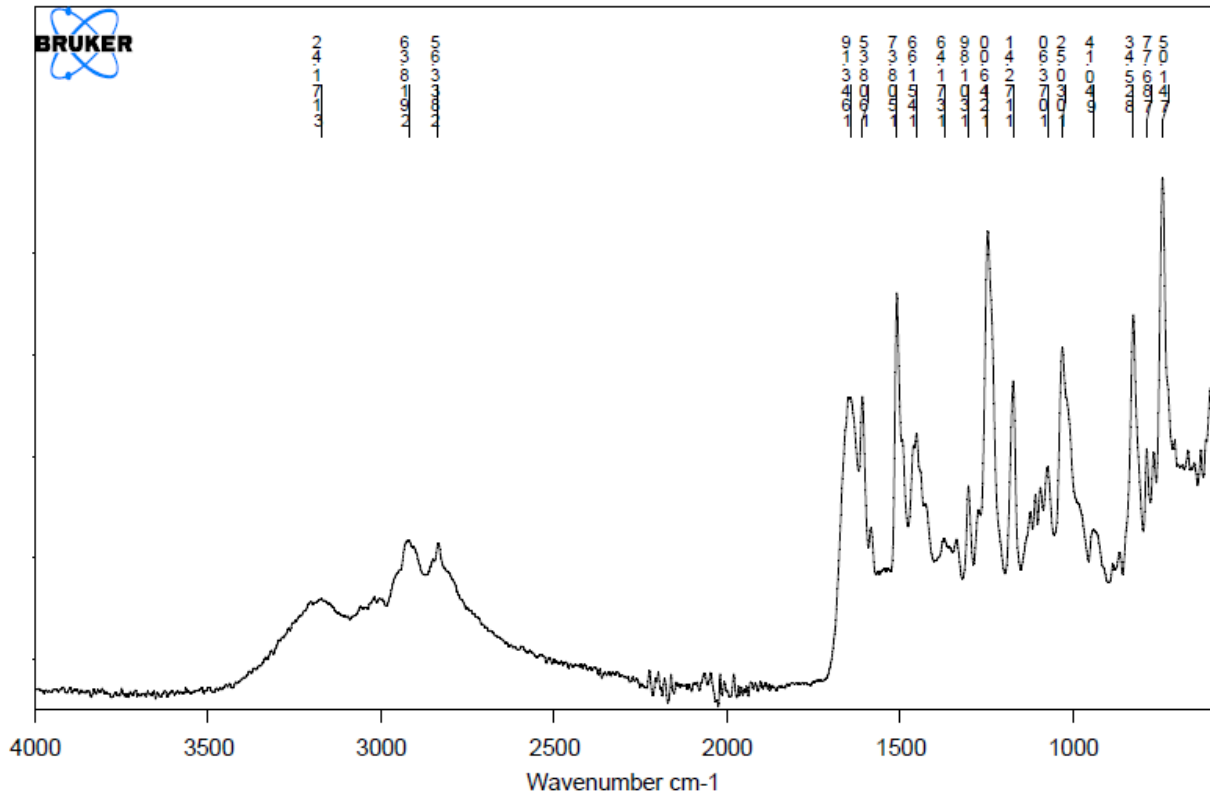




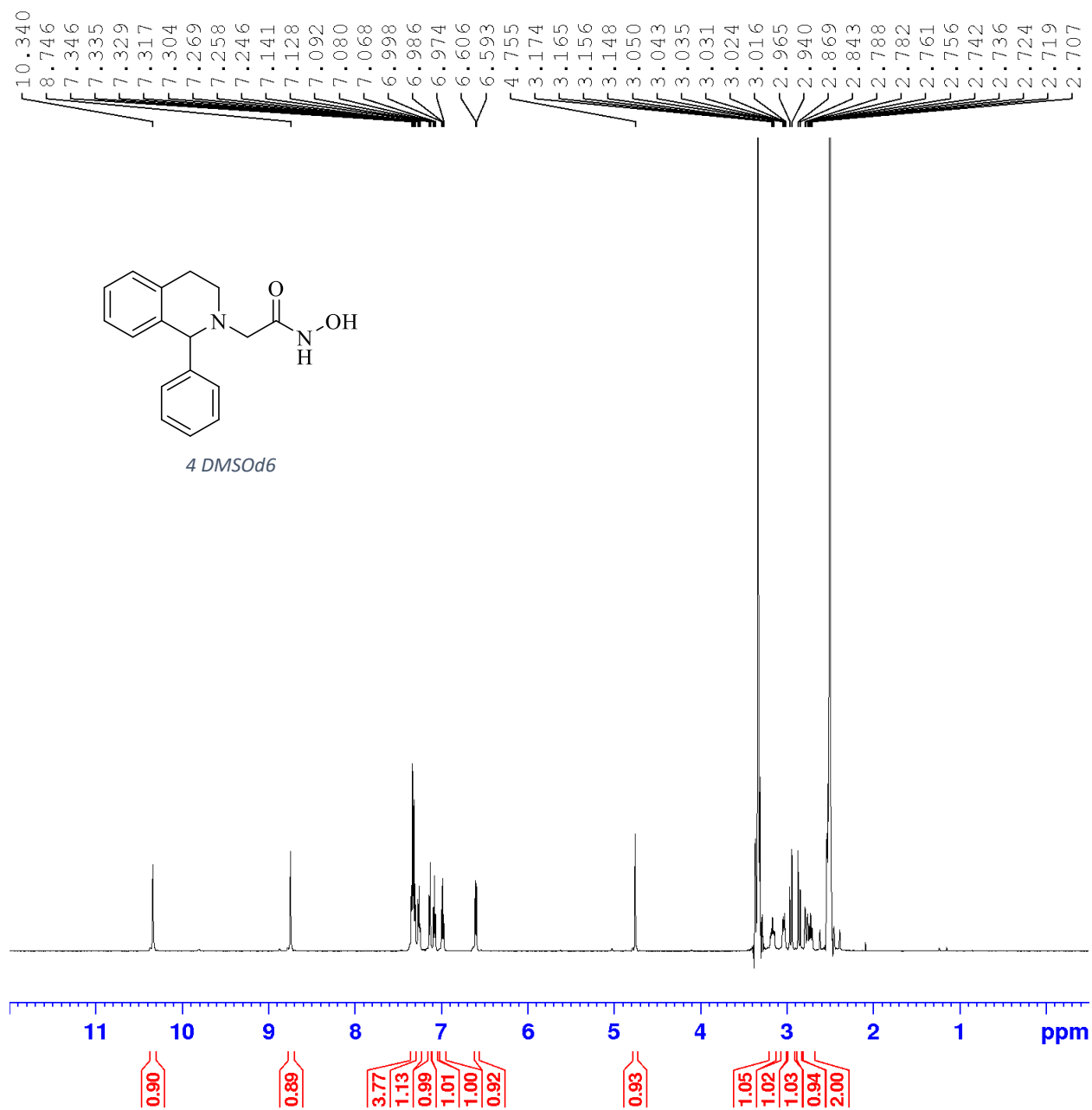
3

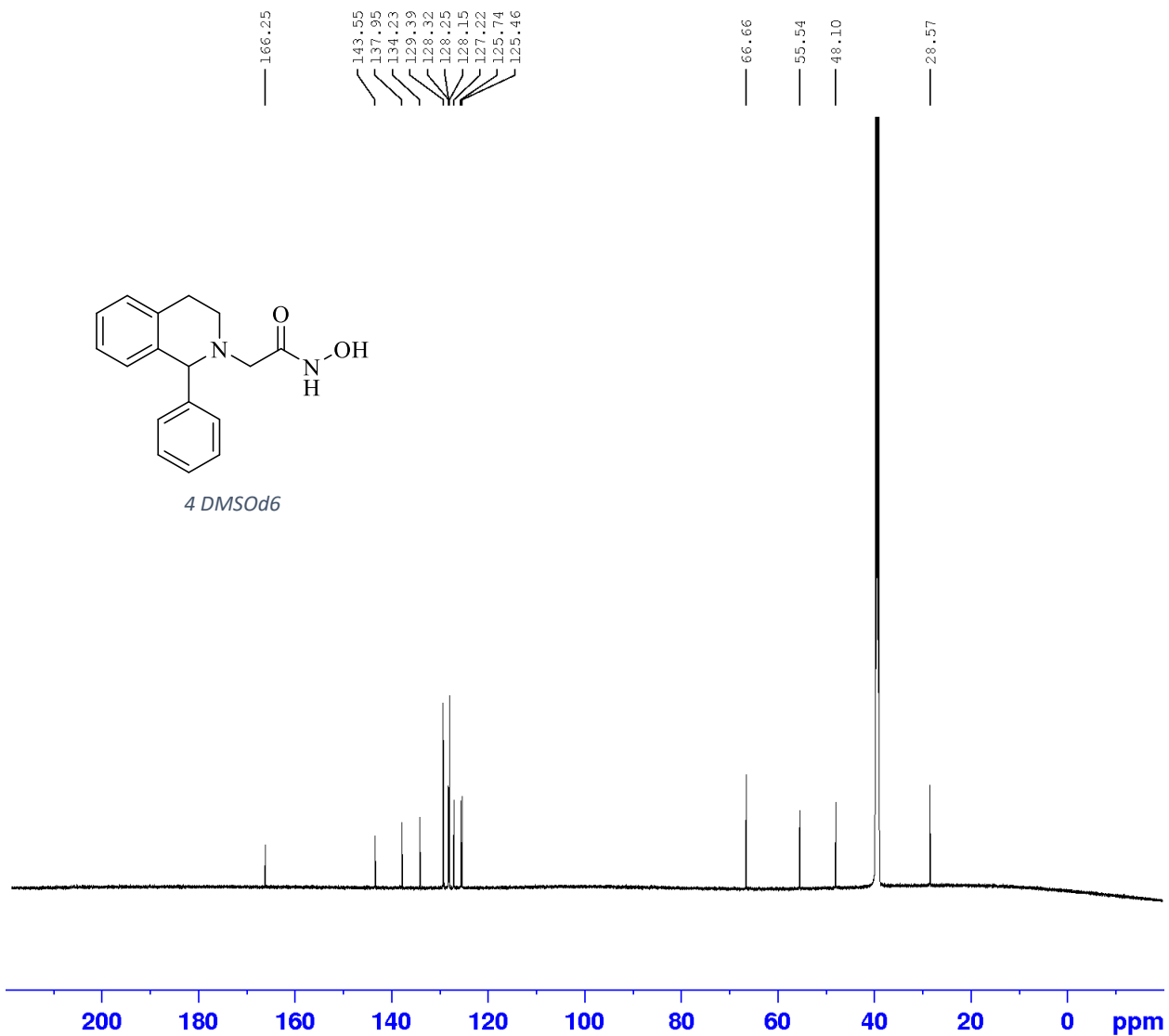


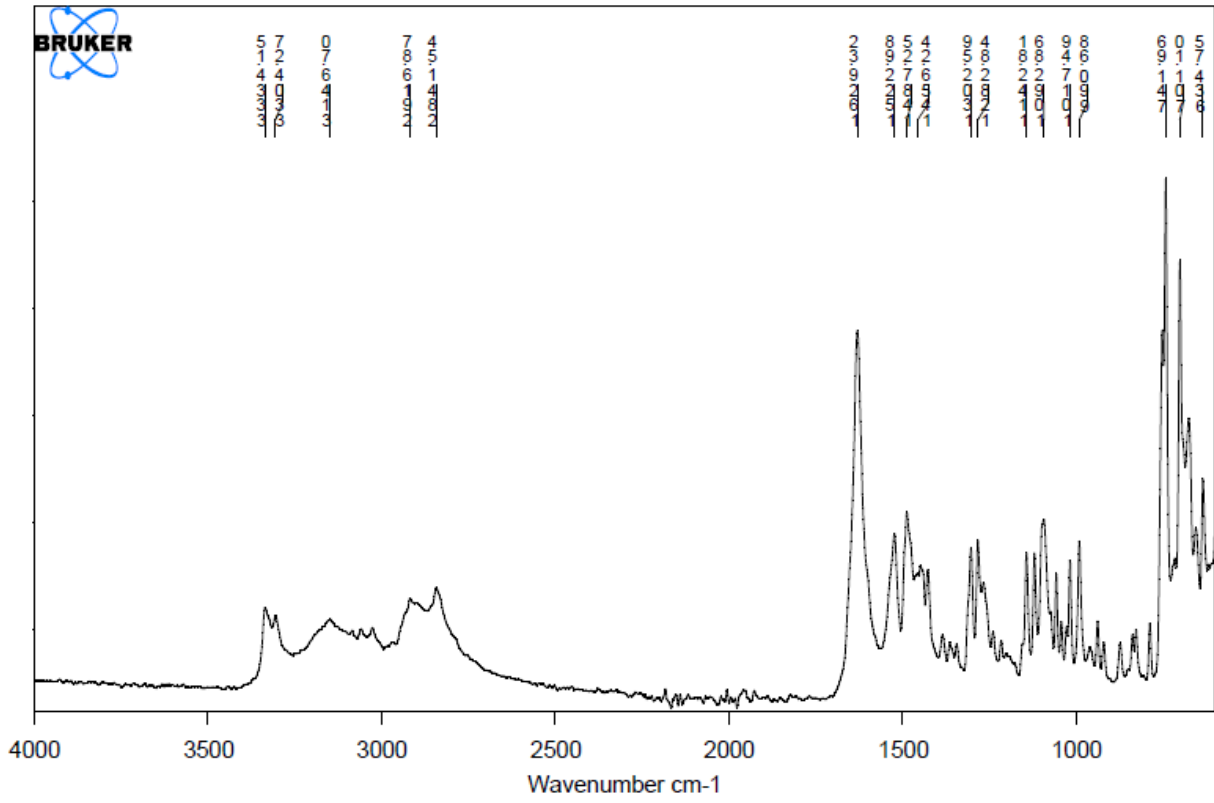




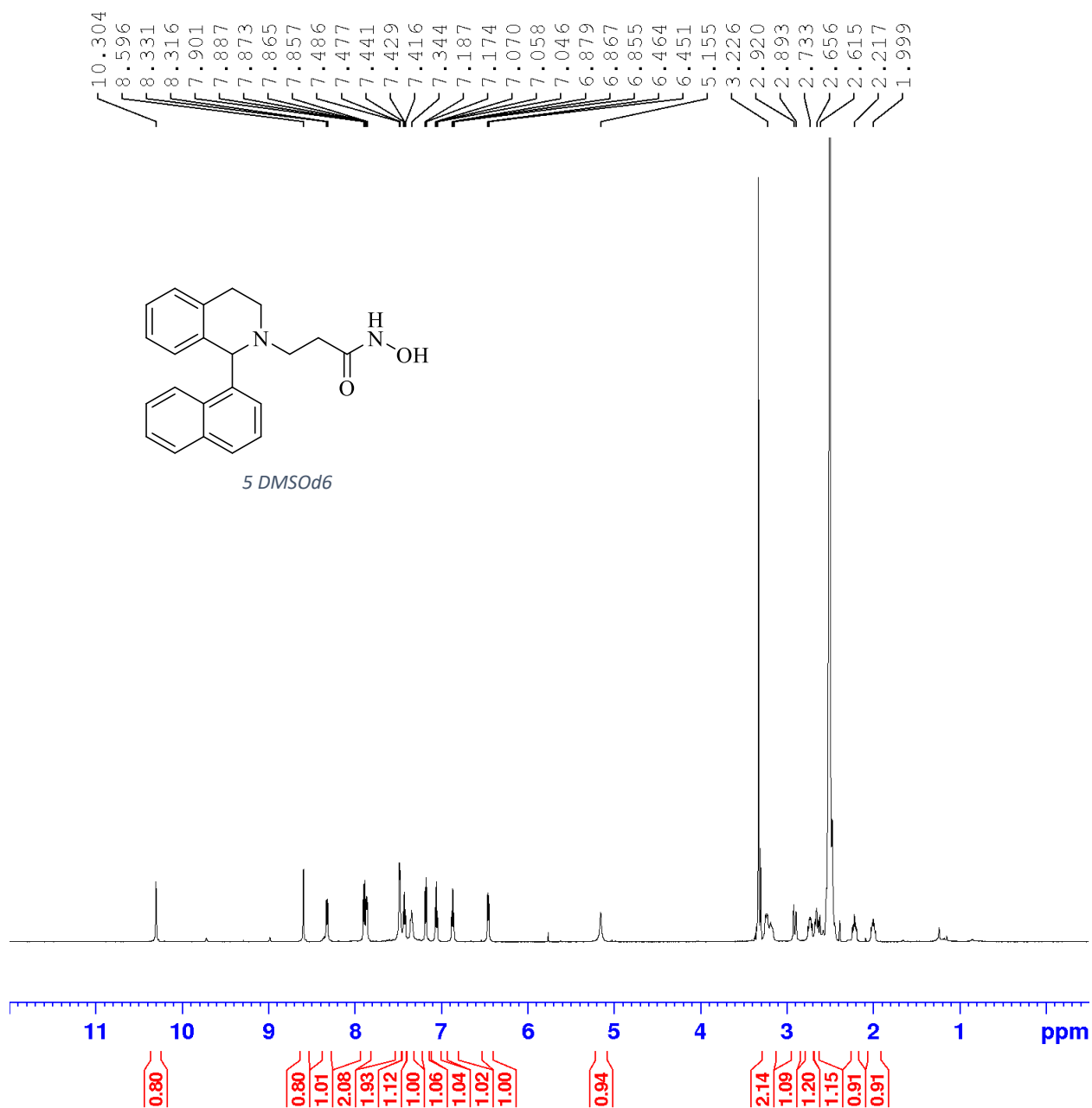
4

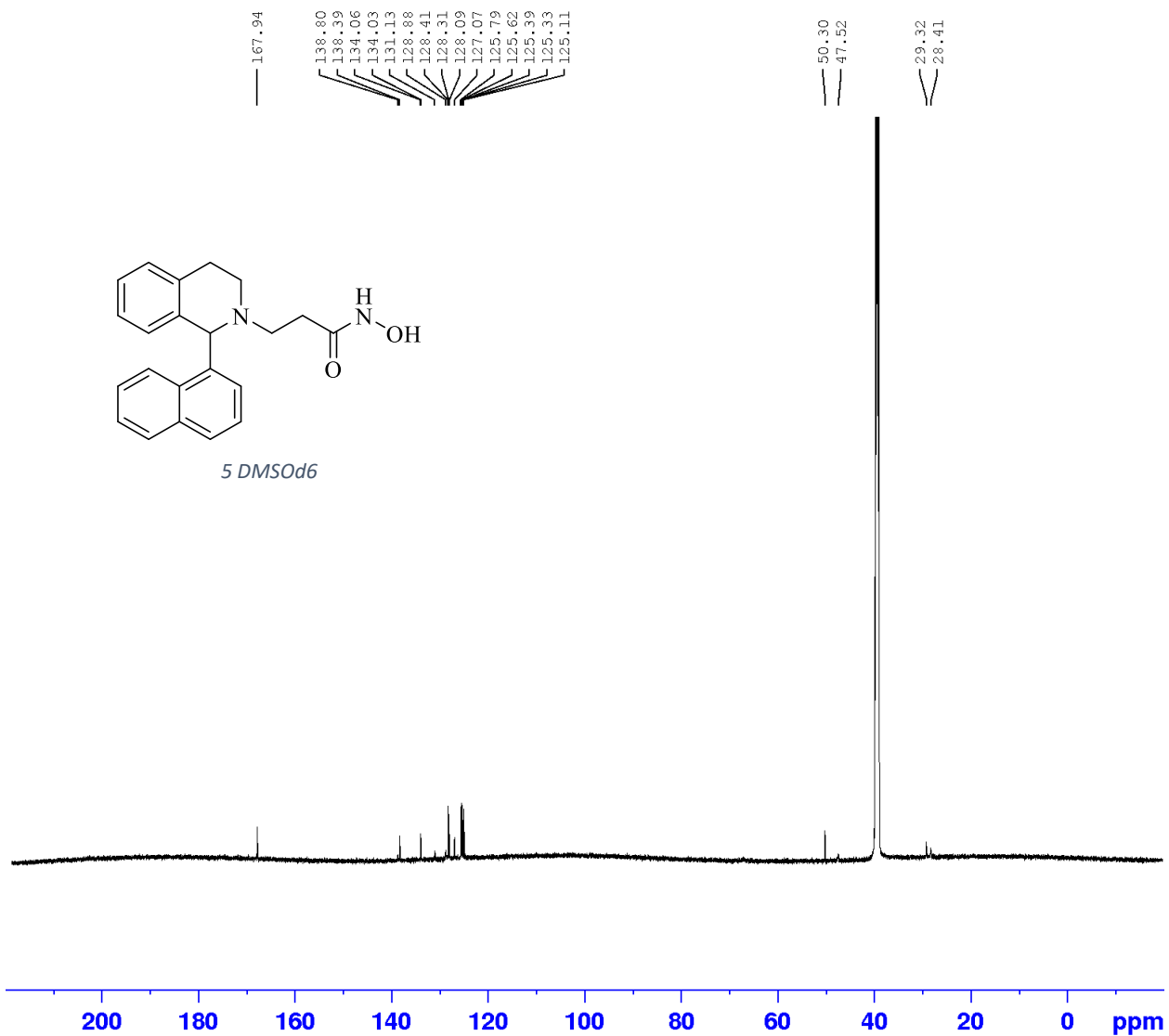


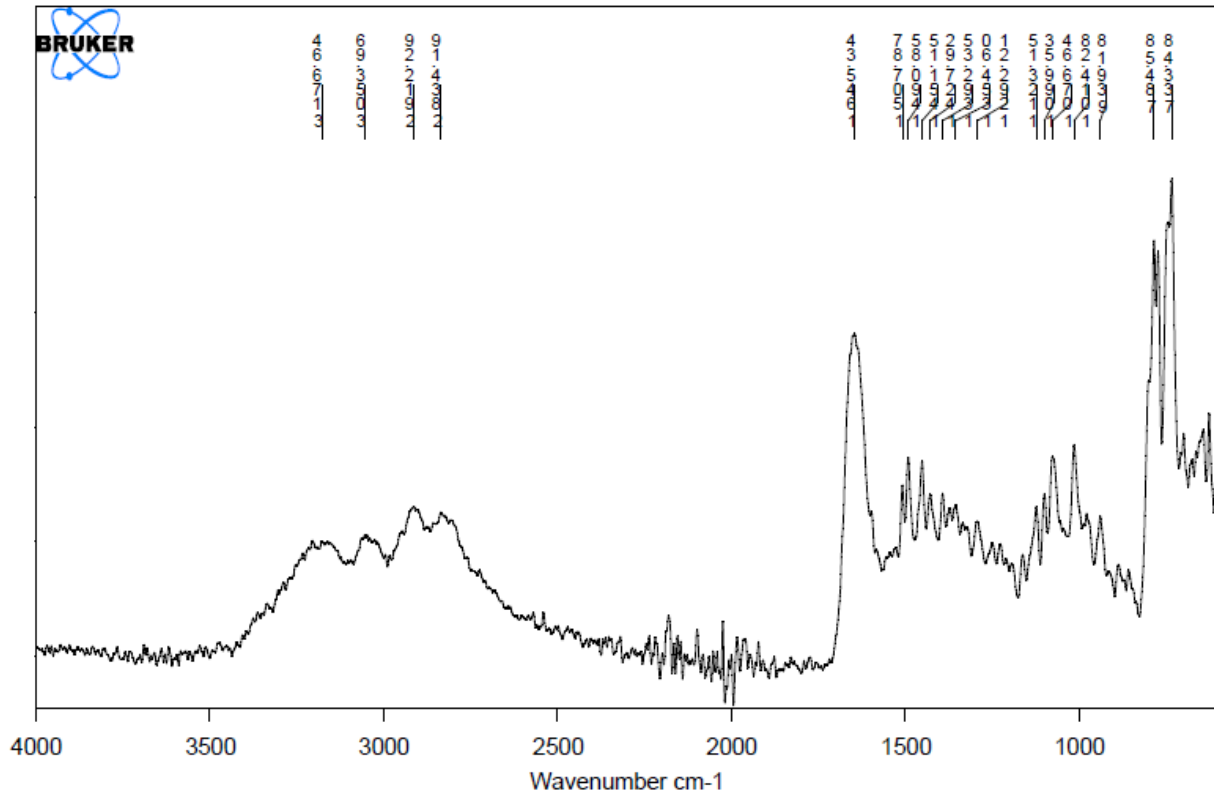




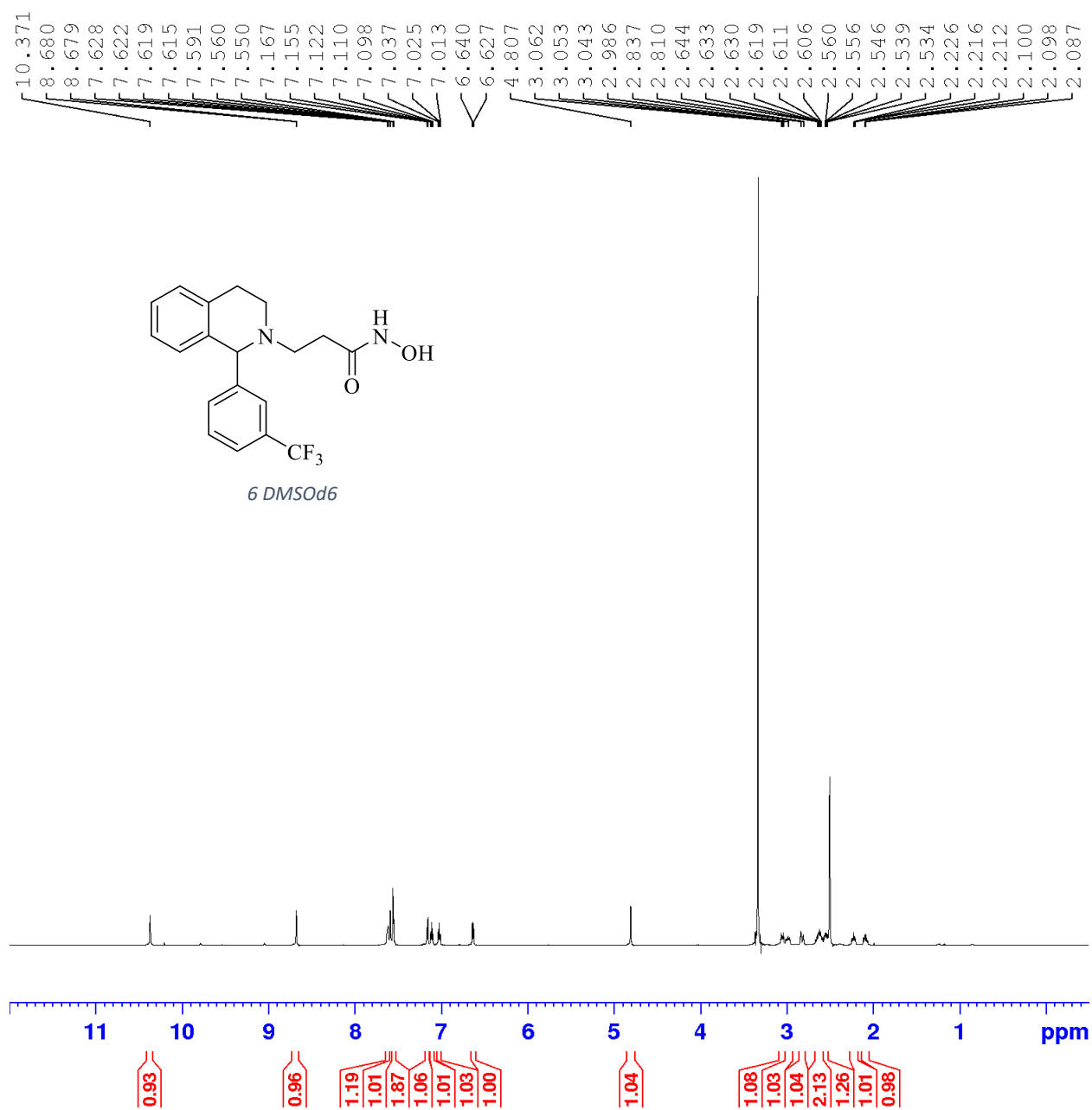
5

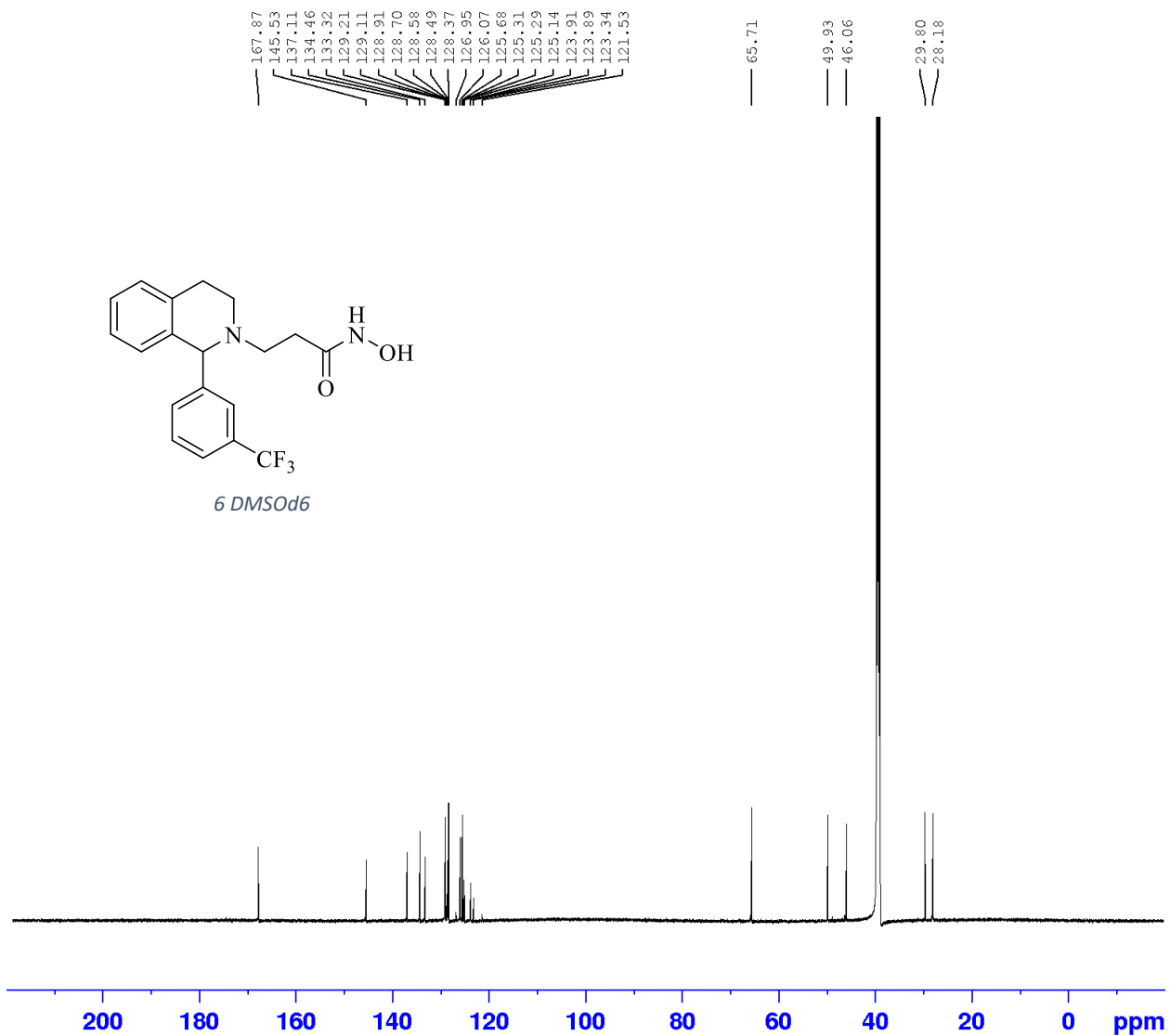


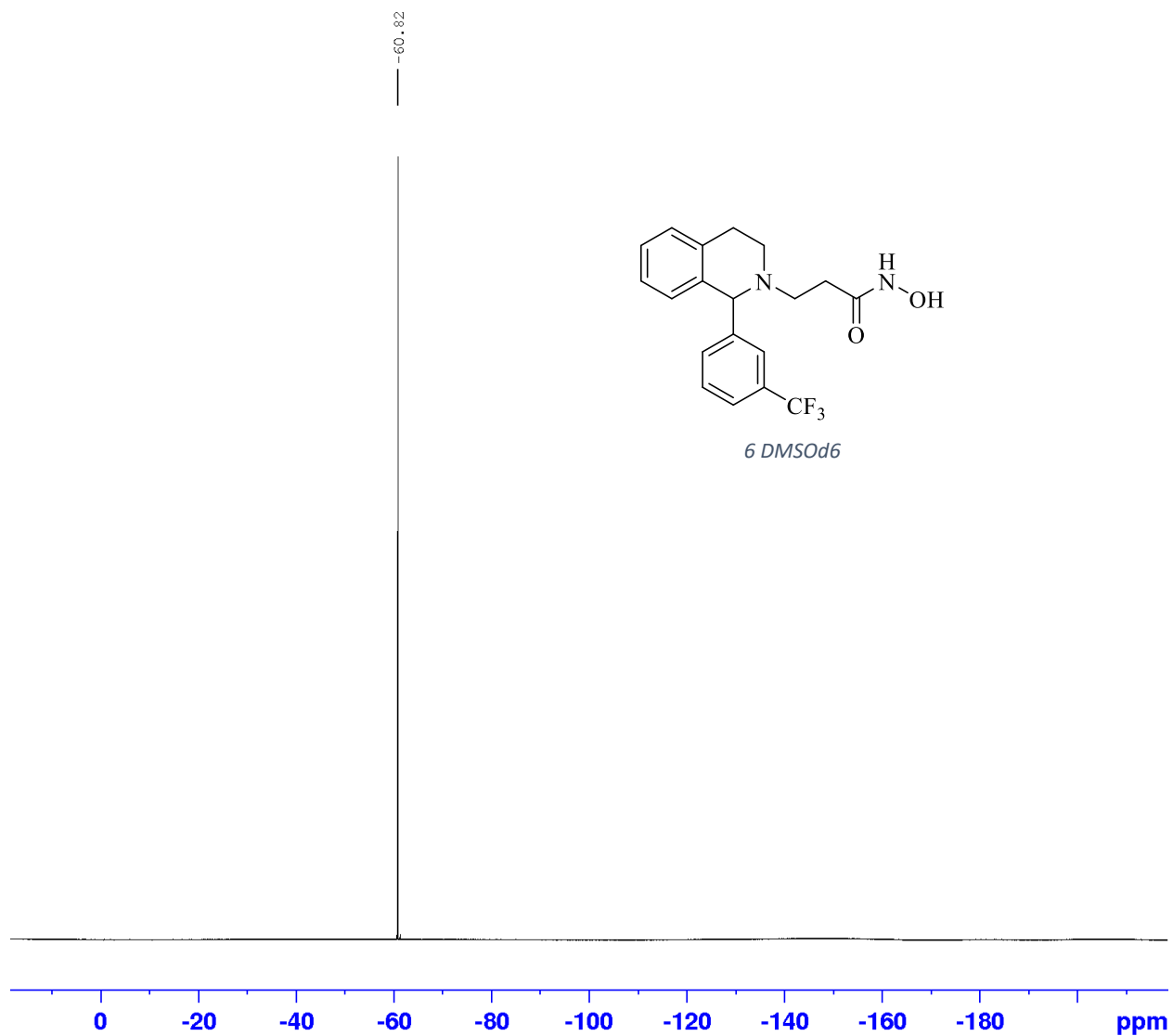




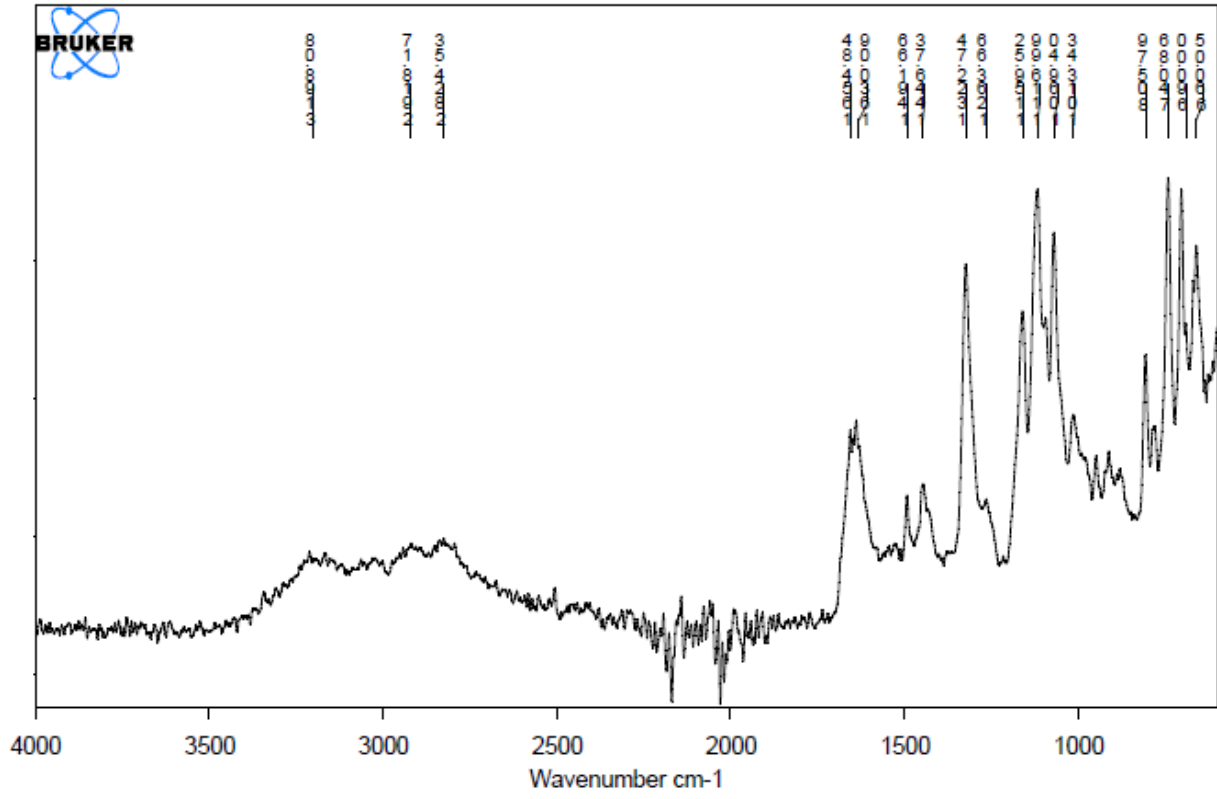
6



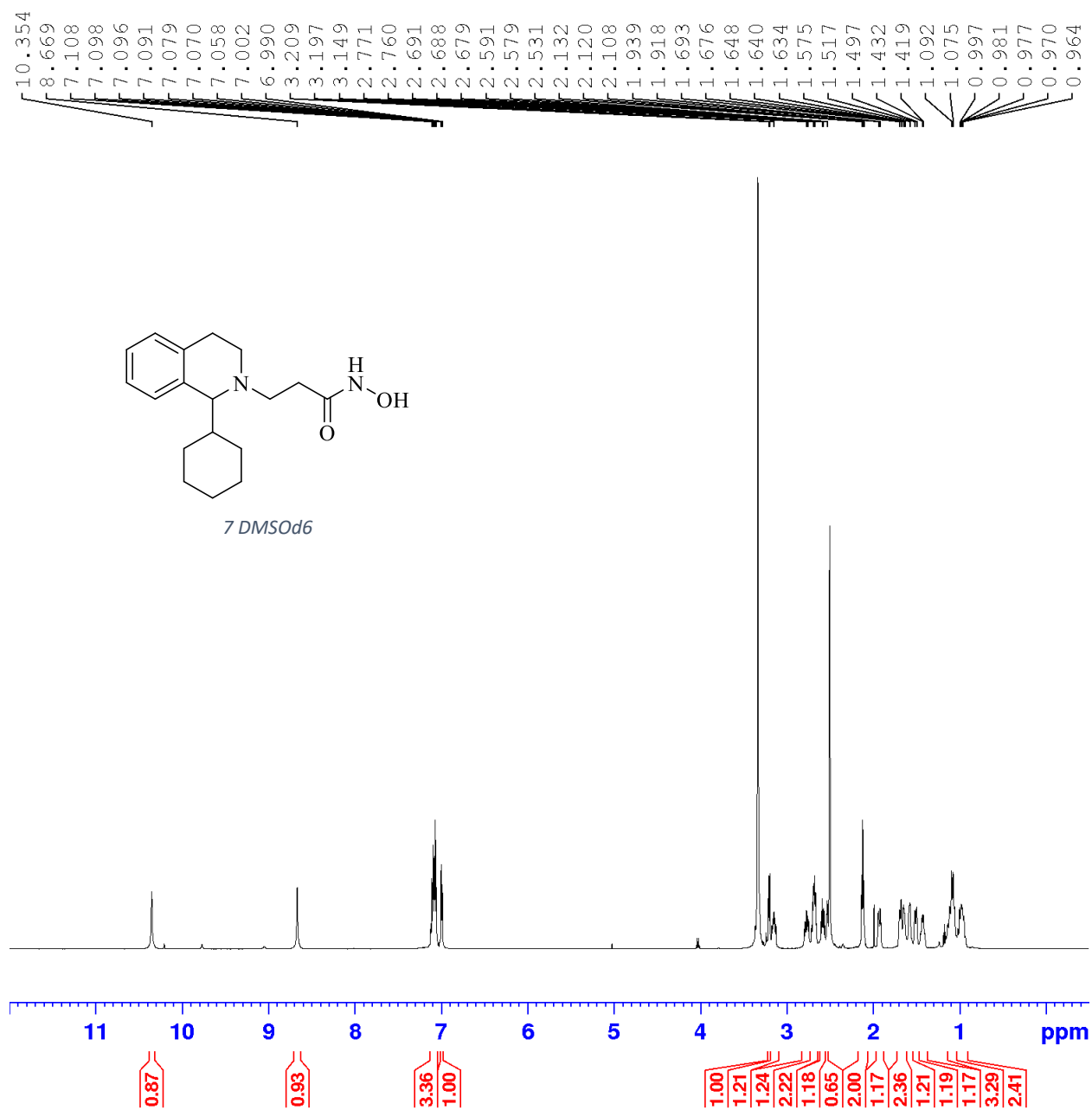


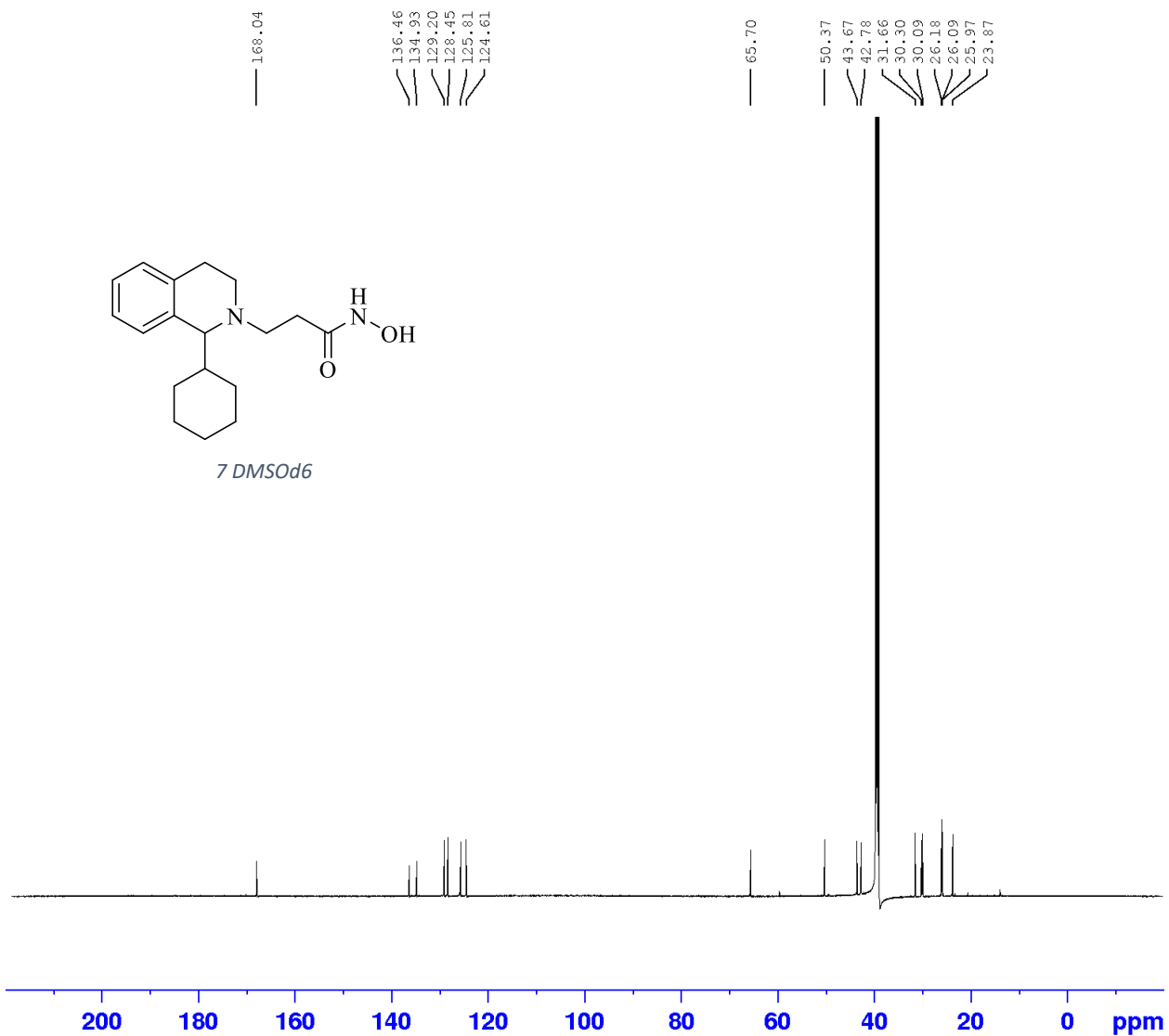


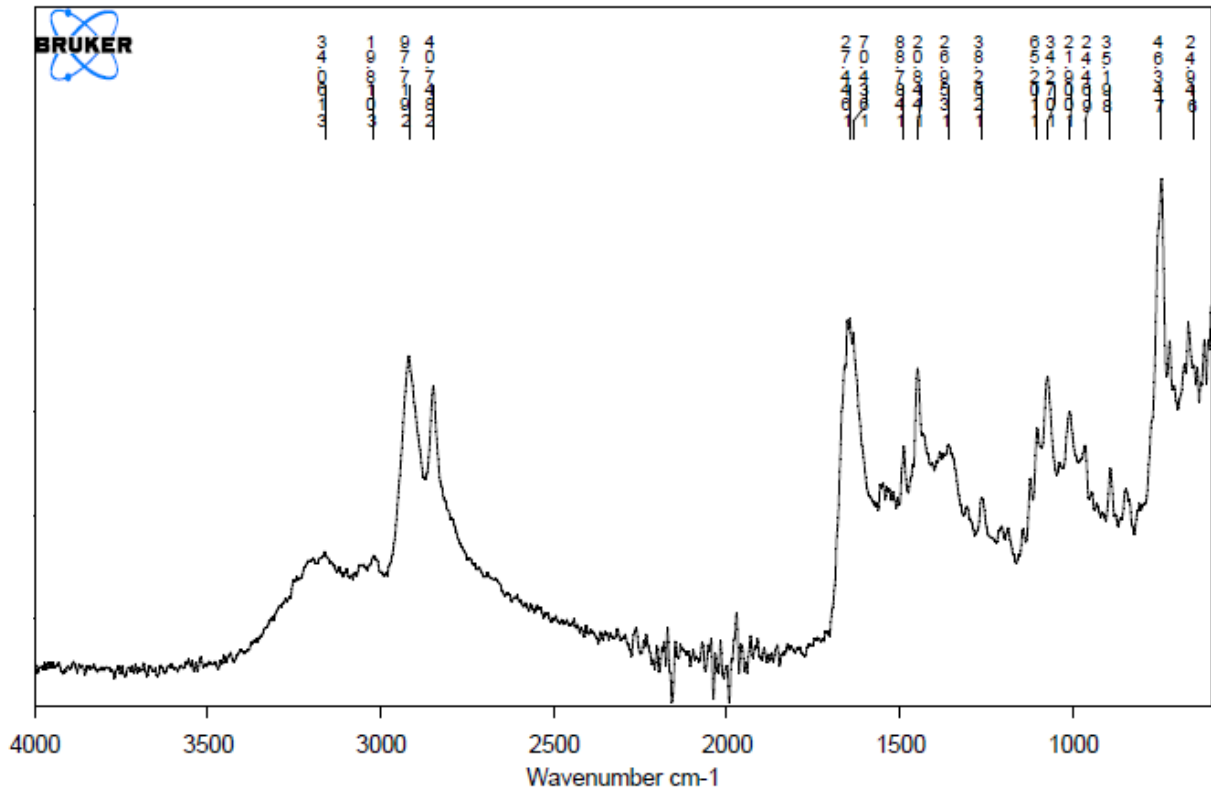
^{19}F NMR



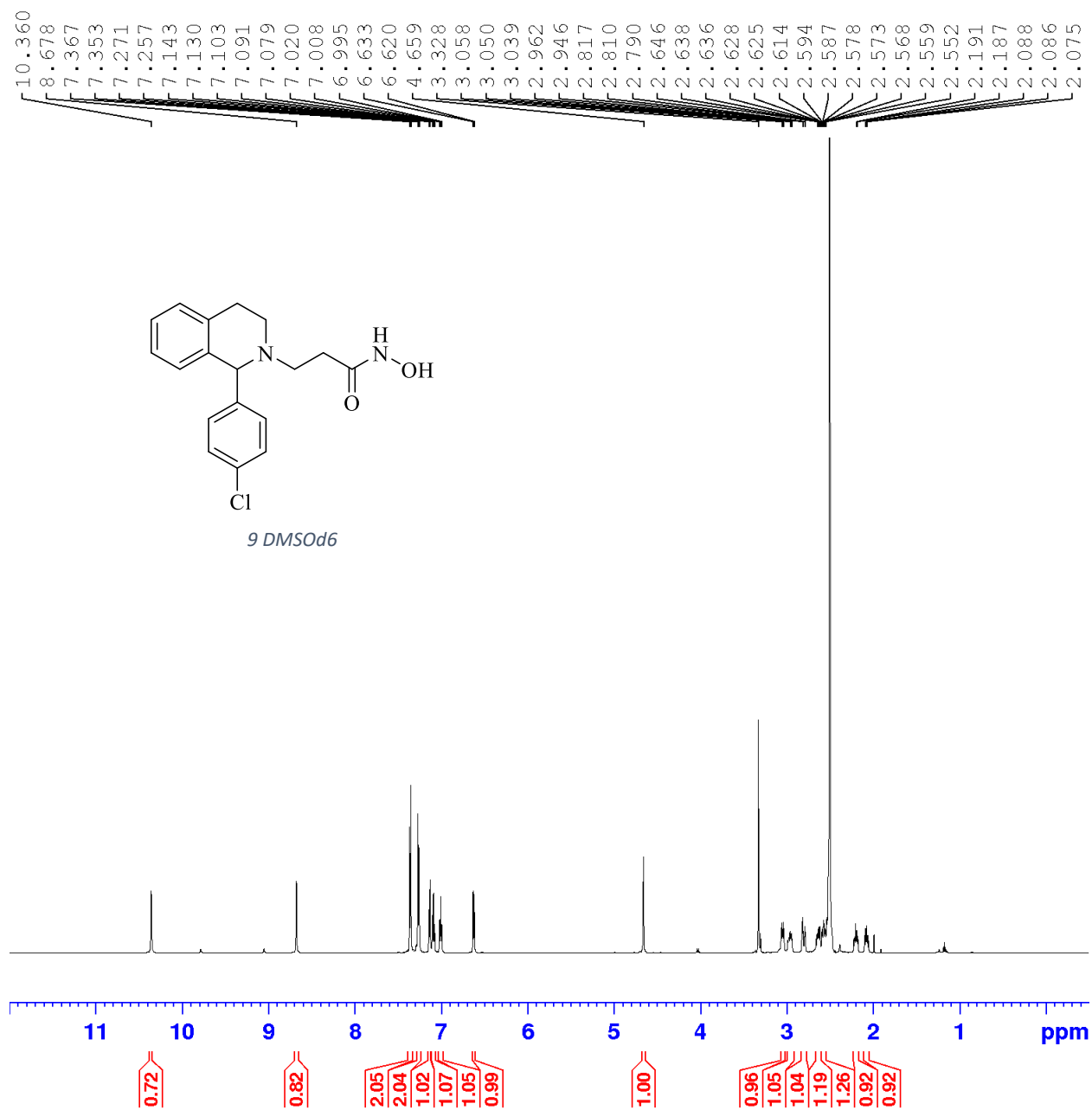
7

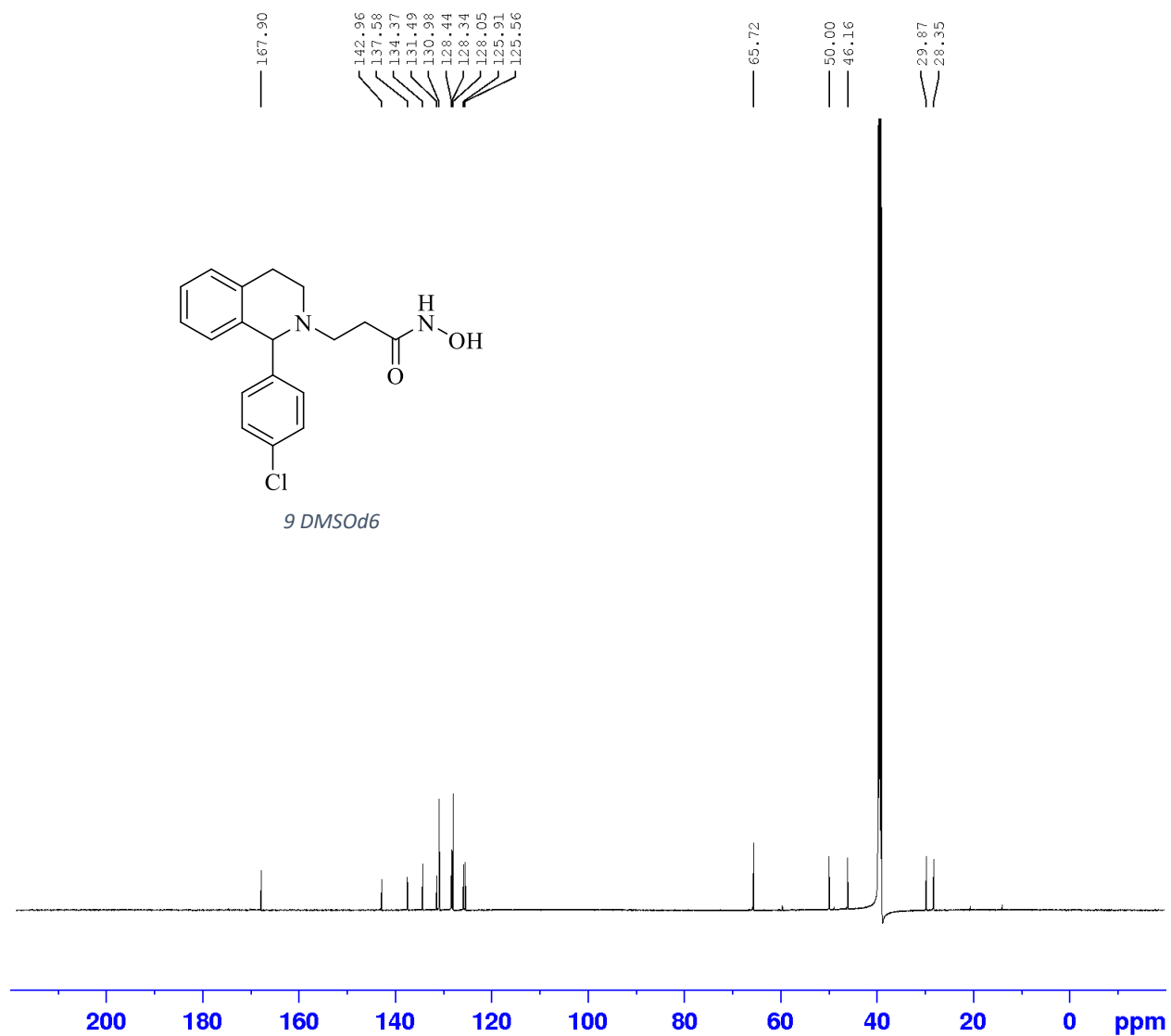


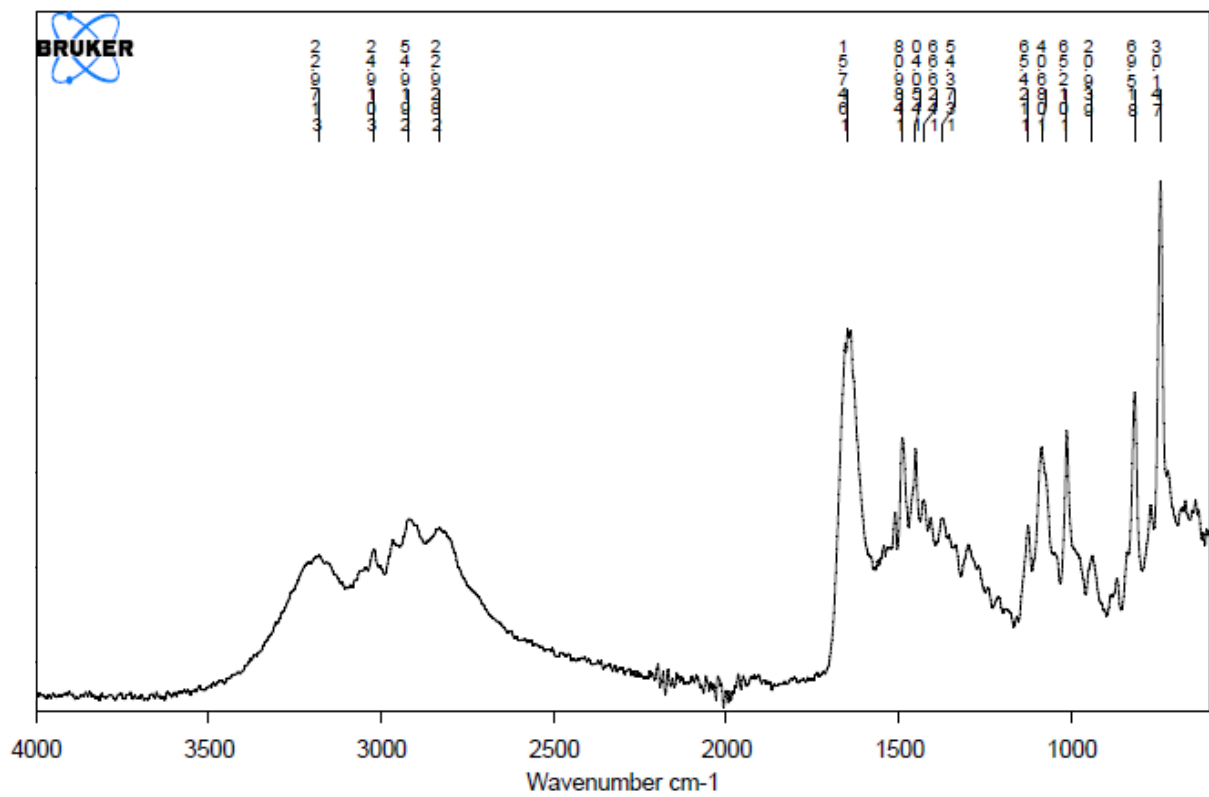




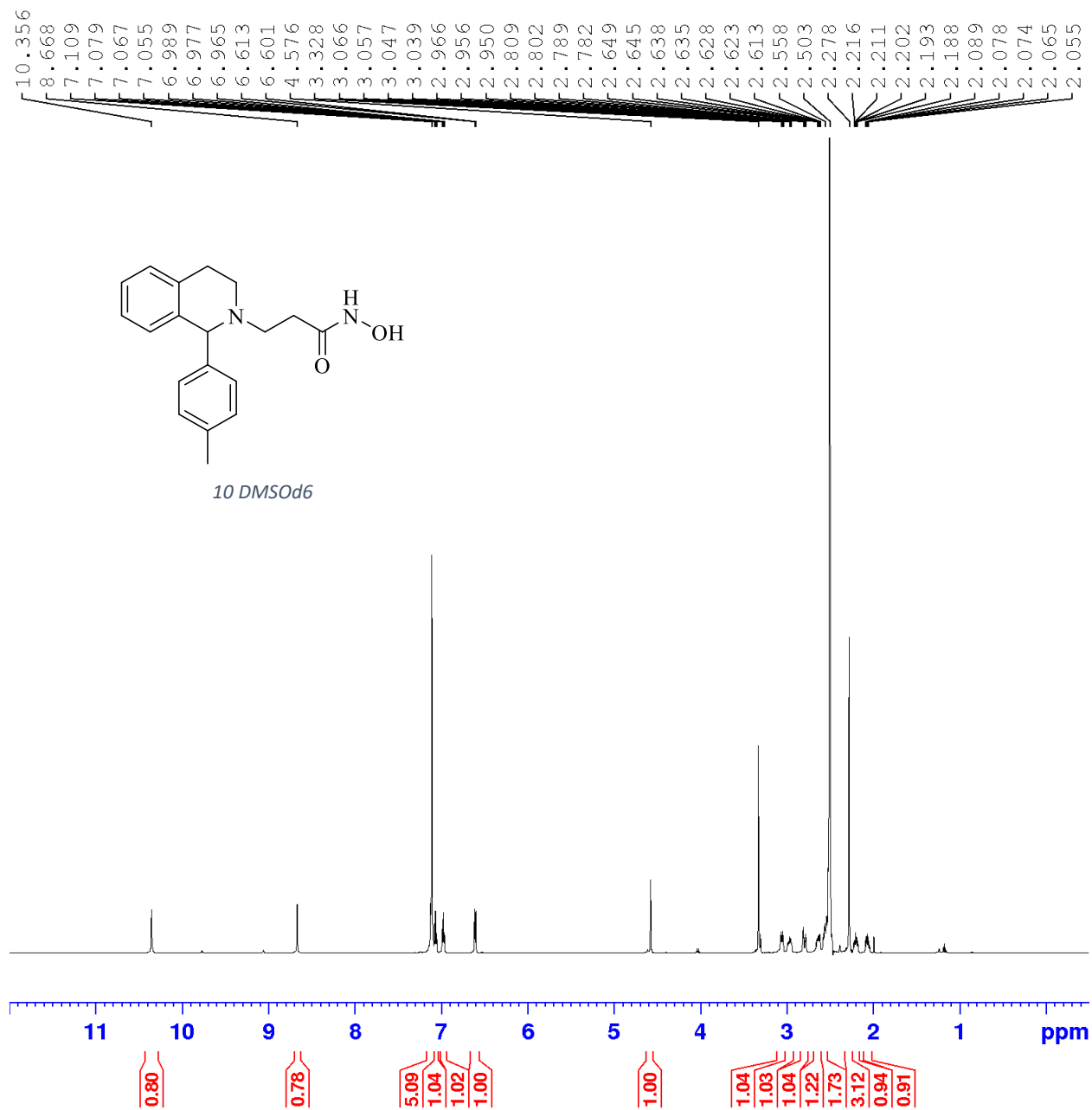
9

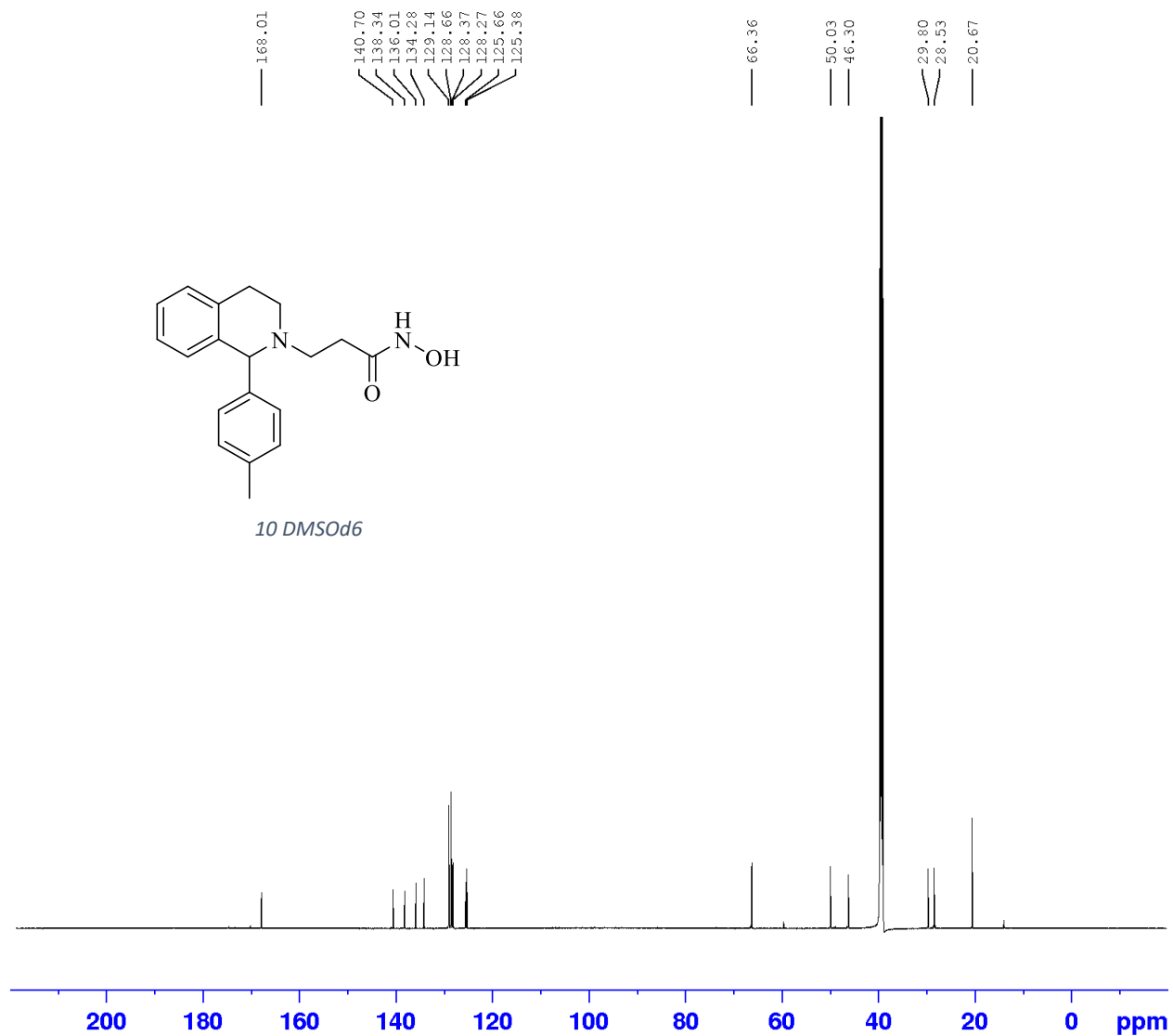


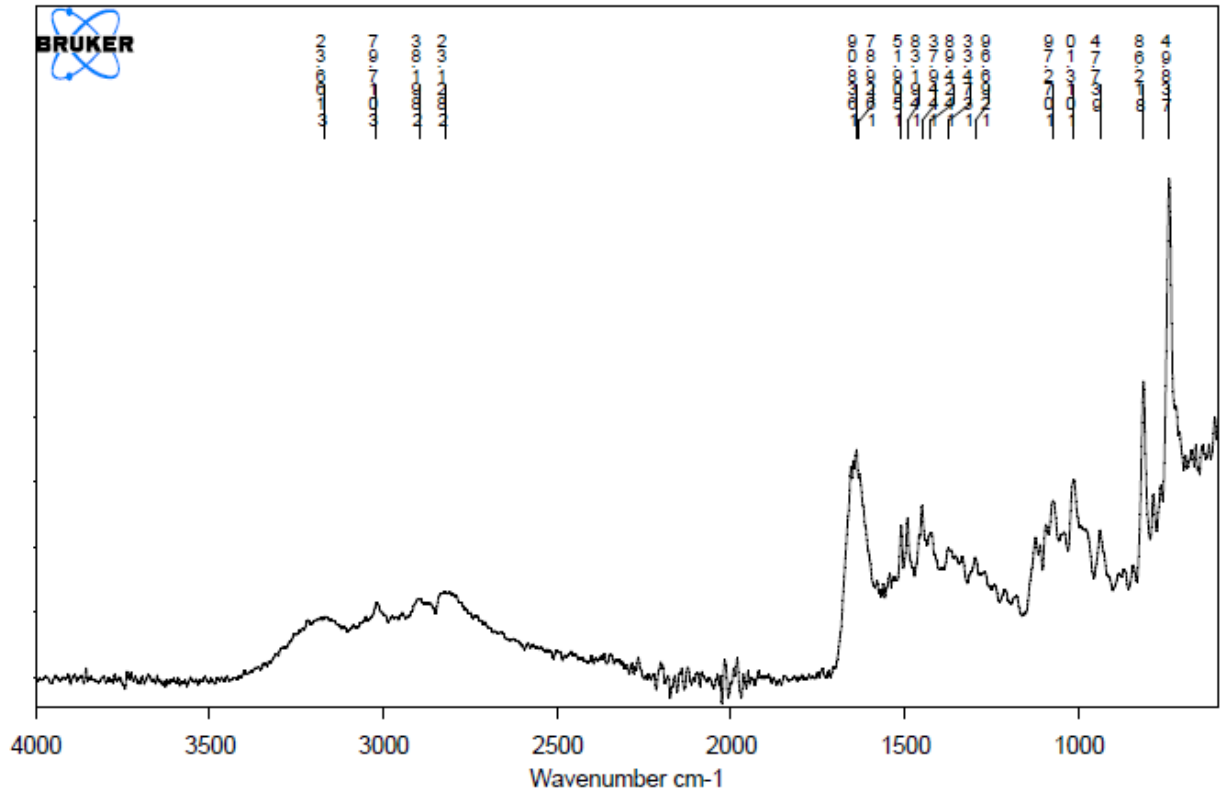




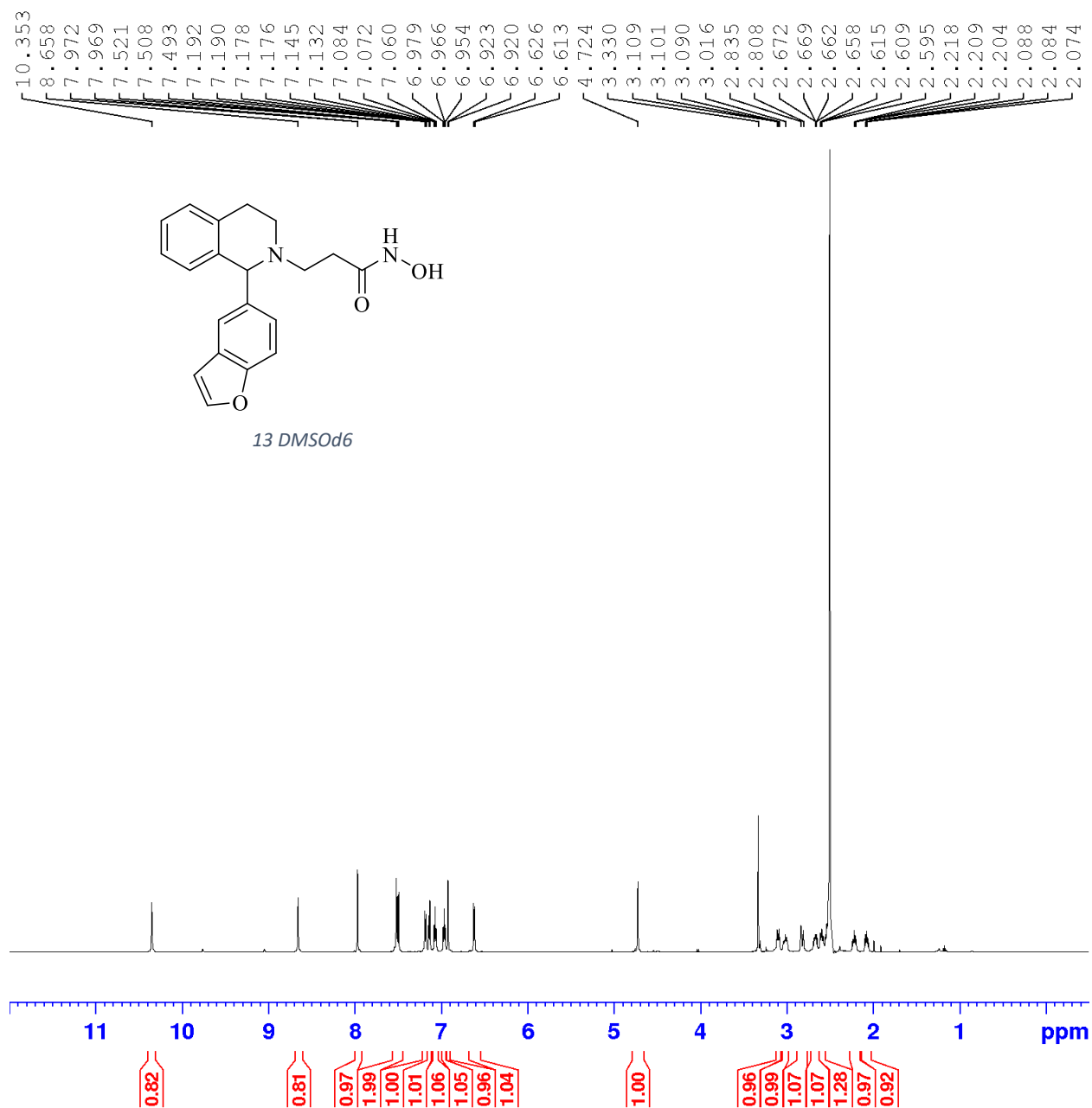
10

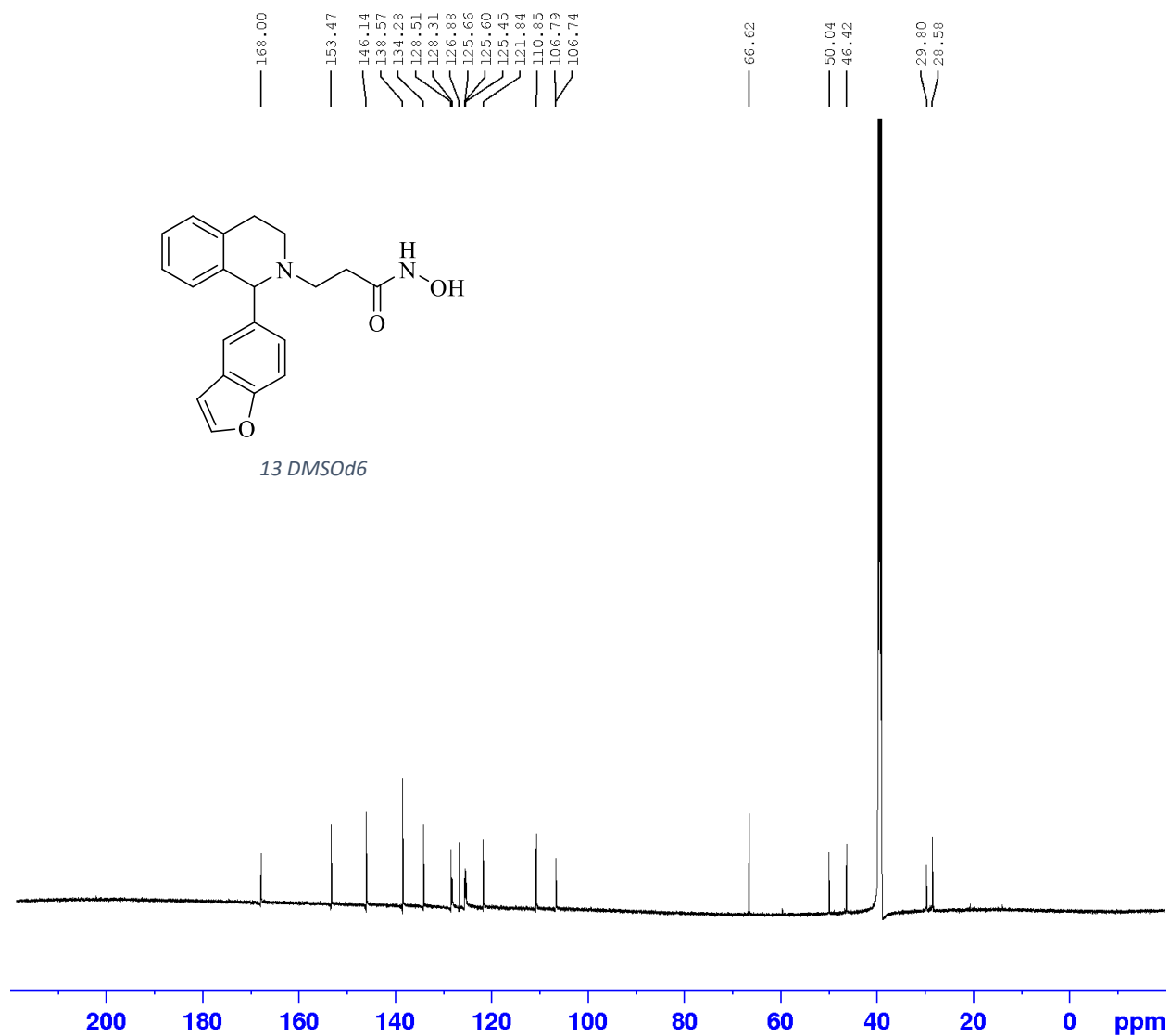


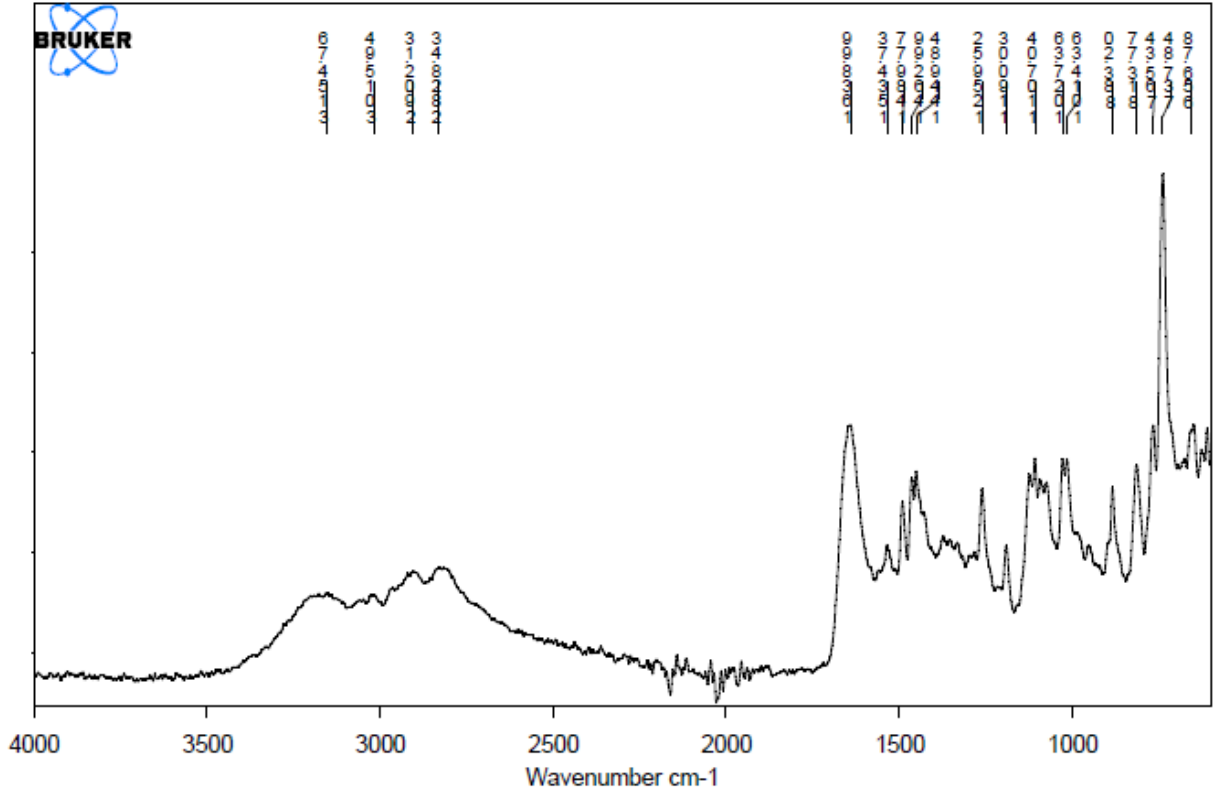




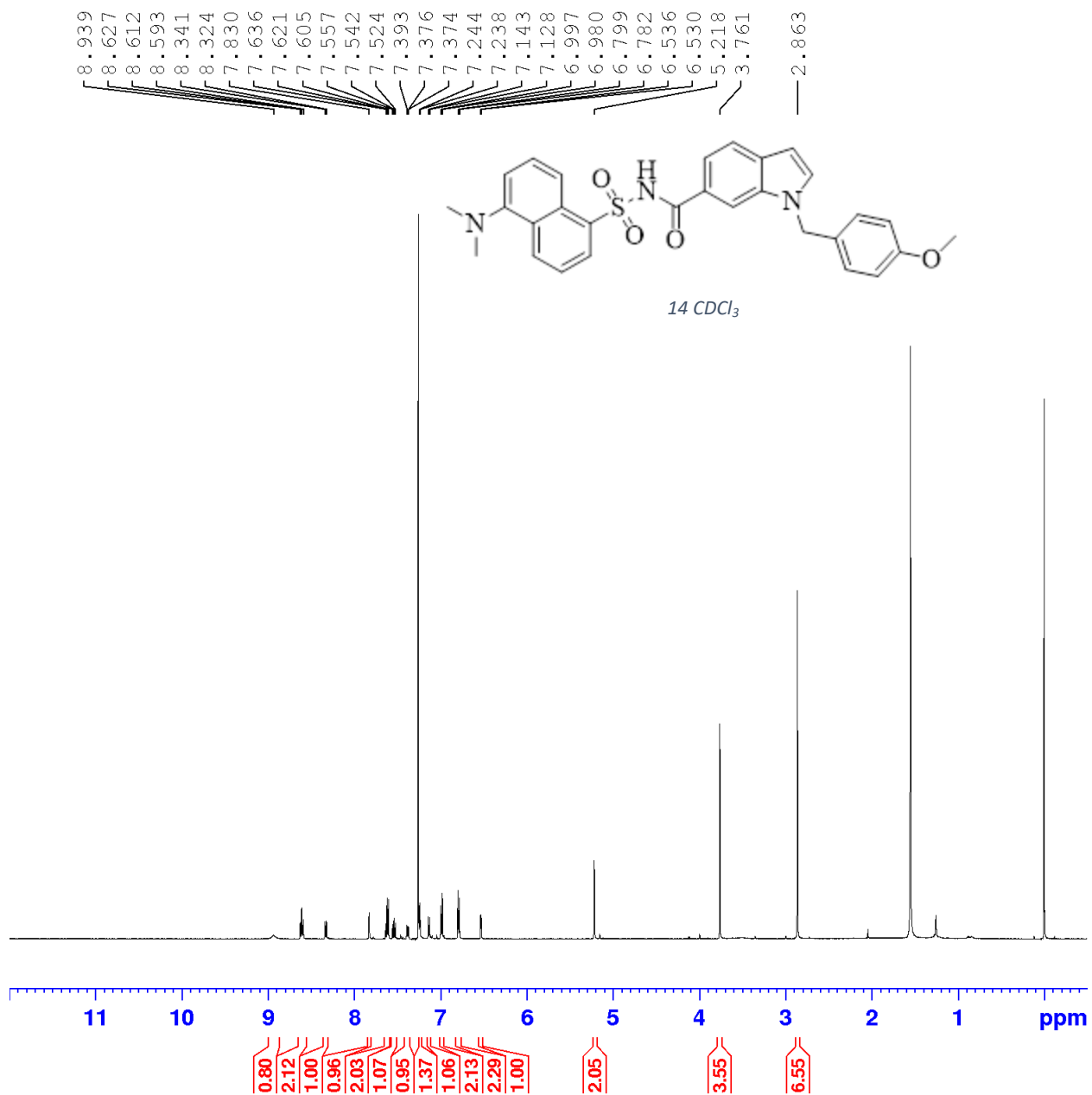
13

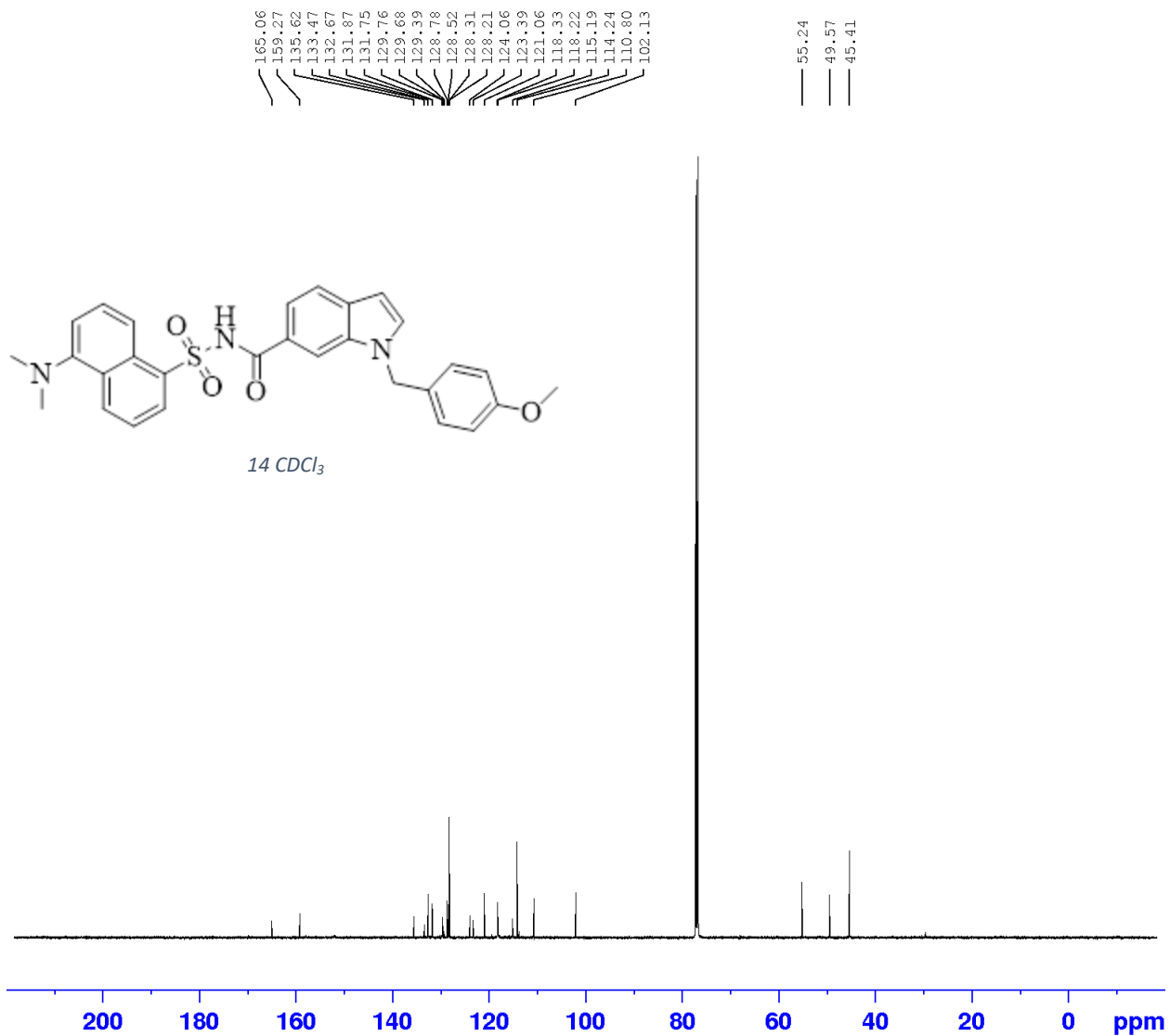


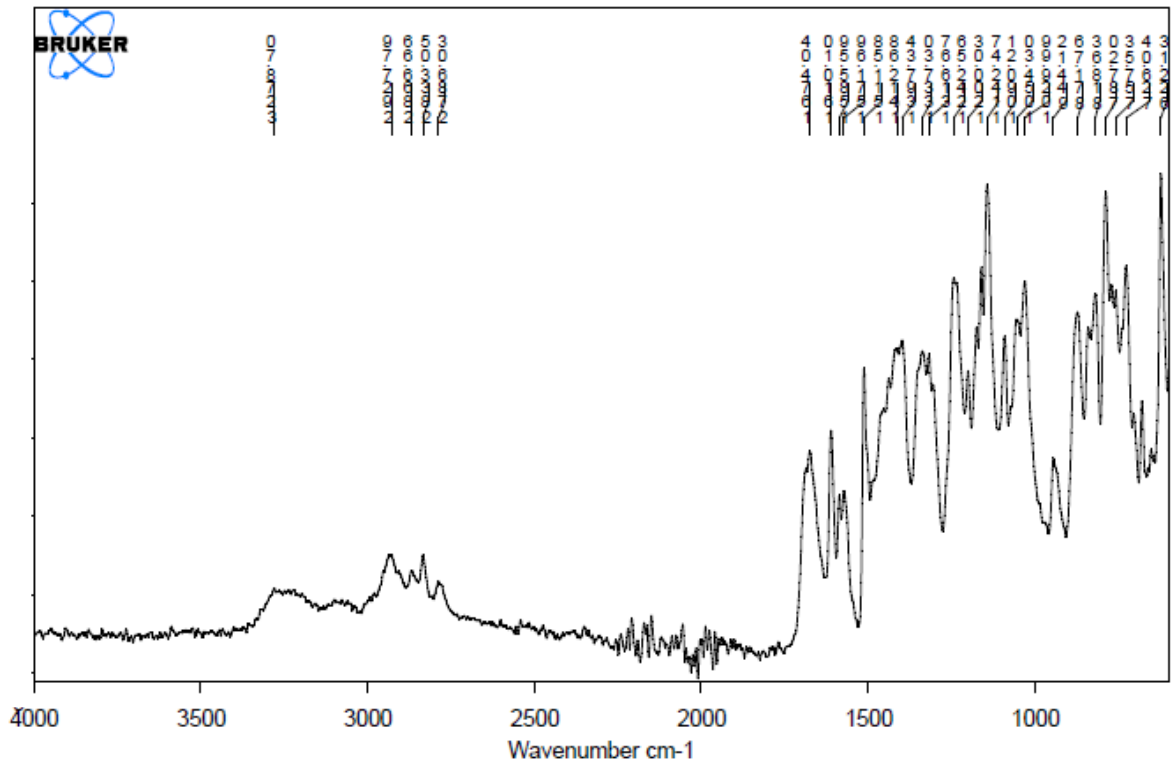




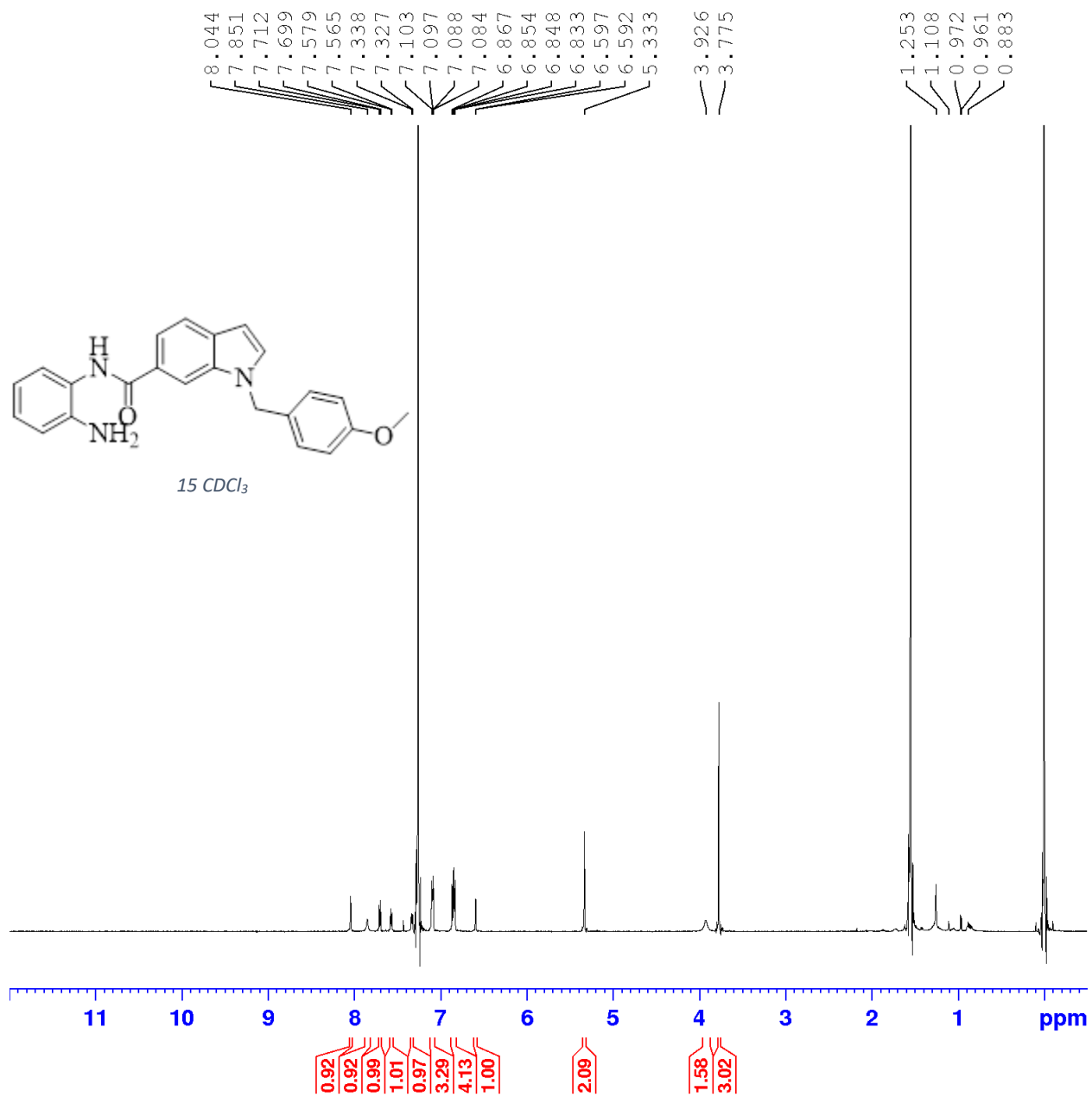
14

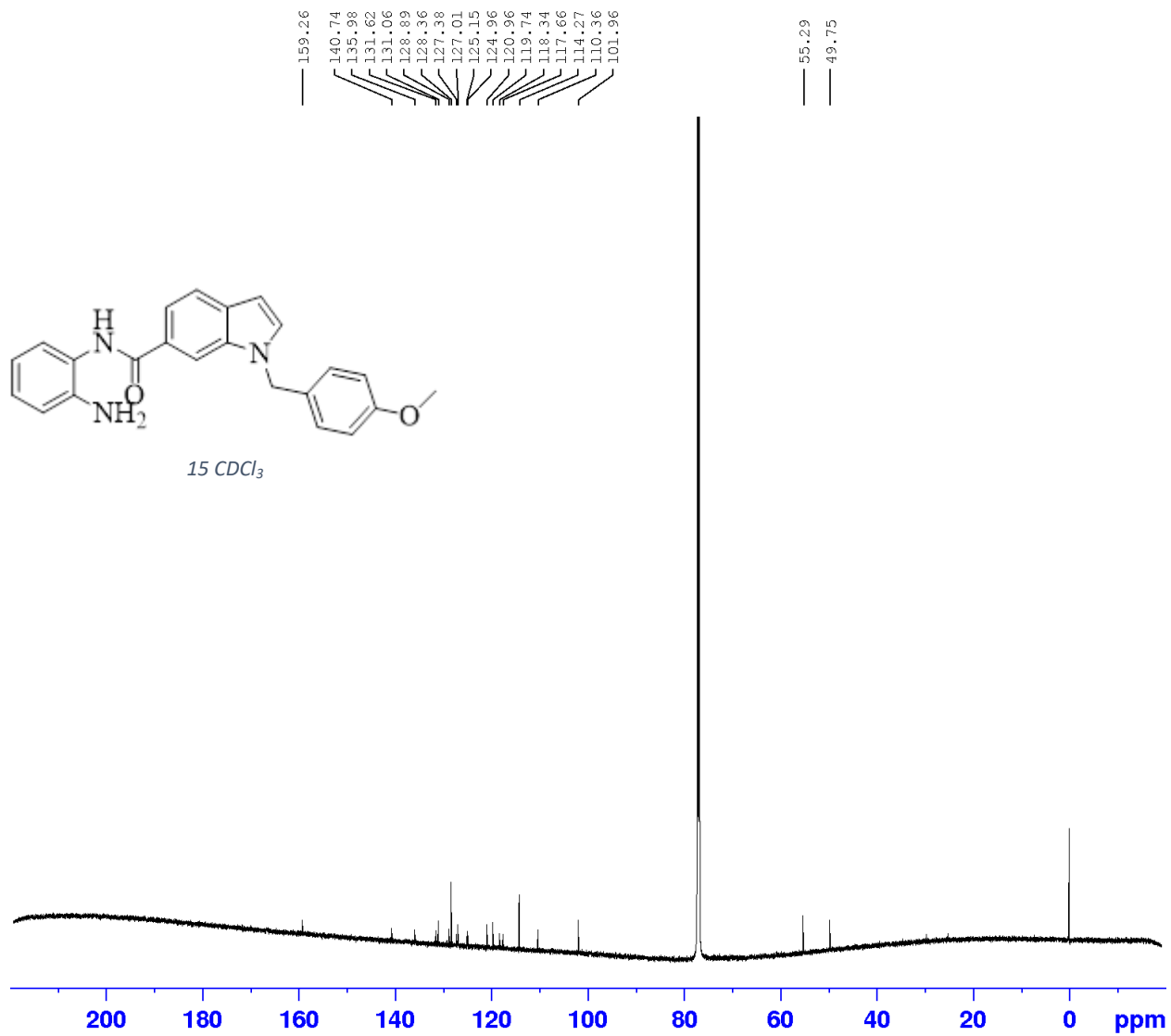


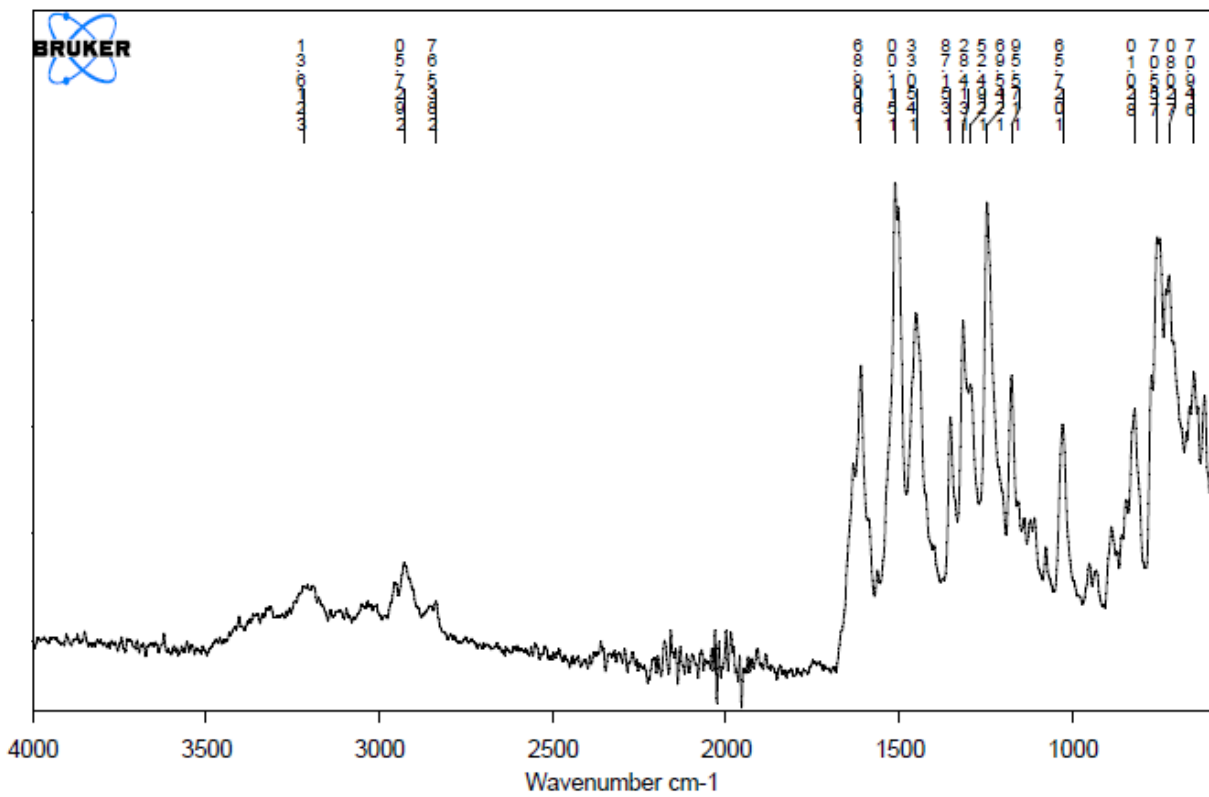




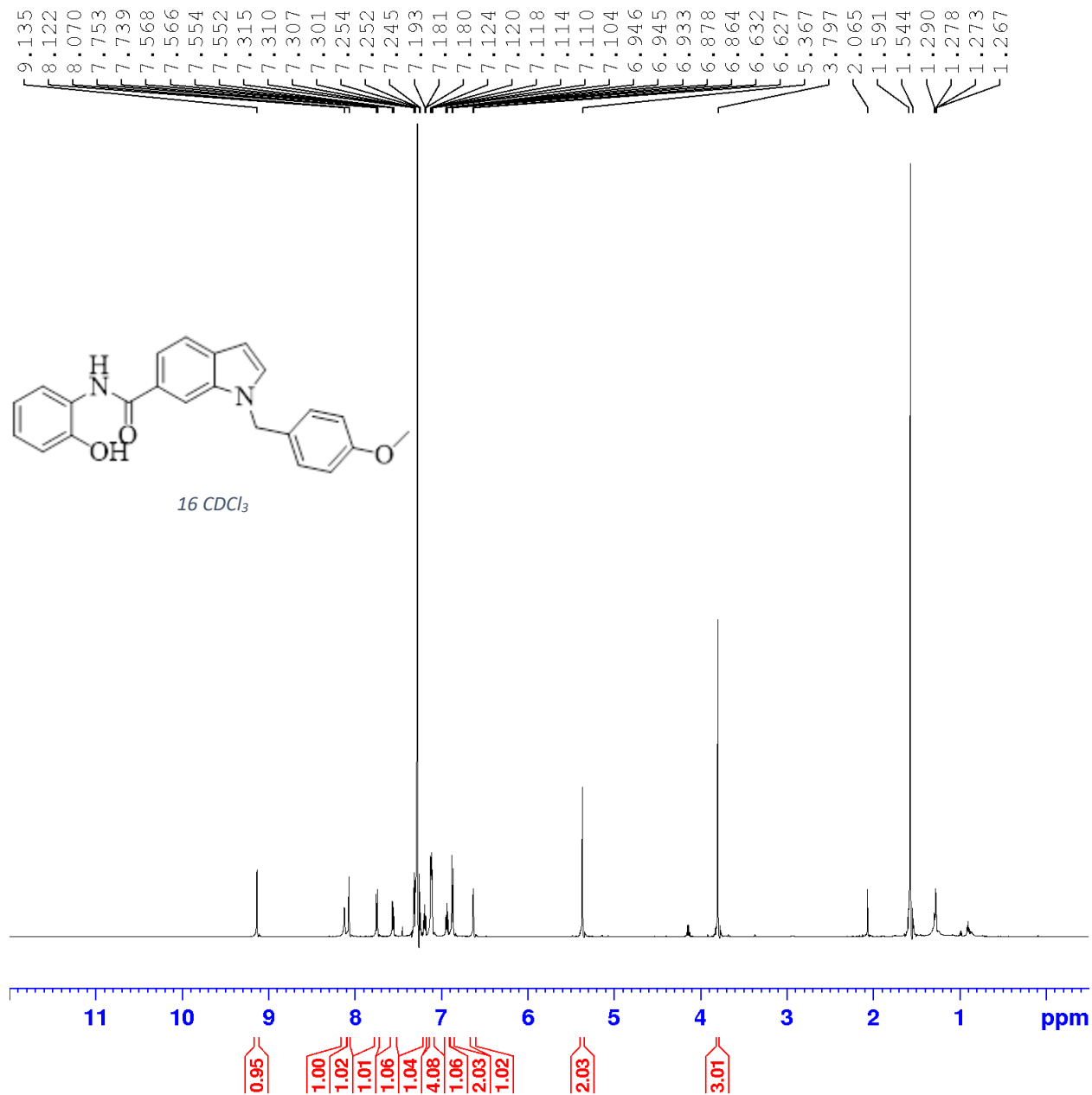
15

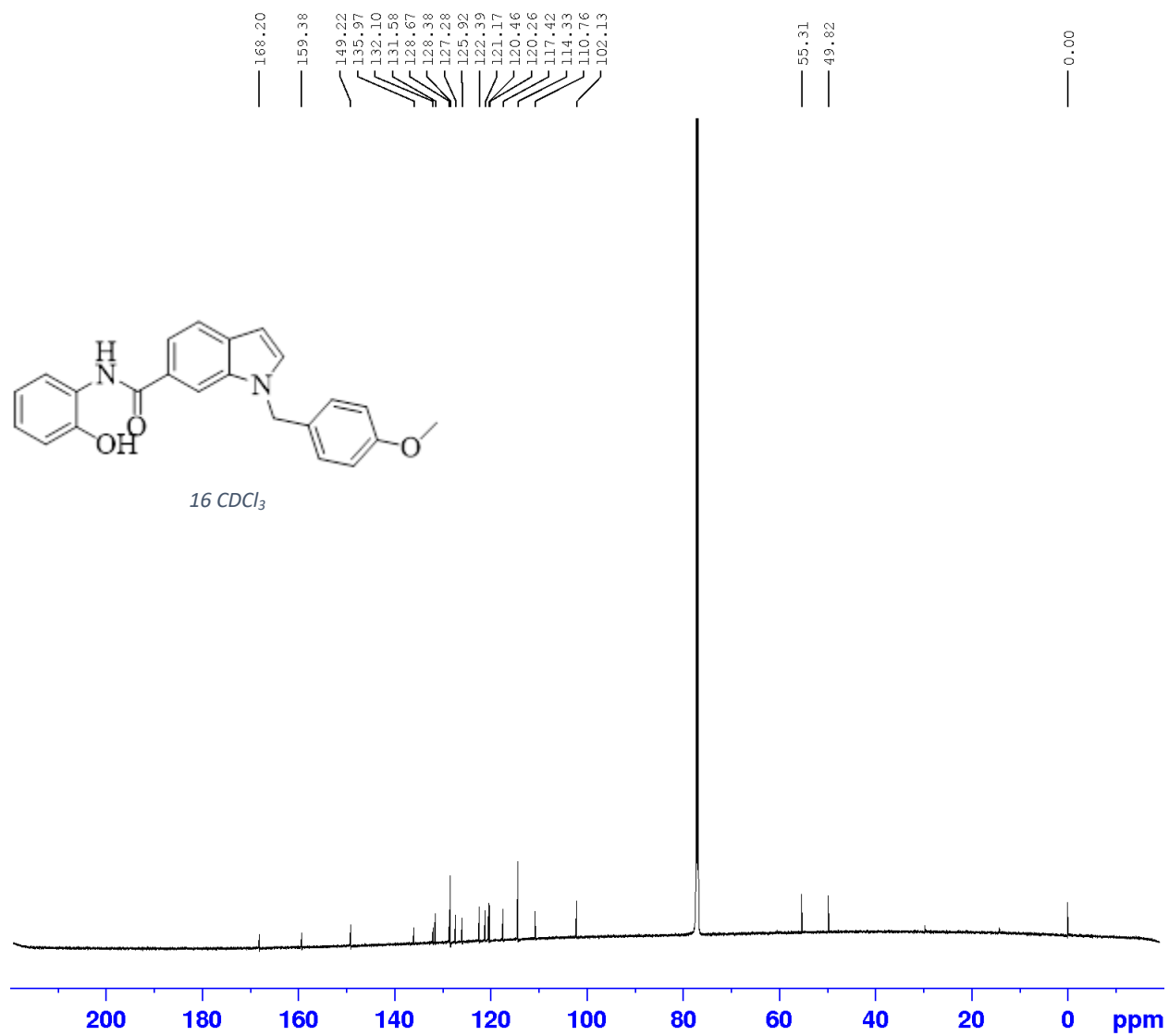


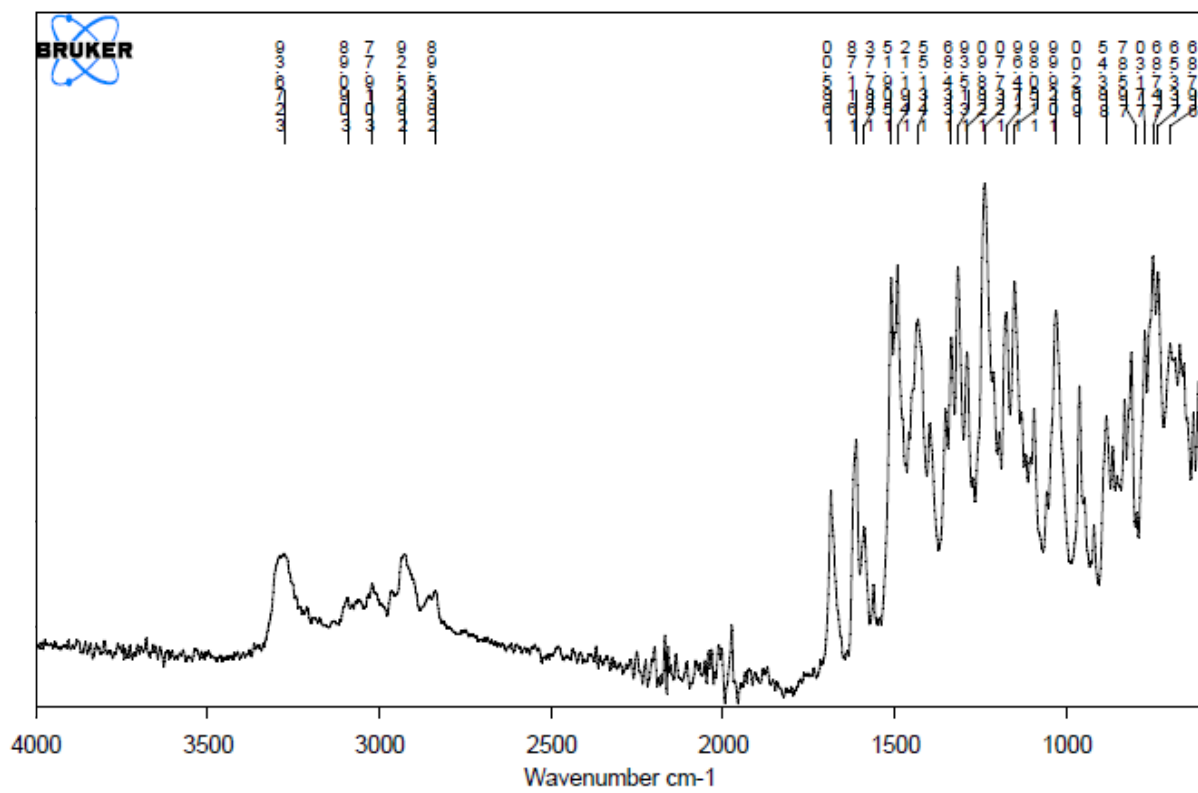




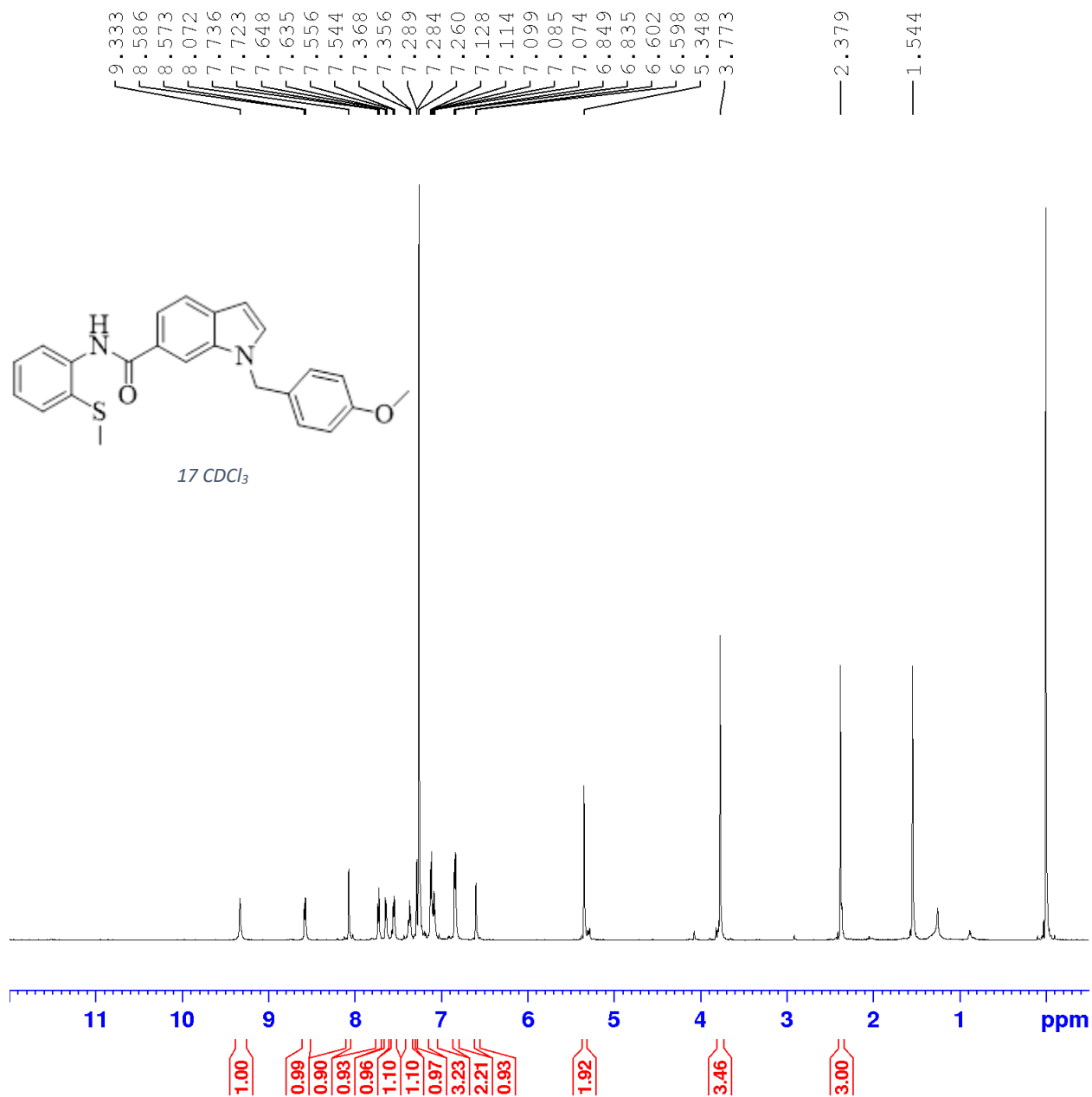
16

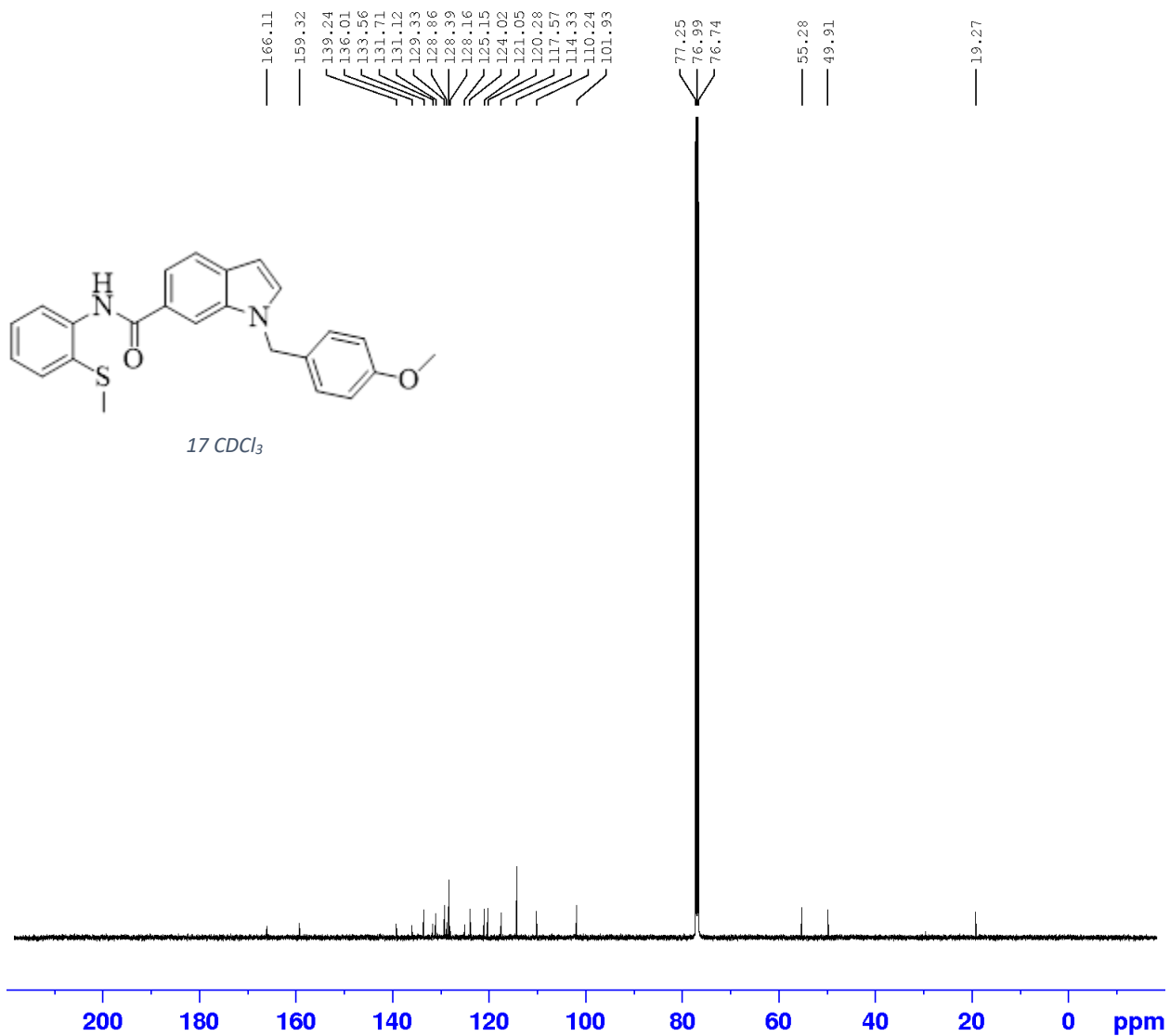


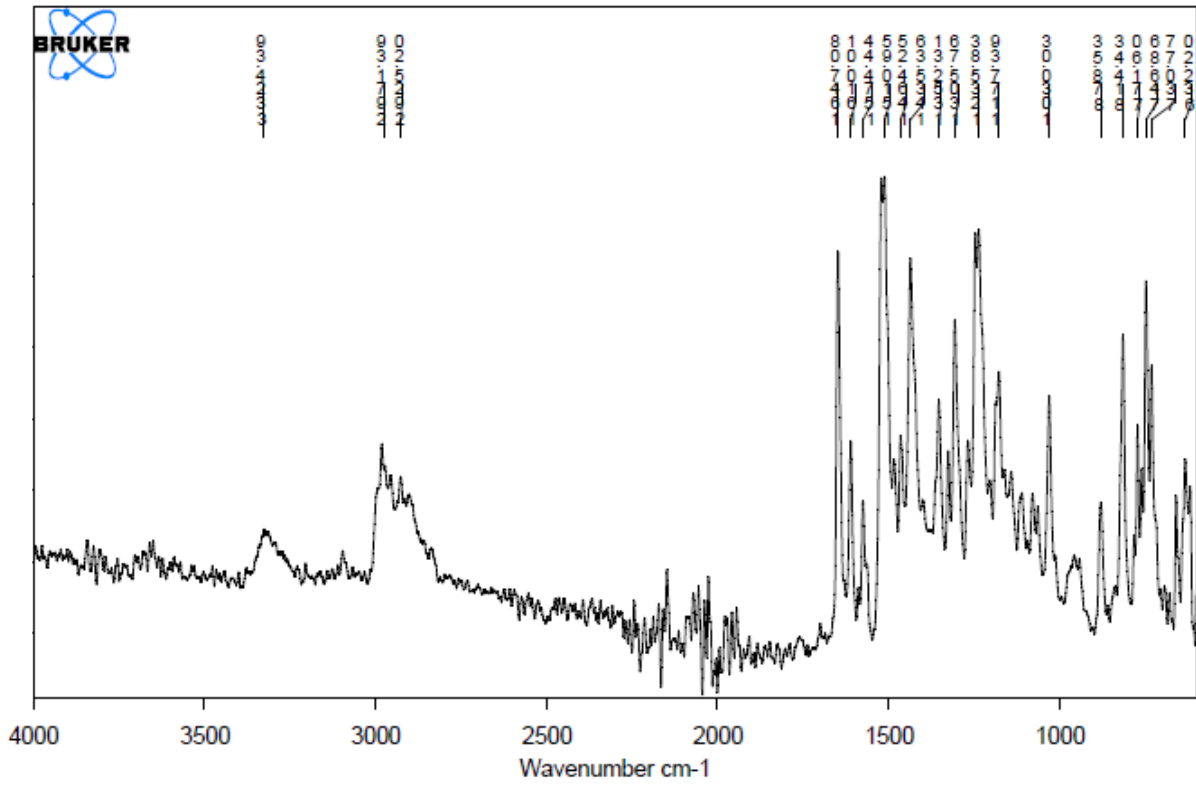




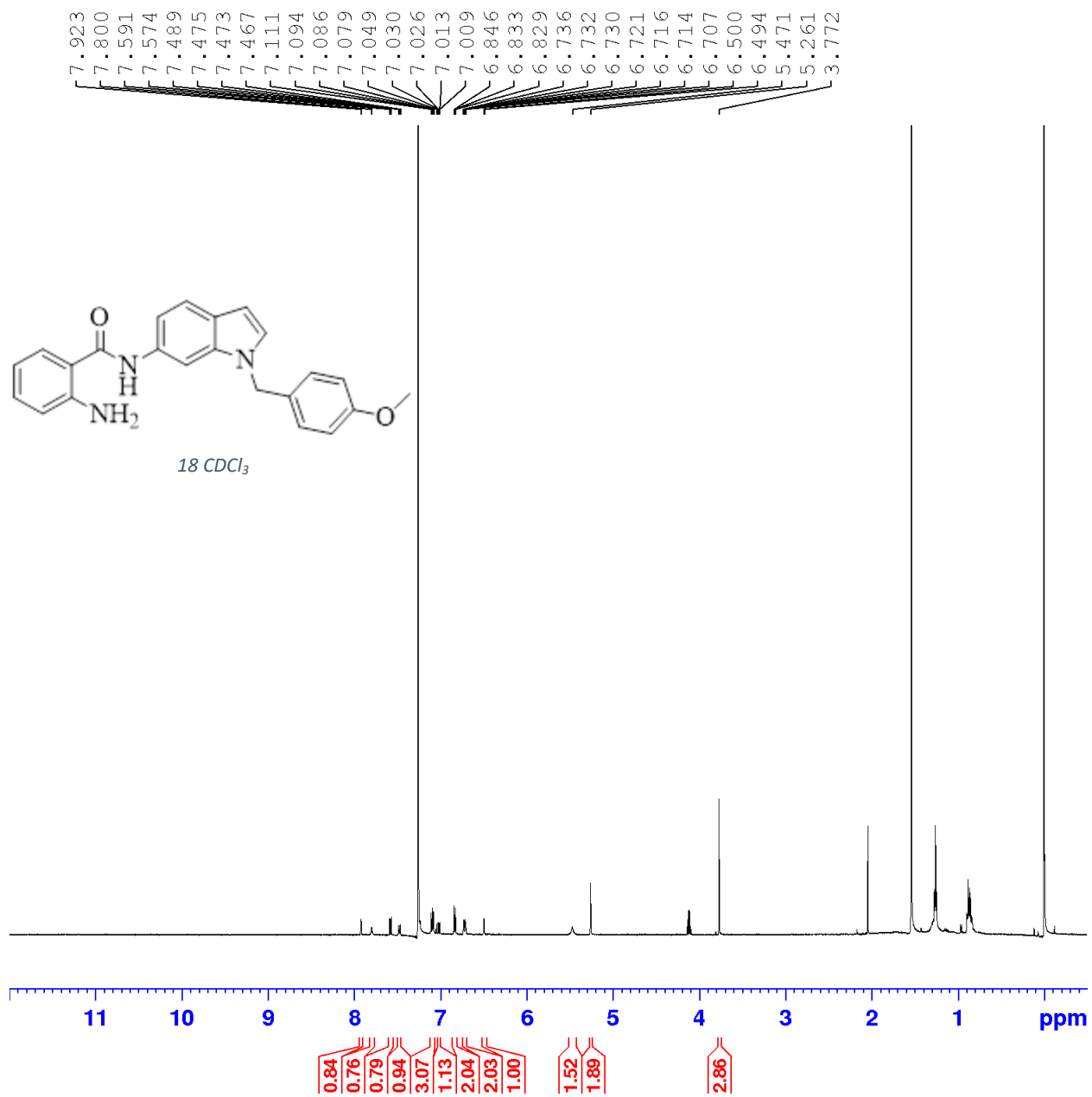
17

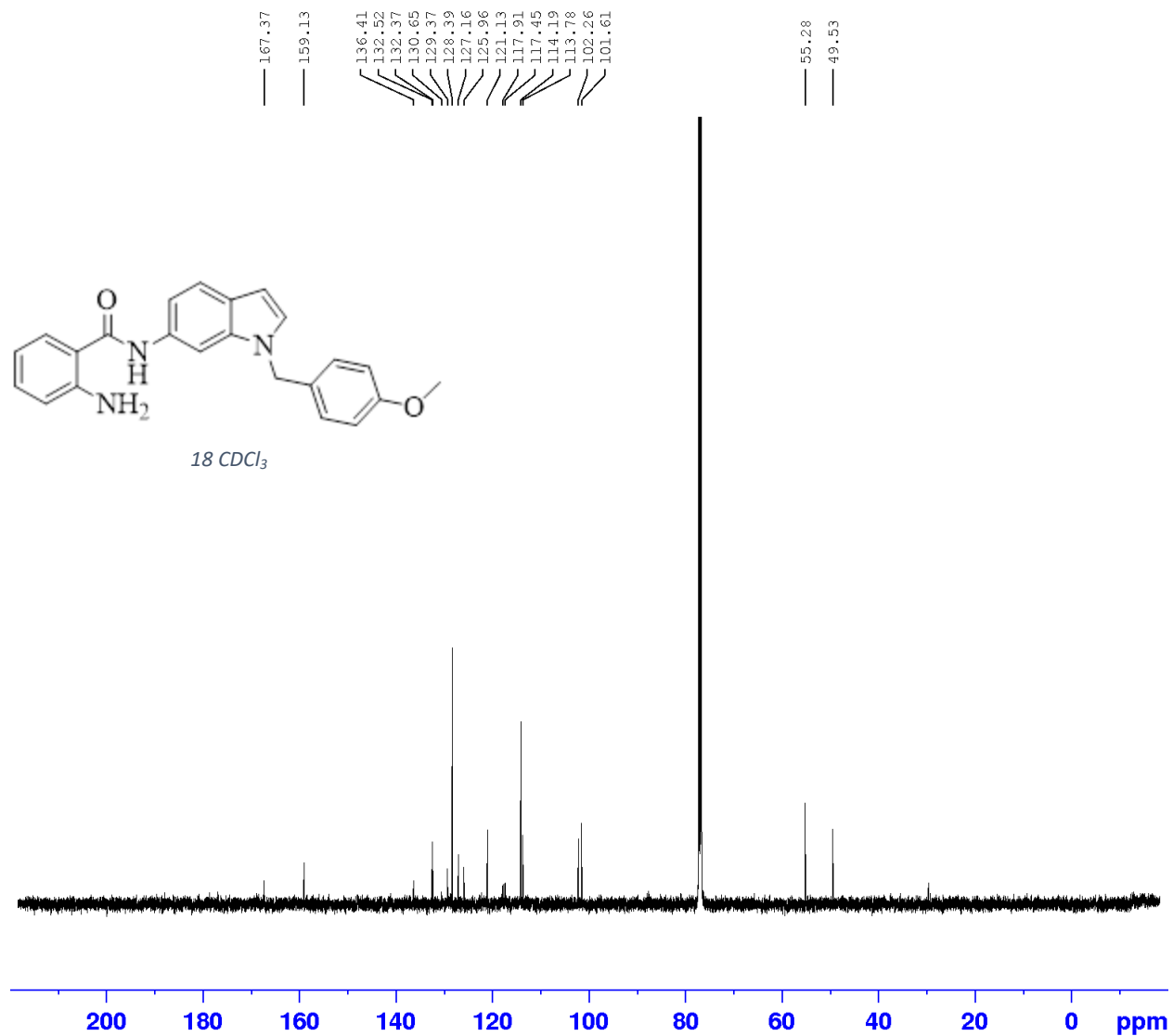


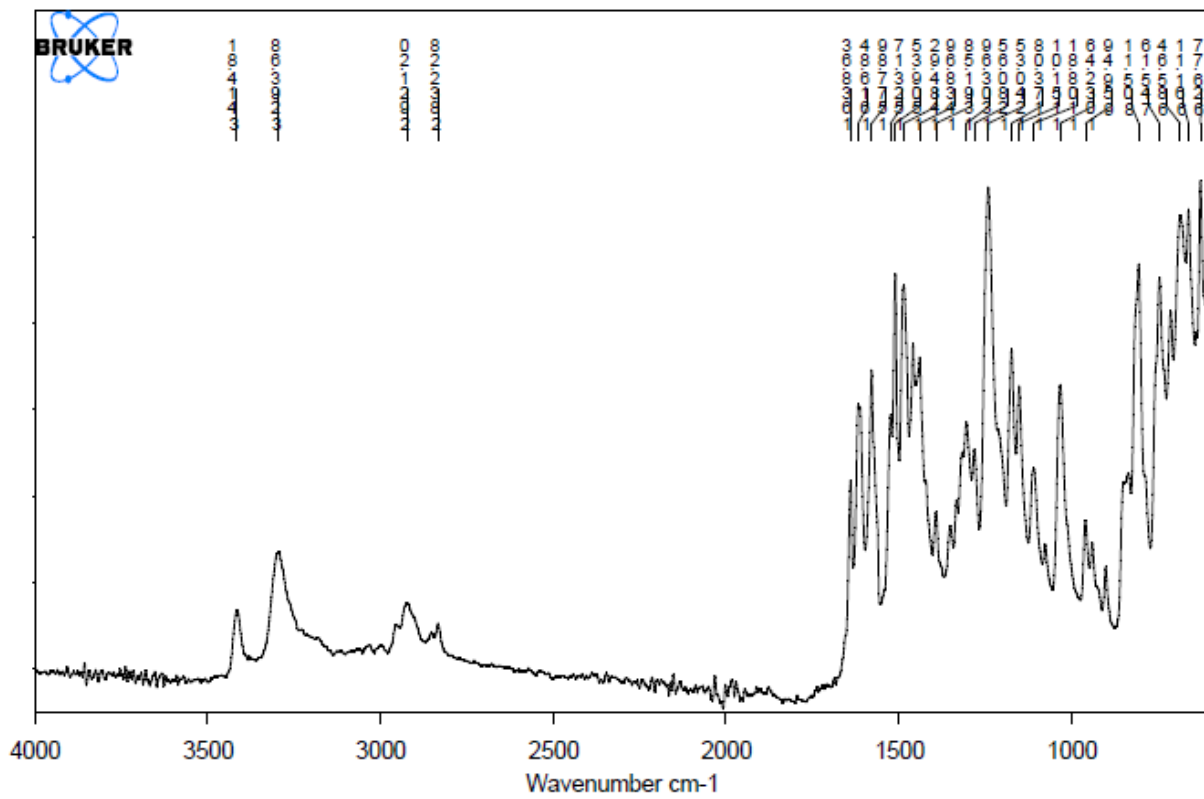




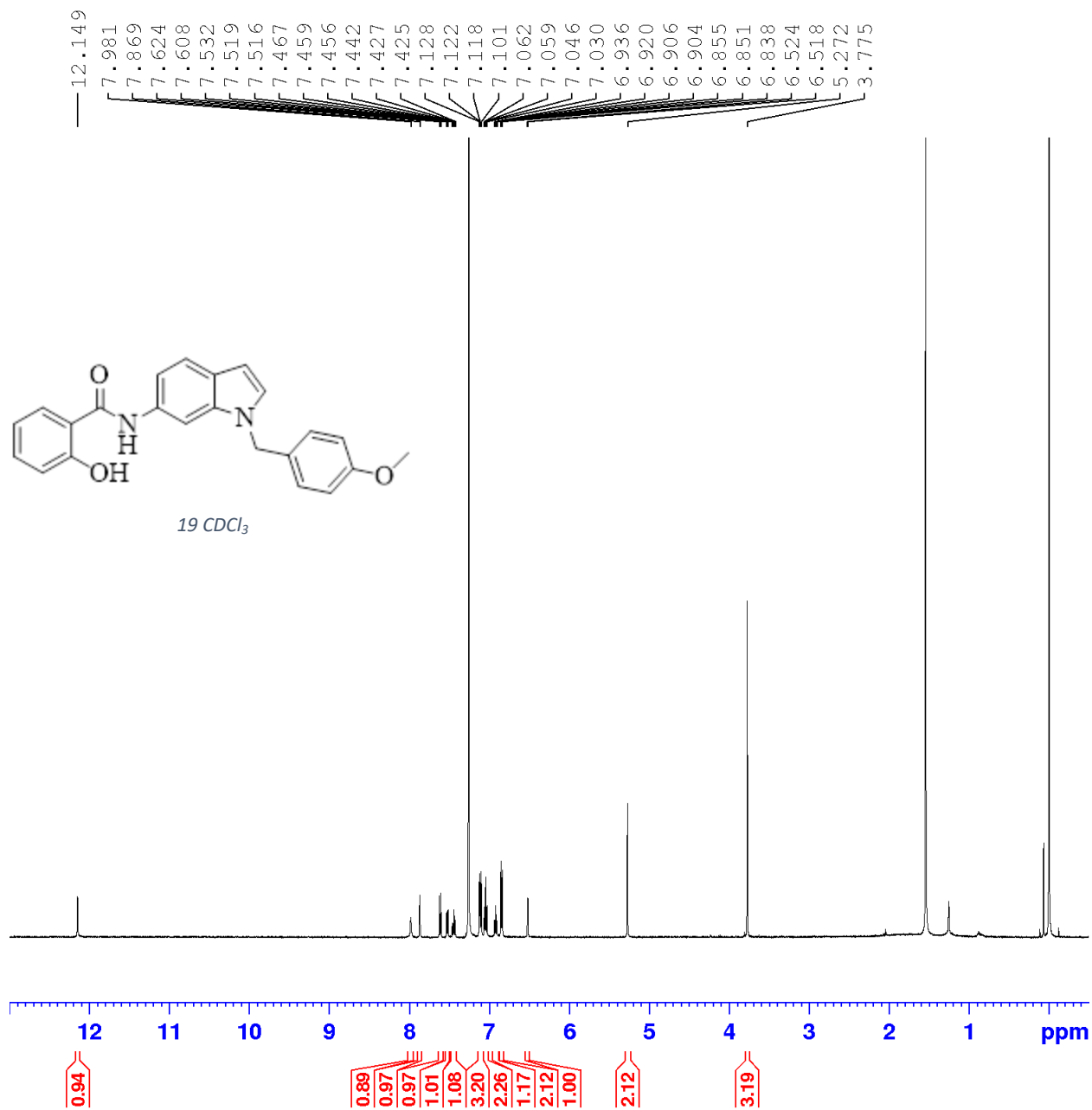
18

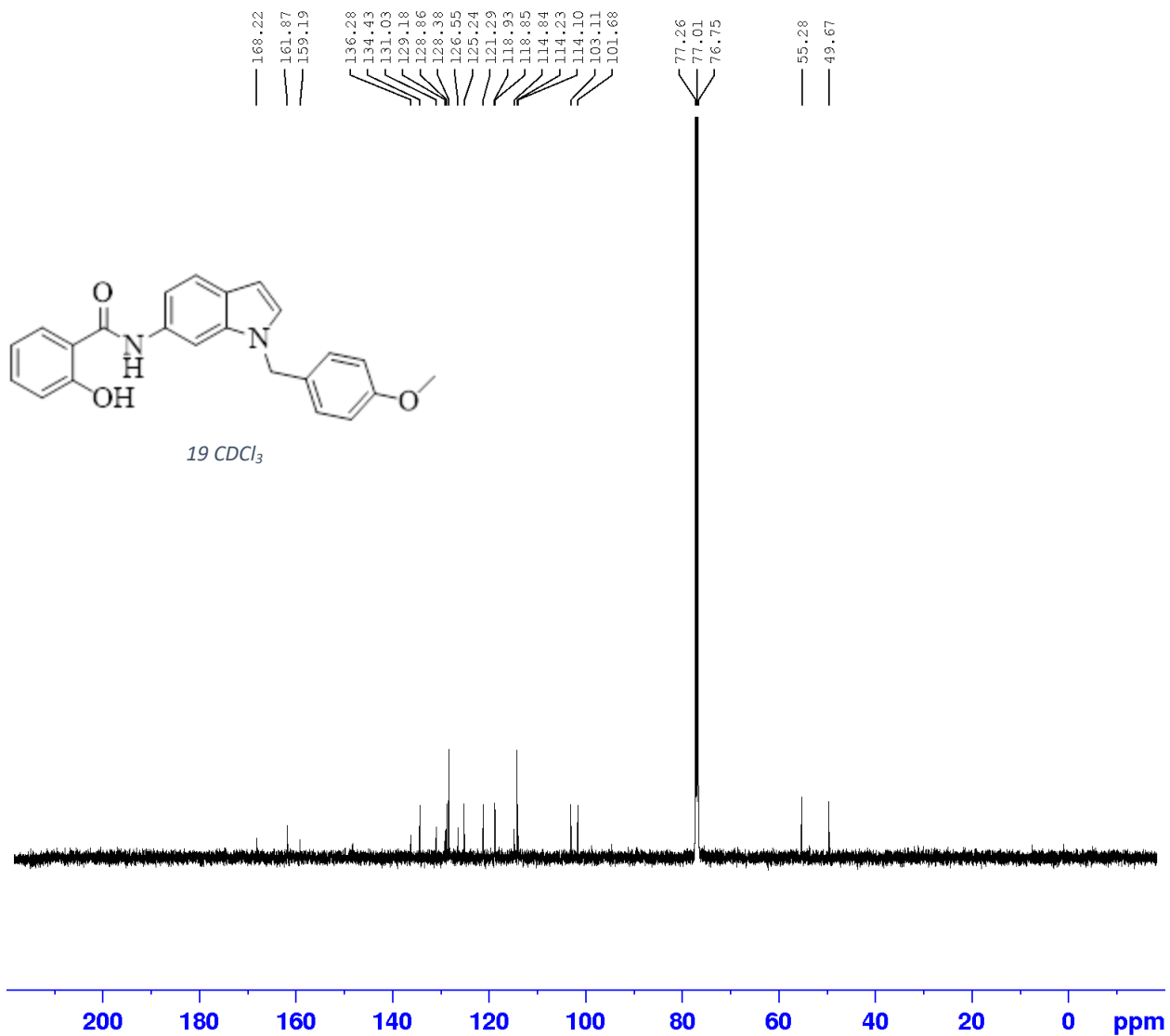


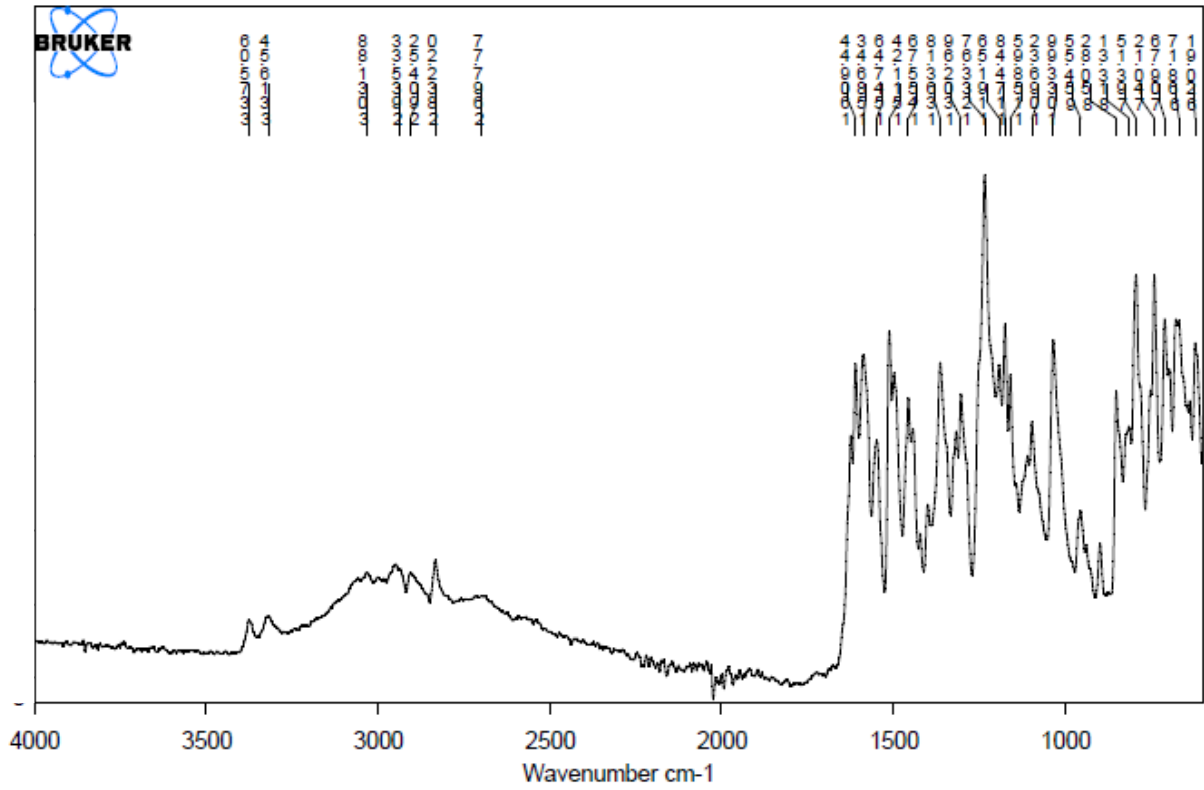




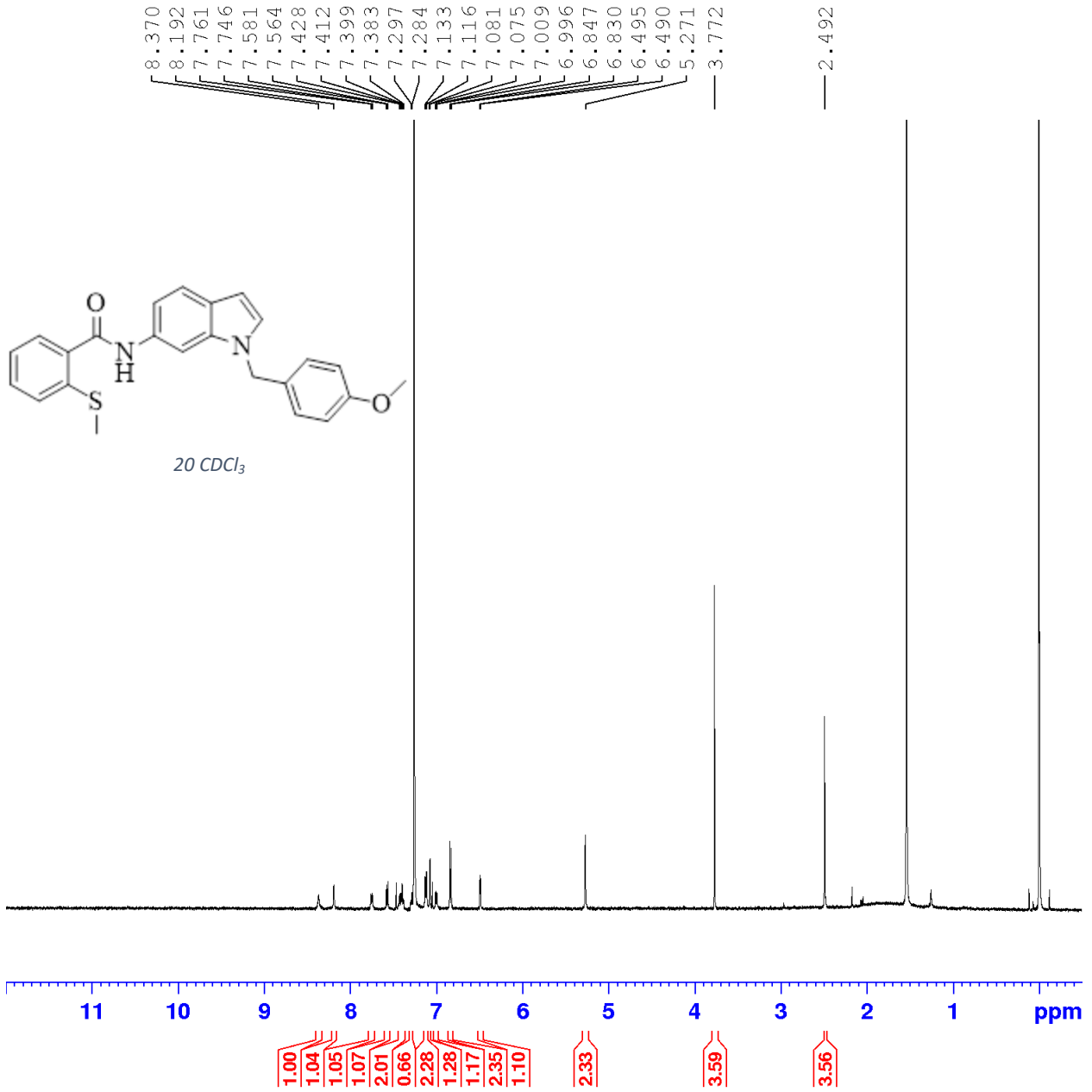
19

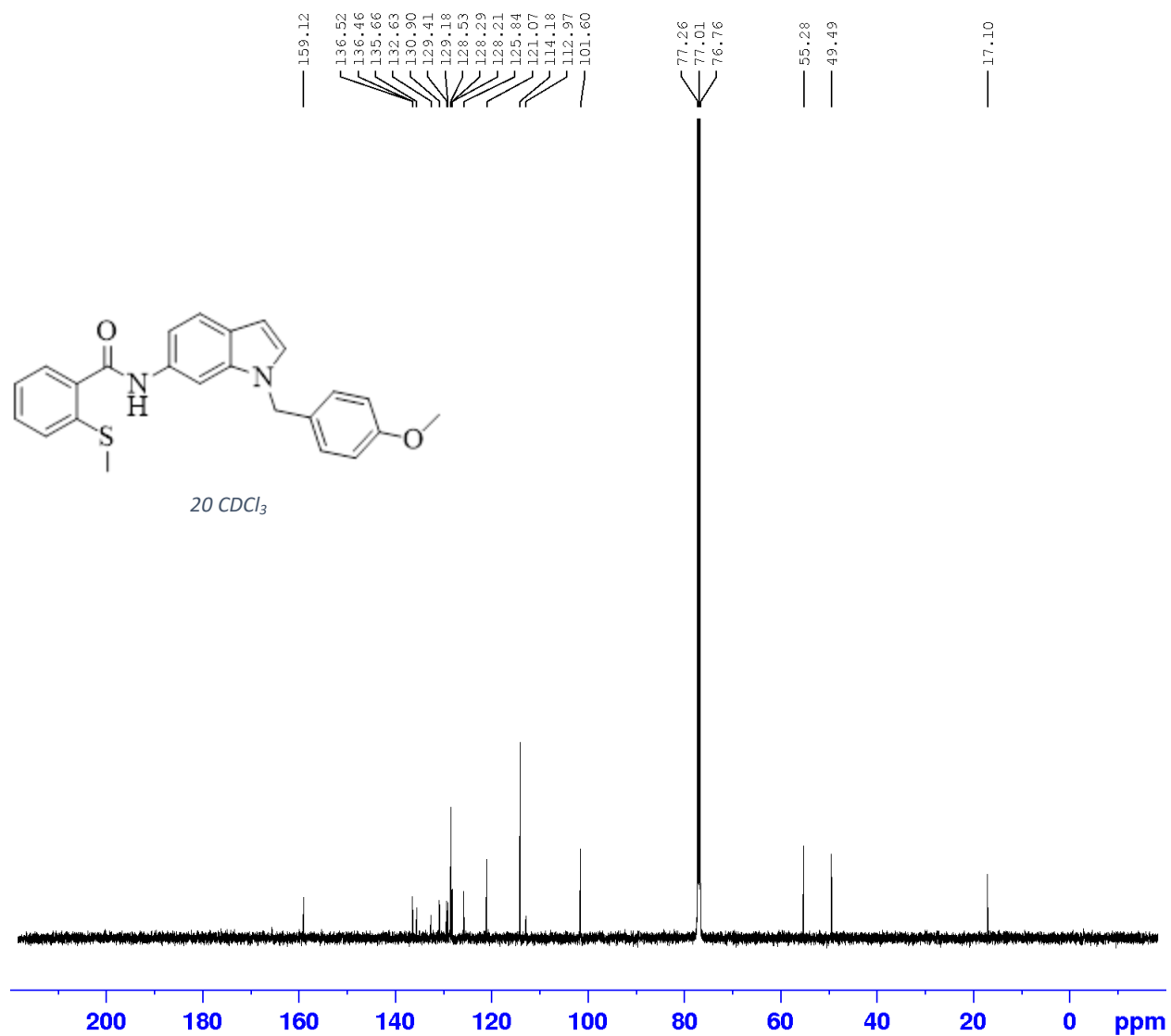


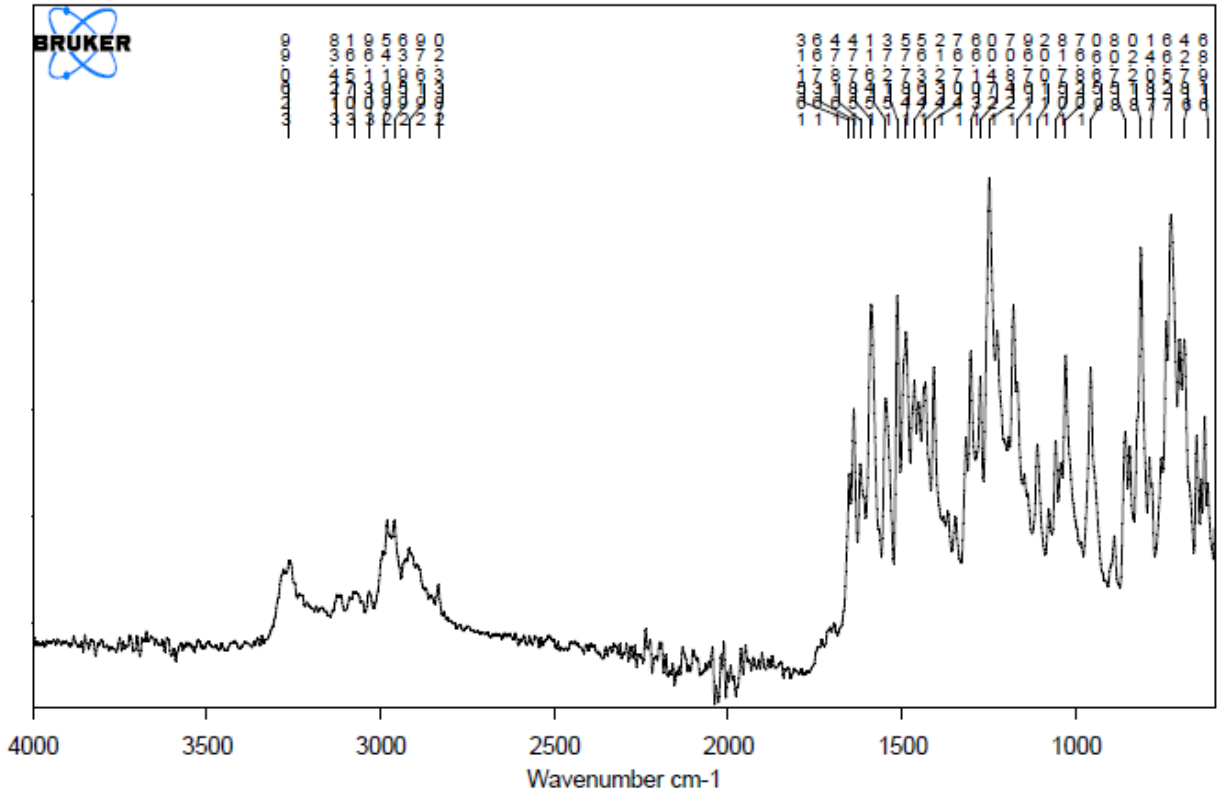




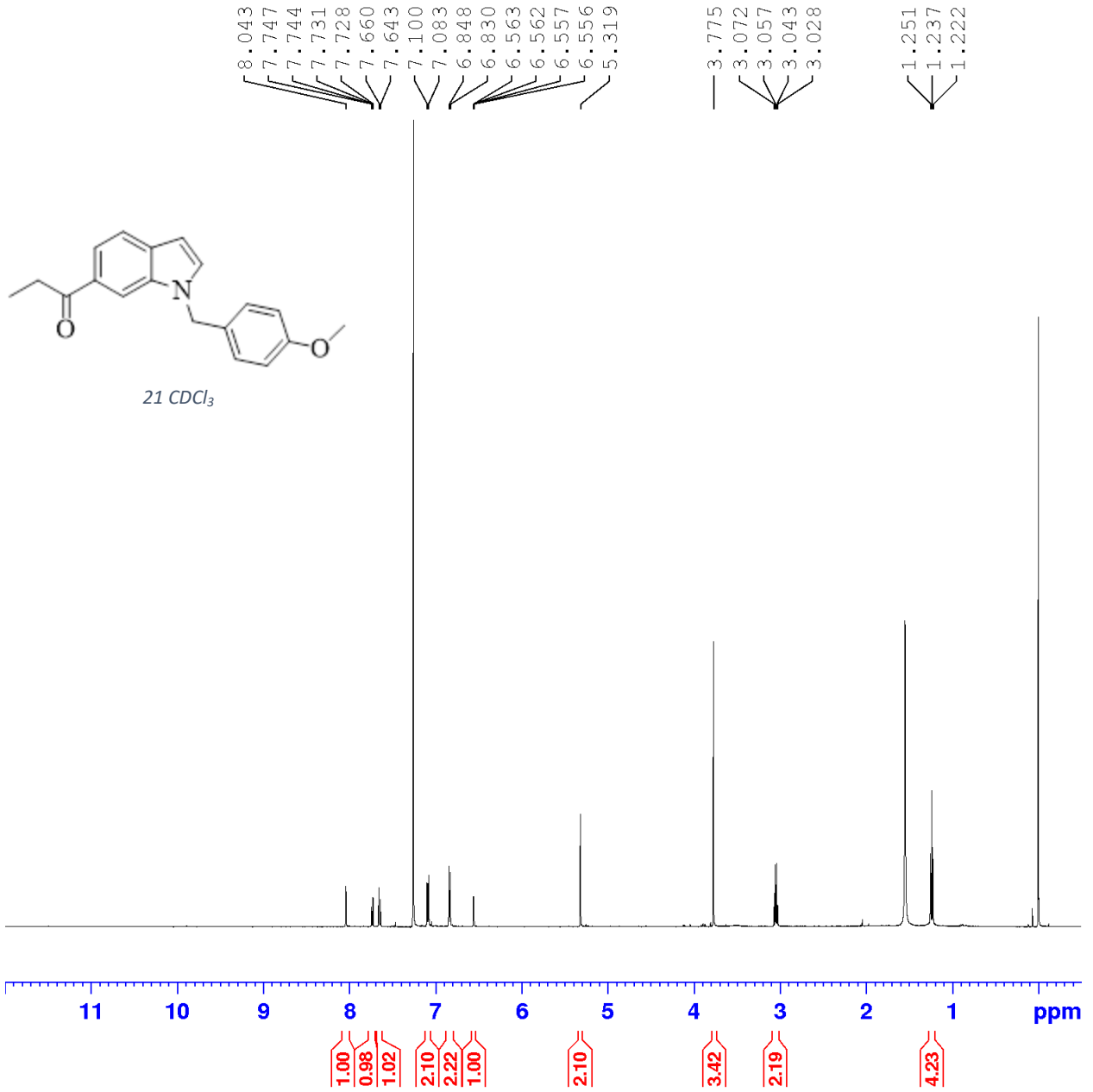
20

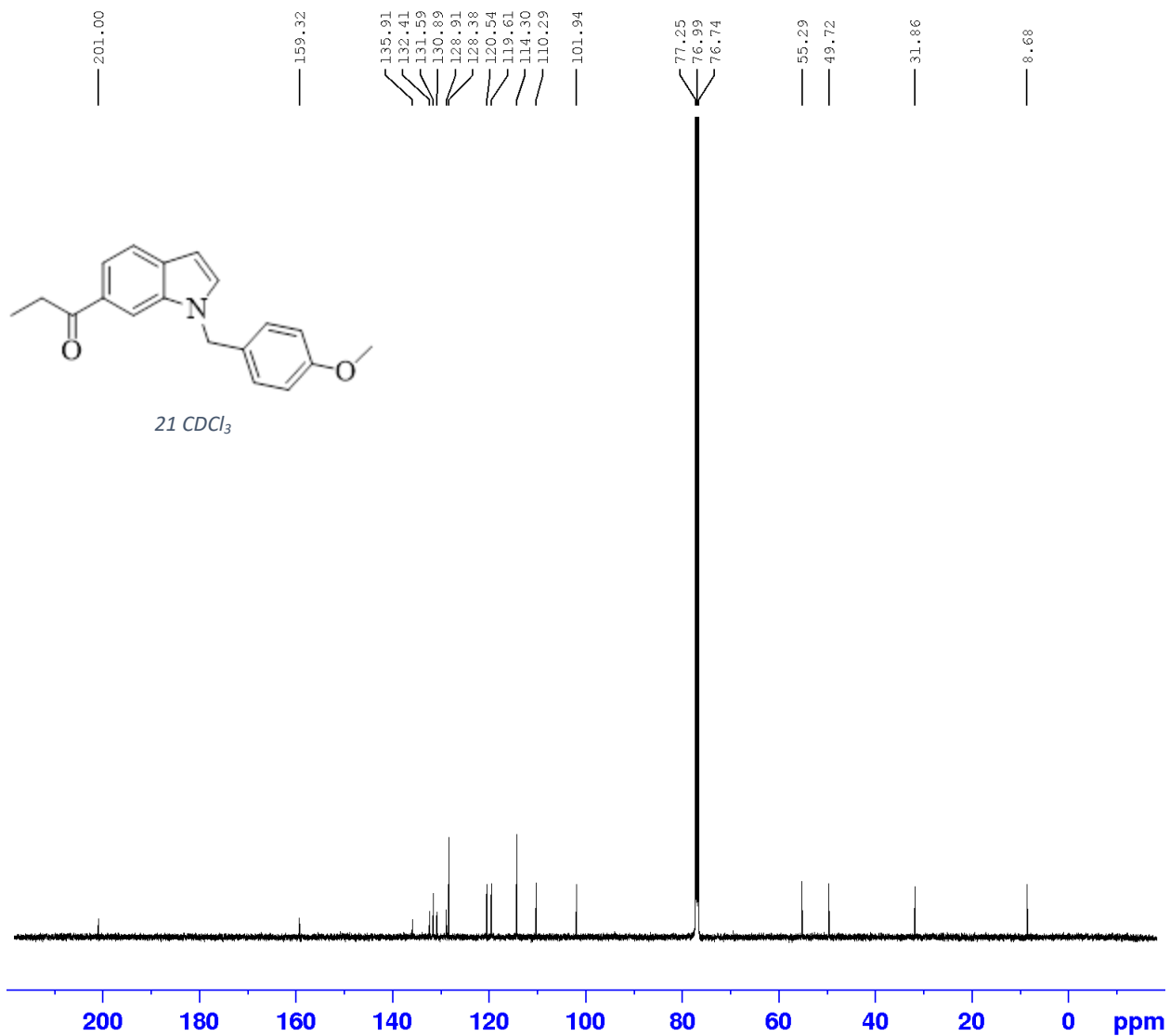


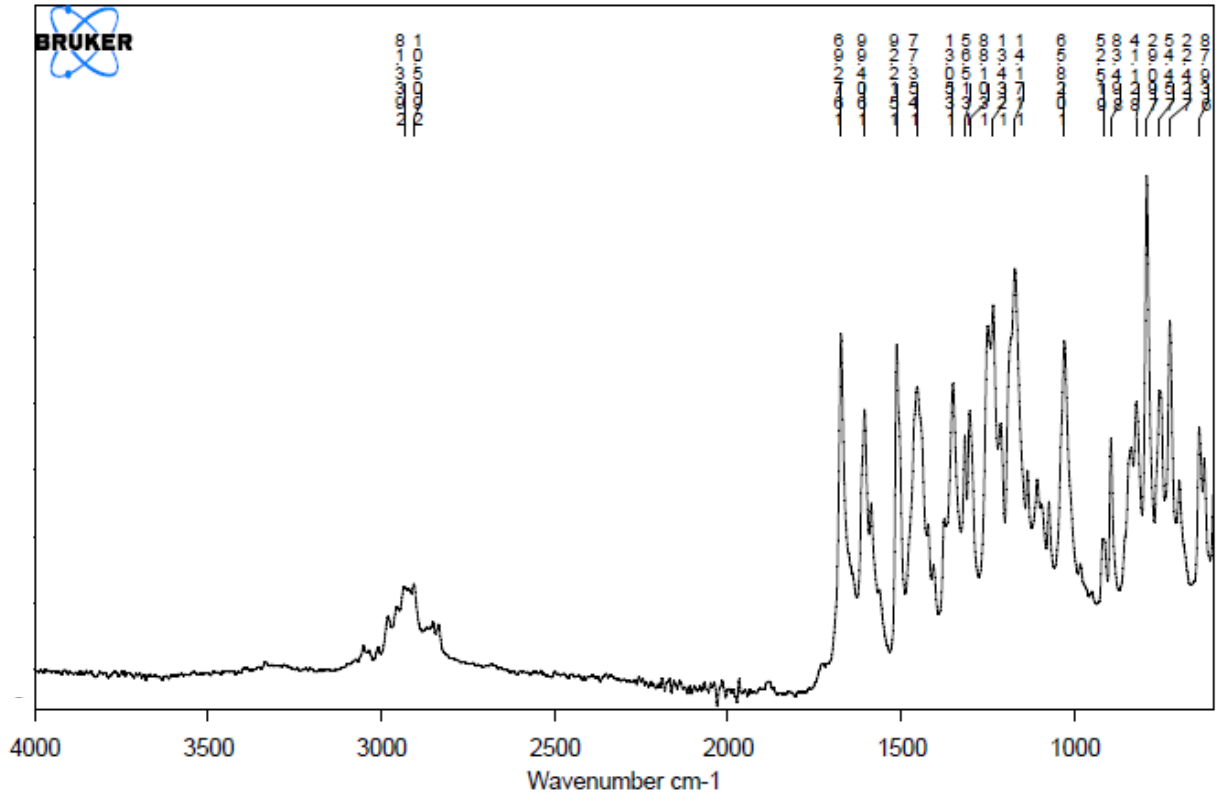




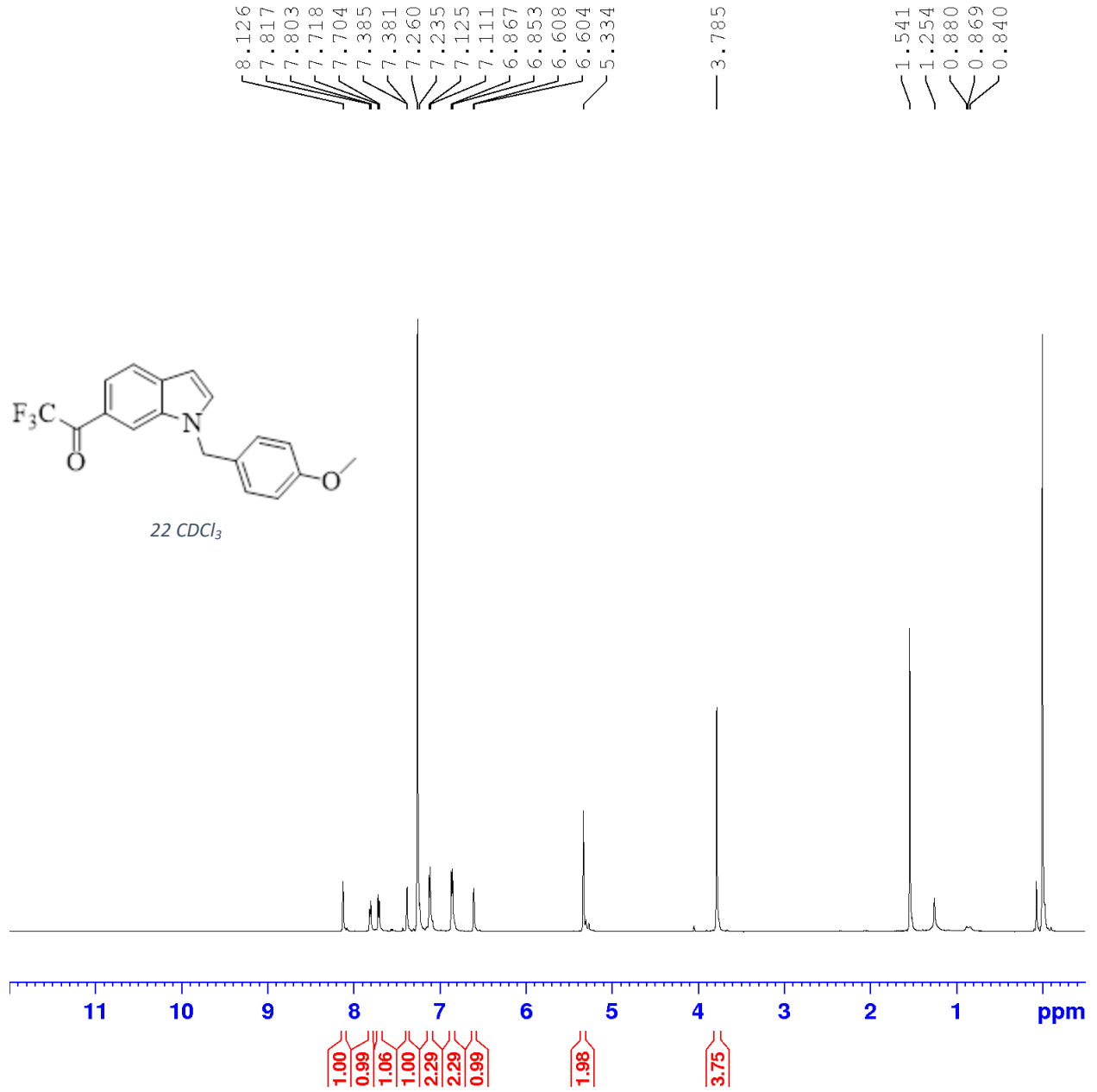
21

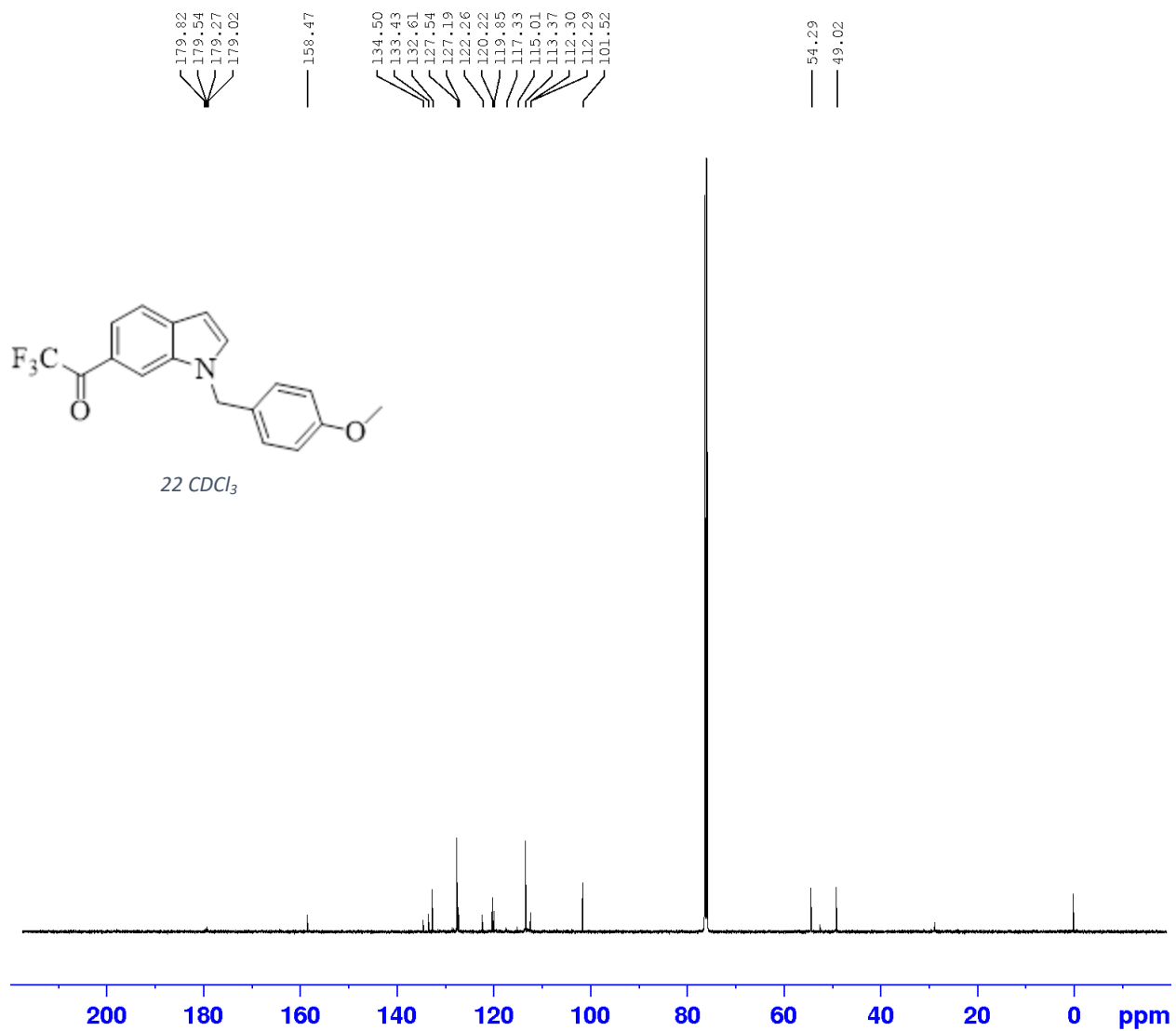




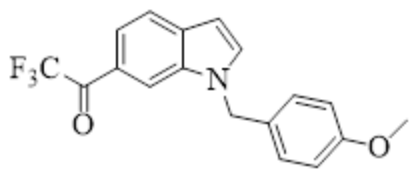


22

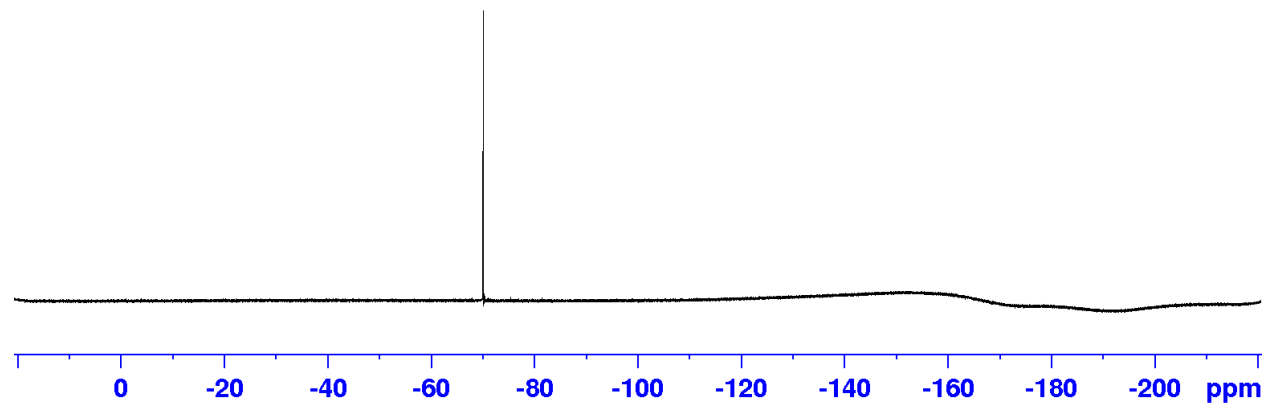




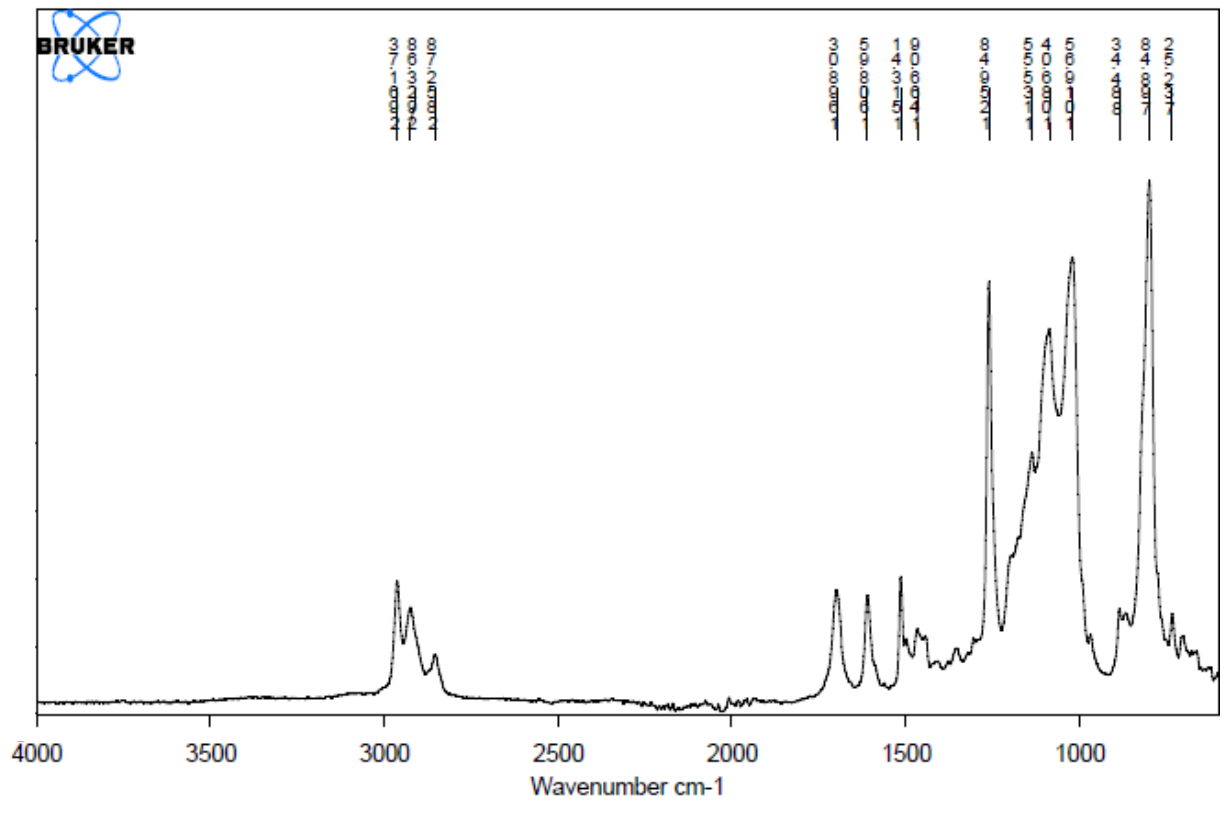
-70.07



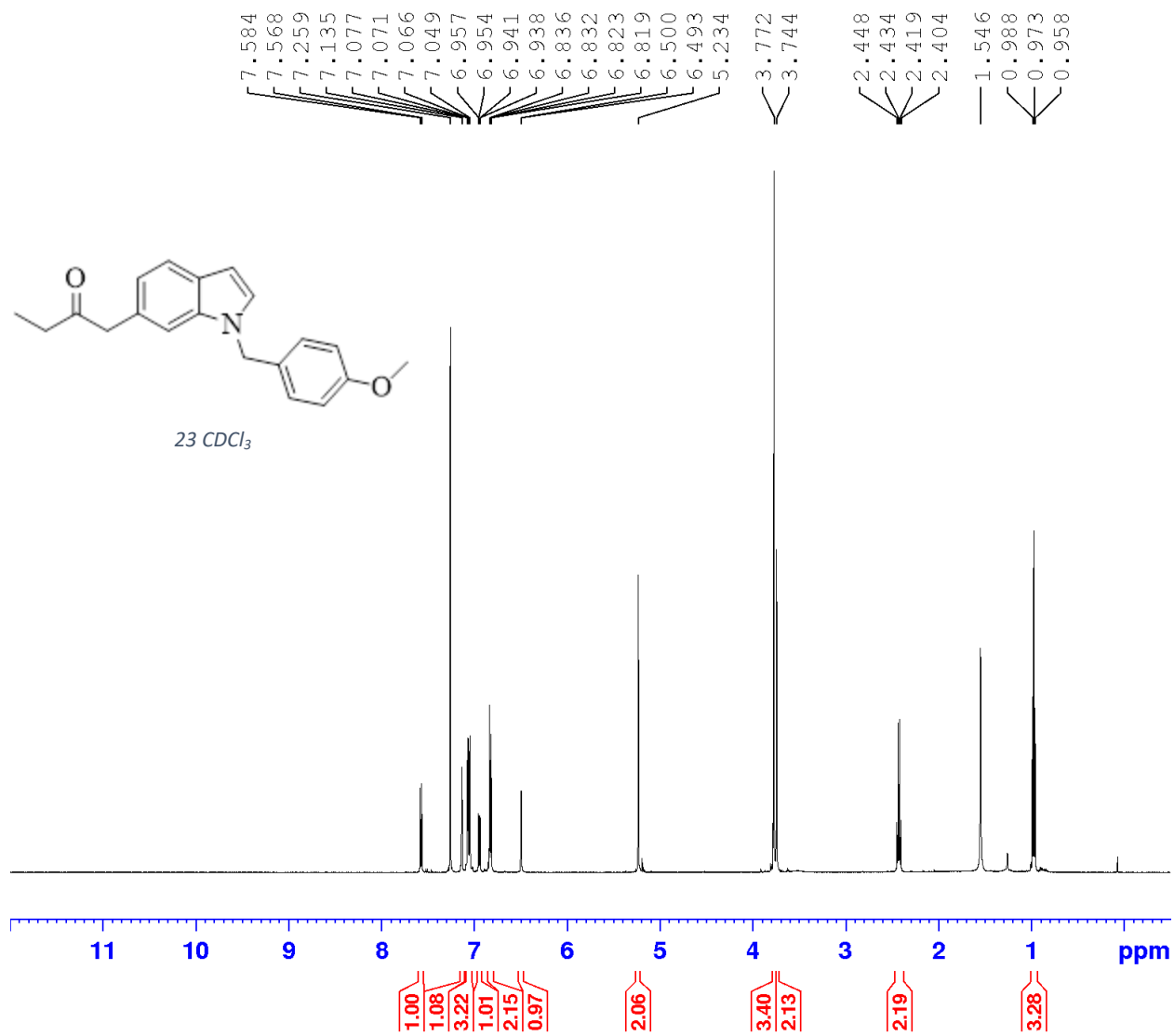
22 CDCl₃

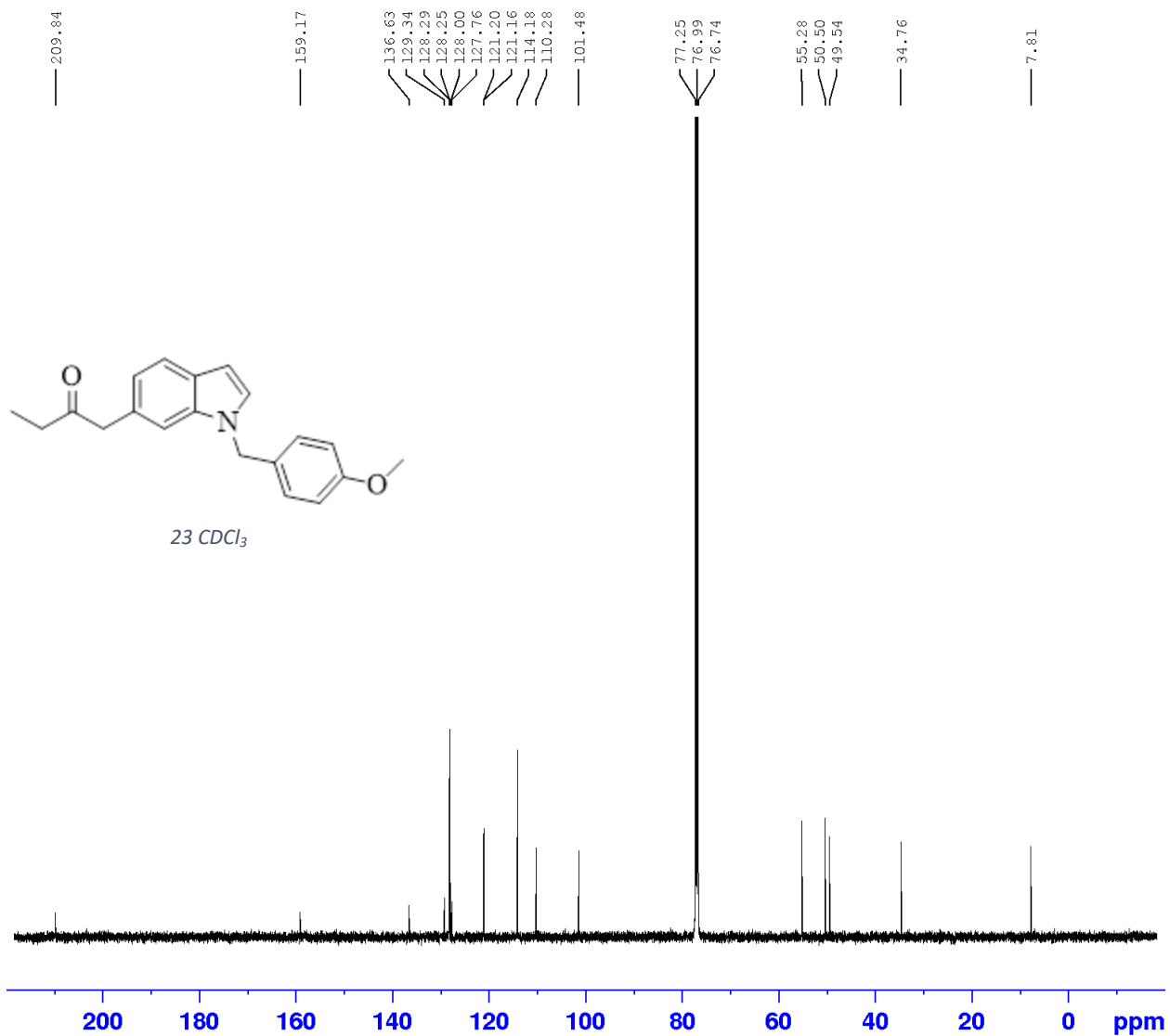


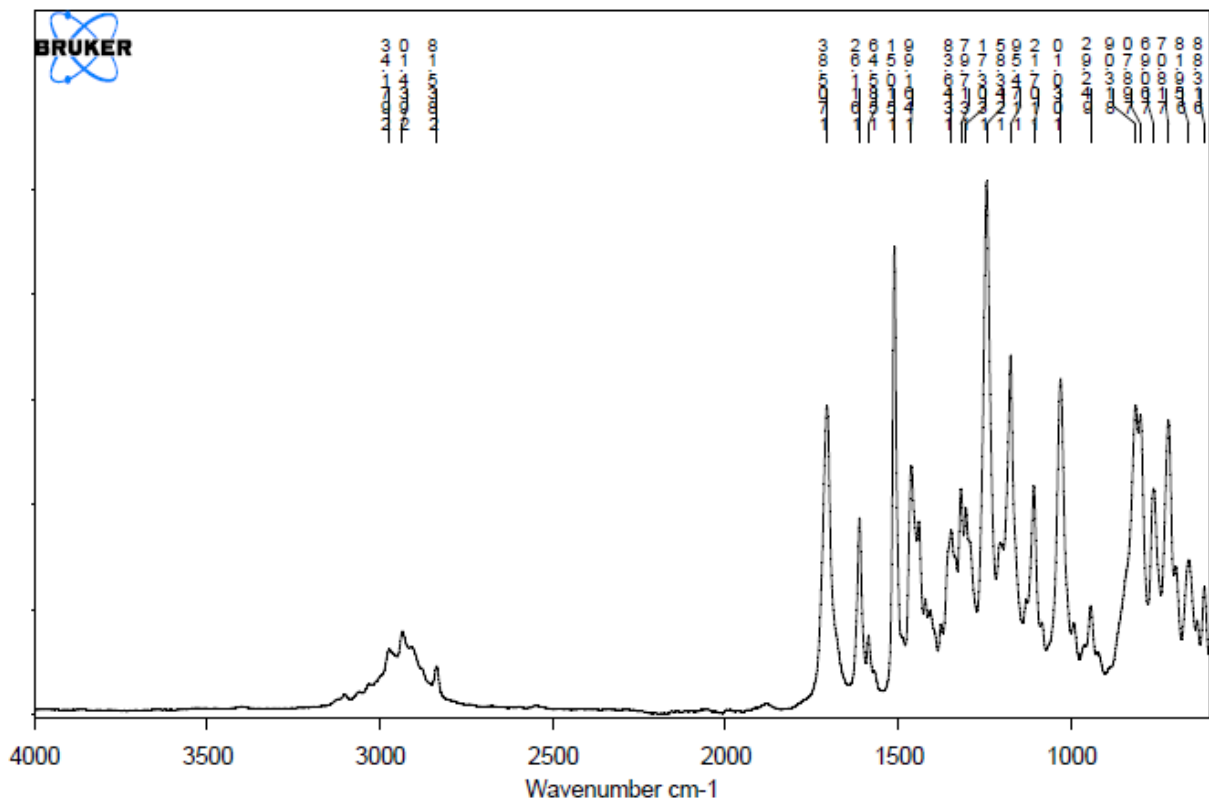
¹⁹F NMR



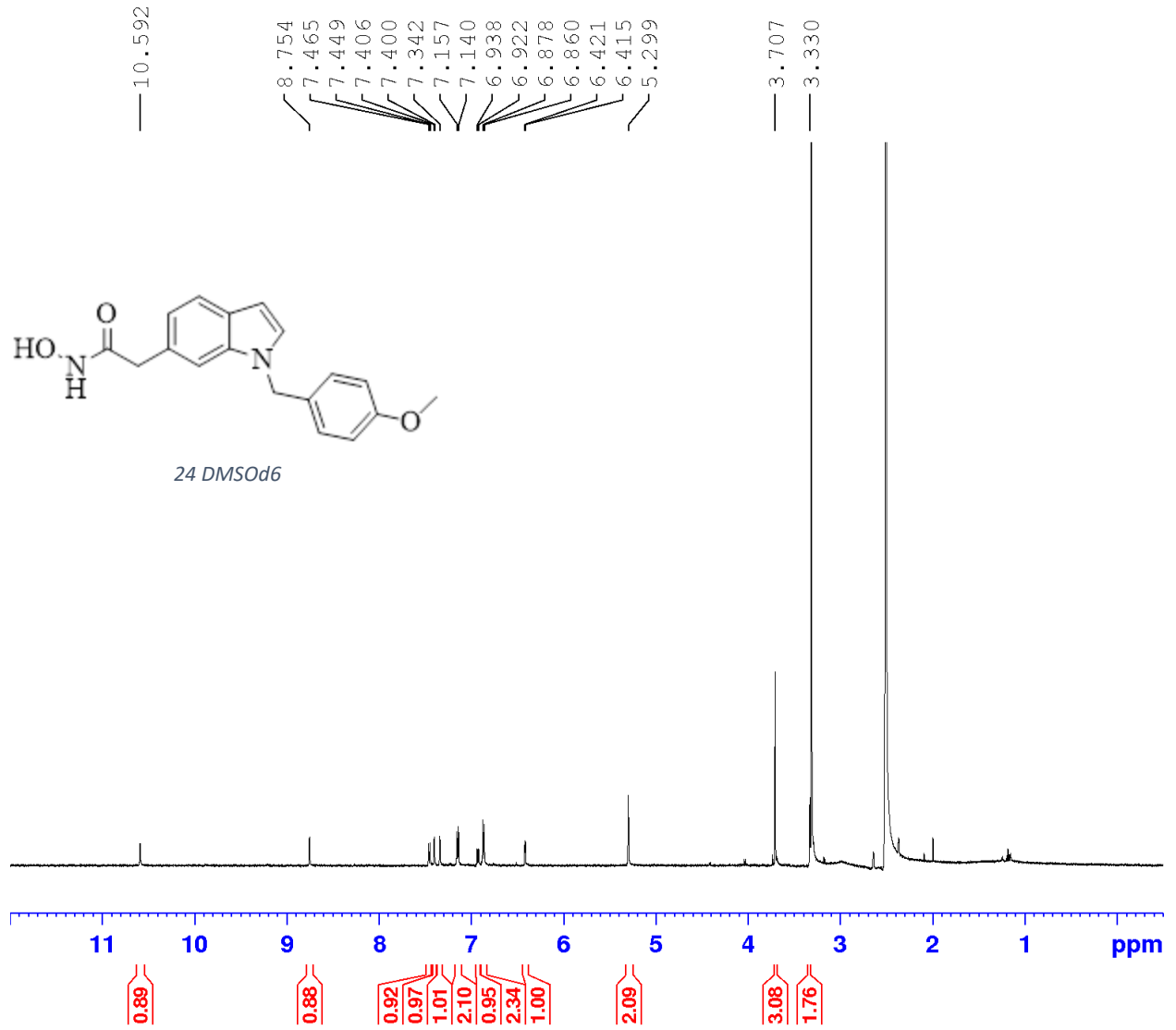
23

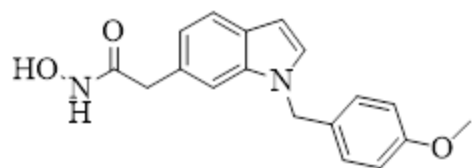




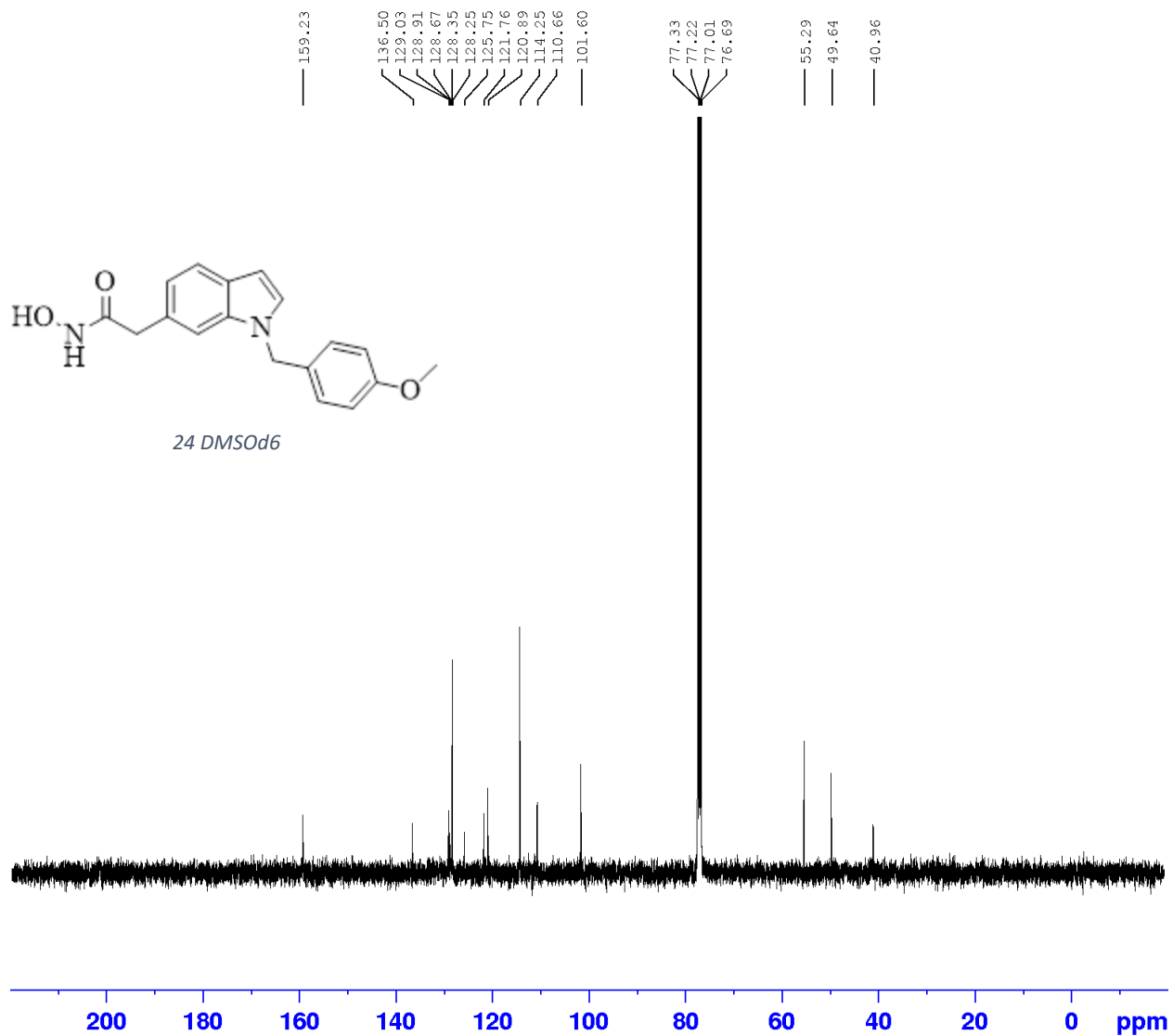


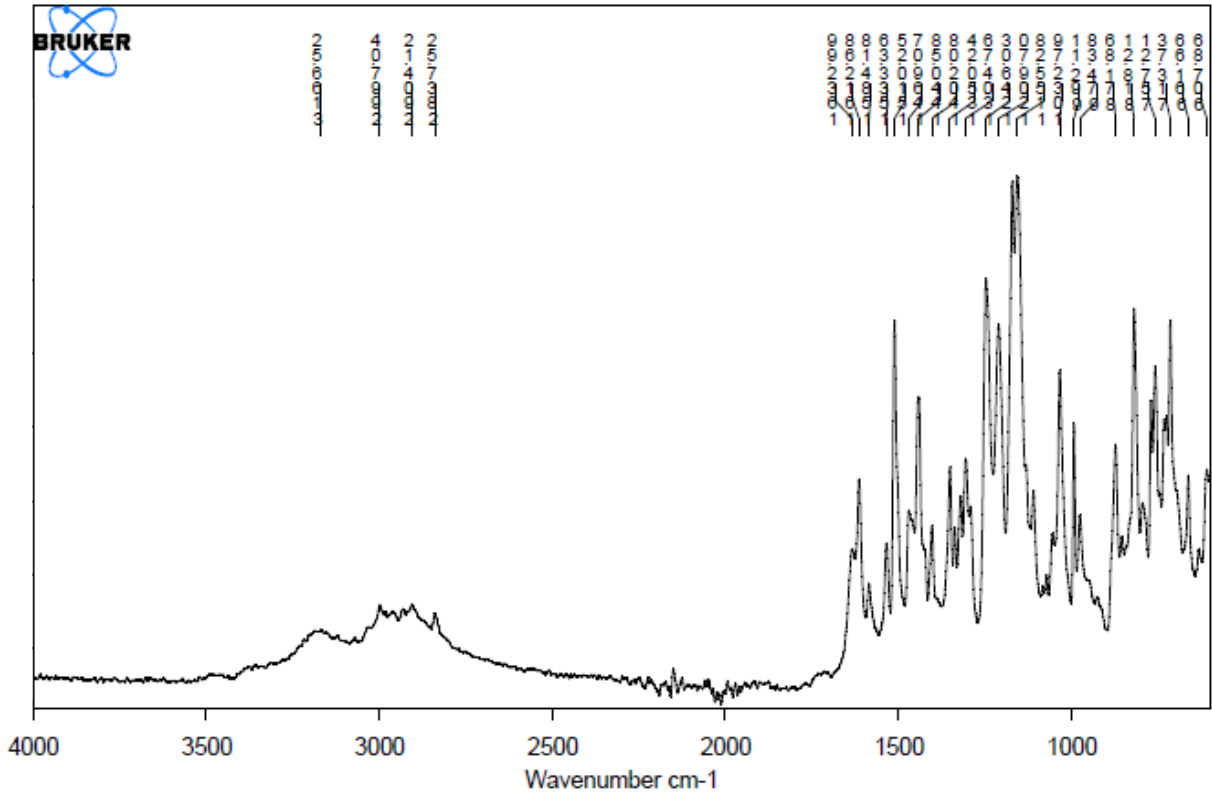
24



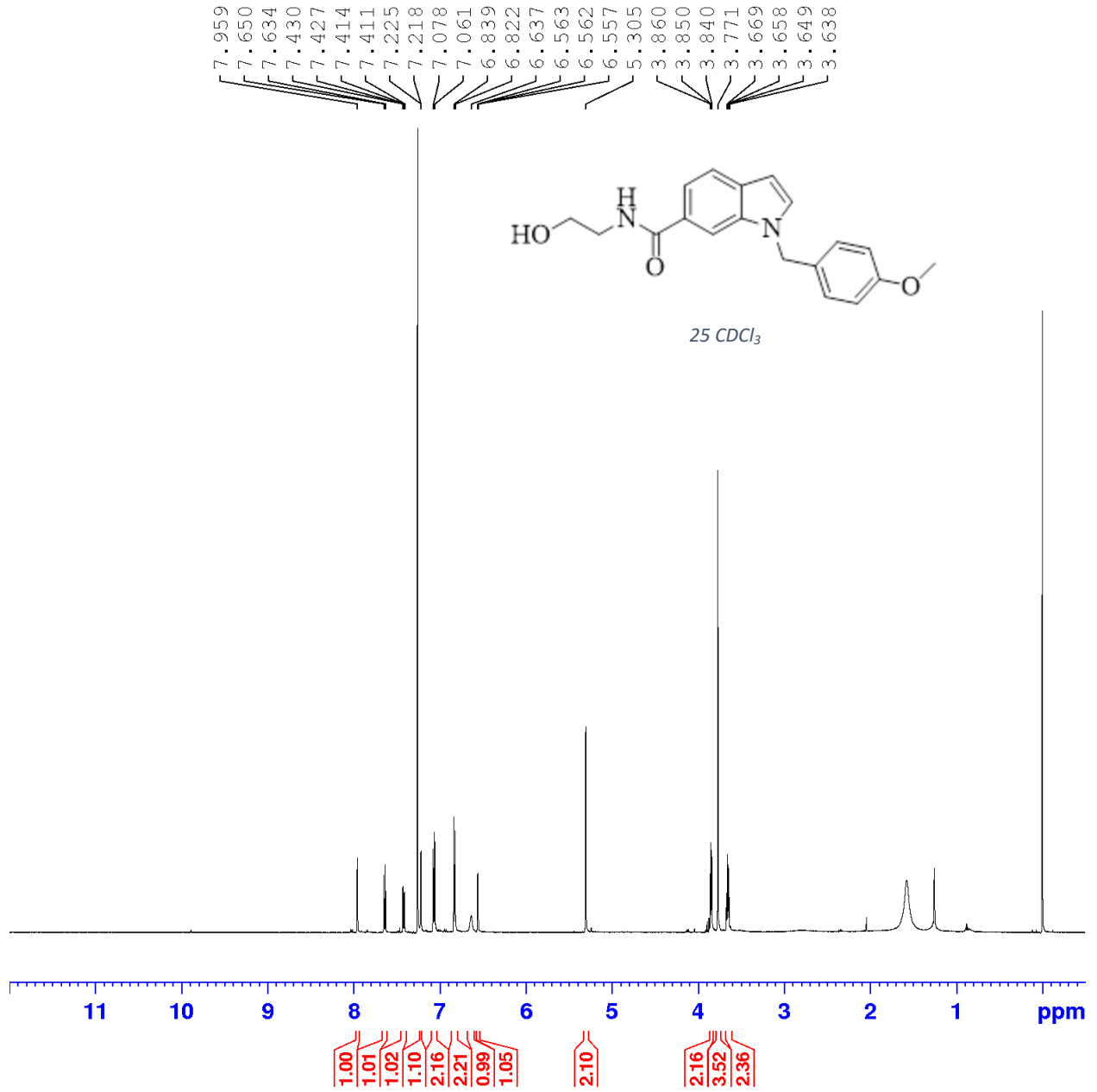


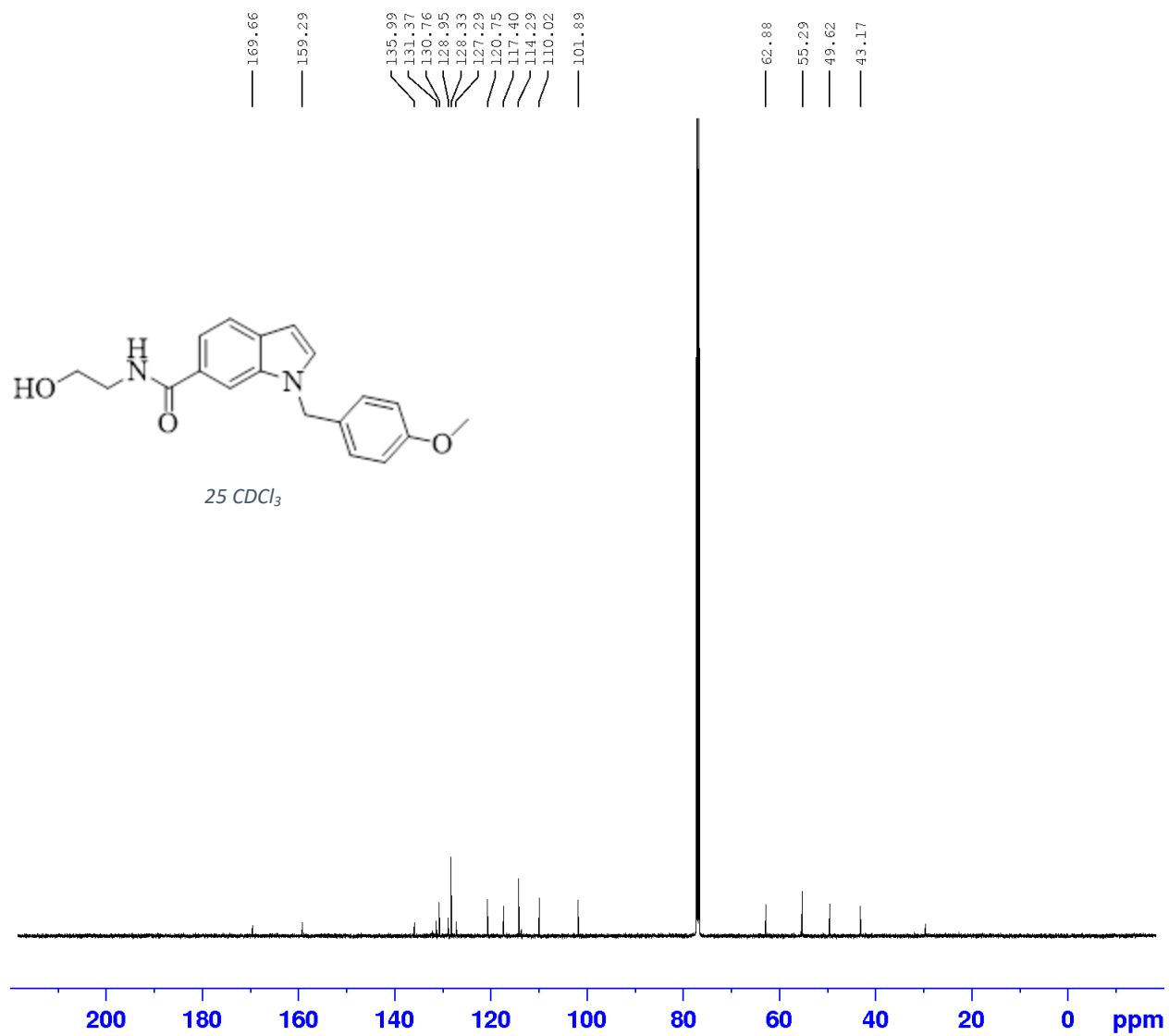
24 DMSO-d6

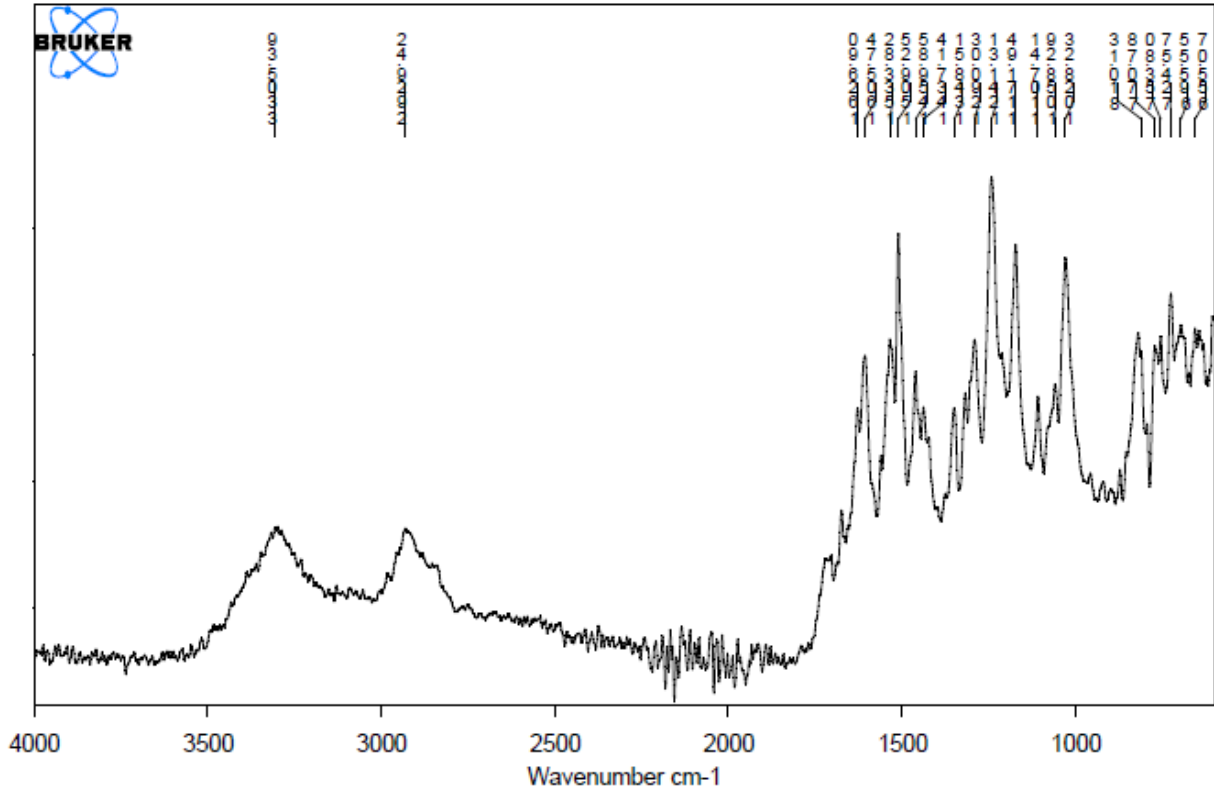


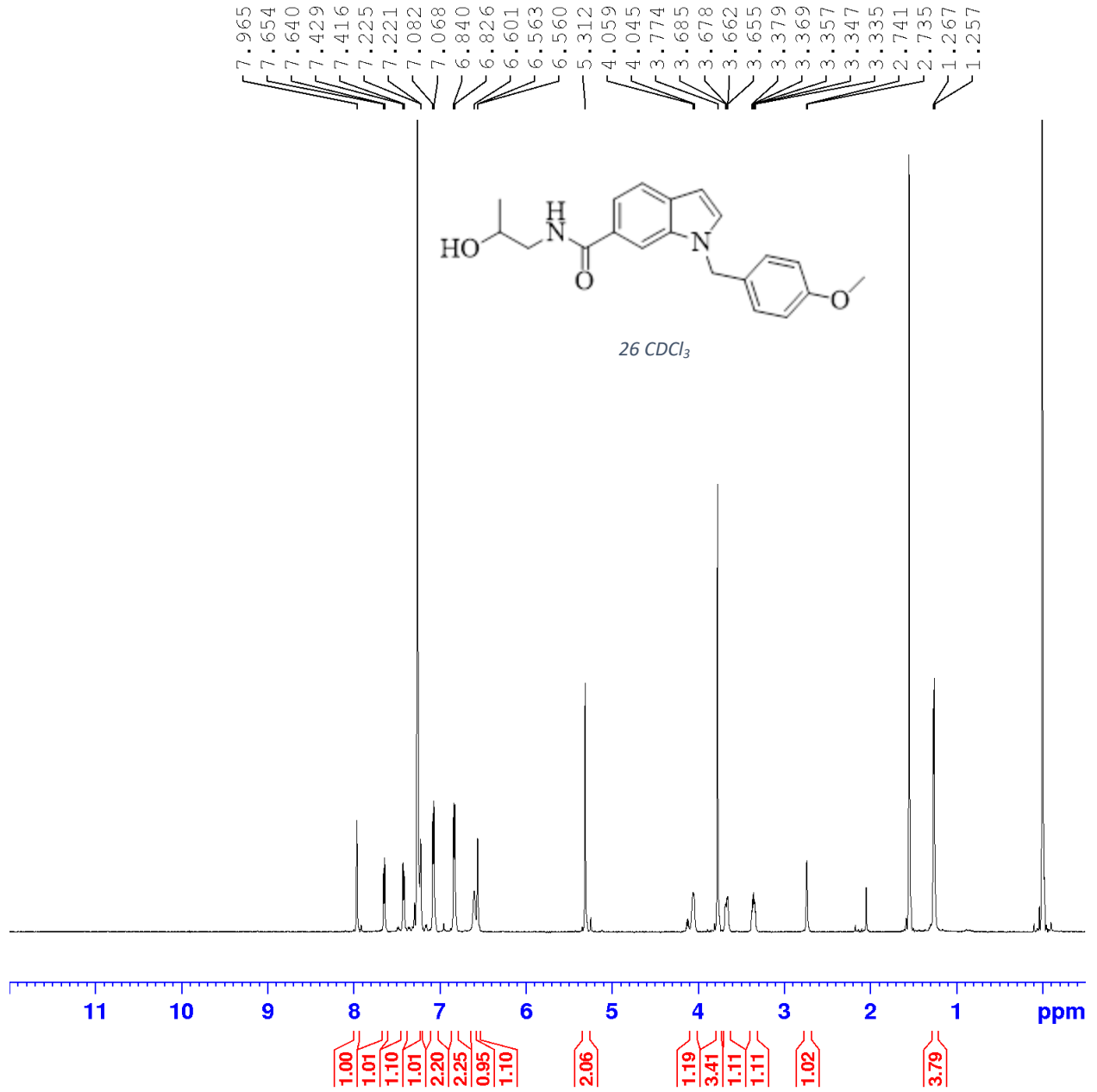


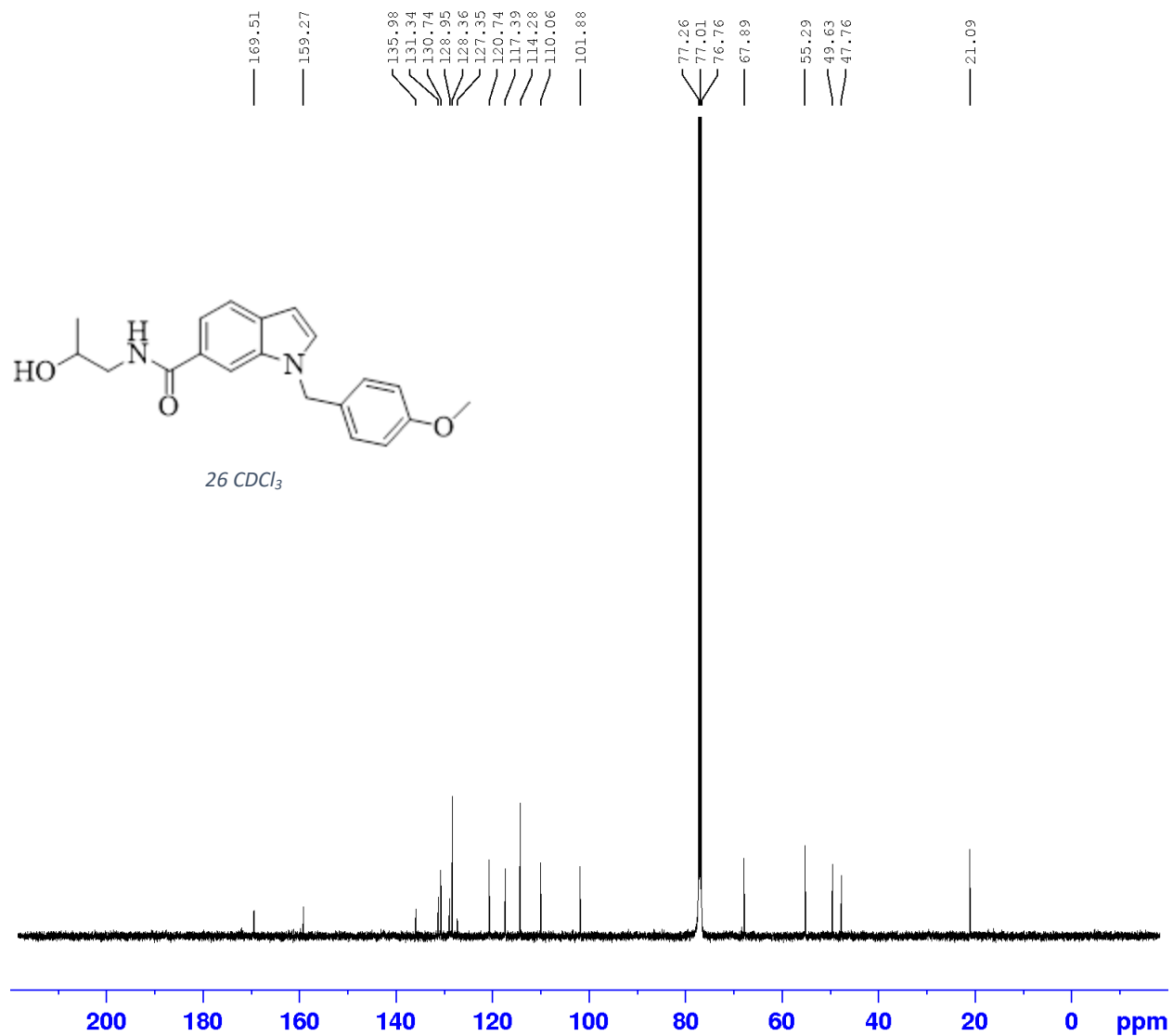
25

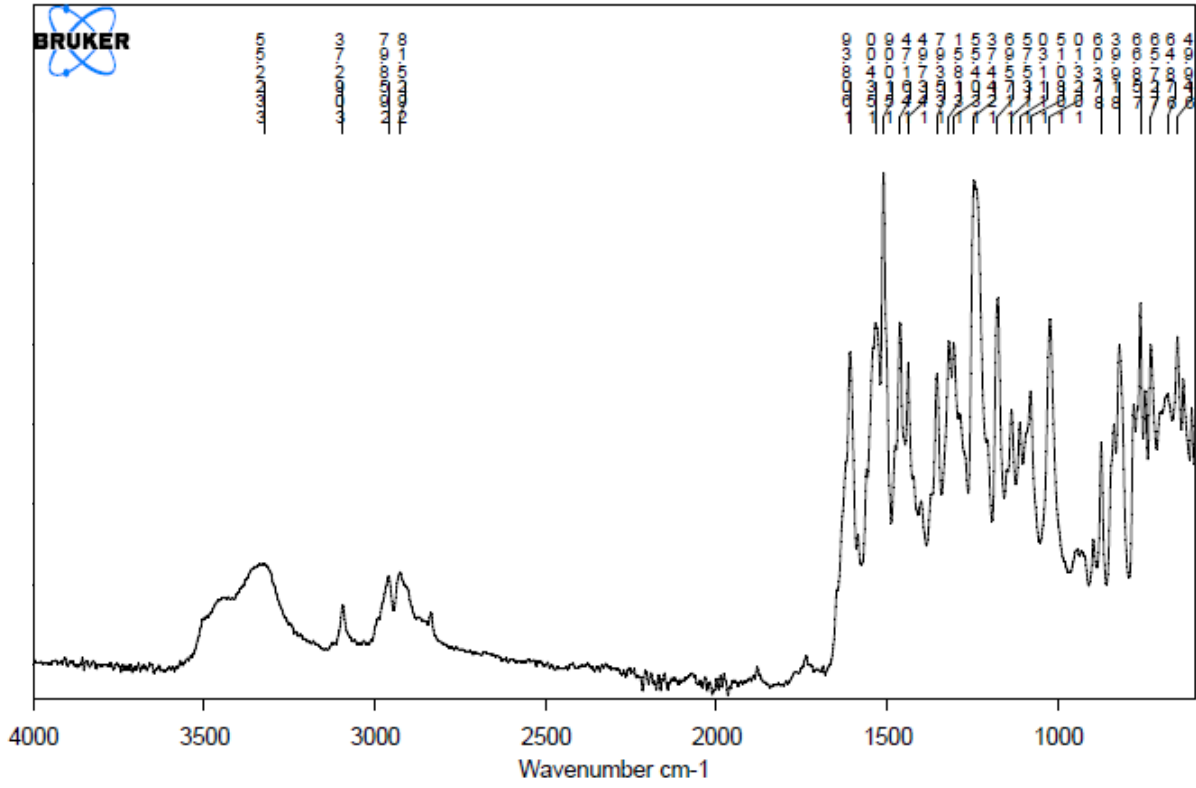




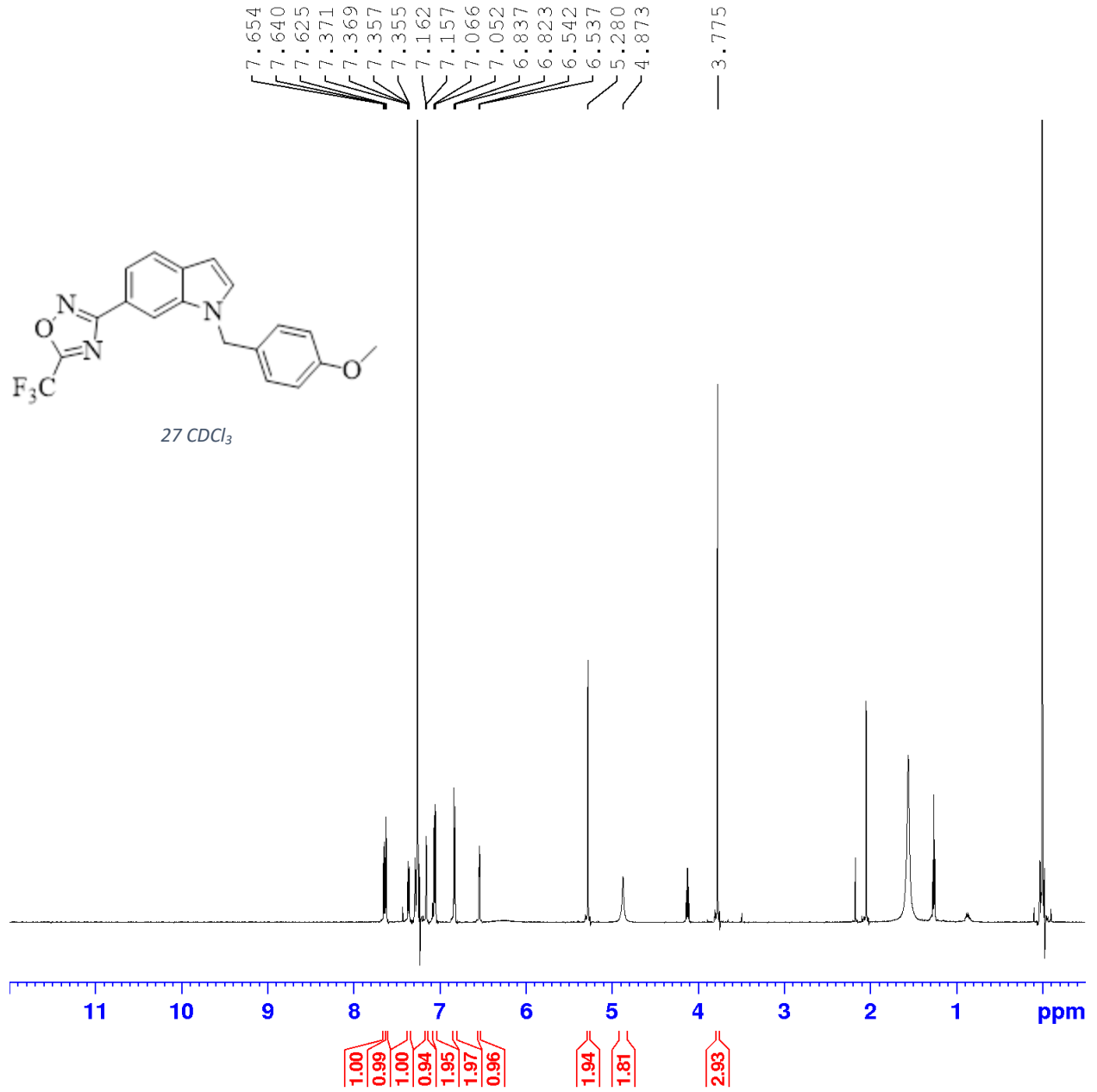


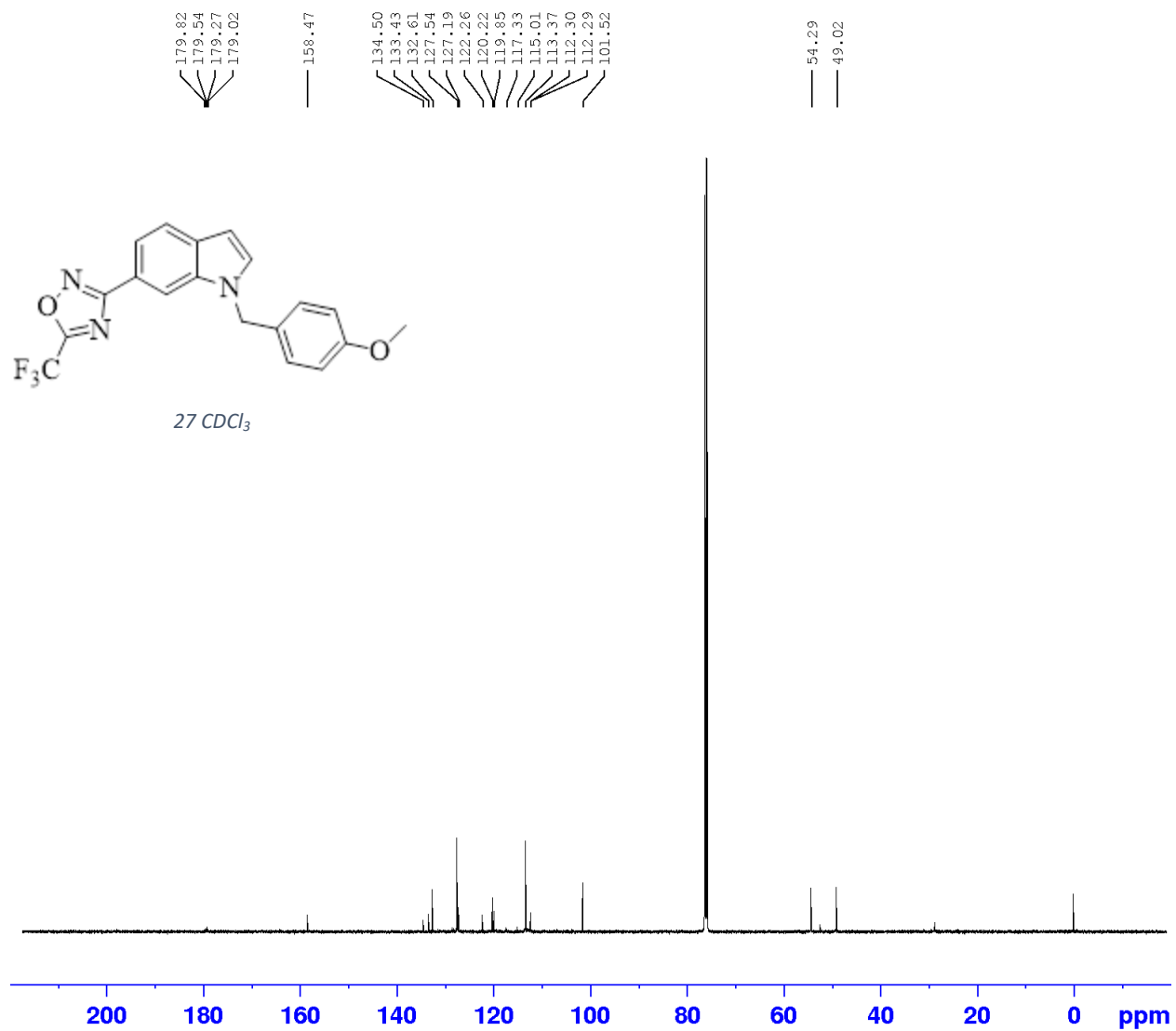


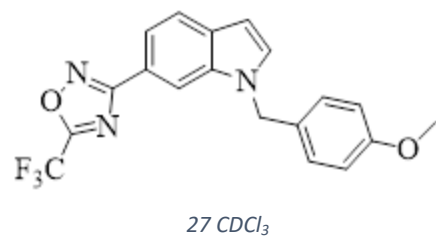




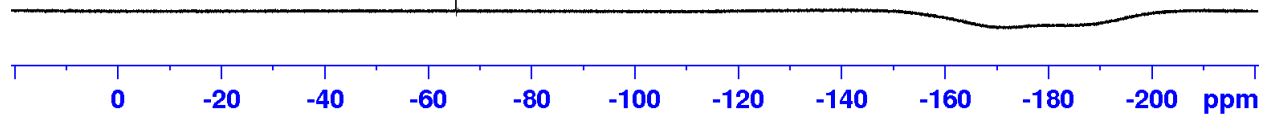
27



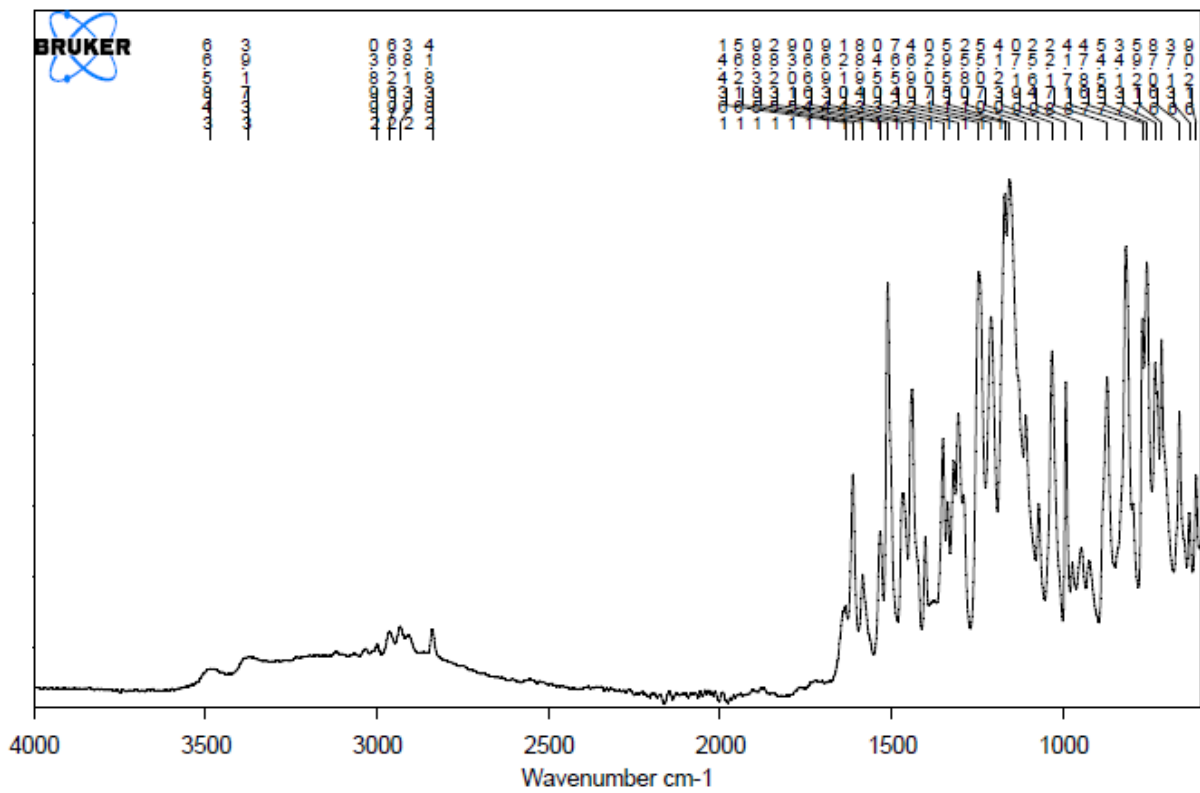




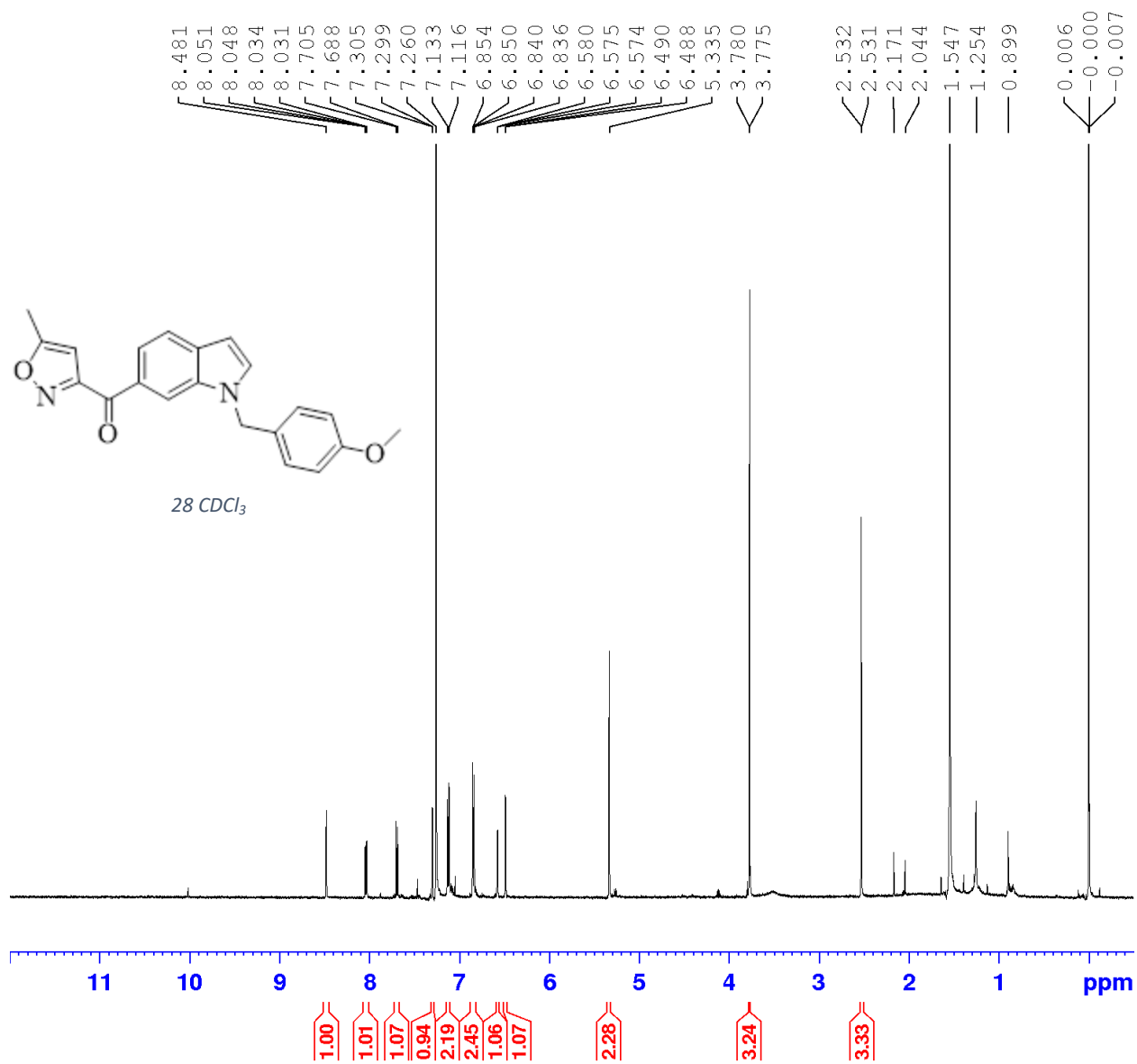
-65.39

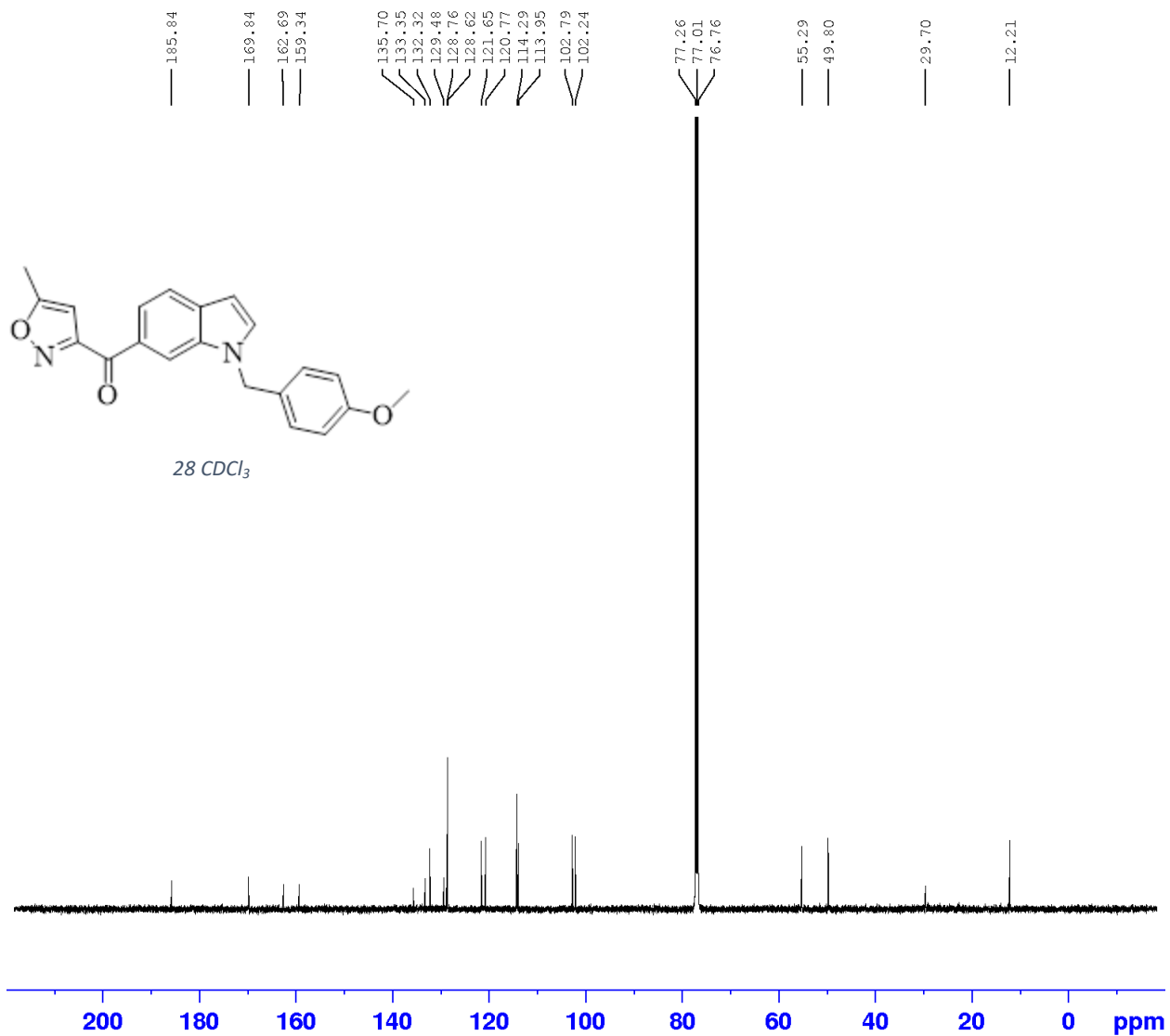


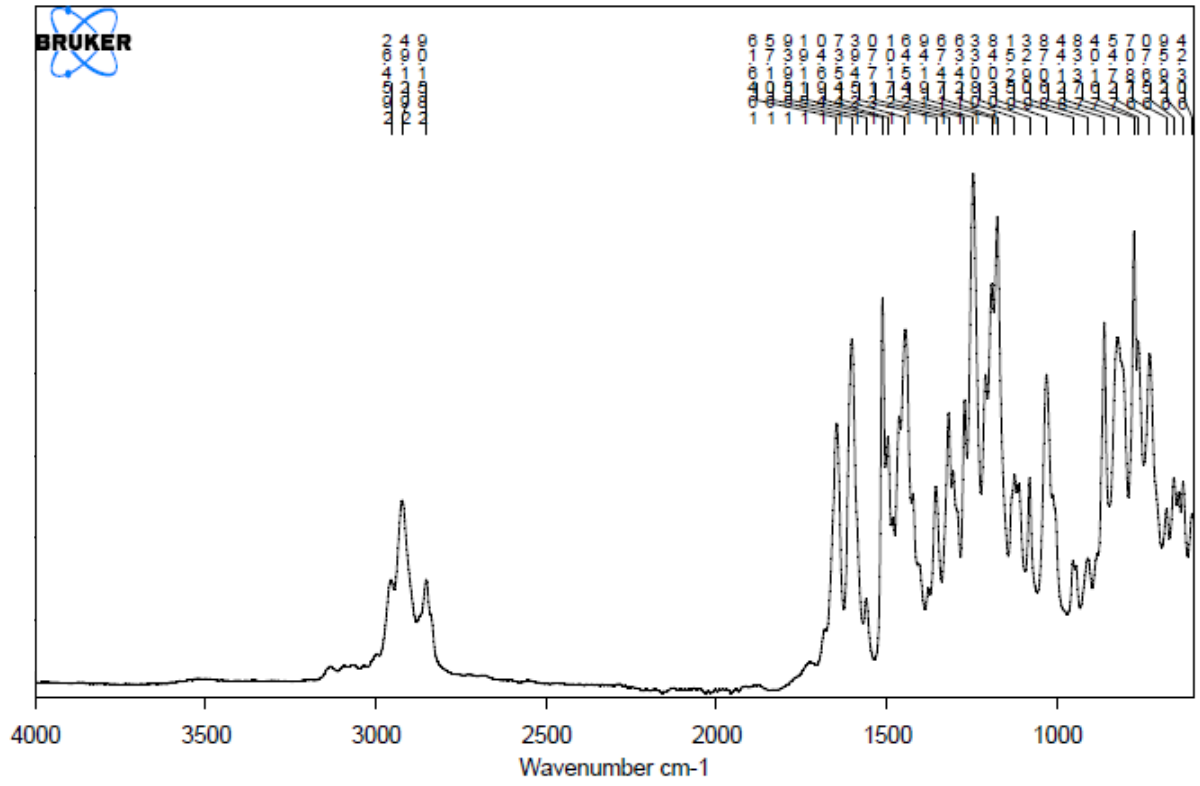
¹⁹F NMR



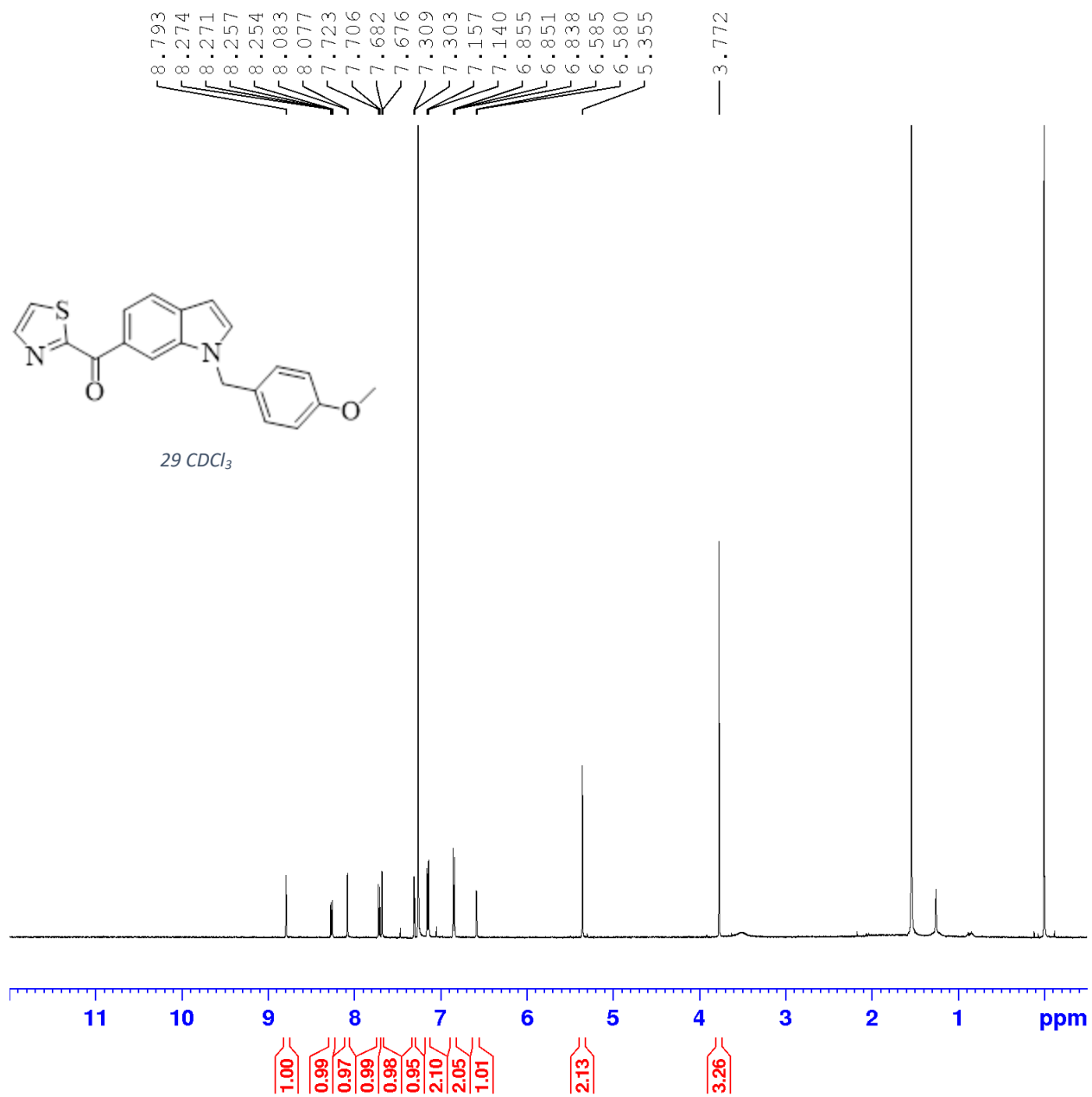
28

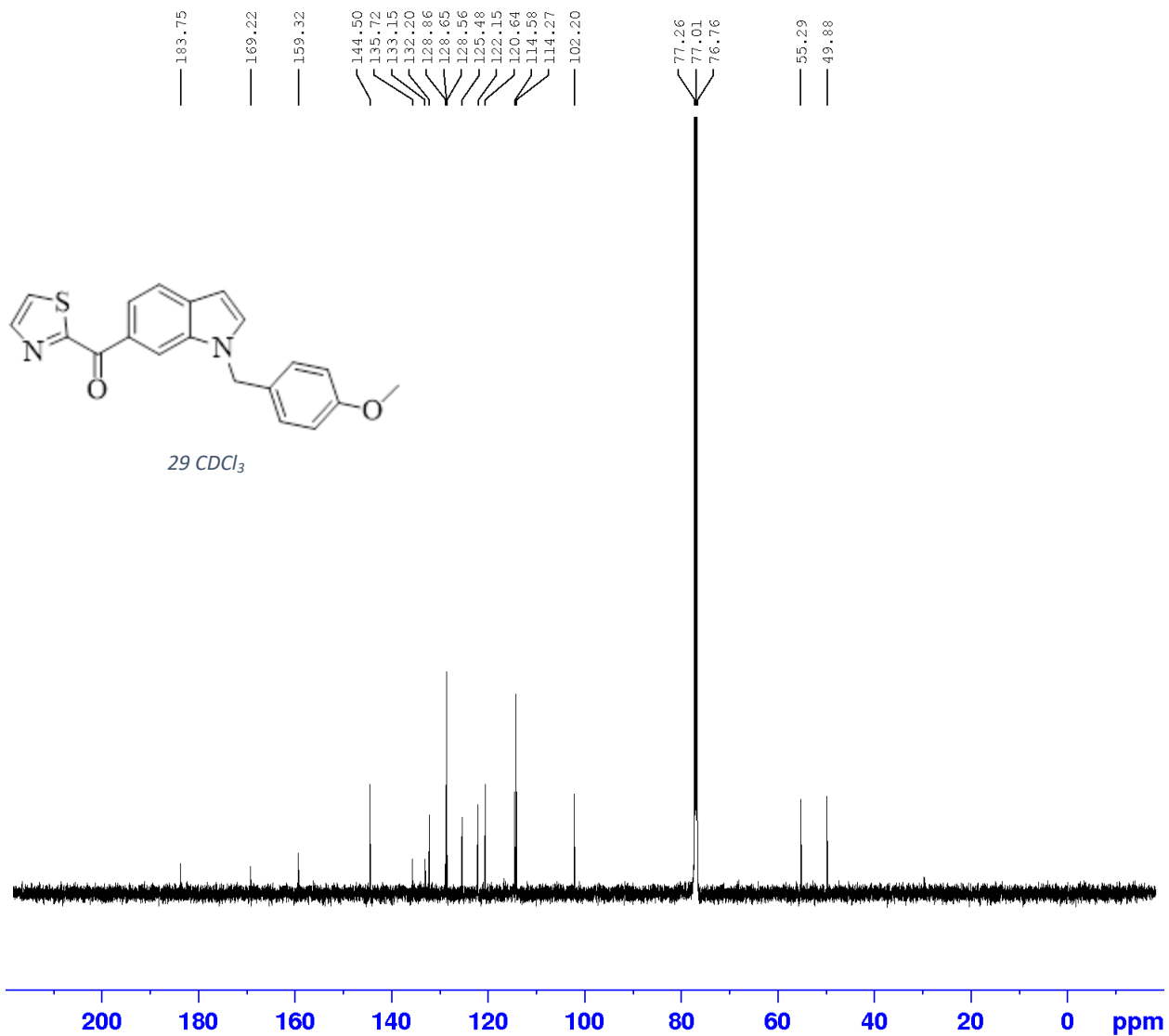


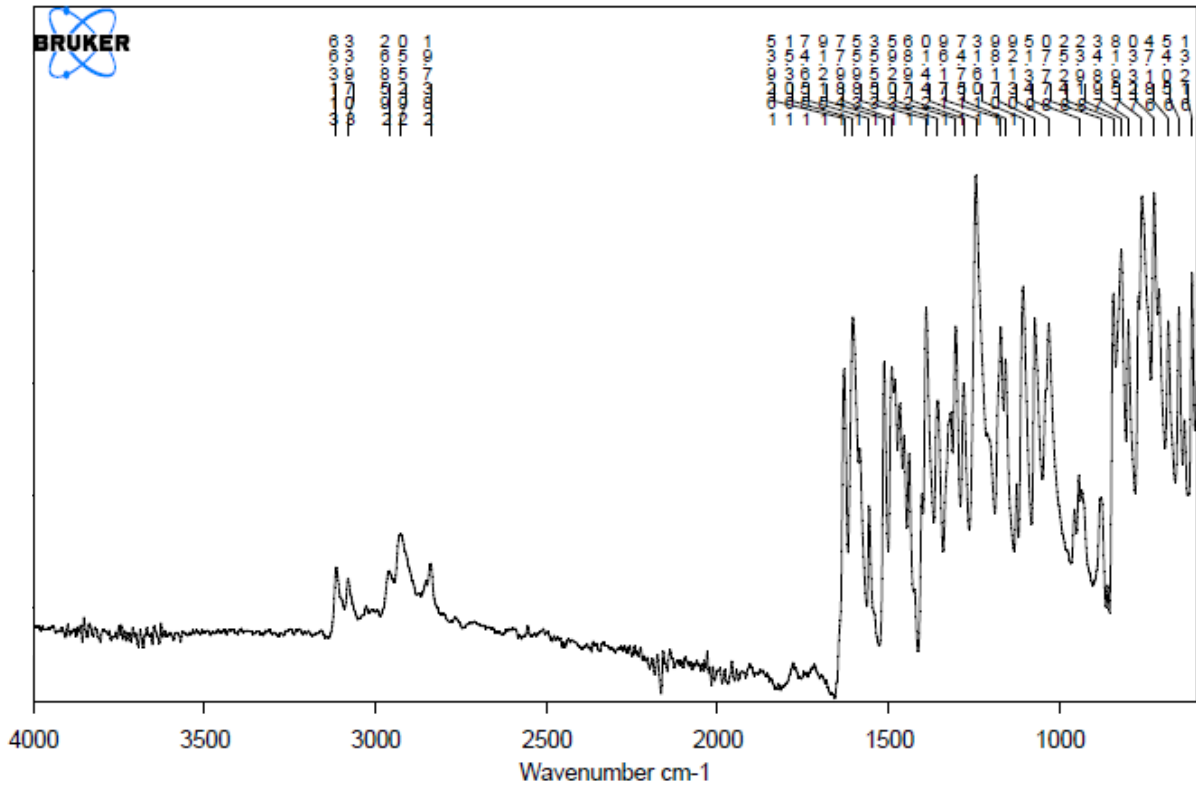




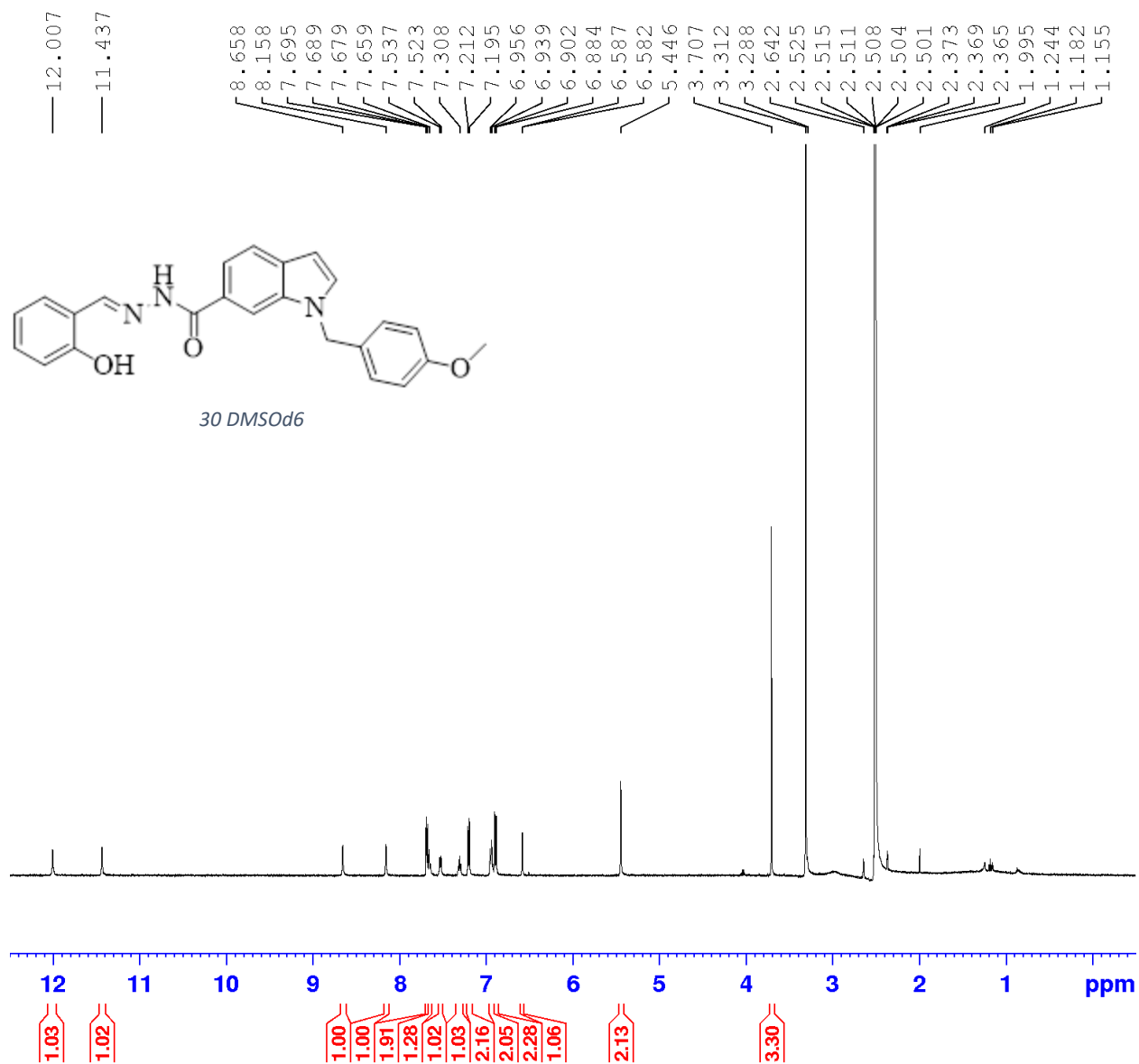
29

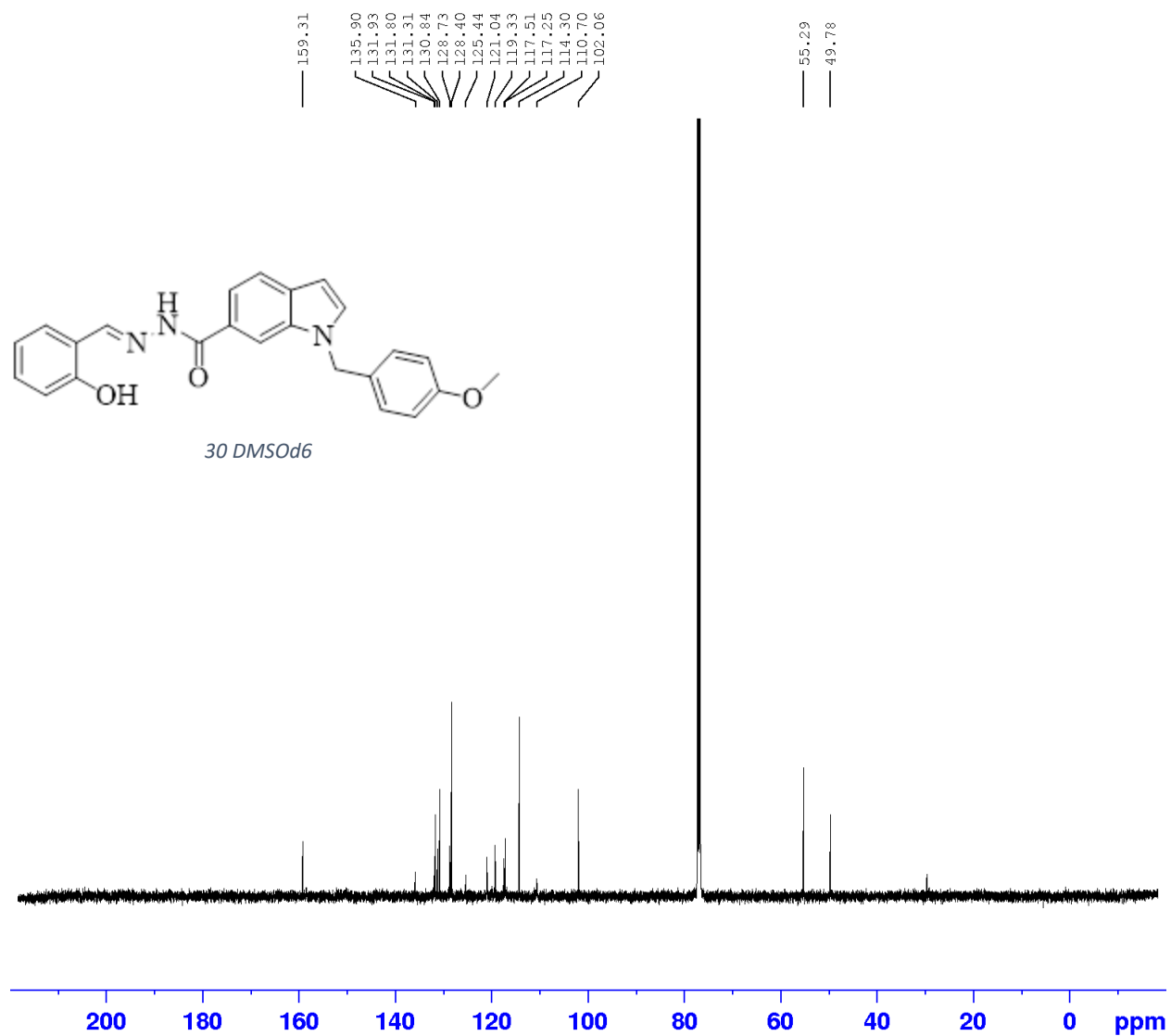


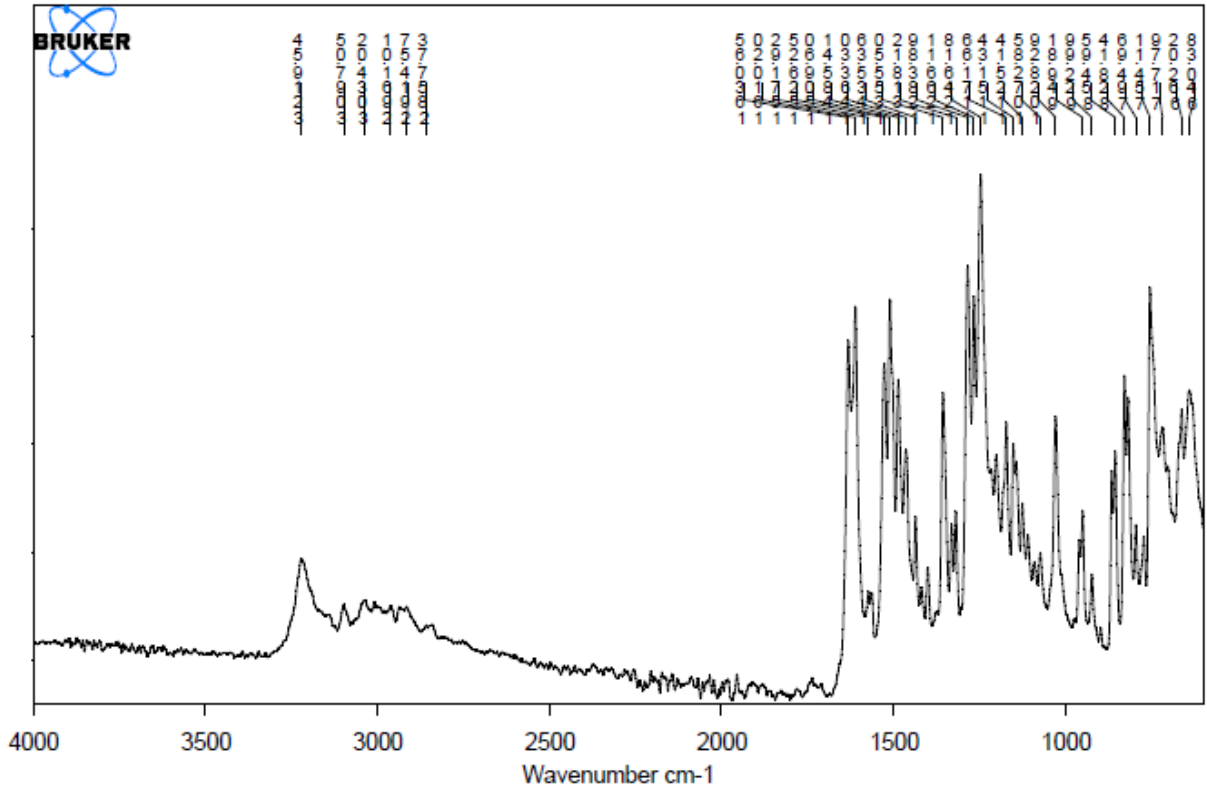




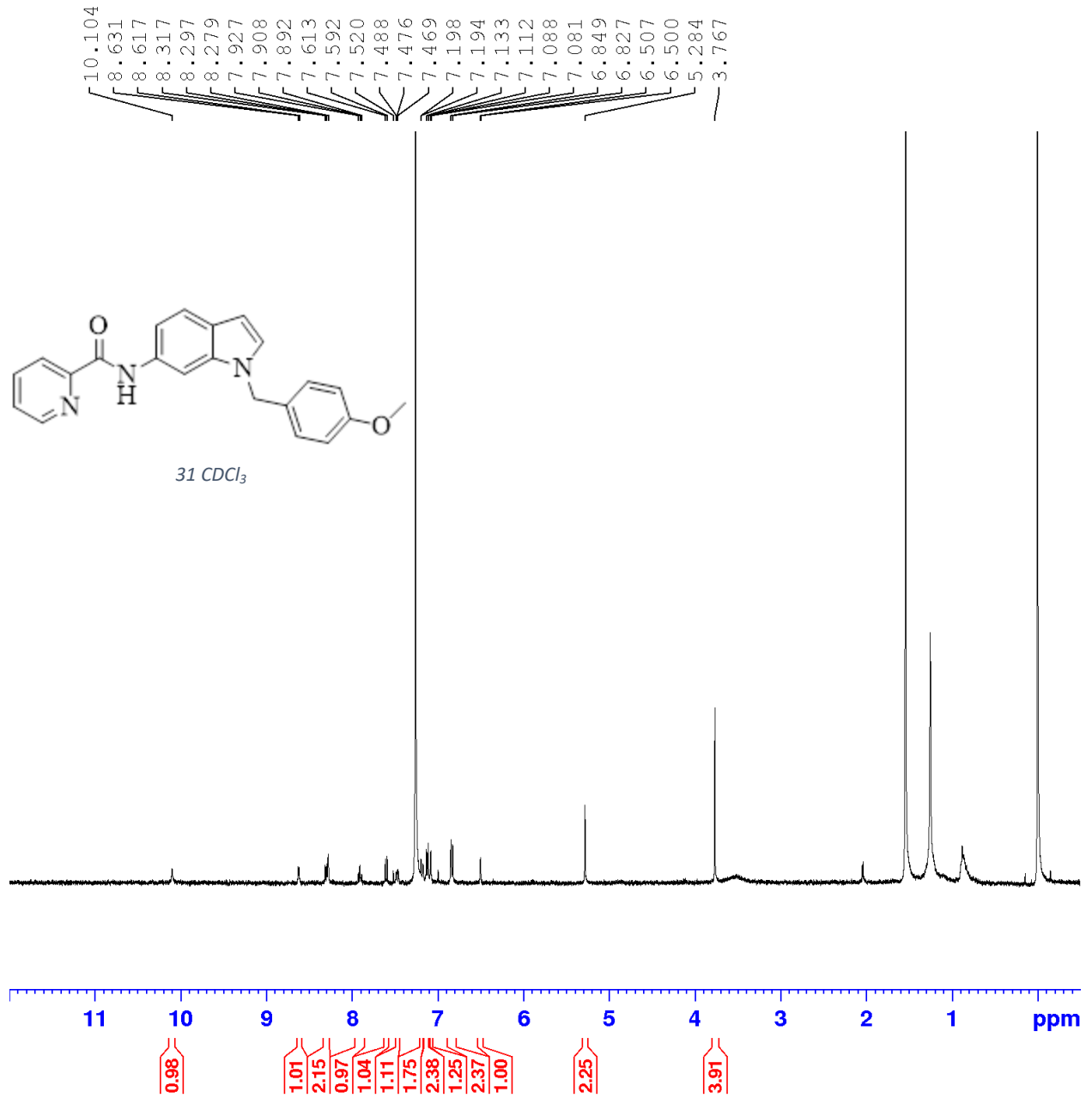
30

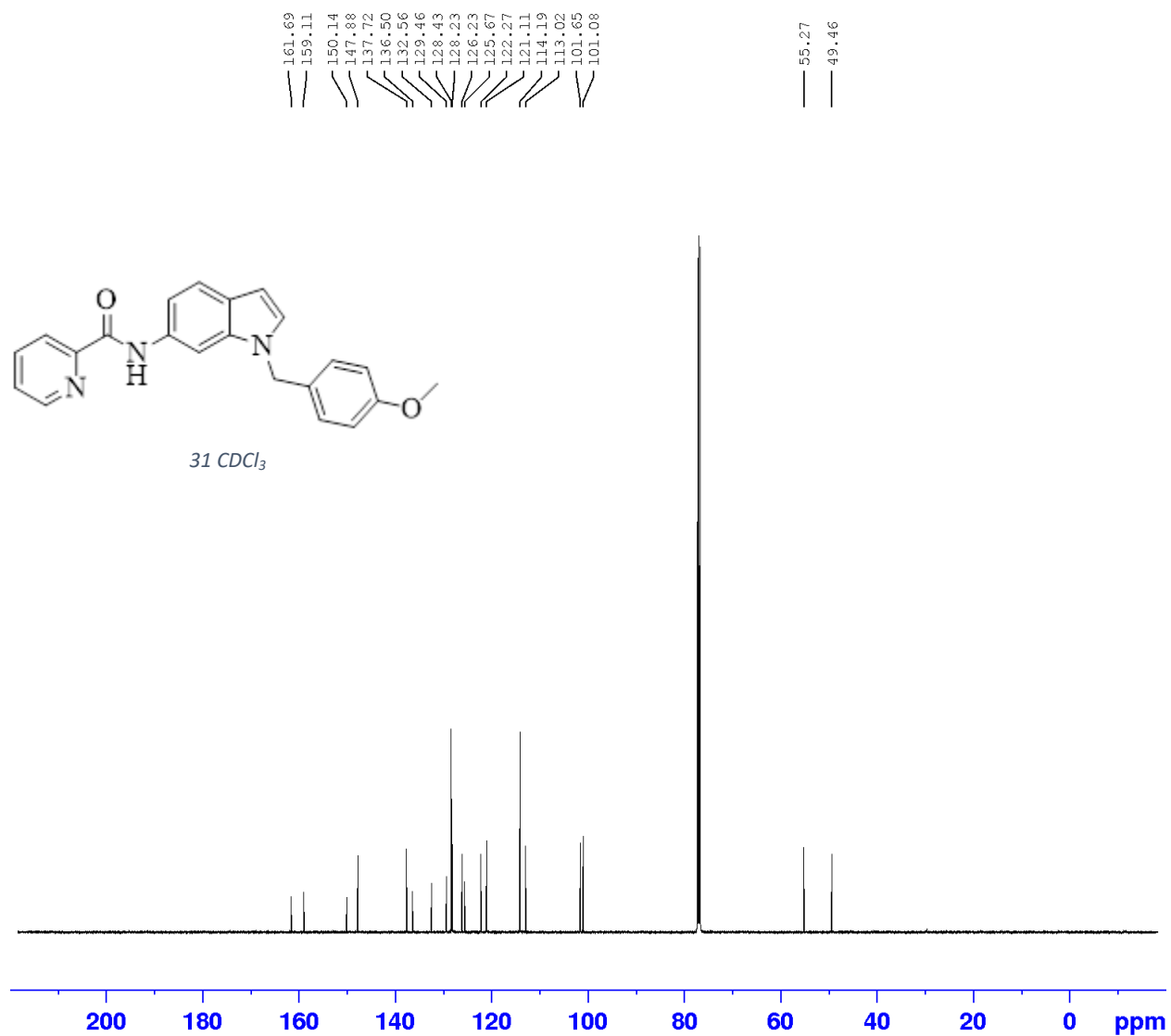


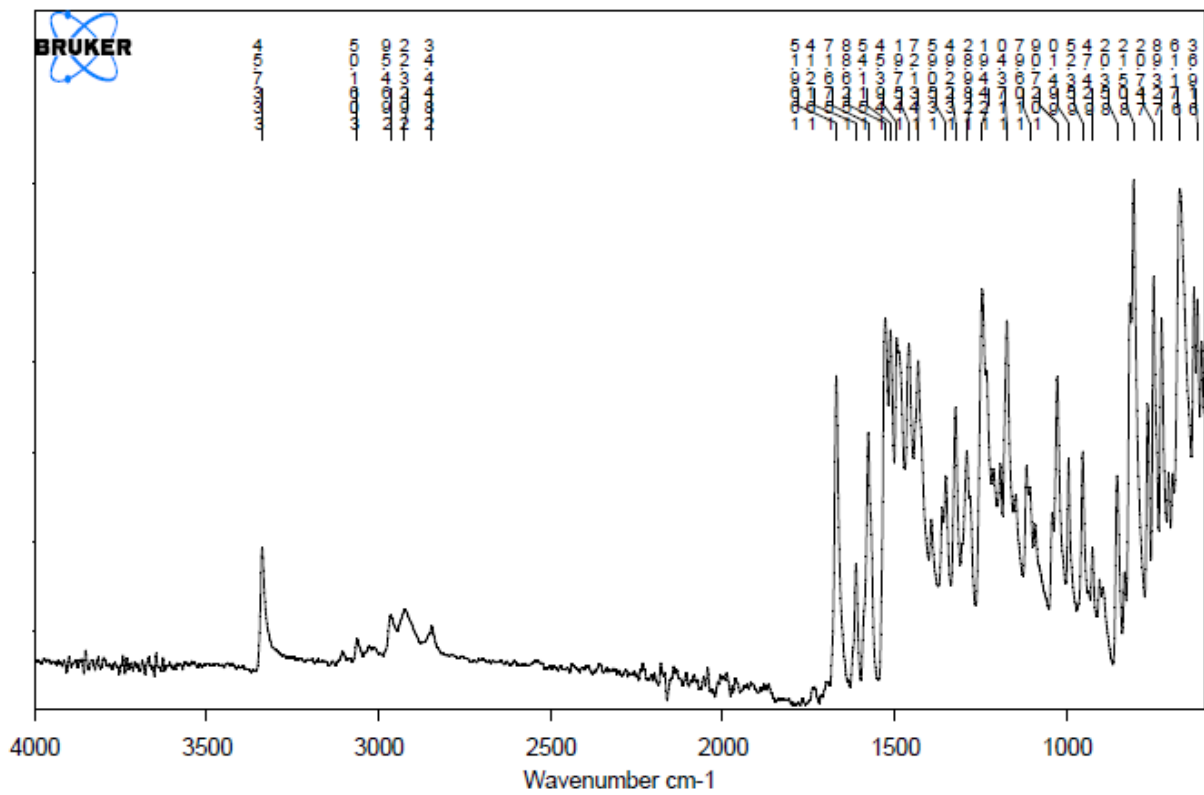




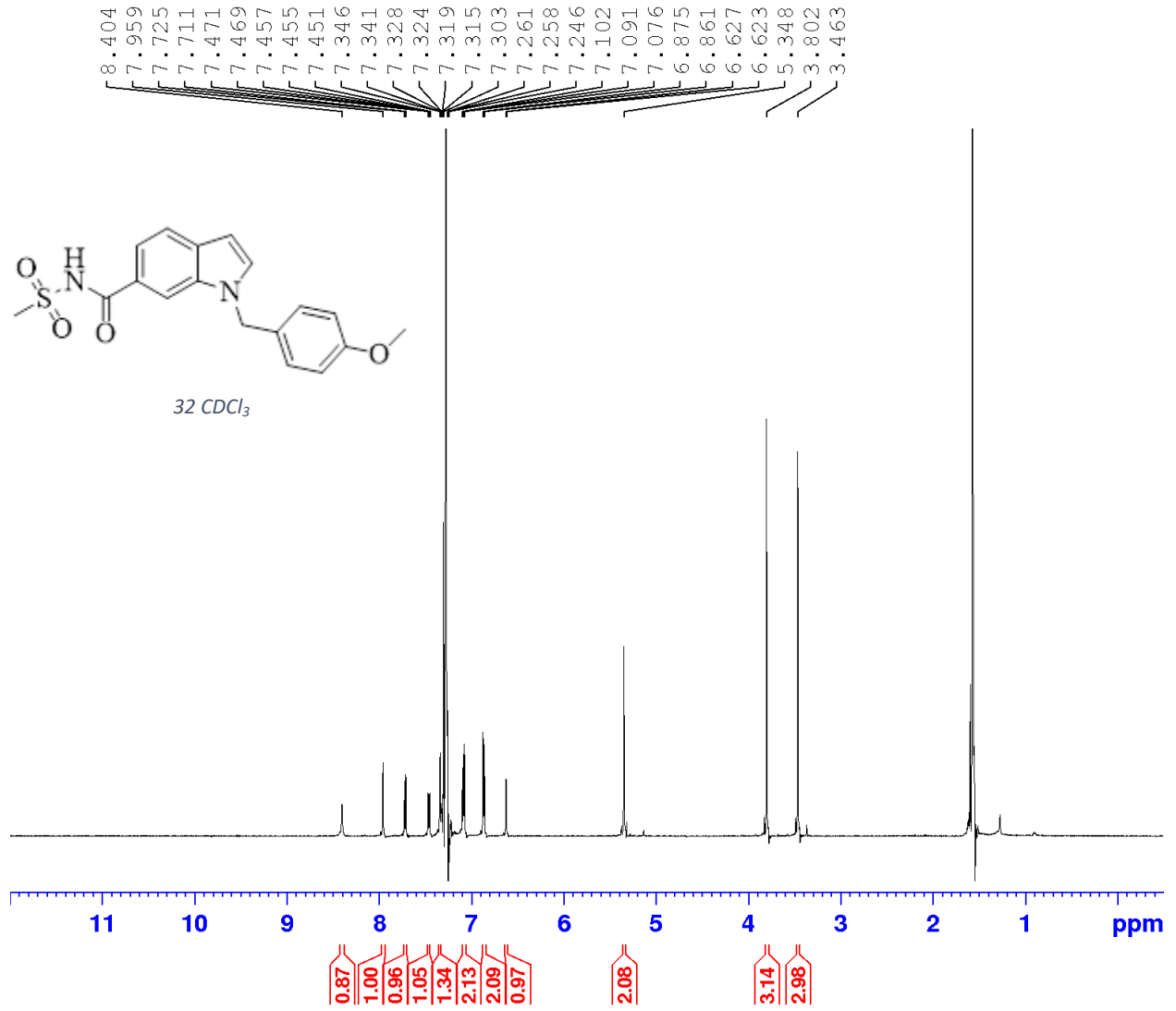
31

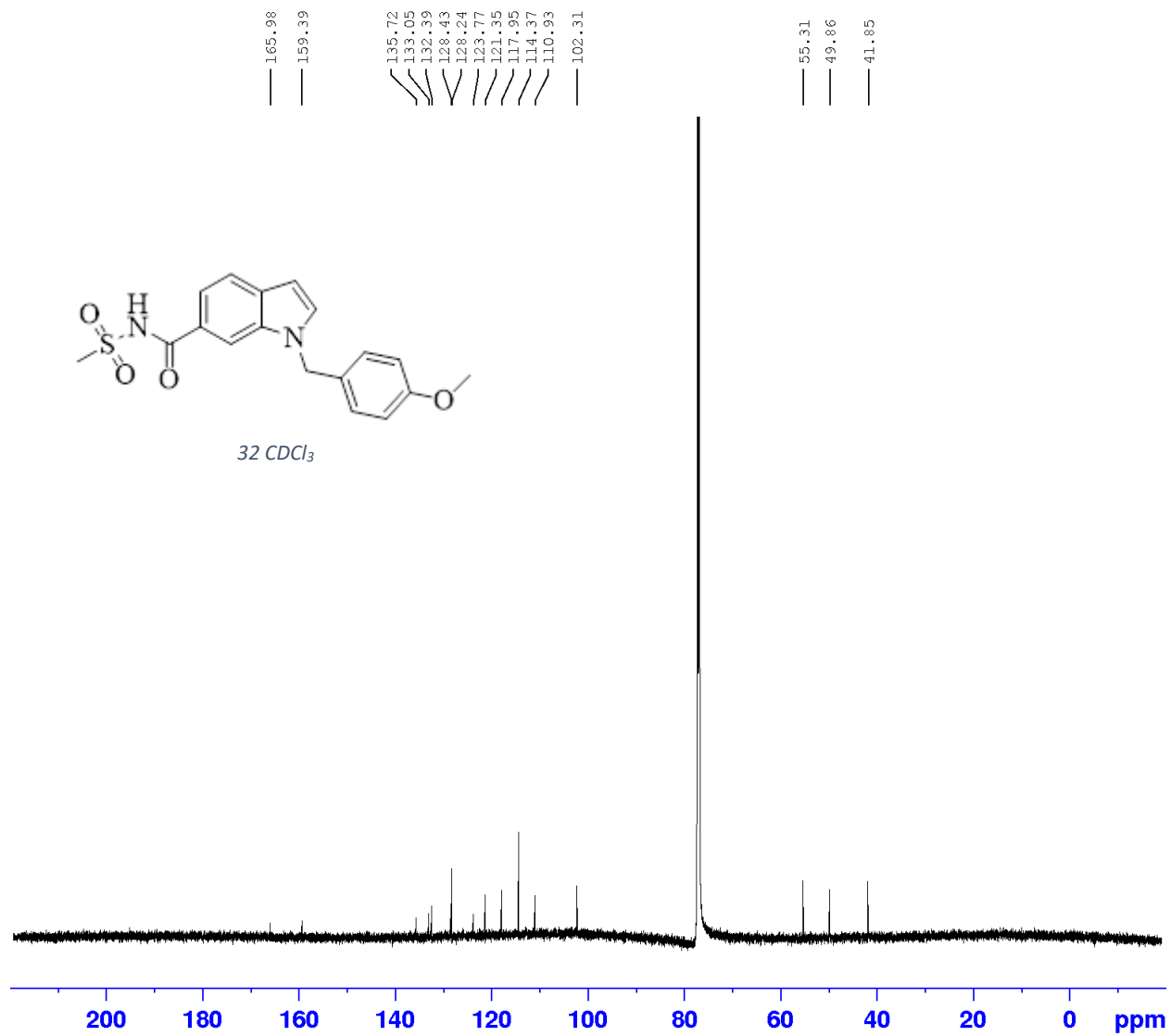


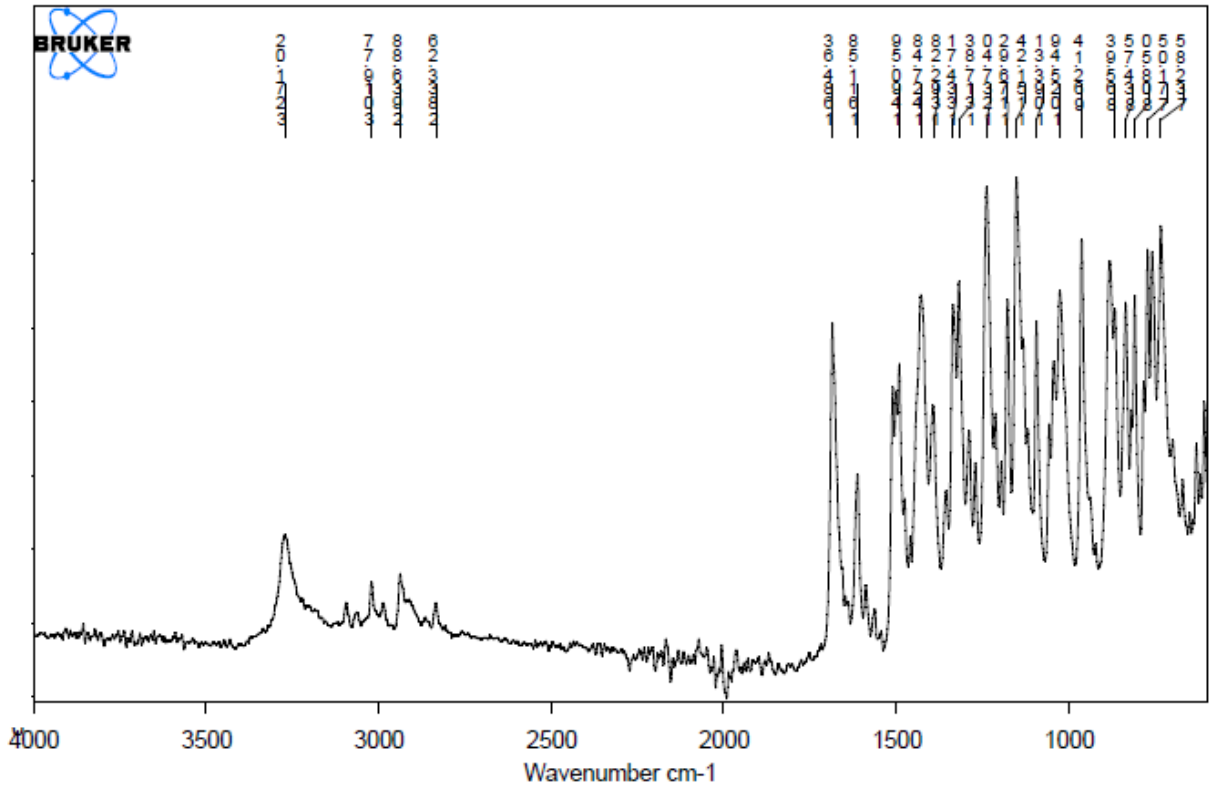




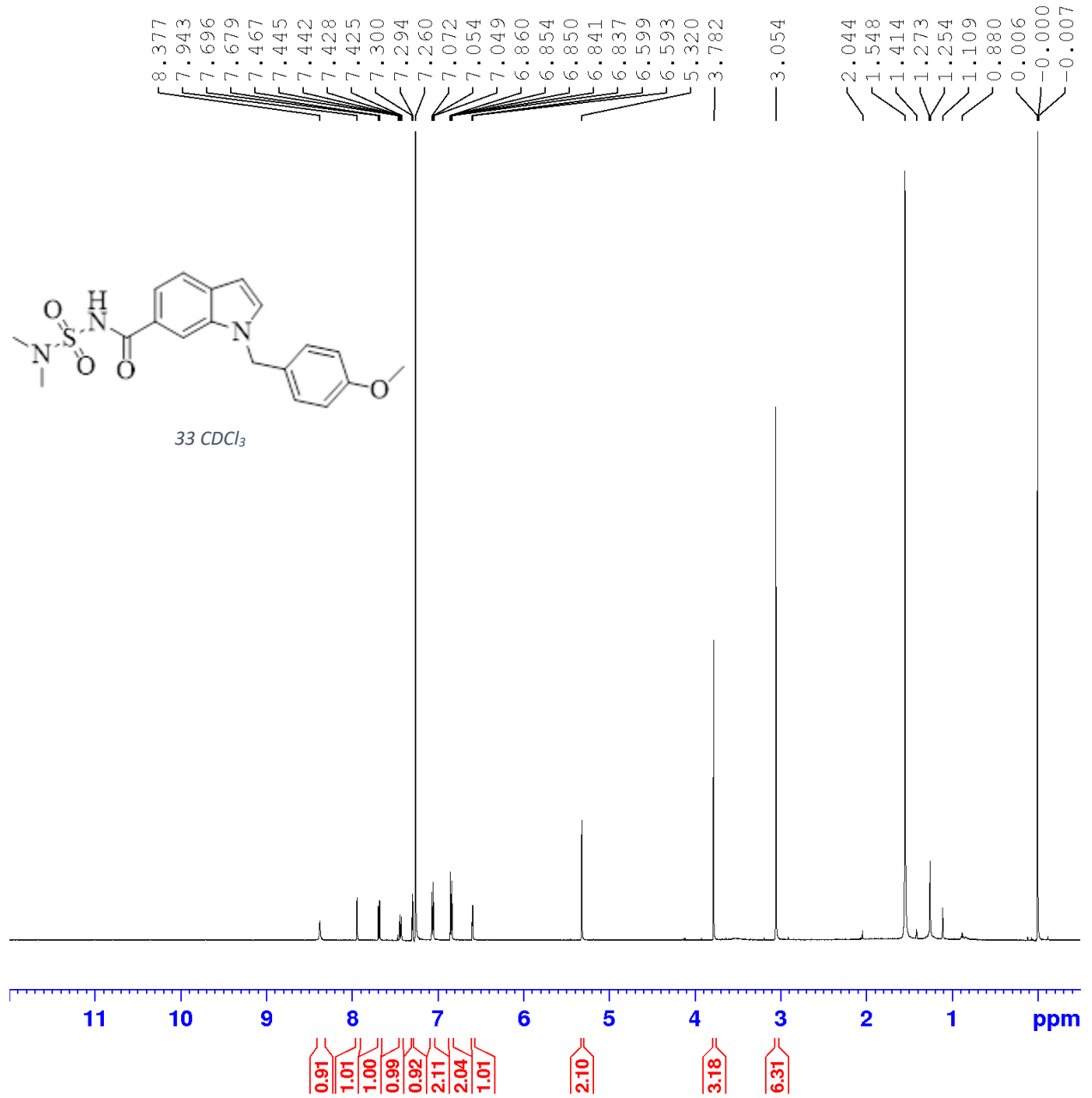
32

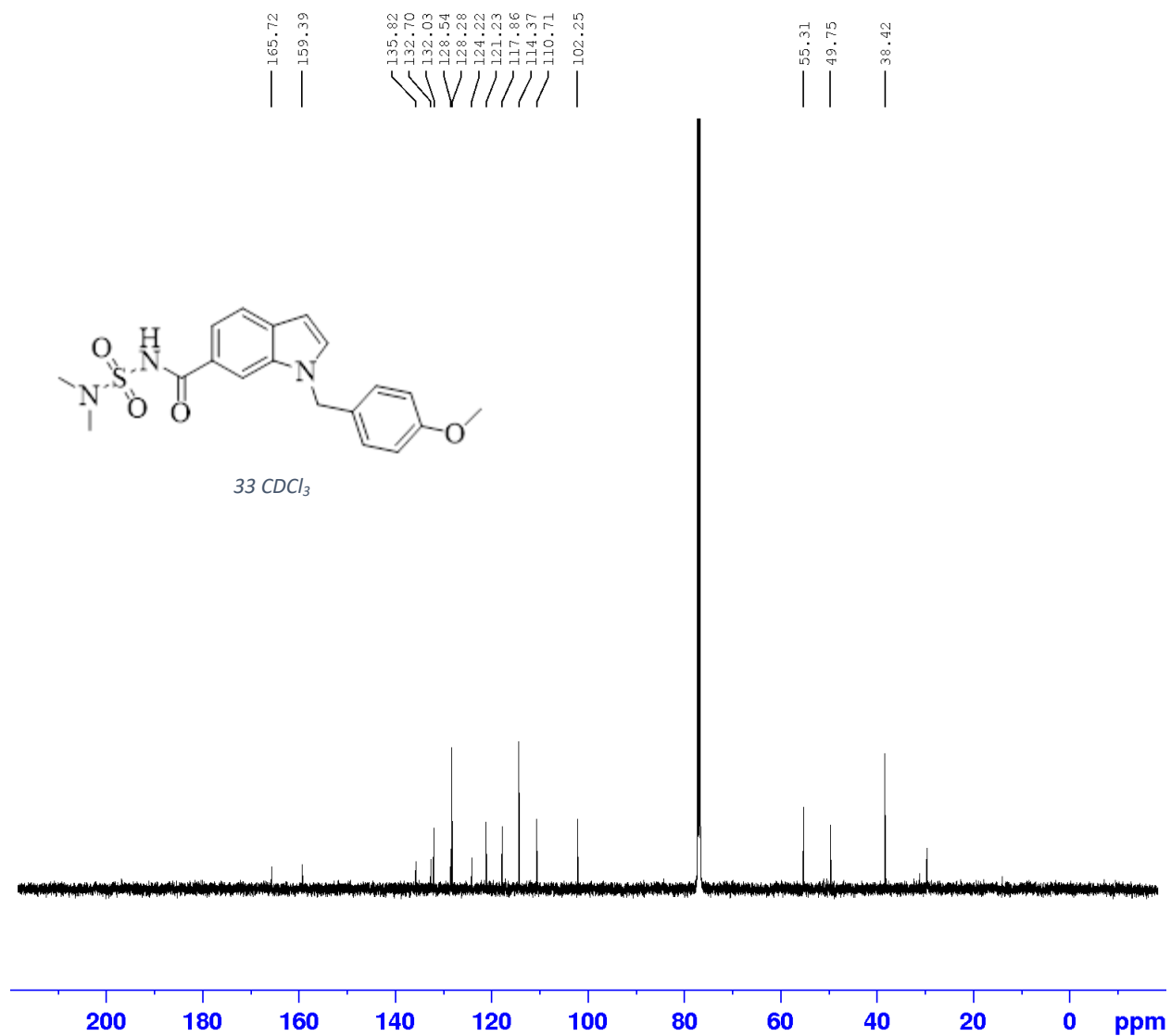


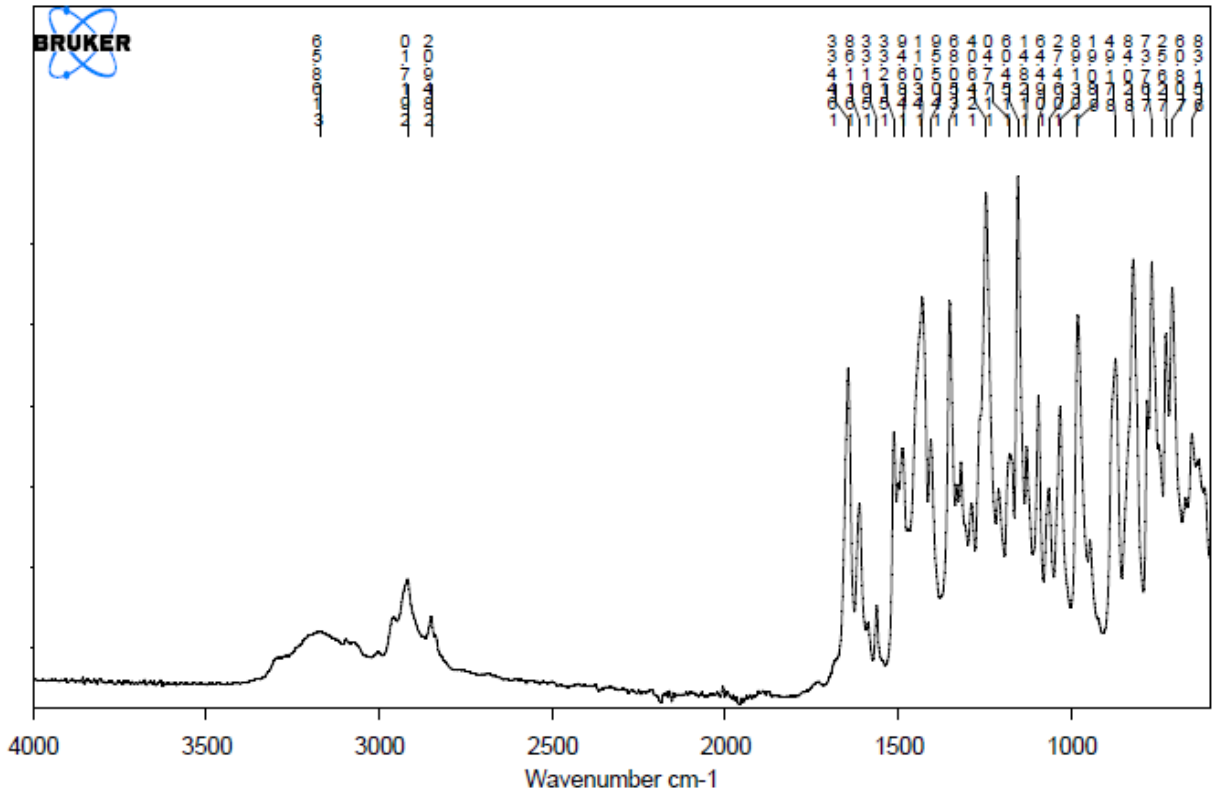




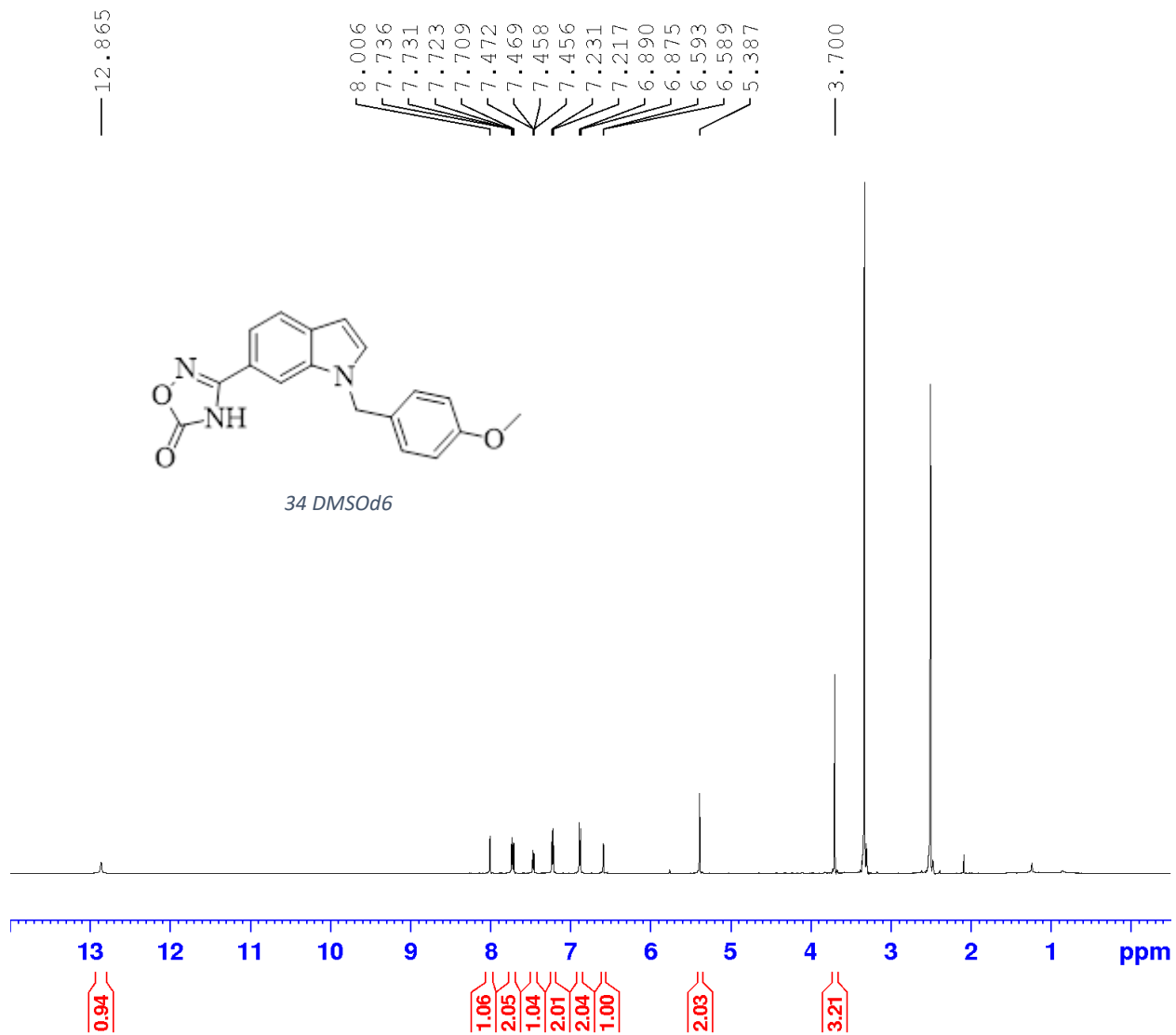
33

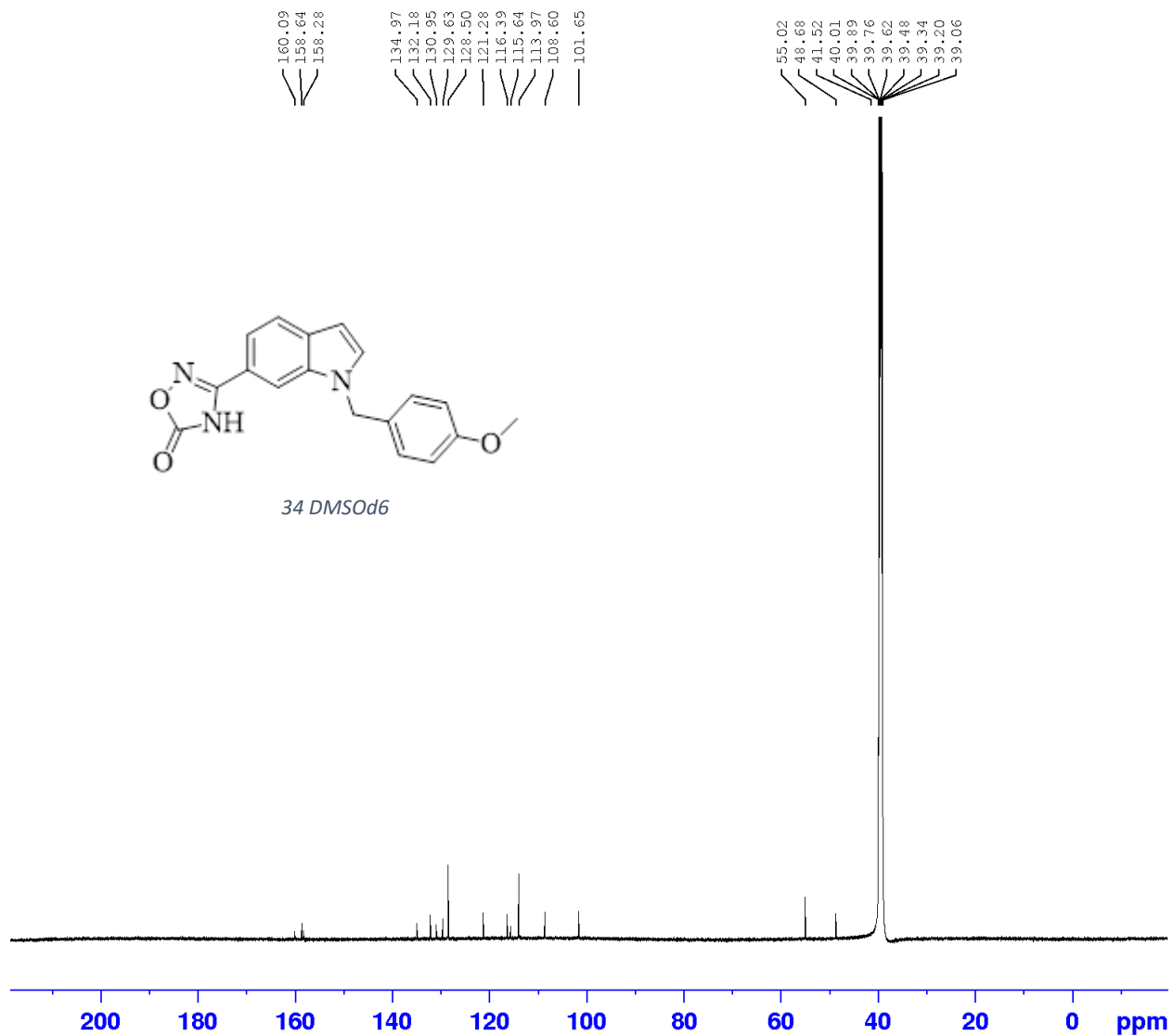


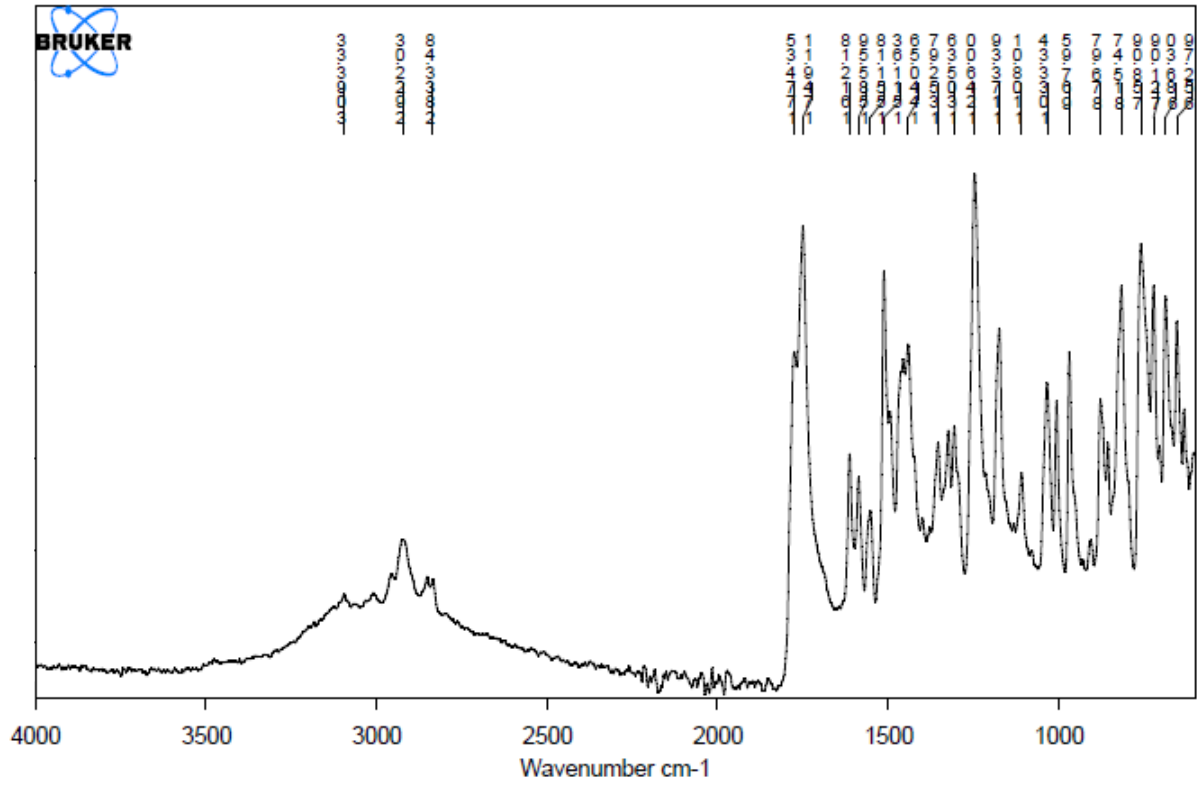




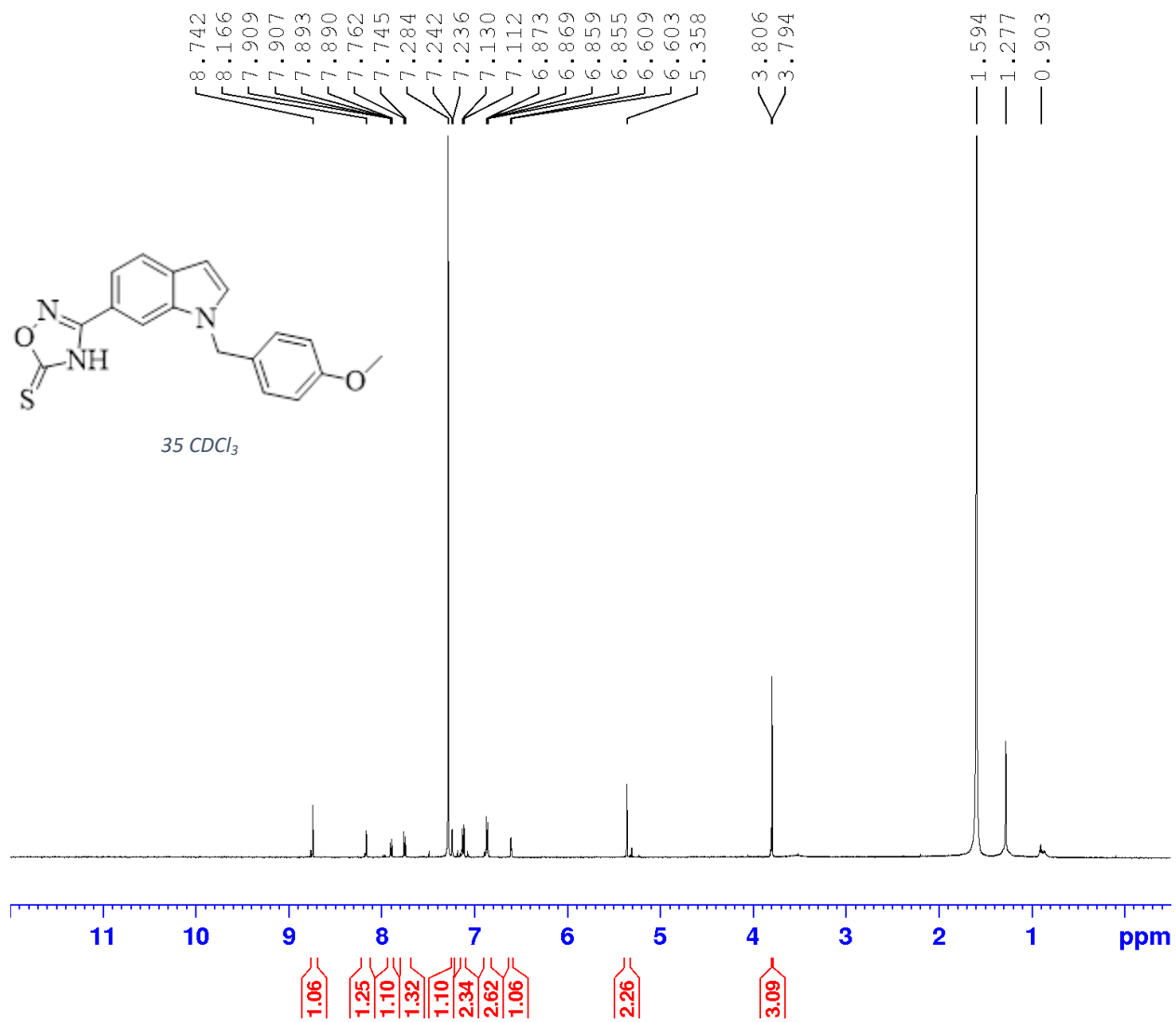
34

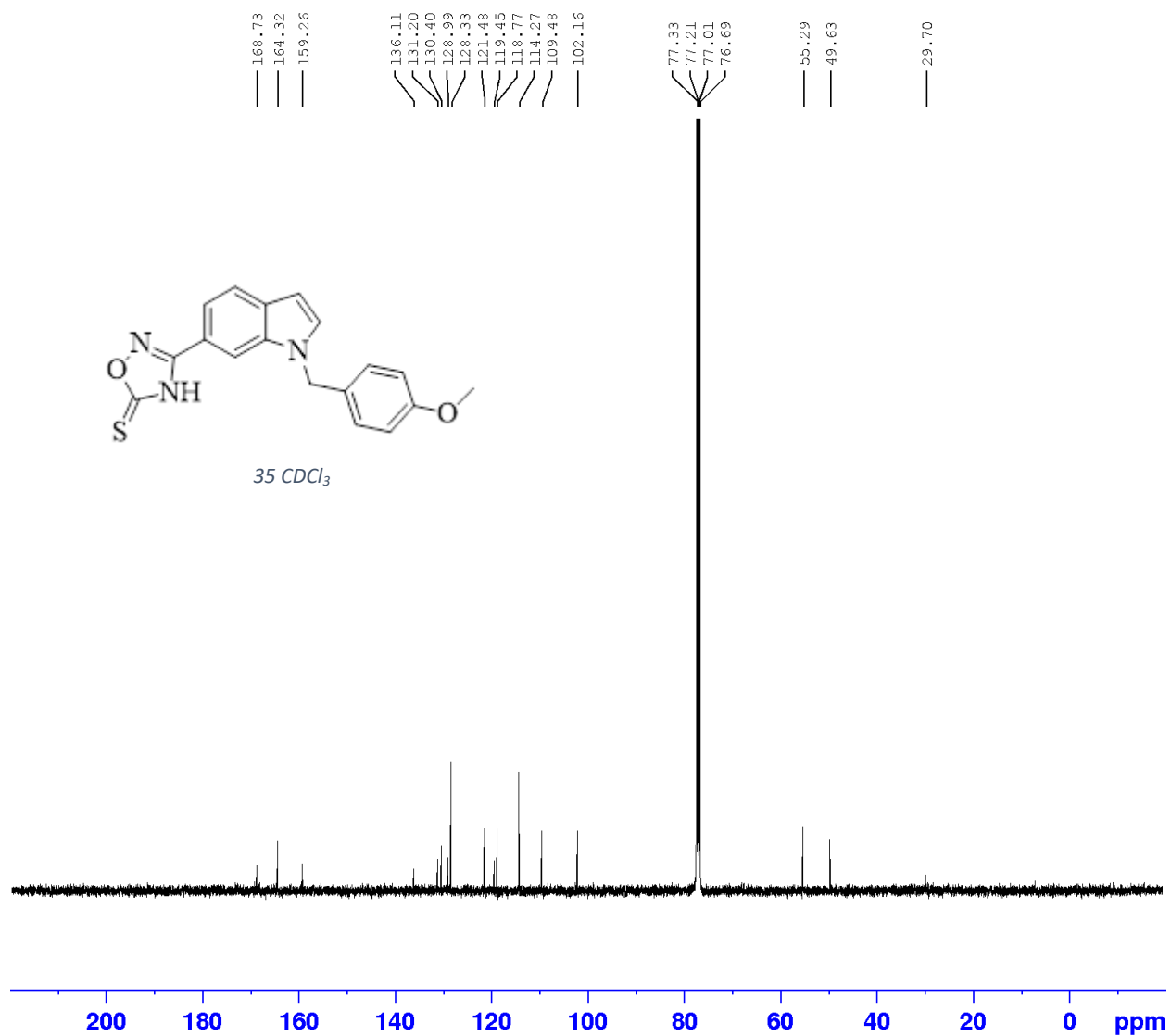


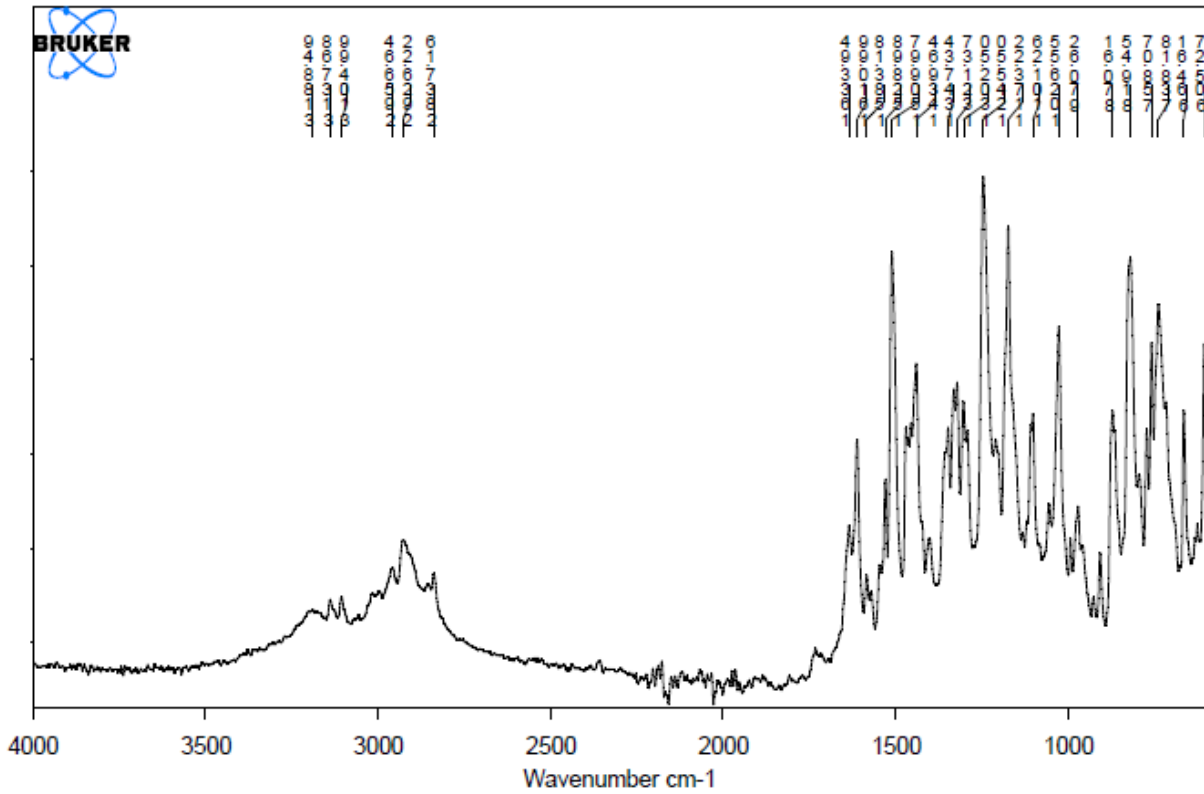




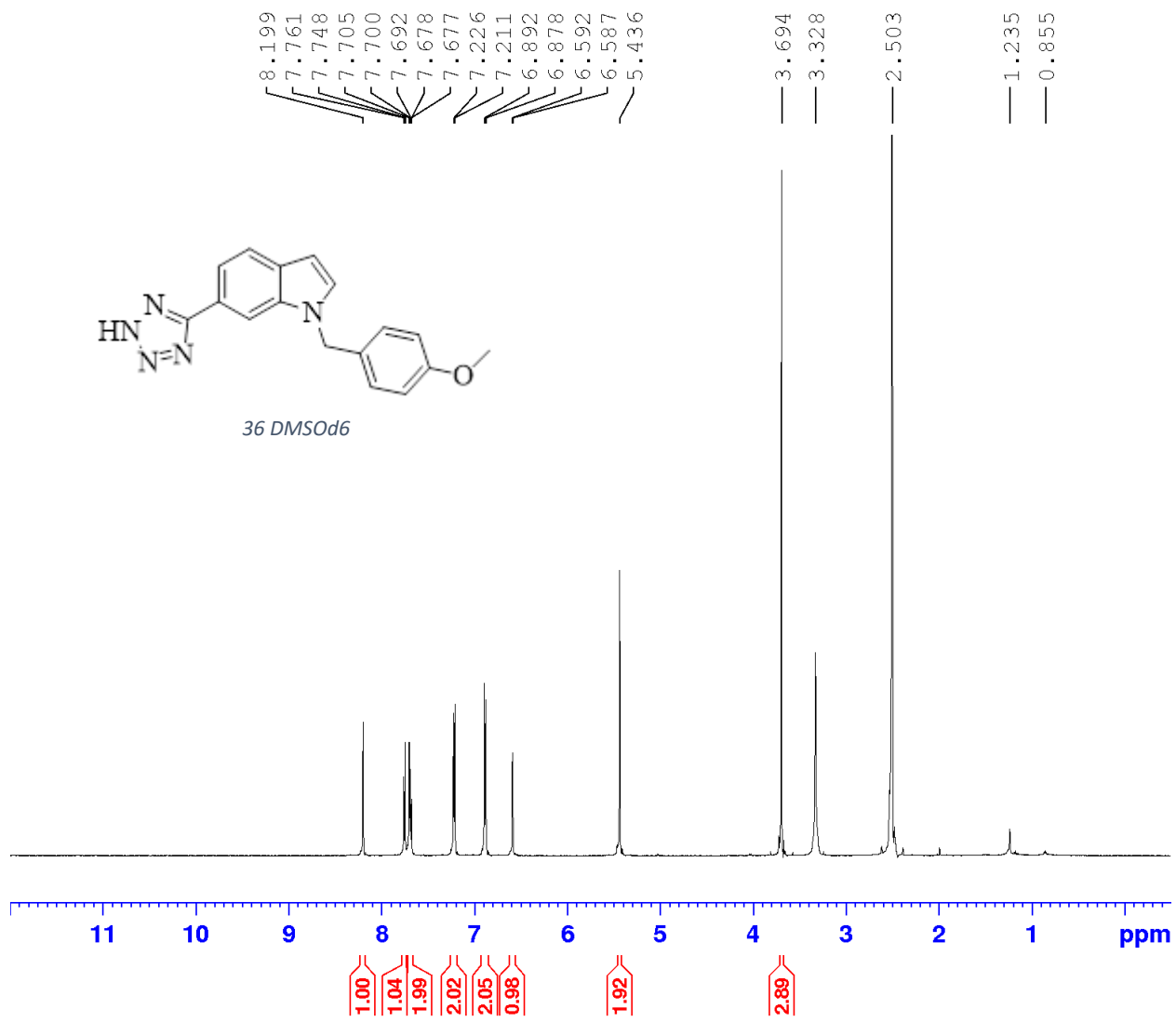
35

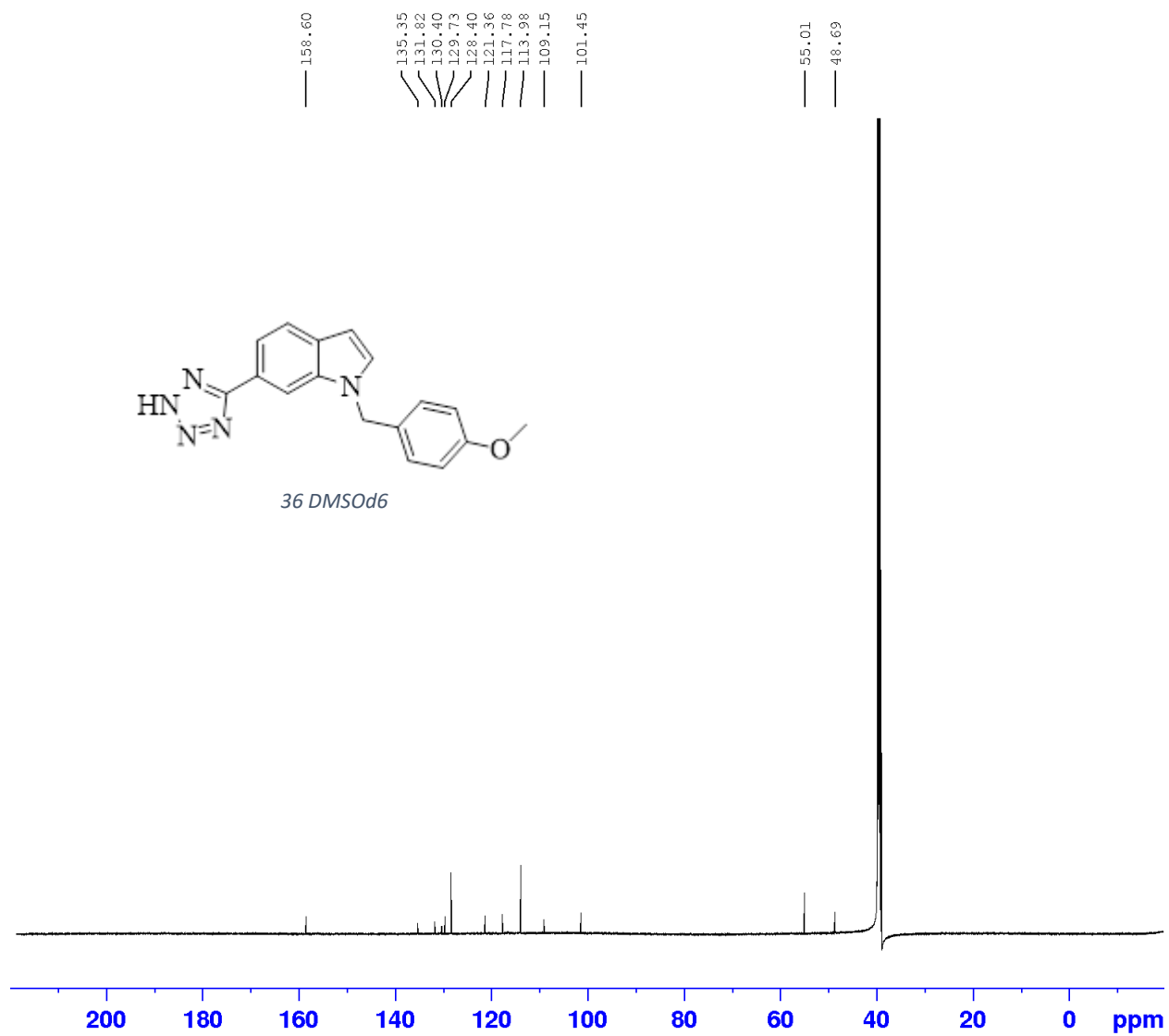


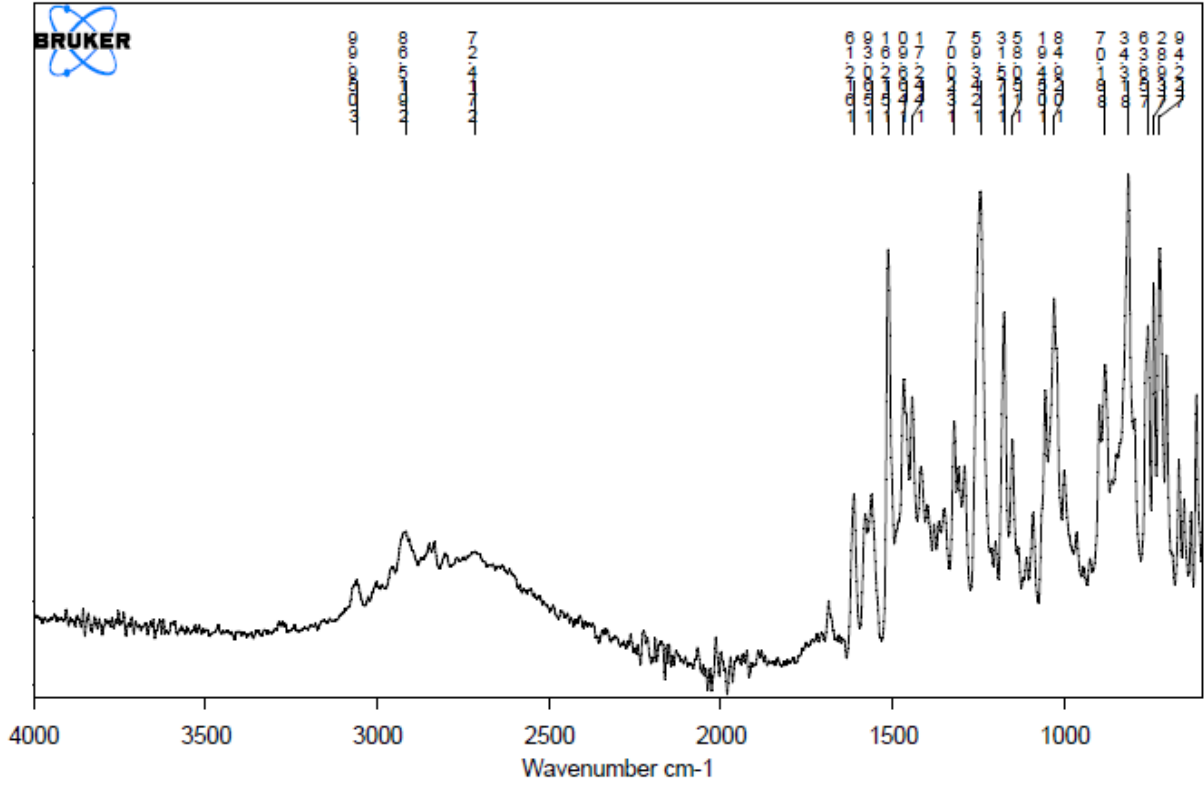




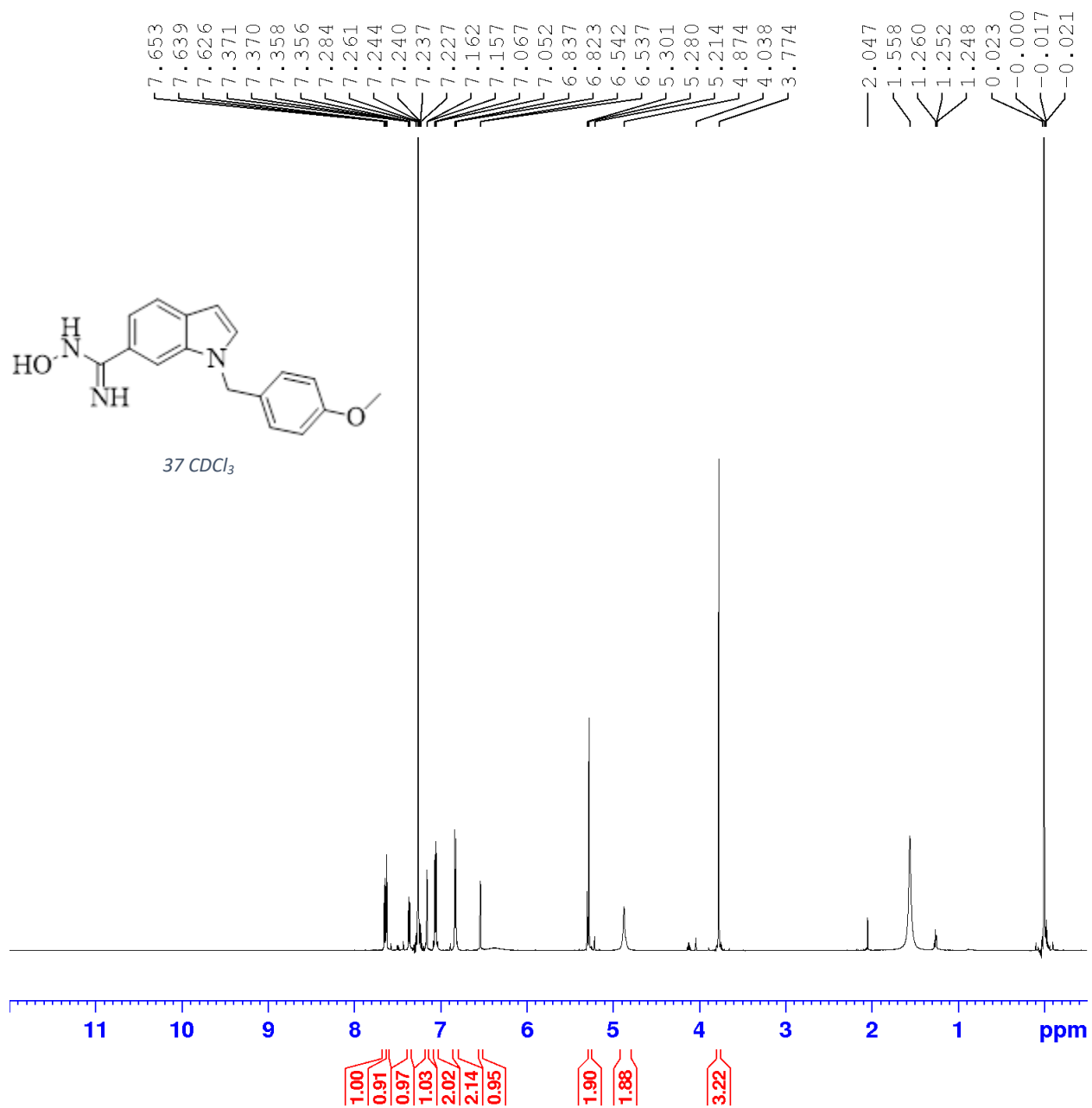
36



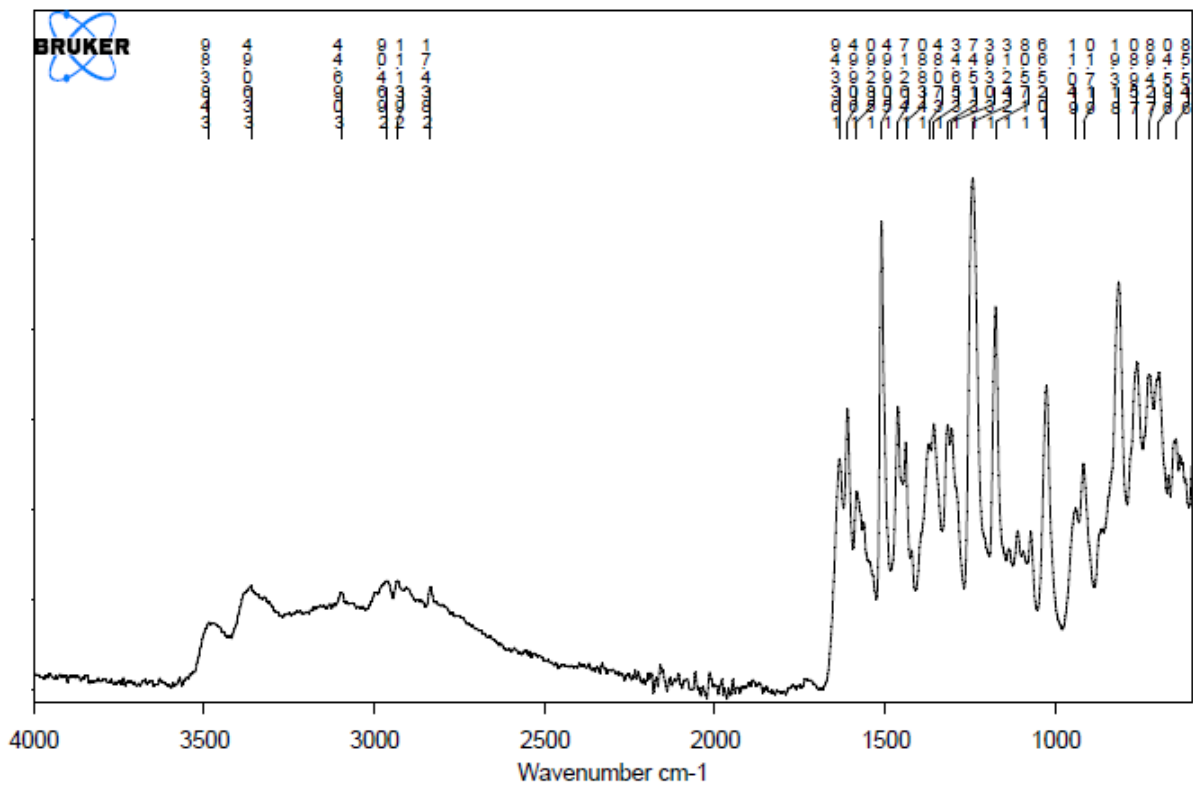




37







References

1. Jewell, T. Kidney Overview. <https://www.healthline.com/human-body-maps/kidney>.
2. Your Kidneys & How They Work. <https://www.niddk.nih.gov/health-information/kidney-disease/kidneys-how-they-work>.
3. Alshogran, O. Y.; Nolin, T. D., Implications of Kidney Disease on Metabolic Reduction. *Curr Drug Metab* **2016**, *17* (7), 663-72.
4. Makris, K.; Spanou, L., Acute Kidney Injury: Definition, Pathophysiology and Clinical Phenotypes. *Clin Biochem Rev* **2016**, *37* (2), 85-98.
5. Gray, M. P.; Barreto, E. F.; Schreier, D. J.; Kellum, J. A.; Suh, K.; Kashani, K. B.; Rule, A. D.; Kane-Gill, S. L., Consensus Obtained for the Nephrotoxic Potential of 167 Drugs in Adult Critically Ill Patients Using a Modified Delphi Method. *Drug Saf* **2022**, *45* (4), 389-398.
6. Faubel, S., Pulmonary complications after acute kidney injury. *Adv Chronic Kidney Dis* **2008**, *15* (3), 284-96.
7. Holgado, J. L.; Lopez, C.; Fernandez, A.; Sauri, I.; Uso, R.; Trillo, J. L.; Vela, S.; Nunez, J.; Redon, J.; Ruiz, A., Acute kidney injury in heart failure: a population study. *ESC Heart Fail* **2020**, *7* (2), 415-422.
8. Chertow, G. M.; Burdick, E.; Honour, M.; Bonventre, J. V.; Bates, D. W., Acute kidney injury, mortality, length of stay, and costs in hospitalized patients. *J Am Soc Nephrol* **2005**, *16* (11), 3365-70.
9. Wilson, F. P.; Shashaty, M.; Testani, J.; Aqeel, I.; Borovskiy, Y.; Ellenberg, S. S.; Feldman, H. I.; Fernandez, H.; Gitelman, Y.; Lin, J.; Negoianu, D.; Parikh, C. R.; Reese, P. P.; Urbani, R.; Fuchs, B., Automated, electronic alerts for acute kidney injury: a single-blind, parallel-group, randomised controlled trial. *Lancet* **2015**, *385* (9981), 1966-74.
10. Silver, S. A.; Long, J.; Zheng, Y.; Chertow, G. M., Cost of Acute Kidney Injury in Hospitalized Patients. *J Hosp Med* **2017**, *12* (2), 70-76.
11. Palevsky, P. M.; Zhang, J. H.; O'Connor, T. Z.; Chertow, G. M.; Crowley, S. T.; Choudhury, D.; Finkel, K.; Kellum, J. A.; Paganini, E.; Schein, R. M.; Smith, M. W.; Swanson, K. M.; Thompson, B. T.; Vijayan, A.; Watnick, S.; Star, R. A.; Peduzzi, P., Intensity of renal support in critically ill patients with acute kidney injury. *N Engl J Med* **2008**, *359* (1), 7-20.
12. Coca, S. G.; Singanamala, S.; Parikh, C. R., Chronic kidney disease after acute kidney injury: a systematic review and meta-analysis. *Kidney Int* **2012**, *81* (5), 442-8.
13. Sharma, N.; Malek, V.; Mulay, S. R.; Gaikwad, A. B., Angiotensin II type 2 receptor and angiotensin-converting enzyme 2 mediate ischemic renal injury in diabetic and non-diabetic rats. *Life Sci* **2019**, *235*, 116796.
14. Yang, Y.; Yu, X.; Zhang, Y.; Ding, G.; Zhu, C.; Huang, S.; Jia, Z.; Zhang, A., Hypoxia-inducible factor prolyl hydroxylase inhibitor roxadustat (FG-4592) protects against cisplatin-induced acute kidney injury. *Clin Sci (Lond)* **2018**, *132* (7), 825-838.
15. Chen, Y.; Wang, N.; Yuan, Q.; Qin, J.; Hu, G.; Li, Q.; Tao, L.; Xie, Y.; Peng, Z., The Protective Effect of Fluorofenidone against Cyclosporine A-Induced Nephrotoxicity. *Kidney Blood Press Res* **2019**, *44* (4), 656-668.
16. Jiang, Y.; Quan, J.; Chen, Y.; Liao, X.; Dai, Q.; Lu, R.; Yu, Y.; Hu, G.; Li, Q.; Meng, J.; Xie, Y.; Peng, Z.; Tao, L., Fluorofenidone protects against acute kidney injury. *FASEB J* **2019**, *33* (12), 14325-14336.
17. Tang, Y.; Zhang, F.; Huang, L.; Yuan, Q.; Qin, J.; Li, B.; Wang, N.; Xie, Y.; Wang, L.; Wang, W.; Kwan, K.; Peng, Z.; Hu, G.; Li, J.; Tao, L., The Protective Mechanism of Fluorofenidone in Renal Interstitial Inflammation and Fibrosis. *Am J Med Sci* **2015**, *350* (3), 195-203.
18. Liles, J. T.; Corkey, B. K.; Notte, G. T.; Budas, G. R.; Lansdon, E. B.; Hinojosa-Kirschenbaum, F.; Badal, S. S.; Lee, M.; Schultz, B. E.; Wise, S.; Pendem, S.; Graupe, M.; Castonguay, L.; Koch, K. A.;

- Wong, M. H.; Papalia, G. A.; French, D. M.; Sullivan, T.; Huntzicker, E. G.; Ma, F. Y.; Nikolic-Paterson, D. J.; Altuhaifi, T.; Yang, H.; Fogo, A. B.; Breckenridge, D. G., ASK1 contributes to fibrosis and dysfunction in models of kidney disease. *J Clin Invest* **2018**, *128* (10), 4485-4500.
19. El Eter, E., NQDI 1, an inhibitor of ASK1 attenuates acute ischemic renal injury by modulating oxidative stress and cell death. *Cardiovasc Hematol Agents Med Chem* **2013**, *11* (3), 179-86.
20. Gong, X.; Duan, Y.; Zheng, J.; Wang, Y.; Wang, G.; Norgren, S.; Hei, T. K., Nephroprotective Effects of N-Acetylcysteine Amide against Contrast-Induced Nephropathy through Upregulating Thioredoxin-1, Inhibiting ASK1/p38MAPK Pathway, and Suppressing Oxidative Stress and Apoptosis in Rats. *Oxid Med Cell Longev* **2016**, *2016*, 8715185.
21. Wang, Y.; Ji, H. X.; Xing, S. H.; Pei, D. S.; Guan, Q. H., SP600125, a selective JNK inhibitor, protects ischemic renal injury via suppressing the extrinsic pathways of apoptosis. *Life Sci* **2007**, *80* (22), 2067-75.
22. Kim, T.; Kim, Y. J.; Han, I. H.; Lee, D.; Ham, J.; Kang, K. S.; Lee, J. W., The synthesis of sulforaphane analogues and their protection effect against cisplatin induced cytotoxicity in kidney cells. *Bioorg Med Chem Lett* **2015**, *25* (1), 62-6.
23. He, X.; Li, L.; Tan, H.; Chen, J.; Zhou, Y., Atorvastatin attenuates contrast-induced nephropathy by modulating inflammatory responses through the regulation of JNK/p38/Hsp27 expression. *J Pharmacol Sci* **2016**, *131* (1), 18-27.
24. Yang, N.; Luo, M.; Li, R.; Huang, Y.; Zhang, R.; Wu, Q.; Wang, F.; Li, Y.; Yu, X., Blockage of JAK/STAT signalling attenuates renal ischaemia-reperfusion injury in rat. *Nephrol Dial Transplant* **2008**, *23* (1), 91-100.
25. Neria, F.; Castilla, M. A.; Sanchez, R. F.; Gonzalez Pacheco, F. R.; Deudero, J. J.; Calabia, O.; Tejedor, A.; Manzarbeitia, F.; Ortiz, A.; Caramelo, C., Inhibition of JAK2 protects renal endothelial and epithelial cells from oxidative stress and cyclosporin A toxicity. *Kidney Int* **2009**, *75* (2), 227-34.
26. Novogrodsky, A.; Vanichkin, A.; Patya, M.; Gazit, A.; Oshero, N.; Levitzki, A., Prevention of lipopolysaccharide-induced lethal toxicity by tyrosine kinase inhibitors. *Science* **1994**, *264* (5163), 1319-22.
27. Novogrodsky, A.; Weisspapir, M.; Patya, M.; Meshorer, A.; Vanichkin, A., Tyrphostin 4-nitrobenzylidene malononitrile reduces chemotherapy toxicity without impairing efficacy. *Cancer Res* **1998**, *58* (11), 2397-403.
28. Uddin, M. J.; Dorotea, D.; Pak, E. S.; Ha, H., Fyn Kinase: A Potential Therapeutic Target in Acute Kidney Injury. *Biomol Ther (Seoul)* **2020**, *28* (3), 213-221.
29. Xiong, C.; Zang, X.; Zhou, X.; Liu, L.; Masucci, M. V.; Tang, J.; Li, X.; Liu, N.; Bayliss, G.; Zhao, T. C.; Zhuang, S., Pharmacological inhibition of Src kinase protects against acute kidney injury in a murine model of renal ischemia/reperfusion. *Oncotarget* **2017**, *8* (19), 31238-31253.
30. Sahu, B. D.; Kalvala, A. K.; Koneru, M.; Mahesh Kumar, J.; Kuncha, M.; Rachamalla, S. S.; Sistla, R., Ameliorative effect of fisetin on cisplatin-induced nephrotoxicity in rats via modulation of NF-kappaB activation and antioxidant defence. *PLoS One* **2014**, *9* (9), e105070.
31. Ren, Q.; Guo, F.; Tao, S.; Huang, R.; Ma, L.; Fu, P., Flavonoid fisetin alleviates kidney inflammation and apoptosis via inhibiting Src-mediated NF-kappaB p65 and MAPK signaling pathways in septic AKI mice. *Biomed Pharmacother* **2020**, *122*, 109772.
32. Takikita-Suzuki, M.; Haneda, M.; Sasahara, M.; Owada, M. K.; Nakagawa, T.; Isono, M.; Takikita, S.; Koya, D.; Ogasawara, K.; Kikkawa, R., Activation of Src kinase in platelet-derived growth factor-B-dependent tubular regeneration after acute ischemic renal injury. *Am J Pathol* **2003**, *163* (1), 277-86.
33. Wang, Y.; Zhang, H.; Yang, Z.; Miao, D.; Zhang, D., Rho Kinase Inhibitor, Fasudil, Attenuates Contrast-induced Acute Kidney Injury. *Basic Clin Pharmacol Toxicol* **2018**, *122* (2), 278-287.

34. Prakash, J.; de Borst, M. H.; Lacombe, M.; Opdam, F.; Klok, P. A.; van Goor, H.; Meijer, D. K.; Moolenaar, F.; Poelstra, K.; Kok, R. J., Inhibition of renal rho kinase attenuates ischemia/reperfusion-induced injury. *J Am Soc Nephrol* **2008**, *19* (11), 2086-97.
35. Kentrup, D.; Reuter, S.; Schnockel, U.; Grabner, A.; Edemir, B.; Pavenstadt, H.; Schober, O.; Schafers, M.; Schlatter, E.; Bussemaker, E., Hydroxyfasudil-mediated inhibition of ROCK1 and ROCK2 improves kidney function in rat renal acute ischemia-reperfusion injury. *PLoS One* **2011**, *6* (10), e26419.
36. Xu, Y.; Ma, H.; Shao, J.; Wu, J.; Zhou, L.; Zhang, Z.; Wang, Y.; Huang, Z.; Ren, J.; Liu, S.; Chen, X.; Han, J., A Role for Tubular Necroptosis in Cisplatin-Induced AKI. *J Am Soc Nephrol* **2015**, *26* (11), 2647-58.
37. Qin, X.; Hu, L.; Shi, S. N.; Chen, X.; Zhuang, C.; Zhang, W.; Jitkaew, S.; Pang, X.; Yu, J.; Tan, Y. X.; Wang, H. Y.; Cai, Z., The Bcr-Abl inhibitor GNF-7 inhibits necroptosis and ameliorates acute kidney injury by targeting RIPK1 and RIPK3 kinases. *Biochem Pharmacol* **2020**, *177*, 113947.
38. Fauster, A.; Rebsamen, M.; Huber, K. V.; Bigenzahn, J. W.; Stukalov, A.; Lardeau, C. H.; Scorzoni, S.; Bruckner, M.; Gridling, M.; Parapatics, K.; Colinge, J.; Bennett, K. L.; Kubicek, S.; Krautwald, S.; Linkermann, A.; Superti-Furga, G., A cellular screen identifies ponatinib and pazopanib as inhibitors of necroptosis. *Cell Death Dis* **2015**, *6*, e1767.
39. Najjar, M.; Suebsuwong, C.; Ray, S. S.; Thapa, R. J.; Maki, J. L.; Nogusa, S.; Shah, S.; Saleh, D.; Gough, P. J.; Bertin, J.; Yuan, J.; Balachandran, S.; Cuny, G. D.; Degterev, A., Structure guided design of potent and selective ponatinib-based hybrid inhibitors for RIPK1. *Cell Rep* **2015**, *10* (11), 1850-60.
40. Aminzadeh, M. A.; Reisman, S. A.; Vaziri, N. D.; Khazaeli, M.; Yuan, J.; Meyer, C. J., The synthetic triterpenoid RTA dh404 (CDDO-dhTFEA) restores Nrf2 activity and attenuates oxidative stress, inflammation, and fibrosis in rats with chronic kidney disease. *Xenobiotica* **2014**, *44* (6), 570-8.
41. Chorvat, R. J., Peripherally restricted CB1 receptor blockers. *Bioorg Med Chem Lett* **2013**, *23* (17), 4751-60.
42. Lecru, L.; Desterke, C.; Grassin-Delyle, S.; Chatziantoniou, C.; Vandermeersch, S.; Devocelle, A.; Vernochet, A.; Ivanovski, N.; Ledent, C.; Ferlicot, S.; Dalia, M.; Said, M.; Beaudreuil, S.; Charpentier, B.; Vazquez, A.; Giron-Michel, J.; Azzarone, B.; Durrbach, A.; Francois, H., Cannabinoid receptor 1 is a major mediator of renal fibrosis. *Kidney Int* **2015**, *88* (1), 72-84.
43. Pacher, P.; Batkai, S.; Kunos, G., The endocannabinoid system as an emerging target of pharmacotherapy. *Pharmacol Rev* **2006**, *58* (3), 389-462.
44. Mukhopadhyay, P.; Rajesh, M.; Pan, H.; Patel, V.; Mukhopadhyay, B.; Batkai, S.; Gao, B.; Hasko, G.; Pacher, P., Cannabinoid-2 receptor limits inflammation, oxidative/nitrosative stress, and cell death in nephropathy. *Free Radic Biol Med* **2010**, *48* (3), 457-67.
45. Nettekoven, M.; Adam, J. M.; Bendels, S.; Bissantz, C.; Fingerle, J.; Grether, U.; Gruner, S.; Guba, W.; Kimbara, A.; Ottaviani, G.; Pullmann, B.; Rogers-Evans, M.; Rover, S.; Rothenhausler, B.; Schmitt, S.; Schuler, F.; Schulz-Gasch, T.; Ullmer, C., Novel Triazolopyrimidine-Derived Cannabinoid Receptor 2 Agonists as Potential Treatment for Inflammatory Kidney Diseases. *ChemMedChem* **2016**, *11* (2), 179-89.
46. Barutta, F.; Grimaldi, S.; Gambino, R.; Vemuri, K.; Makriyannis, A.; Annaratone, L.; di Marzo, V.; Bruno, G.; Gruden, G., Dual therapy targeting the endocannabinoid system prevents experimental diabetic nephropathy. *Nephrol Dial Transplant* **2017**, *32* (10), 1655-1665.
47. Horvath, B.; Mukhopadhyay, P.; Kechrid, M.; Patel, V.; Tanchian, G.; Wink, D. A.; Gertsch, J.; Pacher, P., beta-Caryophyllene ameliorates cisplatin-induced nephrotoxicity in a cannabinoid 2 receptor-dependent manner. *Free Radic Biol Med* **2012**, *52* (8), 1325-33.
48. Zhou, L.; Zhou, S.; Yang, P.; Tian, Y.; Feng, Z.; Xie, X. Q.; Liu, Y., Targeted inhibition of the type 2 cannabinoid receptor is a novel approach to reduce renal fibrosis. *Kidney Int* **2018**, *94* (4), 756-772.
49. Mukhopadhyay, P.; Baggelaar, M.; Erdelyi, K.; Cao, Z.; Cinar, R.; Fezza, F.; Ignatowska-Janlowska, B.; Wilkerson, J.; van Gils, N.; Hansen, T.; Ruben, M.; Soethoudt, M.; Heitman, L.; Kunos,

- G.; Maccarrone, M.; Lichtman, A.; Pacher, P.; Van der Stelt, M., The novel, orally available and peripherally restricted selective cannabinoid CB2 receptor agonist LEI-101 prevents cisplatin-induced nephrotoxicity. *Br J Pharmacol* **2016**, *173* (3), 446-58.
50. Gutierrez, S.; Moron, M.; Griera, M.; Sucunza, D.; Calleros, L.; Garcia-Jerez, A.; Coderch, C.; Hermoso, F. J.; Burgos, C.; Rodriguez-Puyol, M.; de Pascual-Teresa, B.; Diez-Marques, M. L.; Jimenez, A.; Toro-Londono, M.; Rodriguez-Puyol, D.; Vaquero, J. J., Discovery of potent calpain inhibitors based on the azolo-imidazolidenone scaffold. *Eur J Med Chem* **2018**, *157*, 946-959.
51. Tedesco-Silva, H.; Szakaly, P.; Shoker, A.; Sommerer, C.; Yoshimura, N.; Schena, F. P.; Cremer, M.; Hmissi, A.; Mayer, H.; Lang, P.; Group, F. T. Y. C. S., FTY720 versus mycophenolate mofetil in de novo renal transplantation: six-month results of a double-blind study. *Transplantation* **2007**, *84* (7), 885-92.
52. Suleiman, M.; Cury, P. M.; Pestana, J. O.; Burdmann, E. A.; Bueno, V., FTY720 prevents renal T-cell infiltration after ischemia/reperfusion injury. *Transplant Proc* **2005**, *37* (1), 373-4.
53. Tian, T.; Zhang, J.; Zhu, X.; Wen, S.; Shi, D.; Zhou, H., FTY720 ameliorates renal fibrosis by simultaneously affecting leucocyte recruitment and TGF-beta signalling in fibroblasts. *Clin Exp Immunol* **2017**, *190* (1), 68-78.
54. Lien, Y. H.; Yong, K. C.; Cho, C.; Igarashi, S.; Lai, L. W., S1P(1)-selective agonist, SEW2871, ameliorates ischemic acute renal failure. *Kidney Int* **2006**, *69* (9), 1601-8.
55. Peng, Y.; Liu, L.; Wang, Y.; Yao, J.; Jin, F.; Tao, T.; Yuan, H.; Shi, L.; Lu, S., Treatment with toll-like receptor 2 inhibitor ortho-vanillin alleviates lipopolysaccharide-induced acute kidney injury in mice. *Exp Ther Med* **2019**, *18* (6), 4829-4837.
56. Wu, C. H.; Song, J. S.; Chang, K. H.; Jan, J. J.; Chen, C. T.; Chou, M. C.; Yeh, K. C.; Wong, Y. C.; Tseng, C. T.; Wu, S. H.; Yeh, C. F.; Huang, C. Y.; Wang, M. H.; Sadani, A. A.; Chang, C. P.; Cheng, C. Y.; Tsou, L. K.; Shia, K. S., Stem cell mobilizers targeting chemokine receptor CXCR4: renoprotective application in acute kidney injury. *J Med Chem* **2015**, *58* (5), 2315-25.
57. Cugini, D.; Azzollini, N.; Gagliardini, E.; Cassis, P.; Bertini, R.; Colotta, F.; Noris, M.; Remuzzi, G.; Benigni, A., Inhibition of the chemokine receptor CXCR2 prevents kidney graft function deterioration due to ischemia/reperfusion. *Kidney Int* **2005**, *67* (5), 1753-61.
58. Liu, P.; Li, X.; Lv, W.; Xu, Z., Inhibition of CXCL1-CXCR2 axis ameliorates cisplatin-induced acute kidney injury by mediating inflammatory response. *Biomed Pharmacother* **2020**, *122*, 109693.
59. Fountain, J. H.; Lappin, S. L., Physiology, Renin Angiotensin System. In *StatPearls*, Treasure Island (FL), 2022.
60. Choi, S. Y.; Ryu, Y.; Kee, H. J.; Cho, S. N.; Kim, G. R.; Cho, J. Y.; Kim, H. S.; Kim, I. K.; Jeong, M. H., Tubastatin A suppresses renal fibrosis via regulation of epigenetic histone modification and Smad3-dependent fibrotic genes. *Vascul Pharmacol* **2015**, *72*, 130-40.
61. Anemia and Chronic Kidney Disease https://www.kidney.org/atoz/content/what_anemia_ckd.
62. Sanz, A. B.; Santamaria, B.; Ruiz-Ortega, M.; Egido, J.; Ortiz, A., Mechanisms of renal apoptosis in health and disease. *J Am Soc Nephrol* **2008**, *19* (9), 1634-42.
63. Zhang, Q.; Liu, J.; Zhang, M.; Wei, S.; Li, R.; Gao, Y.; Peng, W.; Wu, C., Apoptosis Induction of Fibroblast-Like Synoviocytes Is an Important Molecular-Mechanism for Herbal Medicine along with its Active Components in Treating Rheumatoid Arthritis. *Biomolecules* **2019**, *9* (12).
64. Song, J.; Park, K. A.; Lee, W. T.; Lee, J. E., Apoptosis signal regulating kinase 1 (ASK1): potential as a therapeutic target for Alzheimer's disease. *Int J Mol Sci* **2014**, *15* (2), 2119-29.
65. Polonio-Vallon, T.; Kirkpatrick, J.; Krijgsveld, J.; Hofmann, T. G., Src kinase modulates the apoptotic p53 pathway by altering HIPK2 localization. *Cell Cycle* **2014**, *13* (1), 115-25.
66. Wael, H.; Yoshida, R.; Kudoh, S.; Hasegawa, K.; Niimori-Kita, K.; Ito, T., Notch1 signaling controls cell proliferation, apoptosis and differentiation in lung carcinoma. *Lung Cancer* **2014**, *85* (2), 131-40.

67. Momeni, H. R., Role of calpain in apoptosis. *Cell J* **2011**, *13* (2), 65-72.
68. Amaral, J. D.; Viana, R. J.; Ramalho, R. M.; Steer, C. J.; Rodrigues, C. M., Bile acids: regulation of apoptosis by ursodeoxycholic acid. *J Lipid Res* **2009**, *50* (9), 1721-34.
69. Black, L. M.; Lever, J. M.; Agarwal, A., Renal Inflammation and Fibrosis: A Double-edged Sword. *J Histochem Cytochem* **2019**, *67* (9), 663-681.
70. Obinata, H.; Hla, T., Sphingosine 1-phosphate and inflammation. *Int Immunol* **2019**, *31* (9), 617-625.
71. Ahmed, S. M.; Luo, L.; Namani, A.; Wang, X. J.; Tang, X., Nrf2 signaling pathway: Pivotal roles in inflammation. *Biochim Biophys Acta Mol Basis Dis* **2017**, *1863* (2), 585-597.
72. Ashton, J. C.; Glass, M., The cannabinoid CB2 receptor as a target for inflammation-dependent neurodegeneration. *Curr Neuropharmacol* **2007**, *5* (2), 73-80.
73. Shimokawa, H.; Takeshita, A., Rho-kinase is an important therapeutic target in cardiovascular medicine. *Arterioscler Thromb Vasc Biol* **2005**, *25* (9), 1767-75.
74. Karunakaran, D.; Nguyen, M. A.; Geoffrion, M.; Vreeken, D.; Lister, Z.; Cheng, H. S.; Otte, N.; Essebier, P.; Wyatt, H.; Kandiah, J. W.; Jung, R.; Alenghat, F. J.; Mompeon, A.; Lee, R.; Pan, C.; Gordon, E.; Rasheed, A.; Lusic, A. J.; Liu, P.; Matic, L. P.; Hedin, U.; Fish, J. E.; Guo, L.; Kolodgie, F.; Virmani, R.; van Gils, J. M.; Rayner, K. J., RIPK1 Expression Associates With Inflammation in Early Atherosclerosis in Humans and Can Be Therapeutically Silenced to Reduce NF-kappaB Activation and Atherogenesis in Mice. *Circulation* **2021**, *143* (2), 163-177.
75. Akcay, A.; Nguyen, Q.; Edelstein, C. L., Mediators of inflammation in acute kidney injury. *Mediators Inflamm* **2009**, *2009*, 137072.
76. Horl, W. H., Nonsteroidal Anti-Inflammatory Drugs and the Kidney. *Pharmaceuticals (Basel)* **2010**, *3* (7), 2291-2321.
77. Billings, F. T. t.; Hendricks, P. A.; Schildcrout, J. S.; Shi, Y.; Petracek, M. R.; Byrne, J. G.; Brown, N. J., High-Dose Perioperative Atorvastatin and Acute Kidney Injury Following Cardiac Surgery: A Randomized Clinical Trial. *JAMA* **2016**, *315* (9), 877-88.
78. Wu, Q.; Wu, W.; Jacevic, V.; Franca, T. C. C.; Wang, X.; Kuca, K., Selective inhibitors for JNK signalling: a potential targeted therapy in cancer. *J Enzyme Inhib Med Chem* **2020**, *35* (1), 574-583.
79. Roskoski, R., Jr., Properties of FDA-approved small molecule protein kinase inhibitors: A 2021 update. *Pharmacol Res* **2021**, *165*, 105463.
80. Chakrabarti, A.; Oehme, I.; Witt, O.; Oliveira, G.; Sippl, W.; Romier, C.; Pierce, R. J.; Jung, M., HDAC8: a multifaceted target for therapeutic interventions. *Trends Pharmacol Sci* **2015**, *36* (7), 481-92.
81. Cirio, M. C.; de Caestecker, M. P.; Hukriede, N. A., Zebrafish Models of Kidney Damage and Repair. *Curr Pathobiol Rep* **2015**, *3* (2), 163-170.
82. Cho, Y. S.; Kwon, H. J., Identification and validation of bioactive small molecule target through phenotypic screening. *Bioorg Med Chem* **2012**, *20* (6), 1922-8.
83. Rennekamp, A. J.; Peterson, R. T., 15 years of zebrafish chemical screening. *Curr Opin Chem Biol* **2015**, *24*, 58-70.
84. Moffat, J. G.; Vincent, F.; Lee, J. A.; Eder, J.; Prunotto, M., Opportunities and challenges in phenotypic drug discovery: an industry perspective. *Nat Rev Drug Discov* **2017**, *16* (8), 531-543.
85. Yoganantharajah, P.; Gibert, Y., The Use of the Zebrafish Model to Aid in Drug Discovery and Target Validation. *Curr Top Med Chem* **2017**, *17* (18), 2041-2055.
86. Rubinstein, A. L., Zebrafish assays for drug toxicity screening. *Expert Opin Drug Metab Toxicol* **2006**, *2* (2), 231-40.
87. Taylor, K. L.; Grant, N. J.; Temperley, N. D.; Patton, E. E., Small molecule screening in zebrafish: an in vivo approach to identifying new chemical tools and drug leads. *Cell Commun Signal* **2010**, *8*, 11.
88. Miscovic, F.; Rotstein, O.; Wen, X. Y., Advances in zebrafish high content and high throughput technologies. *Comb Chem High Throughput Screen* **2012**, *15* (7), 515-21.

89. Pickart, M. A.; Klee, E. W., Zebrafish approaches enhance the translational research tackle box. *Transl Res* **2014**, *163* (2), 65-78.
90. Patton, E. E.; Zon, L. I.; Langenau, D. M., Zebrafish disease models in drug discovery: from preclinical modelling to clinical trials. *Nat Rev Drug Discov* **2021**, *20* (8), 611-628.
91. Cianciolo Cosentino, C.; Roman, B. L.; Drummond, I. A.; Hukriede, N. A., Intravenous microinjections of zebrafish larvae to study acute kidney injury. *J Vis Exp* **2010**, (42).
92. Kaplan, E. L. M., P., Non-parametric estimation from incomplete observations. *J. Am. Stat. Assoc.* **1958**, *53*, 457-481.
93. Lipinski, C. A.; Lombardo, F.; Dominy, B. W.; Feeney, P. J., Experimental and computational approaches to estimate solubility and permeability in drug discovery and development settings. *Adv Drug Deliv Rev* **2001**, *46* (1-3), 3-26.
94. Veber, D. F.; Johnson, S. R.; Cheng, H. Y.; Smith, B. R.; Ward, K. W.; Kopple, K. D., Molecular properties that influence the oral bioavailability of drug candidates. *J Med Chem* **2002**, *45* (12), 2615-23.
95. Yang, N. J.; Hinner, M. J., Getting across the cell membrane: an overview for small molecules, peptides, and proteins. *Methods Mol Biol* **2015**, *1266*, 29-53.
96. Richter, M. F.; Drown, B. S.; Riley, A. P.; Garcia, A.; Shirai, T.; Svec, R. L.; Hergenrother, P. J., Predictive compound accumulation rules yield a broad-spectrum antibiotic. *Nature* **2017**, *545* (7654), 299-304.
97. *BIOVIA Discovery Studio*, Dassault Systèmes: San Diego, 2018.
98. Athanasiadis, E.; Cournia, Z.; Spyrou, G., ChemBioServer: a web-based pipeline for filtering, clustering and visualization of chemical compounds used in drug discovery. *Bioinformatics* **2012**, *28* (22), 3002-3.
99. Wishart, D. S.; Feunang, Y. D.; Guo, A. C.; Lo, E. J.; Marcu, A.; Grant, J. R.; Sajed, T.; Johnson, D.; Li, C.; Sayeeda, Z.; Assempour, N.; Iynkkaran, I.; Liu, Y.; Maciejewski, A.; Gale, N.; Wilson, A.; Chin, L.; Cummings, R.; Le, D.; Pon, A.; Knox, C.; Wilson, M., DrugBank 5.0: a major update to the DrugBank database for 2018. *Nucleic Acids Res* **2018**, *46* (D1), D1074-D1082.
100. Shultz, M. D., Two Decades under the Influence of the Rule of Five and the Changing Properties of Approved Oral Drugs. *J Med Chem* **2019**, *62* (4), 1701-1714.
101. *Schrödinger Release 2016-1: Maestro*, Schrödinger, LLC: New York, 2018.
102. Podlewska, S.; Kafel, R., MetStabOn-Online Platform for Metabolic Stability Predictions. *Int J Mol Sci* **2018**, *19* (4).
103. Zhong, H.; Lin, S., Chemical screening with zebrafish embryos. *Methods Mol Biol* **2011**, *716*, 193-205.
104. Fischer, S.; Kluver, N.; Burkhardt-Medicke, K.; Pietsch, M.; Schmidt, A. M.; Wellner, P.; Schirmer, K.; Luckenbach, T., Abcb4 acts as multixenobiotic transporter and active barrier against chemical uptake in zebrafish (*Danio rerio*) embryos. *BMC Biol* **2013**, *11*, 69.
105. Fraher, D.; Sanigorski, A.; Mellett, N. A.; Meikle, P. J.; Sinclair, A. J.; Gibert, Y., Zebrafish Embryonic Lipidomic Analysis Reveals that the Yolk Cell Is Metabolically Active in Processing Lipid. *Cell Rep* **2016**, *14* (6), 1317-1329.
106. de Groh, E. D.; Swanhart, L. M.; Cosentino, C. C.; Jackson, R. L.; Dai, W.; Kitchens, C. A.; Day, B. W.; Smithgall, T. E.; Hukriede, N. A., Inhibition of histone deacetylase expands the renal progenitor cell population. *J Am Soc Nephrol* **2010**, *21* (5), 794-802.
107. Skrypnik, N. I.; Sanker, S.; Skvarca, L. B.; Novitskaya, T.; Woods, C.; Chiba, T.; Patel, K.; Goldberg, N. D.; McDermott, L.; Vinson, P. N.; Calcutt, M. W.; Huryn, D. M.; Verneti, L. A.; Vogt, A.; Hukriede, N. A.; de Caestecker, M. P., Delayed treatment with PTBA analogs reduces postinjury renal fibrosis after kidney injury. *Am J Physiol Renal Physiol* **2016**, *310* (8), F705-F716.
108. Brilli Skvarca, L.; Han, H. I.; Espiritu, E. B.; Missinato, M. A.; Rochon, E. R.; McDaniels, M. D.; Bais, A. S.; Roman, B. L.; Waxman, J. S.; Watkins, S. C.; Davidson, A. J.; Tsang, M.; Hukriede, N. A.,

Enhancing regeneration after acute kidney injury by promoting cellular dedifferentiation in zebrafish. *Dis Model Mech* **2019**, *12* (4).

109. Bantscheff, M.; Hopf, C.; Savitski, M. M.; Dittmann, A.; Grandi, P.; Michon, A. M.; Schlegl, J.; Abraham, Y.; Becher, I.; Bergamini, G.; Boesche, M.; Delling, M.; Dumpelfeld, B.; Eberhard, D.; Huthmacher, C.; Mathieson, T.; Poeckel, D.; Reader, V.; Strunk, K.; Sweetman, G.; Kruse, U.; Neubauer, G.; Ramsden, N. G.; Drewes, G., Chemoproteomics profiling of HDAC inhibitors reveals selective targeting of HDAC complexes. *Nat Biotechnol* **2011**, *29* (3), 255-65.
110. Brillì, L. L.; Swanhart, L. M.; de Caestecker, M. P.; Hukriede, N. A., HDAC inhibitors in kidney development and disease. *Pediatr Nephrol* **2013**, *28* (10), 1909-21.
111. Chun, P., Therapeutic effects of histone deacetylase inhibitors on kidney disease. *Arch Pharm Res* **2018**, *41* (2), 162-183.
112. Hadden, M. J.; Advani, A., Histone Deacetylase Inhibitors and Diabetic Kidney Disease. *Int J Mol Sci* **2018**, *19* (9).
113. Ho, T. C. S.; Chan, A. H. Y.; Ganesan, A., Thirty Years of HDAC Inhibitors: 2020 Insight and Hindsight. *J Med Chem* **2020**, *63* (21), 12460-12484.
114. Liu, N.; Zhuang, S., Treatment of chronic kidney diseases with histone deacetylase inhibitors. *Front Physiol* **2015**, *6*, 121.
115. Zhuang, S., Epigenetic targeting for acute kidney injury. *Nephrology (Carlton)* **2018**, *23 Suppl 4*, 21-25.
116. Wang, B.; Zhu, X.; Kim, Y.; Li, J.; Huang, S.; Saleem, S.; Li, R. C.; Xu, Y.; Dore, S.; Cao, W., Histone deacetylase inhibition activates transcription factor Nrf2 and protects against cerebral ischemic damage. *Free Radic Biol Med* **2012**, *52* (5), 928-36.
117. Tung, C. W.; Hsu, Y. C.; Cai, C. J.; Shih, Y. H.; Wang, C. J.; Chang, P. J.; Lin, C. L., Trichostatin A ameliorates renal tubulointerstitial fibrosis through modulation of the JNK-dependent Notch-2 signaling pathway. *Sci Rep* **2017**, *7* (1), 14495.
118. Liang, D.; Kong, X.; Sang, N., Effects of histone deacetylase inhibitors on HIF-1. *Cell Cycle* **2006**, *5* (21), 2430-5.
119. Saito, T.; Nishida, K.; Furumatsu, T.; Yoshida, A.; Ozawa, M.; Ozaki, T., Histone deacetylase inhibitors suppress mechanical stress-induced expression of RUNX-2 and ADAMTS-5 through the inhibition of the MAPK signaling pathway in cultured human chondrocytes. *Osteoarthritis Cartilage* **2013**, *21* (1), 165-74.
120. Li, W.; Sun, Z., Mechanism of Action for HDAC Inhibitors-Insights from Omics Approaches. *Int J Mol Sci* **2019**, *20* (7).
121. Narita, T.; Weinert, B. T.; Choudhary, C., Functions and mechanisms of non-histone protein acetylation. *Nat Rev Mol Cell Biol* **2019**, *20* (3), 156-174.
122. Mishra, N.; Reilly, C. M.; Brown, D. R.; Ruiz, P.; Gilkeson, G. S., Histone deacetylase inhibitors modulate renal disease in the MRL-lpr/lpr mouse. *J Clin Invest* **2003**, *111* (4), 539-52.
123. Advani, A.; Huang, Q.; Thai, K.; Advani, S. L.; White, K. E.; Kelly, D. J.; Yuen, D. A.; Connelly, K. A.; Marsden, P. A.; Gilbert, R. E., Long-term administration of the histone deacetylase inhibitor vorinostat attenuates renal injury in experimental diabetes through an endothelial nitric oxide synthase-dependent mechanism. *Am J Pathol* **2011**, *178* (5), 2205-14.
124. Choi, H. S.; Song, J. H.; Kim, I. J.; Joo, S. Y.; Eom, G. H.; Kim, I.; Cha, H.; Cho, J. M.; Ma, S. K.; Kim, S. W.; Bae, E. H., Histone deacetylase inhibitor, CG200745 attenuates renal fibrosis in obstructive kidney disease. *Sci Rep* **2018**, *8* (1), 11546.
125. Choi, S. Y.; Kee, H. J.; Kurz, T.; Hansen, F. K.; Ryu, Y.; Kim, G. R.; Lin, M. Q.; Jin, L.; Piao, Z. H.; Jeong, M. H., Class I HDACs specifically regulate E-cadherin expression in human renal epithelial cells. *J Cell Mol Med* **2016**, *20* (12), 2289-2298.

126. Gilbert, R. E.; Huang, Q.; Thai, K.; Advani, S. L.; Lee, K.; Yuen, D. A.; Connelly, K. A.; Advani, A., Histone deacetylase inhibition attenuates diabetes-associated kidney growth: potential role for epigenetic modification of the epidermal growth factor receptor. *Kidney Int* **2011**, *79* (12), 1312-21.
127. Kang, S. W.; Lee, S. M.; Kim, J. Y.; Kim, S. Y.; Kim, Y. H.; Kim, T. H.; Kang, M. S.; Jang, W. H.; Seo, S. K., Therapeutic activity of the histone deacetylase inhibitor SB939 on renal fibrosis. *Int Immunopharmacol* **2017**, *42*, 25-31.
128. Kinugasa, F.; Noto, T.; Matsuoka, H.; Urano, Y.; Sudo, Y.; Takakura, S.; Mutoh, S., Prevention of renal interstitial fibrosis via histone deacetylase inhibition in rats with unilateral ureteral obstruction. *Transpl Immunol* **2010**, *23* (1-2), 18-23.
129. Liu, J.; Livingston, M. J.; Dong, G.; Tang, C.; Su, Y.; Wu, G.; Yin, X. M.; Dong, Z., Histone deacetylase inhibitors protect against cisplatin-induced acute kidney injury by activating autophagy in proximal tubular cells. *Cell Death Dis* **2018**, *9* (3), 322.
130. Manson, S. R.; Song, J. B.; Hruska, K. A.; Austin, P. F., HDAC dependent transcriptional repression of Bmp-7 potentiates TGF-beta mediated renal fibrosis in obstructive uropathy. *J Urol* **2014**, *191* (1), 242-52.
131. Noh, H.; Oh, E. Y.; Seo, J. Y.; Yu, M. R.; Kim, Y. O.; Ha, H.; Lee, H. B., Histone deacetylase-2 is a key regulator of diabetes- and transforming growth factor-beta1-induced renal injury. *Am J Physiol Renal Physiol* **2009**, *297* (3), F729-39.
132. Pang, M.; Kothapally, J.; Mao, H.; Tolbert, E.; Ponnusamy, M.; Chin, Y. E.; Zhuang, S., Inhibition of histone deacetylase activity attenuates renal fibroblast activation and interstitial fibrosis in obstructive nephropathy. *Am J Physiol Renal Physiol* **2009**, *297* (4), F996-F1005.
133. Ranganathan, P.; Hamad, R.; Mohamed, R.; Jayakumar, C.; Muthusamy, T.; Ramesh, G., Histone deacetylase-mediated silencing of AMWAP expression contributes to cisplatin nephrotoxicity. *Kidney Int* **2016**, *89* (2), 317-26.
134. Van Beneden, K.; Geers, C.; Pauwels, M.; Mannaerts, I.; Wissing, K. M.; Van den Branden, C.; van Grunsven, L. A., Comparison of trichostatin A and valproic acid treatment regimens in a mouse model of kidney fibrosis. *Toxicol Appl Pharmacol* **2013**, *271* (2), 276-84.
135. Hyndman, K. A.; Kasztan, M.; Mendoza, L. D.; Monteiro-Pai, S., Dynamic changes in histone deacetylases following kidney ischemia-reperfusion injury are critical for promoting proximal tubule proliferation. *Am J Physiol Renal Physiol* **2019**, *316* (5), F875-F888.
136. Ren, J.; Liao, X.; Vieson, M. D.; Chen, M.; Scott, R.; Kazmierczak, J.; Luo, X. M.; Reilly, C. M., Selective HDAC6 inhibition decreases early stage of lupus nephritis by down-regulating both innate and adaptive immune responses. *Clin Exp Immunol* **2018**, *191* (1), 19-31.
137. Zhang, Y.; Zou, J.; Tolbert, E.; Zhao, T. C.; Bayliss, G.; Zhuang, S., Identification of histone deacetylase 8 as a novel therapeutic target for renal fibrosis. *FASEB J* **2020**, *34* (6), 7295-7310.
138. Holm Nielsen, S.; Willumsen, N.; Leeming, D. J.; Daniels, S. J.; Brix, S.; Karsdal, M. A.; Genovese, F.; Nielsen, M. J., Serological Assessment of Activated Fibroblasts by alpha-Smooth Muscle Actin (alpha-SMA): A Noninvasive Biomarker of Activated Fibroblasts in Lung Disorders. *Transl Oncol* **2019**, *12* (2), 368-374.
139. Simoes-Pires, C.; Zwick, V.; Nurisso, A.; Schenker, E.; Carrupt, P. A.; Cuendet, M., HDAC6 as a target for neurodegenerative diseases: what makes it different from the other HDACs? *Mol Neurodegener* **2013**, *8*, 7.
140. Liu, N.; He, S.; Ma, L.; Ponnusamy, M.; Tang, J.; Tolbert, E.; Bayliss, G.; Zhao, T. C.; Yan, H.; Zhuang, S., Blocking the class I histone deacetylase ameliorates renal fibrosis and inhibits renal fibroblast activation via modulating TGF-beta and EGFR signaling. *PLoS One* **2013**, *8* (1), e54001.
141. Regna, N. L.; Vieson, M. D.; Luo, X. M.; Chafin, C. B.; Puthiyaveetil, A. G.; Hammond, S. E.; Caudell, D. L.; Jarpe, M. B.; Reilly, C. M., Specific HDAC6 inhibition by ACY-738 reduces SLE pathogenesis in NZB/W mice. *Clin Immunol* **2016**, *162*, 58-73.

142. Shi, Y.; Xu, L.; Tang, J.; Fang, L.; Ma, S.; Ma, X.; Nie, J.; Pi, X.; Qiu, A.; Zhuang, S.; Liu, N., Inhibition of HDAC6 protects against rhabdomyolysis-induced acute kidney injury. *Am J Physiol Renal Physiol* **2017**, *312* (3), F502-F515.
143. Tang, J.; Yan, Y.; Zhao, T. C.; Gong, R.; Bayliss, G.; Yan, H.; Zhuang, S., Class I HDAC activity is required for renal protection and regeneration after acute kidney injury. *Am J Physiol Renal Physiol* **2014**, *307* (3), F303-16.
144. Feng, Y.; Huang, R.; Guo, F.; Liang, Y.; Xiang, J.; Lei, S.; Shi, M.; Li, L.; Liu, J.; Feng, Y.; Ma, L.; Fu, P., Selective Histone Deacetylase 6 Inhibitor 23BB Alleviated Rhabdomyolysis-Induced Acute Kidney Injury by Regulating Endoplasmic Reticulum Stress and Apoptosis. *Front Pharmacol* **2018**, *9*, 274.
145. Bradner, J. E.; West, N.; Grachan, M. L.; Greenberg, E. F.; Haggarty, S. J.; Warnow, T.; Mazitschek, R., Chemical phylogenetics of histone deacetylases. *Nat Chem Biol* **2010**, *6* (3), 238-243.
146. Hu, E.; Dul, E.; Sung, C. M.; Chen, Z.; Kirkpatrick, R.; Zhang, G. F.; Johanson, K.; Liu, R.; Lago, A.; Hofmann, G.; Macarron, R.; de los Frailes, M.; Perez, P.; Krawiec, J.; Winkler, J.; Jaye, M., Identification of novel isoform-selective inhibitors within class I histone deacetylases. *J Pharmacol Exp Ther* **2003**, *307* (2), 720-8.
147. Khan, N.; Jeffers, M.; Kumar, S.; Hackett, C.; Boldog, F.; Khramtsov, N.; Qian, X.; Mills, E.; Berghs, S. C.; Carey, N.; Finn, P. W.; Collins, L. S.; Tumber, A.; Ritchie, J. W.; Jensen, P. B.; Lichenstein, H. S.; Sehested, M., Determination of the class and isoform selectivity of small-molecule histone deacetylase inhibitors. *Biochem J* **2008**, *409* (2), 581-9.
148. Dasgupta, T.; Antony, J.; Braithwaite, A. W.; Horsfield, J. A., HDAC8 Inhibition Blocks SMC3 Deacetylation and Delays Cell Cycle Progression without Affecting Cohesin-dependent Transcription in MCF7 Cancer Cells. *J Biol Chem* **2016**, *291* (24), 12761-12770.
149. Glenisson, W.; Castronovo, V.; Waltregny, D., Histone deacetylase 4 is required for TGFbeta1-induced myofibroblastic differentiation. *Biochim Biophys Acta* **2007**, *1773* (10), 1572-82.
150. Banerjee, S.; Adhikari, N.; Amin, S. A.; Jha, T., Histone deacetylase 8 (HDAC8) and its inhibitors with selectivity to other isoforms: An overview. *Eur J Med Chem* **2019**, *164*, 214-240.
151. Balasubramanian, S.; Ramos, J.; Luo, W.; Sirisawad, M.; Verner, E.; Buggy, J. J., A novel histone deacetylase 8 (HDAC8)-specific inhibitor PCI-34051 induces apoptosis in T-cell lymphomas. *Leukemia* **2008**, *22* (5), 1026-34.
152. Taha, T. Y.; Aboukhatwa, S. M.; Knopp, R. C.; Ikegaki, N.; Abdelkarim, H.; Neerasa, J.; Lu, Y.; Neelarapu, R.; Hanigan, T. W.; Thatcher, G. R. J.; Petukhov, P. A., Design, Synthesis, and Biological Evaluation of Tetrahydroisoquinoline-Based Histone Deacetylase 8 Selective Inhibitors. *ACS Med Chem Lett* **2017**, *8* (8), 824-829.
153. Kovacic, P.; Edwards, C. L., Hydroxamic acids (therapeutics and mechanism): chemistry, acyl nitroso, nitroxyl, reactive oxygen species, and cell signaling. *J Recept Signal Transduct Res* **2011**, *31* (1), 10-9.
154. Olson, D. E.; Sleiman, S. F.; Bourassa, M. W.; Wagner, F. F.; Gale, J. P.; Zhang, Y. L.; Ratan, R. R.; Holson, E. B., Hydroxamate-based histone deacetylase inhibitors can protect neurons from oxidative stress via a histone deacetylase-independent catalase-like mechanism. *Chem Biol* **2015**, *22* (4), 439-445.
155. Whitehead, L.; Dobler, M. R.; Radetich, B.; Zhu, Y.; Atadja, P. W.; Claiborne, T.; Grob, J. E.; McRiner, A.; Pancost, M. R.; Patnaik, A.; Shao, W.; Shultz, M.; Tichkule, R.; Tommasi, R. A.; Vash, B.; Wang, P.; Stams, T., Human HDAC isoform selectivity achieved via exploitation of the acetate release channel with structurally unique small molecule inhibitors. *Bioorg Med Chem* **2011**, *19* (15), 4626-34.
156. <https://bpsbioscience.com/fluorogenic-hdac8-assay-kit-50068>.
157. Cianciolo Cosentino, C.; Skrypnik, N. I.; Brilli, L. L.; Chiba, T.; Novitskaya, T.; Woods, C.; West, J.; Korotchenko, V. N.; McDermott, L.; Day, B. W.; Davidson, A. J.; Harris, R. C.; de Caestecker, M. P.; Hukriede, N. A., Histone deacetylase inhibitor enhances recovery after AKI. *J Am Soc Nephrol* **2013**, *24* (6), 943-53.

158. Chiba, T.; Skrypnyk, N. I.; Skvarca, L. B.; Penchev, R.; Zhang, K. X.; Rochon, E. R.; Fall, J. L.; Pauksakon, P.; Yang, H.; Alford, C. E.; Roman, B. L.; Zhang, M. Z.; Harris, R.; Hukriede, N. A.; de Caestecker, M. P., Retinoic Acid Signaling Coordinates Macrophage-Dependent Injury and Repair after AKI. *J Am Soc Nephrol* **2016**, *27* (2), 495-508.
159. Perazella, M. A., Onco-nephrology: renal toxicities of chemotherapeutic agents. *Clin J Am Soc Nephrol* **2012**, *7* (10), 1713-21.
160. Novitskaya, T.; McDermott, L.; Zhang, K. X.; Chiba, T.; Pauksakon, P.; Hukriede, N. A.; de Caestecker, M. P., A PTBA small molecule enhances recovery and reduces postinjury fibrosis after aristolochic acid-induced kidney injury. *Am J Physiol Renal Physiol* **2014**, *306* (5), F496-504.
161. Buggy, J. J., Balasubramanian, S., Verner, E., Tai, V., Lee, C. Indole Derivatives as Inhibitors of Histone Deacetylase. 2007.
162. Verner, E., Balasubramanian, S., Buggy, J. Selective Inhibitors of Histone Deacetylase. 2009.
163. Santos-Barrriopedro, I.; Li, Y.; Bahl, S.; Seto, E., HDAC8 affects MGMT levels in glioblastoma cell lines via interaction with the proteasome receptor ADRM1. *Genes Cancer* **2019**, *10* (5-6), 119-133.
164. Mormino, A.; Coccozza, G.; Fontemaggi, G.; Valente, S.; Esposito, V.; Santoro, A.; Bernardini, G.; Santoni, A.; Fazi, F.; Mai, A.; Limatola, C.; Garofalo, S., Histone-deacetylase 8 drives the immune response and the growth of glioma. *Glia* **2021**, *69* (11), 2682-2698.
165. Hassan, M. M.; Israelian, J.; Nawar, N.; Ganda, G.; Manaswiyoungkul, P.; Raouf, Y. S.; Armstrong, D.; Sedighi, A.; Olaoye, O. O.; Erdogan, F.; Cabral, A. D.; Angeles, F.; Altintas, R.; de Araujo, E. D.; Gunning, P. T., Characterization of Conformationally Constrained Benzanilide Scaffolds for Potent and Selective HDAC8 Targeting. *J Med Chem* **2020**, *63* (15), 8634-8648.
166. Gawel, J. M.; Shouksmith, A. E.; Raouf, Y. S.; Nawar, N.; Toutah, K.; Bukhari, S.; Manaswiyoungkul, P.; Olaoye, O. O.; Israelian, J.; Radu, T. B.; Cabral, A. D.; Sina, D.; Sedighi, A.; de Araujo, E. D.; Gunning, P. T., PTG-0861: A novel HDAC6-selective inhibitor as a therapeutic strategy in acute myeloid leukaemia. *Eur J Med Chem* **2020**, *201*, 112411.
167. Gerald, M.; Morgen, M.; Sehr, P.; Steimbach, R. R.; Moi, D.; Ridinger, J.; Oehme, I.; Witt, O.; Malz, M.; Nogueira, M. S.; Koch, O.; Gunkel, N.; Miller, A. K., Selective Inhibition of Histone Deacetylase 10: Hydrogen Bonding to the Gatekeeper Residue is Implicated. *J Med Chem* **2019**, *62* (9), 4426-4443.
168. Gryder, B. E.; Sodji, Q. H.; Oyelere, A. K., Targeted cancer therapy: giving histone deacetylase inhibitors all they need to succeed. *Future Med Chem* **2012**, *4* (4), 505-24.
169. Huang, W. J.; Wang, Y. C.; Chao, S. W.; Yang, C. Y.; Chen, L. C.; Lin, M. H.; Hou, W. C.; Chen, M. Y.; Lee, T. L.; Yang, P.; Chang, C. I., Synthesis and biological evaluation of ortho-aryl N-hydroxycinnamides as potent histone deacetylase (HDAC) 8 isoform-selective inhibitors. *ChemMedChem* **2012**, *7* (10), 1815-24.
170. Lin, X.; Chen, W.; Qiu, Z.; Guo, L.; Zhu, W.; Li, W.; Wang, Z.; Zhang, W.; Zhang, Z.; Rong, Y.; Zhang, M.; Yu, L.; Zhong, S.; Zhao, R.; Wu, X.; Wong, J. C.; Tang, G., Design and synthesis of orally bioavailable aminopyrrolidinone histone deacetylase 6 inhibitors. *J Med Chem* **2015**, *58* (6), 2809-20.
171. Neelarapu, R.; Holzle, D. L.; Velaparthi, S.; Bai, H.; Brunsteiner, M.; Blond, S. Y.; Petukhov, P. A., Design, synthesis, docking, and biological evaluation of novel diazide-containing isoxazole- and pyrazole-based histone deacetylase probes. *J Med Chem* **2011**, *54* (13), 4350-64.
172. Rodrigues, D. A.; Ferreira-Silva, G. A.; Ferreira, A. C.; Fernandes, R. A.; Kwee, J. K.; Sant'Anna, C. M.; Ionta, M.; Fraga, C. A., Design, Synthesis, and Pharmacological Evaluation of Novel N-Acylhydrazone Derivatives as Potent Histone Deacetylase 6/8 Dual Inhibitors. *J Med Chem* **2016**, *59* (2), 655-70.
173. Suzuki, T.; Ota, Y.; Ri, M.; Bando, M.; Gotoh, A.; Itoh, Y.; Tsumoto, H.; Tatum, P. R.; Mizukami, T.; Nakagawa, H.; Iida, S.; Ueda, R.; Shirahige, K.; Miyata, N., Rapid discovery of highly potent and selective inhibitors of histone deacetylase 8 using click chemistry to generate candidate libraries. *J Med Chem* **2012**, *55* (22), 9562-75.

174. Tang, G.; Wong, J. C.; Zhang, W.; Wang, Z.; Zhang, N.; Peng, Z.; Zhang, Z.; Rong, Y.; Li, S.; Zhang, M.; Yu, L.; Feng, T.; Zhang, X.; Wu, X.; Wu, J. Z.; Chen, L., Identification of a novel aminotetralin class of HDAC6 and HDAC8 selective inhibitors. *J Med Chem* **2014**, *57* (19), 8026-34.
175. Tang, W.; Luo, T.; Greenberg, E. F.; Bradner, J. E.; Schreiber, S. L., Discovery of histone deacetylase 8 selective inhibitors. *Bioorg Med Chem Lett* **2011**, *21* (9), 2601-5.
176. Wang, H.; Lim, Z. Y.; Zhou, Y.; Ng, M.; Lu, T.; Lee, K.; Sangthongpitag, K.; Goh, K. C.; Wang, X.; Wu, X.; Khng, H. H.; Goh, S. K.; Ong, W. C.; Bonday, Z.; Sun, E. T., Acylurea connected straight chain hydroxamates as novel histone deacetylase inhibitors: Synthesis, SAR, and in vivo antitumor activity. *Bioorg Med Chem Lett* **2010**, *20* (11), 3314-21.
177. Zhang, L.; Wang, X.; Li, X.; Zhang, L.; Xu, W., Discovery of a series of hydroxamic acid derivatives as potent histone deacetylase inhibitors. *J Enzyme Inhib Med Chem* **2014**, *29* (4), 582-9.
178. Zhang, Y.; Feng, J.; Jia, Y.; Xu, Y.; Liu, C.; Fang, H.; Xu, W., Design, synthesis and primary activity assay of tripeptidomimetics as histone deacetylase inhibitors with linear linker and branched cap group. *Eur J Med Chem* **2011**, *46* (11), 5387-97.
179. Zhang, Y.; Feng, J.; Liu, C.; Zhang, L.; Jiao, J.; Fang, H.; Su, L.; Zhang, X.; Zhang, J.; Li, M.; Wang, B.; Xu, W., Design, synthesis and preliminary activity assay of 1,2,3,4-tetrahydroisoquinoline-3-carboxylic acid derivatives as novel Histone deacetylases (HDACs) inhibitors. *Bioorg Med Chem* **2010**, *18* (5), 1761-72.
180. Zhao, C.; Zang, J.; Ding, Q.; Inks, E. S.; Xu, W.; Chou, C. J.; Zhang, Y., Discovery of meta-sulfamoyl N-hydroxybenzamides as HDAC8 selective inhibitors. *Eur J Med Chem* **2018**, *150*, 282-291.
181. De Vreese, R.; Van Steen, N.; Verhaeghe, T.; Desmet, T.; Bougarne, N.; De Bosscher, K.; Benoy, V.; Haeck, W.; Van Den Bosch, L.; D'Hooghe, M., Synthesis of benzothiophene-based hydroxamic acids as potent and selective HDAC6 inhibitors. *Chem Commun (Camb)* **2015**, *51* (48), 9868-71.
182. Marek, L.; Hamacher, A.; Hansen, F. K.; Kuna, K.; Gohlke, H.; Kassack, M. U.; Kurz, T., Histone deacetylase (HDAC) inhibitors with a novel connecting unit linker region reveal a selectivity profile for HDAC4 and HDAC5 with improved activity against chemoresistant cancer cells. *J Med Chem* **2013**, *56* (2), 427-36.
183. Suzuki, T.; Muto, N.; Bando, M.; Itoh, Y.; Masaki, A.; Ri, M.; Ota, Y.; Nakagawa, H.; Iida, S.; Shirahige, K.; Miyata, N., Design, synthesis, and biological activity of NCC149 derivatives as histone deacetylase 8-selective inhibitors. *ChemMedChem* **2014**, *9* (3), 657-64.
184. Shen, S.; Kozikowski, A. P., Why Hydroxamates May Not Be the Best Histone Deacetylase Inhibitors--What Some May Have Forgotten or Would Rather Forget? *ChemMedChem* **2016**, *11* (1), 15-21.
185. Skipper, P. L.; Tannenbaum, S. R.; Thilly, W. G.; Furth, E. E.; Bishop, W. W., Mutagenicity of hydroxamic acids and the probable involvement of carbamoylation. *Cancer Res* **1980**, *40* (12), 4704-8.
186. Wang, C. Y., Mutagenicity of hydroxamic acids for *Salmonella typhimurium*. *Mutat Res* **1977**, *56* (1), 7-12.
187. *How many doses of an Ames-Positive/Mutagenic (DNA Reactive) Drug can be safely administered to Healthy Subjects?*; U.S. Food & Drug Administration: November 4, 2019.
188. Mulder, G. J.; Meerman, J. H., Sulfation and glucuronidation as competing pathways in the metabolism of hydroxamic acids: the role of N,O-sulfonation in chemical carcinogenesis of aromatic amines. *Environ Health Perspect* **1983**, *49*, 27-32.
189. Flipo, M.; Charton, J.; Hocine, A.; Dassonneville, S.; Deprez, B.; Deprez-Poulain, R., Hydroxamates: relationships between structure and plasma stability. *J Med Chem* **2009**, *52* (21), 6790-802.

190. Gunaydin, H.; Altman, M. D.; Ellis, J. M.; Fuller, P.; Johnson, S. A.; Lahue, B.; Lapointe, B., Strategy for Extending Half-life in Drug Design and Its Significance. *ACS Med Chem Lett* **2018**, *9* (6), 528-533.
191. Kelly, W. K.; O'Connor, O. A.; Krug, L. M.; Chiao, J. H.; Heaney, M.; Curley, T.; MacGregore-Cortelli, B.; Tong, W.; Secrist, J. P.; Schwartz, L.; Richardson, S.; Chu, E.; Olgac, S.; Marks, P. A.; Scher, H.; Richon, V. M., Phase I study of an oral histone deacetylase inhibitor, suberoylanilide hydroxamic acid, in patients with advanced cancer. *J Clin Oncol* **2005**, *23* (17), 3923-31.
192. Konsoula, R.; Jung, M., In vitro plasma stability, permeability and solubility of mercaptoacetamide histone deacetylase inhibitors. *Int J Pharm* **2008**, *361* (1-2), 19-25.
193. Calvo, E.; Reddy, G.; Boni, V.; Garcia-Canamaque, L.; Song, T.; Tjornelund, J.; Choi, M. R.; Allen, L. F., Pharmacokinetics, metabolism, and excretion of (14)C-labeled belinostat in patients with recurrent or progressive malignancies. *Invest New Drugs* **2016**, *34* (2), 193-201.
194. Long, K.; Vaughn, Z.; McDaniels, M. D.; Joyasawal, S.; Przepiorski, A.; Parasky, E.; Sander, V.; Close, D.; Johnston, P. A.; Davidson, A. J.; de Caestecker, M.; Hukriede, N. A.; Hury, D. M., Validation of HDAC8 Inhibitors as Drug Discovery Starting Points to Treat Acute Kidney Injury. *ACS Pharmacol Transl Sci* **2022**, *5* (4), 207-215.
195. Connolly, R. M.; Rudek, M. A.; Piekarczyk, R., Entinostat: a promising treatment option for patients with advanced breast cancer. *Future Oncol* **2017**, *13* (13), 1137-1148.
196. Liu, J.; Yu, Y.; Kelly, J.; Sha, D.; Alhassan, A. B.; Yu, W.; Maletic, M. M.; Duffy, J. L.; Klein, D. J.; Holloway, M. K.; Carroll, S.; Howell, B. J.; Barnard, R. J. O.; Wolkenberg, S.; Kozlowski, J. A., Discovery of Highly Selective and Potent HDAC3 Inhibitors Based on a 2-Substituted Benzamide Zinc Binding Group. *ACS Med Chem Lett* **2020**, *11* (12), 2476-2483.
197. Liu, J.; Kelly, J.; Yu, W.; Clausen, D.; Yu, Y.; Kim, H.; Duffy, J. L.; Chung, C. C.; Myers, R. W.; Carroll, S.; Klein, D. J.; Fells, J.; Holloway, M. K.; Wu, J.; Wu, G.; Howell, B. J.; Barnard, R. J. O.; Kozlowski, J. A., Selective Class I HDAC Inhibitors Based on Aryl Ketone Zinc Binding Induce HIV-1 Protein for Clearance. *ACS Med Chem Lett* **2020**, *11* (7), 1476-1483.
198. Madsen, A. S.; Kristensen, H. M.; Lanz, G.; Olsen, C. A., The effect of various zinc binding groups on inhibition of histone deacetylases 1-11. *ChemMedChem* **2014**, *9* (3), 614-26.
199. Hou, X.; Du, J.; Liu, R.; Zhou, Y.; Li, M.; Xu, W.; Fang, H., Enhancing the Sensitivity of Pharmacophore-Based Virtual Screening by Incorporating Customized ZBG Features: A Case Study Using Histone Deacetylase 8. *J Chem Inf Model* **2015**, *55* (4), 861-71.
200. He, J.; Wang, S.; Liu, X.; Lin, R.; Deng, F.; Jia, Z.; Zhang, C.; Li, Z.; Zhu, H.; Tang, L.; Yang, P.; He, D.; Jia, Q.; Zhang, Y., Synthesis and Biological Evaluation of HDAC Inhibitors With a Novel Zinc Binding Group. *Front Chem* **2020**, *8*, 256.
201. Lobera, M.; Madauss, K. P.; Pohlhaus, D. T.; Wright, Q. G.; Trocha, M.; Schmidt, D. R.; Baloglu, E.; Trump, R. P.; Head, M. S.; Hofmann, G. A.; Murray-Thompson, M.; Schwartz, B.; Chakravorty, S.; Wu, Z.; Mander, P. K.; Kruidenier, L.; Reid, R. A.; Burkhart, W.; Turunen, B. J.; Rong, J. X.; Wagner, C.; Moyer, M. B.; Wells, C.; Hong, X.; Moore, J. T.; Williams, J. D.; Soler, D.; Ghosh, S.; Nolan, M. A., Selective class IIa histone deacetylase inhibition via a nonchelating zinc-binding group. *Nat Chem Biol* **2013**, *9* (5), 319-25.
202. Roth, H. S.; Hergenrother, P. J., Derivatives of Procaspase-Activating Compound 1 (PAC-1) and their Anticancer Activities. *Curr Med Chem* **2016**, *23* (3), 201-41.
203. Dick, B. L.; Cohen, S. M., Metal-Binding Isosteres as New Scaffolds for Metalloenzyme Inhibitors. *Inorg Chem* **2018**, *57* (15), 9538-9543.
204. Sixto-Lopez, Y.; Bello, M.; Correa-Basurto, J., Exploring the inhibitory activity of valproic acid against the HDAC family using an MMGBSA approach. *J Comput Aided Mol Des* **2020**, *34* (8), 857-878.
205. Zhang, L.; Zhang, J.; Jiang, Q.; Zhang, L.; Song, W., Zinc binding groups for histone deacetylase inhibitors. *J Enzyme Inhib Med Chem* **2018**, *33* (1), 714-721.

206. Amin, S. A.; Adhikari, N.; Jha, T., Structure-activity relationships of HDAC8 inhibitors: Non-hydroxamates as anticancer agents. *Pharmacol Res* **2018**, *131*, 128-142.
207. Lassalas, P.; Gay, B.; Lasfargeas, C.; James, M. J.; Tran, V.; Vijayendran, K. G.; Brunden, K. R.; Kozlowski, M. C.; Thomas, C. J.; Smith, A. B., 3rd; Huryn, D. M.; Ballatore, C., Structure Property Relationships of Carboxylic Acid Isosteres. *J Med Chem* **2016**, *59* (7), 3183-203.
208. Gurard-Levin, Z. A.; Scholle, M. D.; Eisenberg, A. H.; Mrksich, M., High-throughput screening of small molecule libraries using SAMDI mass spectrometry. *ACS Comb Sci* **2011**, *13* (4), 347-50.
209. Yoshida, M.; Kijima, M.; Akita, M.; Beppu, T., Potent and specific inhibition of mammalian histone deacetylase both in vivo and in vitro by trichostatin A. *J Biol Chem* **1990**, *265* (28), 17174-9.
210. Catapano, M. C.; Tvrdy, V.; Karlickova, J.; Micolini, L.; Mladenka, P., A simple, cheap but reliable method for evaluation of zinc chelating properties. *Bioorg Chem* **2018**, *77*, 287-292.
211. Citarella, A.; Moi, D.; Pinzi, L.; Bonanni, D.; Rastelli, G., Hydroxamic Acid Derivatives: From Synthetic Strategies to Medicinal Chemistry Applications. *ACS Omega* **2021**, *6* (34), 21843-21849.
212. Moreno-Yruela, C.; Olsen, C. A., Determination of Slow-Binding HDAC Inhibitor Potency and Subclass Selectivity. *ACS Med Chem Lett* **2022**, *13* (5), 779-785.
213. Goossen, L. J.; Ghosh, K., Palladium-Catalyzed Synthesis of Aryl Ketones from Boronic Acids and Carboxylic Acids or Anhydrides We thank M. Rossig and L. Winkel for technical assistance, Prof. Dr. M. T. Reetz for generous support and constant encouragement, and the DFG for financial support. *Angew Chem Int Ed Engl* **2001**, *40* (18), 3458-3460.
214. Leuci R., B. L., Laghezza A., Liodice F., Tortorella P., and Piemontese L., Importance of Biometals as Targets in Medicinal Chemistry: An Overview about the Role of Zinc (II) Chelating Agents. *Applied Sciences* **2020**, *10*.
215. Patil, V.; Sodji, Q. H.; Kornacki, J. R.; Mrksich, M.; Oyelere, A. K., 3-Hydroxypyridin-2-thione as novel zinc binding group for selective histone deacetylase inhibition. *J Med Chem* **2013**, *56* (9), 3492-506.
216. Puerta, D. T.; Lewis, J. A.; Cohen, S. M., New beginnings for matrix metalloproteinase inhibitors: identification of high-affinity zinc-binding groups. *J Am Chem Soc* **2004**, *126* (27), 8388-9.
217. Samant, B. S., Synthesis of 3-hydroxypyrid-2-ones from furfural for treatment against iron overload and iron deficiency. *Eur J Med Chem* **2008**, *43* (9), 1978-82.
218. Botta, C. B.; Cabri, W.; Cini, E.; De Cesare, L.; Fattorusso, C.; Giannini, G.; Persico, M.; Petrella, A.; Rondinelli, F.; Rodriguez, M.; Russo, A.; Taddei, M., Oxime amides as a novel zinc binding group in histone deacetylase inhibitors: synthesis, biological activity, and computational evaluation. *J Med Chem* **2011**, *54* (7), 2165-82.
219. Muthyala, R.; Shin, W. S.; Xie, J.; Sham, Y. Y., Discovery of 1-hydroxypyridine-2-thiones as selective histone deacetylase inhibitors and their potential application for treating leukemia. *Bioorg Med Chem Lett* **2015**, *25* (19), 4320-4.
220. Pidugu, V. R.; Yarla, N. S.; Pedada, S. R.; Kalle, A. M.; Satya, A. K., Design and synthesis of novel HDAC8 inhibitory 2,5-disubstituted-1,3,4-oxadiazoles containing glycine and alanine hybrids with anti cancer activity. *Bioorg Med Chem* **2016**, *24* (21), 5611-5617.
221. Suzuki, T.; Matsuura, A.; Kouketsu, A.; Nakagawa, H.; Miyata, N., Identification of a potent non-hydroxamate histone deacetylase inhibitor by mechanism-based drug design. *Bioorg Med Chem Lett* **2005**, *15* (2), 331-5.
222. Chen, K.; Xu, L.; Wiest, O., Computational exploration of zinc binding groups for HDAC inhibition. *J Org Chem* **2013**, *78* (10), 5051-5.
223. Westerfield, M., *The zebrafish book. A guide for the laboratory use of zebrafish (Danio rerio)*. 4th ed ed.; University of Oregon Press: Eugene, OR, 2000.

224. Przepiorski, A.; Sander, V.; Tran, T.; Hollywood, J. A.; Sorrenson, B.; Shih, J. H.; Wolvetang, E. J.; McMahon, A. P.; Holm, T. M.; Davidson, A. J., A Simple Bioreactor-Based Method to Generate Kidney Organoids from Pluripotent Stem Cells. *Stem Cell Reports* **2018**, *11* (2), 470-484.
225. Przepiorski, A.; Crunk, A. E.; Holm, T. M.; Sander, V.; Davidson, A. J.; Hukriede, N. A., A Simplified Method for Generating Kidney Organoids from Human Pluripotent Stem Cells. *J Vis Exp* **2021**, (170).
226. Scarfe, L.; Schock-Kusch, D.; Ressel, L.; Friedemann, J.; Shulhevich, Y.; Murray, P.; Wilm, B.; de Caestecker, M., Transdermal Measurement of Glomerular Filtration Rate in Mice. *J Vis Exp* **2018**, (140).
227. Scarfe, L.; Menshikh, A.; Newton, E.; Zhu, Y.; Delgado, R.; Finney, C.; de Caestecker, M. P., Long-term outcomes in mouse models of ischemia-reperfusion-induced acute kidney injury. *Am J Physiol Renal Physiol* **2019**, *317* (4), F1068-F1080.